

**The Light Harvesting 2 Antenna Complex of  
*Rhodobacter sphaeroides***



**John Anthony Timney**

**A thesis submitted for the degree of Doctor of Philosophy at the  
University of Sheffield.**

**Department of Molecular Biology  
and Biotechnology**

**March 2007**

“Look what I just found.....fill that sink up”

**Dr Jaimey Tucker,**  
a pretty slow summer’s afternoon in the Hunter lab.

To my parents.

## Summary

This thesis presents an analysis of the contribution that the polypeptide Puc2B makes to the binding of BChl(s) within the purified LH2 complexes. Mass spectroscopy established for the first time that Puc2B is incorporated within the LH2 in native complexes. The effect the second *puc* operon has on the ability of the cell to adapt to high light conditions was measured; it was shown that the *puc2BA* gene pair is crucial in modulating levels of LH2 complex assembly under these conditions. Using AFM, initial attempts were made to analyse the effects of the second *puc* operon upon the membrane architecture. Images of *Rba. sphaeroides* 2.4.1.  $\Delta 2BA$  membranes were obtained, with large scale hexagonally packed arrays of LH2 observed for the first time.

The development of a purification protocol for a LH2 complex possessing only Puc1B as its  $\beta$ -polypeptide (LH2-1B1A) is described. The crystallisation of LH2 complexes purified using this protocol is detailed, along with the unsuccessful attempts to obtain structural data from the resulting crystals by X-ray crystallography. A previously undescribed protein, RSP6124, was identified during the purification of LH2-1B1A. A bio-informatic analysis of this protein is presented. Although its role within the organism is still unclear, there is evidence which suggests that strong electrostatic interactions between RSP6124 and the extrinsic regions of the LH2 complex may exist. Contamination of the purified LH2-1B1A sample with RSP6124 provides an alternative explanation for current failures to obtain crystals of sufficient quality to yield high resolution diffraction data.

Two new deletion strains of *Rba. sphaeroides* 2.4.1. that lack the ability to assemble any LH2, LH1 or RC complex have been created. Assembly levels of the LH2 complex in the deletion strains lacking both *puc* operons were shown to be markedly lower than in a deletion strain which carries *puc2BA* on its genome. The spectroscopic characteristics of LH2 complexes comprising exclusively Puc1B, Puc2B or a mixture of both were analysed while bound within the native membrane. Puc2B is shown to be integral to B800 BChl binding within the LH2 complex of *Rba. sphaeroides* 2.4.1. A hypothesis to account for the reduction of B800 BChl binding in the absence of Puc2B is proposed.

The final chapter describes the specific attachment of purified LH2 complexes from *Rba. sphaeroides* to patterned self assembled monolayers on the micron scale. Surface plasmon resonance studies were used to select SAMs possessing tail groups with specific chemical properties. Two surfaces that have contrasting attractive and repulsive responses to membrane protein adsorption have been identified. Confocal microscopy was used to demonstrate the functionality of the purified LH2 complexes whilst they are covalently attached to the surface.

## Acknowledgements

First and foremost I must thank my supervisor Professor Neil Hunter, who has provided me with immense support throughout my PhD, as well as keeping my intake of chorizo burgers and moonshine up to scratch over the last few months. Thanks for everything Neil.

In relation to the work presented in this thesis, I must thank a number of people for their professional support; Professor Richard Cogdell for his help establishing the crystallography project and Dr Miroslav Papiz for his work on the LH2 crystals; Dr Arthur Moir and Dr Mark Dickman for their help with protein sequencing and all those involved in the micron patterning collaboration.

My thanks must go out to all those in the lab past and present for making my PhD an unforgettable experience. Firstly those past: Pat for teaching me the ways of the Don; Al for his loud sound effects; Dez for teaching me how to use internet gambling sites and for throwing up on my shoes; Jo for being a real friend and the gossip queen and Jim for west wing chats. Special thanks must go to Mark 'mentor' Hoggins for the start he gave me in the lab, coupled with his flawless method of encouragement (it's not nice to set people on fire). Your help and friendship over the past few months has been invaluable and much appreciated, cheers mate.

A big thank you to everybody still in the lab: John for being the guru of everything and putting up with my constant badgering. Jaimey for the passive smoking, near death mountain bike experiences, dusting the ash off my thesis in a phoenix like manner and for making my time in labs so memorable. Thanks for everything mate. Paul must be thanked for his fabulousness whilst having no human emotions whatsoever, as well as proof reading my thesis with such good grace. I must also thank Emma for her tireless proof reading, Dan for his unflinching support of Liverpool football club (we won it five times), Nev for being the poshest man I know and Qian for all his help.

Special thanks must go to Reenie, who has put up with my hideous mood over the past few months and made it all that bit easier. You've been a massive support throughout and one I certainly didn't deserve at times. Thanks for everything skanky.

My time at university has been blessed by the friendship of my three housemates, Fi, Doosh and Fizz. The loving support you have all shown me over the past seven years (and the last six months in particular) has been immense. I never imagined that when I came to Sheffield I would find a second family. Thanks for always being there.

I must also thank my friends at SheffieldVolunteering for making my PhD days plenty of fun. Stella and Helen, thank you for all your support and for believing in us. Dave and Bobby, thanks for the drinks, laughs, memories and for the fANTastic last two years. Can't believe it's nearly all over.

Finally and most of all I must thank my family, Mum, Dad, Helen, Liz and Grandma. Thank you for all the love and support you have shown me and for always believing in me, it has meant so much.

## Contents

<b>Summary</b> .....	<b>i</b>
<b>Acknowledgements</b> .....	<b>ii</b>
<b>Contents</b> .....	<b>iii</b>
<b>List of Figures</b> .....	<b>viii</b>
<b>Abbreviations</b> .....	<b>xii</b>
<b>Chapter 1: Introduction</b> .....	<b>1</b>
1.1 Photosynthesis .....	1
1.2 Photosynthetic bacteria.....	2
1.2.1 <i>Rhodobacter sphaeroides</i> .....	3
1.3 Pigment Biosynthesis.....	5
1.3.1 Bacteriochlorophyll biosynthesis.....	5
1.3.2 Carotenoid Biosynthesis .....	9
1.4 The light harvesting complexes of <i>Rba. sphaeroides</i> .....	14
1.4.1 The peripheral light harvesting complex LH2 .....	15
1.4.1.2 The structure of LH2 .....	15
1.4.1.3 The B800 BChl(s) in LH2 .....	18
1.4.1.4 The B850 BChl(s) in LH2 .....	19
1.4.1.5 The carotenoids of LH2 .....	20
1.4.2 The core light harvesting complex LH1 .....	21
1.4.3 The Reaction Centre .....	25
1.4.4 The LH1-RC Core complex.....	29
1.4.5 PufX.....	33
1.4.6 The function of bacteriochlorophyll in light-harvesting complexes.....	36
1.5 Electron flow and ATP synthesis in the photosynthetic membrane .....	37
1.5.1 Light-driven electron flow in the RC.....	37
1.5.2 The cytochrome <i>bc</i> <sub>1</sub> complex .....	38
1.5.3 ATP synthase .....	40
1.6 Photosynthetic gene clusters of <i>Rba. sphaeroides</i> and other purple bacteria.....	40
1.6.1 The <i>puf</i> operon.....	41
1.6.2 The function of <i>pufQ</i> and <i>pufK</i> .....	42
1.6.3 The <i>puhA</i> operon.....	43
1.6.4 The <i>puc</i> operon .....	46
1.6.5 A second <i>puc</i> operon in <i>Rba. sphaeroides</i> .....	47
1.6.6 The role of the <i>puc2BA</i> operon in LH2 assembly.....	50
1.7 The organisation of the photosynthetic membrane.....	51
1.7.1 The native architecture of the photosynthetic membrane in <i>Rba. sphaeroides</i> .....	52
1.7.2 A comparison of photosynthetic membranes in purple bacteria .....	53

1.8	Protein patterning utilising self assembled monolayers .....	57
1.8.1	Self assembled monolayers.....	59
1.8.2	Photolithography.....	60
1.9	Principles of atomic force microscopy .....	63

## **Chapter 2: Materials and Methods .....** 65

2.1	Materials .....	65
2.2	Standard buffers, reagents and media .....	65
2.3	<i>Escherichia coli</i> strains.....	65
2.4	Production of <i>E. coli</i> competent cells.....	66
2.5	Transformation of <i>E.coli</i> competent cells.....	66
2.6	Nucleic acid manipulation .....	66
2.6.1	Small-scale preparation of plasmid DNA (mini-prep) .....	66
2.6.2	Larger-scale preparation of plasmid DNA (midi-prep).....	67
2.6.3	Polymerase chain reaction (PCR).....	67
2.6.4	Restriction enzyme digestions .....	67
2.6.5	Dephosphorylation of DNA.....	68
2.6.6	Agarose gel electrophoresis of DNA .....	68
2.6.7	Recovery of DNA from agarose gels.....	68
2.6.8	Ligation of DNA fragments.....	68
2.7	DNA sequencing.....	69
2.8	Protein Manipulation .....	69
2.8.1	SDS-polyacrylamide gel electrophoresis (SDS-PAGE).....	69
2.8.2	Purification of proteins featured in this thesis .....	69
2.8.3	Quantification of LH2 complex.....	69
2.8.4	Crystallisation trials of purified LH2.....	70
2.9	<i>Rba. sphaeroides</i> strains .....	71
2.10	Growth of <i>Rba. sphaeroides</i> .....	71
2.10.1	Semi-aerobic growth.....	72
2.10.2	Photosynthetic growth .....	72
2.11	Conjugative transfer of plasmid DNA from <i>E. coli</i> to <i>Rba. sphaeroides</i> .....	72
2.12	Membrane preparation from <i>Rba. sphaeroides</i> .....	73
2.12.1	Intracytoplasmic membrane preparation .....	73
2.12.2	ICM partial solubilisation and fractionation.....	73
2.13	Spectroscopy.....	73
2.13.1	Room temperature absorbance spectra .....	73
2.13.2	Low temperature absorbance spectra.....	73
2.13.3	Fluorescence spectroscopy .....	74
2.14	Electron microscopy .....	74
2.15	Self Assembled Monolayers .....	74
2.15.1	Formation of evaporated gold surfaces.....	74
2.15.2	Self Assembled Monolayer formation.....	75
2.15.3	Photopatterning of SAMs .....	75
2.16	Atomic force microscopy .....	75
2.16.1	AFM of membrane fragments .....	75
2.16.2	Atomic force fluorescence microscopy (AFFM).....	76

2.16.3	Friction Force Microscopy .....	76
2.17	Surface Plasmon Resonance .....	77

### **Chapter 3: The role of the Puc2B polypeptide in the LH2 complex of *Rhodobacter sphaeroides*..... 78**

3.2	Introduction.....	79
3.3	Results.....	80
3.3.1	The creation of the strain <i>Rba. sphaeroides</i> 2.4.1. $\Delta 1BA-\Delta 2BA$ (pRKCBC1-2B1AC), which has an LH2 complex comprising Puc2B1A.....	80
3.3.1.1	Site directed mutagenesis of <i>puc1B</i> .....	80
3.3.1.2	Subcloning of the <i>puc2B1A</i> genes and conjugation into the deletion mutant <i>Rba. sphaeroides</i> $\Delta 1BA-\Delta 2BA$ .....	81
3.3.2	Spectroscopic comparison of purified LH2 complexes containing differing $\beta$ -polypeptide compositions.....	84
3.3.2.1	Purification of the LH2 complexes.....	84
3.3.2.2	LH2 absorbance properties .....	84
3.3.2.3	Fluorescence excitation properties of WT and mutant LH2 complexes.....	87
3.3.2.4	Fluorescence emission properties of WT and mutant LH2 complexes.....	91
3.3.3	Analysis of the contribution of the Puc2B polypeptide to wild type LH2 complexes.....	92
3.3.3.1	Growth curve comparison of <i>Rba. sphaeroides</i> 2.4.1. and <i>Rba. sphaeroides</i> 2.4.1. $\Delta 2BA$ .....	92
3.3.3.2	Electrospray mass spectroscopy analysis of purified WT-LH2 and LH2-1B1A complexes.....	94
3.3.3.3	AFM analysis of low light membranes from <i>Rba. sphaeroides</i> 2.4.1. $\Delta 2BA$ .....	96
3.4	Discussion.....	103
3.4.1	Context.....	103
3.4.2	The spectroscopic properties of WT-LH2, LH2-1B1A and LH2-2B1A .....	103
3.4.3	Analysis of the contribution the second <i>puc</i> operon and its resulting polypeptides makes to the phenotype of <i>Rba. sphaeroides</i> 2.4.1. ....	105
3.4.4	The analysis of the LH2 complex by electrospray mass spectroscopy .....	107
3.4.4	AFM analysis of the ICM from <i>Rba. sphaeroides</i> 2.4.1. $\Delta 2BA$ .....	107

**Chapter 4: The purification and crystallisation of LH2-1B1A, and the identification of the novel protein RSP6124 from *Rhodobacter sphaeroides*. ..... 111**

4.1	Summary.....	111
4.2	Introduction.....	112
4.3	Results.....	113
4.3.1	Mutant strains of <i>Rba. sphaeroides</i> .....	113
4.3.2	The purification of LH2-1B1A .....	113
4.3.3	Identification of different populations of LH2-1B1A by Source 15Q ion exchange chromatography .....	115
4.3.4	N-terminal sequencing analysis of purified LH2-1B1A.....	120
4.3.5	Electrospray mass spectroscopy analysis of purified LH2-1B1A .....	124
4.3.6	Bioinformatic analysis of RSP6124.....	124
4.3.7	Crystallisation trials of LH2-1B1A.....	129
4.3.8	Diffraction of LH2-1B1A crystals.....	132
4.4	Discussion.....	136
4.4.1	Context.....	136
4.4.2	The purification of LH2-1B1A.....	136
4.4.3	RSP6124: a novel protein in <i>Rba. sphaeroides</i> .....	137
4.4.4	Crystallisation of LH2-1B1A .....	139

**Chapter 5: The creation of the *Rba. sphaeroides* deletion mutants  $\Delta 3$  and  $\Delta 4$ , and the comparison of LH2-only membranes containing WT- LH2, LH2-1B1A and LH2-2B1A ..... 141**

5.1	Summary.....	141
5.2	Introduction.....	142
5.3	Results.....	143
5.3.1	Creation of the <i>Rba. sphaeroides</i> deletion strains $\Delta 3$ and $\Delta 4$ .....	143
5.3.1.2	Conjugative transfer of the suicide plasmid pSUP202 $\Delta$ BALM.....	145
5.3.2	Analysis of LH2 assembly within <i>Rba. sphaeroides</i> $\Delta 3$ and $\Delta 4$ .....	146
5.3.3	A comparison of LH2-only membranes comprising WT-LH2, LH2-1B1A and LH2-2B1A. ....	146
5.3.3.1	Low temperature (77 K) absorbance properties of WT-LH2, LH2-1B1A and LH2-2B1A. ....	149
5.4	Discussion.....	155
5.4.1	Context.....	155
5.4.2	Analysis of LH2 assembly in $\Delta 3$ and $\Delta 4$ .....	156
5.4.3	The spectroscopic properties of WT-LH2, LH2-1B1A and LH2-2B1A .....	157
5.4.3.1	Absorbance properties .....	157
5.4.3.2	Fluorescence excitation properties.....	159

5.4.3.3	Fluorescence emission properties .....	160
5.4.3.4	The role of the $\beta$ -polypeptide in the LH2 complex .....	161

## **Chapter 6: Micron patterning of functional light harvesting 2 complexes by specific covalent attachment to N-hydroxysuccimide ester self-assembled monolayers..... 166**

6.1	Summary .....	166
6.2	Introduction.....	167
6.3	Results.....	169
6.3.1	Purification of WT-LH2 .....	169
6.3.2	The creation of SAMs.....	169
6.3.3	SPR .....	172
6.3.4	Micron patterning .....	174
6.3.4	Fluorescence imaging of LH2 bound to photopatterned SAMs .....	176
6.4	Discussion .....	179
6.4.1	Context.....	179
6.4.2	SPR analysis of SAM properties .....	179
6.4.3	Micron patterning of purified LH2 complexes.....	180

## **Appendix I..... 181**

## **Appendix II..... 183**

## **References ..... 185**

# List of Figures

	Page
<b>Chapter 1</b>	
<b>Figure 1.1</b> Taxonomy and absorption spectra of photosynthetic organisms.....	4
<b>Figure 1.2(a)</b> The bacteriochlorophyll biosynthetic pathway.....	7
<b>Figure 1.2(b)</b> The bacteriochlorophyll biosynthetic pathway.....	8
<b>Figure 1.3</b> The role of carotenoids in photoprotection.....	10
<b>Figure 1.4</b> The carotenoid biosynthetic pathway.....	12
<b>Figure 1.5</b> The structure of the <i>Rps. acidophila</i> LH2 complex.....	16
<b>Figure 1.6</b> The structure of the <i>Rps. palustris</i> LH1-RC-PufW complex.....	22
<b>Figure 1.7</b> Schematic model of B875 bchls within the LH1 complex .....	26
<b>Figure 1.8</b> Structure of the RC from <i>Rba. sphaeroides</i> .....	27
<b>Figure 1.9</b> The core complex dimer of <i>Rba. sphaeroides</i> resolved to 8.5 Å.....	31
<b>Figure 1.10</b> The NMR structure of PufX.....	35
<b>Figure 1.11</b> Cyclic electron flow within the photosynthetic apparatus of <i>Rba. sphaeroides</i> .....	39
<b>Figure 1.12</b> The <i>Rba. sphaeroides</i> photosynthesis gene cluster.....	42
<b>Figure 1.13</b> A sequence alignment of the polypeptides encoded by the two <i>puc</i> operons from <i>Rba. sphaeroides</i> 2.4.1.....	49
<b>Figure 1.14</b> AFM images of native membranes from <i>Rba. sphaeroides</i> .....	54
<b>Figure 1.15</b> A comparison of differing membrane architectures in purple photosynthetic bacteria.....	56
<b>Figure 1.16</b> Analysis of membrane organisation and its associated structures in <i>Rps. palustris</i> by AFM.....	58
<b>Figure 1.17</b> Self Assembled Monolayers (SAMs).....	61

## Chapter 3

Figure 3.1	<i>A puc2B1A</i> gene pair created by site directed mutagenesis.....	82
Figure 3.2	Creation of transconjugant strain <i>Rba. sphaeroides</i> <i>Δ1BA-2BA</i> (pRKCBC1-2B1A).....	83
Figure 3.3	Purification of WT-LH2, LH2-1B1A and LH2-2B1A.....	86
Figure 3.4	Spectroscopic analysis of WT-LH2 at 77 K.....	88
Figure 3.5	Spectroscopic analysis of LH2-1B1A at 77 K.....	89
Figure 3.6	Spectroscopic analysis of LH2-2B1A at 77 K.....	90
Figure 3.7	Growth curve comparison.....	93
Figure 3.8	A comparison of light harvesting complex expression under high light conditions.....	95
Figure 3.9	Identification of Puc1B in purified WT LH2 complexes by mass spectroscopy.....	97
Figure 3.10	Identification of Puc2B in purified WT LH2 complexes by mass spectroscopy .....	98
Figure 3.11	Sucrose gradient purification of ICM fragments from <i>Rba. sphaeroides</i> 2.4.1 <i>Δ2BA</i> .....	99
Figure 3.12	A comparison of LH2 arrangement in LH2-only and <i>Rba. sphaeroides</i> <i>Δ2BA</i> membranes.....	101
Figure 3.13	An AFM topograph and height profile of ordered LH2 arrays within the membrane.....	102
Figure 3.14	Modelling the movement of LH2 on mica.....	109

## Chapter 4

Figure 4.1	Purification of LH2-1B1A.....	116
Figure 4.2	Recorded spectra of LH2-1B1A throughout purification.....	117
Figure 4.3	Monodispersed LH2 for crystallisation.....	118
Figure 4.4	Source 15-Q column elution profile with low sample loading.....	119
Figure 4.5	Source 15-Q column elution profile with high sample loading....	121
Figure 4.6	Comparison of $Q_y$ absorbance maxima between elution peaks...	122

Figure 4.7	N-terminal sequence analysis of purified LH2-1B1A.....	123
Figure 4.8	Identification of RSP6124 by electrospray mass spectroscopy....	125
Figure 4.9	DNA and protein sequence alignments.....	126
Figure 4.10	Predict protein analysis of RSP6124.....	128
Figure 4.11	Sequence alignments of oxygen sensitive promoters.....	130
Figure 4.12	Crystallisation of the purified LH2-1B1A.....	131
Figure 4.13	Crystal growth and screening at Daresbury SRS ( i ).....	133
Figure 4.14	Crystal growth and screening at Daresbury SRS ( ii ).....	134
Figure 4.15	Crystal growth and screening at Daresbury SRS ( iii ).....	135

## Chapter 5

Figure 5.1	The creation of deletion mutants $\Delta 3$ and $\Delta 4$ .....	144
Figure 5.2	<i>Rba. sphaeroides</i> deletion backgrounds.....	147
Figure 5.3	LH2 complex expression in DD13, $\Delta 3$ and $\Delta 4$ .....	148
Figure 5.4	Absorbance spectra at low temperature (77 K).....	150
Figure 5.5	Absorbance spectra in the carotenoid and near IR regions at 77 K.....	151
Figure 5.6	Fluorescence excitation at low temperature (77 K).....	153
Figure 5.7	Fluorescence emission spectra at low temperature (77 K).....	154
Figure 5.8	B800:B850 absorbance comparison at 77 K.....	158
Figure 5.9	Mapping of <i>Rba. sphaeroides</i> 2.4.1. $\beta$ -polypeptide residues onto the <i>Rps. acidophila</i> LH2 3D crystal structure (McDermott <i>et al.</i> , 1995).....	162
Figure 5.10	Rhodopin-glucoside within the LH2 structure (McDermott <i>et al.</i> , 1995).....	164

## Chapter 6

Figure 6.1	Purification of WT-LH2.....	170
Figure 6.2	Spectroscopic analysis of WT-LH2 at 77 K.....	171
Figure 6.3	SPR analysis of SAMs after exposure to purified WT-LH2 complex.....	173

<b>Figure 6.4</b>	<b>Micron patterning of WT-LH2 imaged by AFM.....</b>	<b>175</b>
<b>Figure 6.5</b>	<b>Fluorescence images of patterned purified WT-LH2 complex.....</b>	<b>177</b>
<b>Figure 6.6</b>	<b>The fluorescence emission spectra of covalently bound.....</b>	<b>178</b>

## Abbreviations

3-D	Three-dimensional
2-D	Two-dimensional
AFM	Atomic force microscopy
AFFM	Atomic force fluorescence microscopy
AU	Absorbance units
ADP	Adenosine diphosphate
ATP	Adenosine triphosphate
BChl	Bacteriochlorophyll
Crt	Carotenoid
CCD	Charge coupled device
DDM	Dodecyl maltoside
DNase I	Deoxyribonuclease I
EDC	N(3-Dimethylaminopropyl)-N'ethylcarbodiimide
EDTA	Ethylenediaminetetraacetic acid
EM	Electron microscopy
HEPES	4-(2-Hydroxyethyl)piperazine-N-(4-butanesulfonic acid)
ICM	Intra cytoplasmic membrane
IR	Infra red
LDAO	N,N-Dimethyldodecylamine-N-oxide
LH	Light-harvesting
MUA	Mercaptoundecanoic acid
MW	Molecular weight
MR	Molecular replacement
NAD(P)	Nicotinamide adenine dinucleotide phosphate
NCBI	National Centre for Biotechnology Information
NHS	N-hydroxysuccimide ester
NMR	Nuclear magnetic resonance
OEG	Oligo ethylene glycol
Pfot	1H,1H,2H,2H-Perfluorooctanethiol
PGC	Photosynthesis gene cluster

PMF	Proton motive force
Psi	Pounds per square inch
Q	Quinone
<i>Rba.</i>	<i>Rhodobacter</i>
RC	Reaction centre
RMS	Root mean square
<i>Rps.</i>	<i>Rhodopseudomonas</i>
RPM	Revolutions per minute
<i>Rsp.</i>	<i>Rhodospirillum</i>
SAMs	Self Assembled Monolayers
SDS-PAGE	Sodium dodecyl sulphate polyacrylamide electrophoresis
Tn	Transposon
Tris	Tris hydroxymethyl methylamine
Uv-vis	Ultraviolet-visible

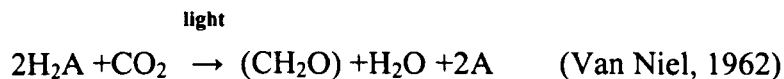
# Chapter 1: Introduction

## 1.1 Photosynthesis

### Introduction and overview

Solar energy harnessed through the process of photosynthesis is the primary source of energy for the biosphere; the only exception being chemolithotrophs which are the only organisms which live independently of incident solar energy. Photosynthetic organisms therefore represent the basis of nearly all eco-systems on earth. Photosynthesis is carried out by plants, algae, cyanobacteria and photosynthetic bacteria. Photosynthesis initiates with the absorption of a single photon by a pigment molecule, and culminates with the production of adenosine-5'-triphosphate (ATP). Hydrolysis of ATP to produce adenosine-5'-diphosphate (ADP) releases the stored chemical energy, initially created by the proton motive force that drives ATP synthase. This hydrolysis reaction is used throughout the cell to drive energy requiring metabolic processes.

Photosynthesis can be represented by the general equation:



where  $\text{H}_2\text{A}$  is the source of hydrogen ions and electrons used to reduce carbon dioxide to carbohydrate ( $\text{CH}_2\text{O}$ ), and  $\text{A}$  is the oxidation product. In plants, algae and cyanobacteria, water is the reductant and oxygen is the oxidation product (oxygenic photosynthesis). Photosynthetic bacteria other than cyanobacteria utilise a number of different compounds as the reductant including molecular hydrogen, reduced sulphur compounds and organic acids such as acetate or succinate. Consequently oxygen is not evolved from these reactions (anoxygenic photosynthesis).

In the first stage of photosynthesis (the 'light reactions'), solar radiation excites an electron in a pigment molecule housed within the organism. The energy is conserved as a charge separation, then as a proton gradient and finally as ATP. The second stage of photosynthesis (the 'dark reactions') comprises of a series of reductive carbon fixation reactions, driven by ATP and NAD(P)H, which assimilate carbon dioxide to carbohydrate.

There are three major groups of pigment molecules involved in light absorption during photosynthesis. Chlorophylls, carotenoids and phycobilins have distinct absorption spectra that indicate the specific wavelengths of light they are capable of harvesting. Pigment and protein molecules associate to form, pigment protein complexes, which come together to form part of the photosynthetic membrane. The wavelength of light a pigment molecule is capable of absorbing can be partially dictated by its local protein environment. The energy absorbed by the light harvesting complexes is transferred to the reaction centre pigment protein complexes, where charge separation occurs.

## 1.2 Photosynthetic bacteria

Photosynthetic bacteria are generally found inhabiting marine and freshwater aquatic environments. There are four main classifications:

1. Green bacteria, which can be subdivided into sulphur or *Chlorobiaceae* and non-sulphur bacteria or *Chloroflexaceae*. The *Chlorobiaceae* are strict anaerobes and utilise sulphide or thiosulphide as an electron source. The *Chloroflexaceae* are facultative anaerobes and utilise reduced carbon compounds as electron donors.
2. Purple sulphur bacteria or *Chromatiaceae*, which can use H<sub>2</sub>S as a photosynthetic electron donor.

3. Purple non-sulphur bacteria or *Rhodospirillaceae*, which are unable to utilise H<sub>2</sub>S, and require simple organic compounds as electron donors. *Rhodobacter sphaeroides* is included in this group.
4. Cyanobacteria, which are oxygenic phototrophs and include the species *Synechocystis*, *Cyanothece* and *Synechococcus*.

The metabolic differences between the groups has resulted in the colonisation of different habitats, consequently the photosynthetic apparatus of each organism have evolved to absorb different wavelengths of light (Figure 1.1).

### 1.2.1 *Rhodobacter sphaeroides*

The purple non-sulphur bacterium *Rba. sphaeroides* belongs to the phylum *Rhodospirillaceae*, which includes other species such as *Rhodobacter capsulatus* and *Rhodospirillum rubrum*. These organisms are metabolically diverse, possessing an extensive range of energy acquiring mechanisms. Their preferred mode of growth is photoheterotrophy, utilising various simple organic substrates, under anaerobic conditions in the light, typically in non-stratified deep lakes or the sediment of shallow lakes (Pfennig, 1978; Madigan, 1988; Drews and Imhoff, 1991). *Rhodospirillaceae* are also capable of photoautotrophic growth, using either molecular hydrogen or sulphide as the reductant and carbon dioxide as the sole carbon source. In addition most can also grow as chemoheterotrophs under microaerobic to aerobic conditions in the dark, and a few are capable of chemolithotrophy (Madigan and Gest, 1979; Drews and Imhoff, 1991). *Rba. sphaeroides* has the unique ability to detoxify a number of rare metal oxides and is the subject of ongoing studies in bioremediation (Kobayashi, 1995; O’Gara *et al.*, 1997). It is also known to utilise the regulatory systems involved in quorum sensing (Puskas *et al.*, 1997). Other studies have revealed the methods of motility and environmental sensing in relation to bacterial taxis and movement in *Rba. sphaeroides* are unique both genetically and physiologically (Hamblin *et al.*, 1997). It possesses a relatively small genome and facile methodologies for genetic

**A**

Photosynthetic Bacteria				
Purple		Green		Cyanobacteria
Non-sulphur	Sulphur	Non-sulphur	Sulphur	
<i>Rhodospirillum</i> <i>Rhodopseudomonas</i> <i>Rhodobacter</i> <i>Rhodocyclus</i> <i>Rhodomicrobium</i> <i>Heliobacterium</i>	<i>Thiospirillum</i> <i>Chromatium</i> <i>Thiocapsa</i> <i>Amoebacter</i> <i>Thiopedia</i> <i>Ectothiorhodospira</i>	<i>Chloroflexus</i>	<i>Chlorobium</i> <i>Prosthecochloris</i> <i>Pelodictyon</i> "Chlorochromatium" "Pelochromatium"	<i>Synechocystis</i> <i>Synechococcus</i> <i>Cyanothece</i> <i>Phormidium</i> <i>Plectonema</i>

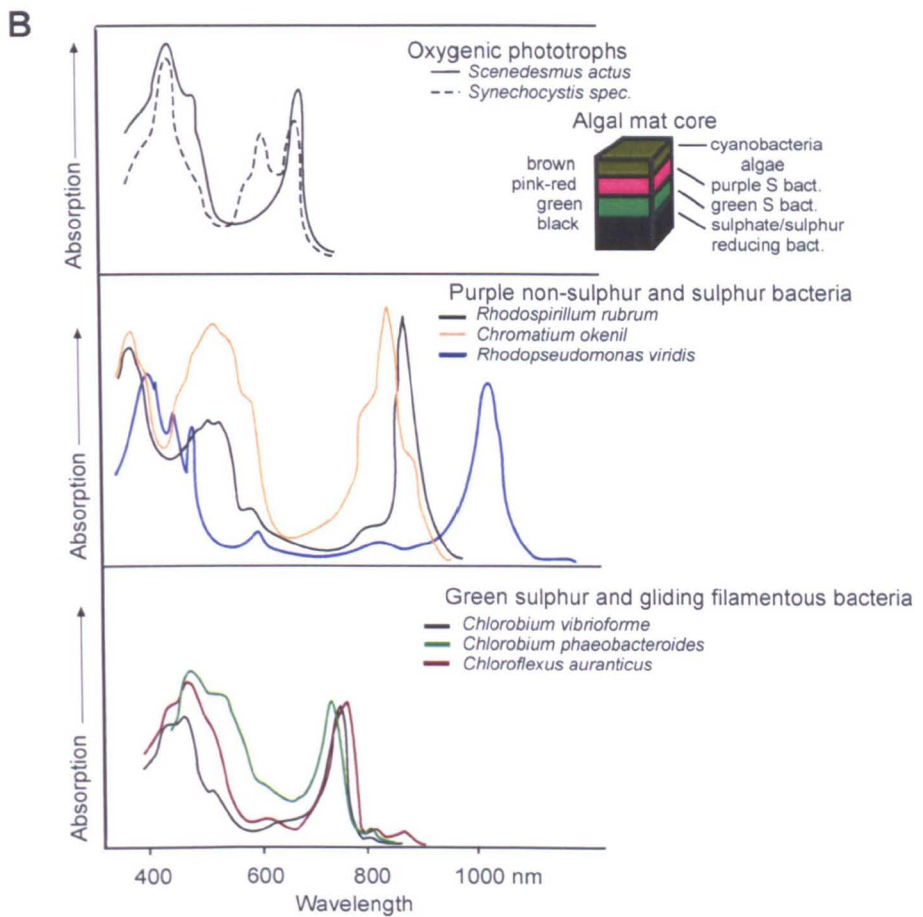


**Figure 1.1 Taxonomy and absorption spectra of photosynthetic organisms**

**A** - Taxonomy and absorption of photosynthetic bacteria.

**B** - Absorption spectra of living photosynthetic organisms.

manipulations, gene transfers, genetic analysis and chromosomal mobilisation. The simple genomes of such bacteria, and in particular *Rba. sphaeroides*, and their facultative photosynthetic nature, permit the study of mutants deficient in essential components of the photosynthetic apparatus. This has aided the identification of genes encoding the reaction centre (RC) and light harvesting polypeptides, as well as those responsible for pigment biosynthesis.

## 1.3 Pigment Biosynthesis

### 1.3.1 Bacteriochlorophyll biosynthesis

Bacteriochlorophylls (BChl) are the central photopigments of photosynthetic bacteria. These tetrapyrrole compounds absorb NIR light and funnel this energy to the RC pigments, where it is converted to a charge separation. The incorporation of a metal ion by tetrapyrroles can modify their electronic and redox properties, resulting in a wide variety of metal-containing enzymes and cofactors from a common biosynthetic precursor (Rüdiger and Schoch, 1988). In addition, slight variations of the common porphyrin ring structure results in the eight different forms of BChl, designated BChl*a-g* (Scheer, 1991).

BChl*a* is widely distributed throughout anoxygenic photosynthetic organisms and is the principal photosynthetic pigment of *Rba. sphaeroides*. This BChl is esterified with the C<sub>20</sub> isoprenoid alcohol, phytol. This phytol moiety constitutes 30 % of the total molecular weight of the molecule, and greatly influences the properties of BChl*a*, including investing it with much of its hydrophobicity. Attachment of the phytol appears to be crucial for both stability and function of the bacterial photosynthetic pigment-protein complexes and is vital for their assembly, (Bollivar *et al.*, 1994a; Addelee and Hunter, 1999). Crystallography studies of LH2 from *Rps. acidophila* revealed that the phytol chains of the BChl(s) intertwined with the carotenoid molecules within the LH2 complex (McDermott *et al.*, 1995; Freer *et al.*, 1996).

All tetrapyrroles are built in a complex sequence of reactions from small biosynthetic precursors. The first intermediate, which is common to all tetrapyrrole formation, is 5'-amino levulinic acid (ALA), which can be formed either from glycine and succinyl coenzyme A via the Shemin pathway (Shemin, 1956), or by the C<sub>5</sub> pathway of glutamate conversion (Beale and Castelfranco, 1974). The C<sub>5</sub> pathway occurs in higher plants, algae and cyanobacteria, plus some photosynthetic and non-photosynthetic bacteria (reviewed by Kannangara *et al.*, 1988). The Shemin pathway occurs in animals, yeast, fungi and some bacteria. The formation of *Rba. sphaeroides* BChl<sub>a</sub> via the Shemin pathway was confirmed by <sup>13</sup>C NMR studies (Oh-Hama *et al.*, 1985). These reactions are catalysed by HemA and HemB ALA synthetase enzymes. (Tai *et al.*, 1988). HemA catalyses the formation of ALA by condensation of succinyl-CoA and glycine, while HemB catalyses the condensation of two molecules of ALA to form porphobilinogen (PBG), the first pyrrole compound in the pathway. The subsequent action of the *hemC-hemG* encoded enzymes leads to the formation of protoporphyrin IX, an aromatic compound with the capacity to chelate a wide variety of metal ions, including magnesium ions which commits it to the chlorophyll biosynthesis pathway and directs the tetrapyrrole ring away from the production of haem by ferrochelatase (reviewed by Willows, 2003).

Figures 1.2a and 1.2b represent the current scheme of the pathway from protoporphyrin IX to BChl<sub>a</sub>. In *Rba. sphaeroides* there are eleven steps in BChl biosynthesis following the chelation of protoporphyrin IX with magnesium; these include a series of hydration, reduction and oxidation reactions. Most of the loci encoding the enzymes catalysing these steps have now been identified and sequenced (Naylor *et al.*, 1999). They have all been found to lie within the 45.7 kb photosynthesis gene cluster, which also contains genes encoding subunits of the reaction centre (RC), the light-harvesting (LH) 1 complex, and enzymes for carotenoid biosynthesis (Figure 1.12).

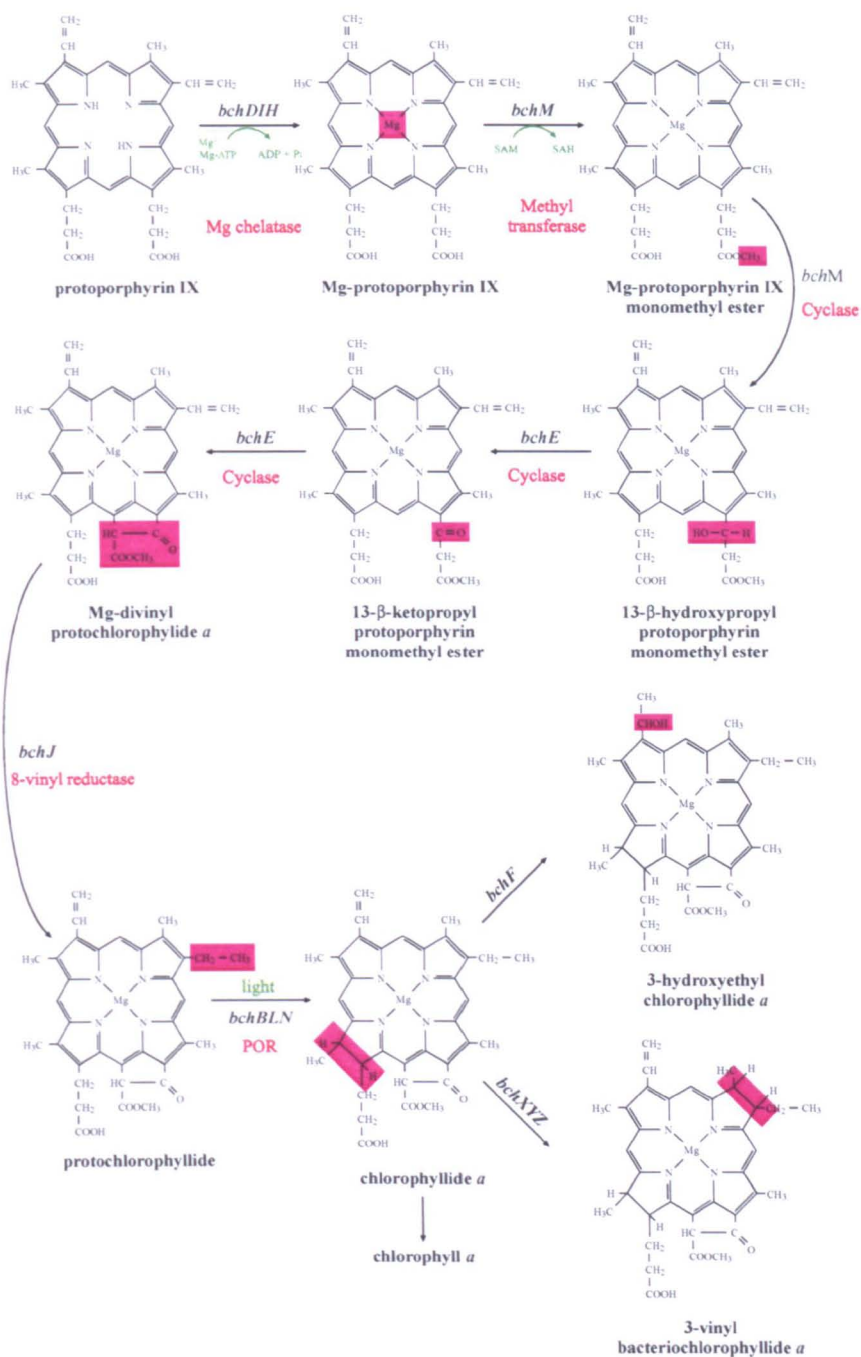


**Figure 1.2(a) The bacteriochlorophyll biosynthetic pathway**

The bacteriochlorophyll biosynthetic pathway from magnesium insertion up to the interchangeable steps catalysed by the *bchF* and *bchXYZ* gene products.

The gene assigned to each step is in italics and where possible the name of the gene product is given in red. Groups modified at each step are coloured magenta. The acrylate intermediate of isocyclic ring formation is not shown. The steps up to chlorophyllide are shared by the chlorophyll biosynthetic pathway; esterification of chlorophyllide leads to chlorophyll (adapted from Bollivar *et al.*, 1994b).

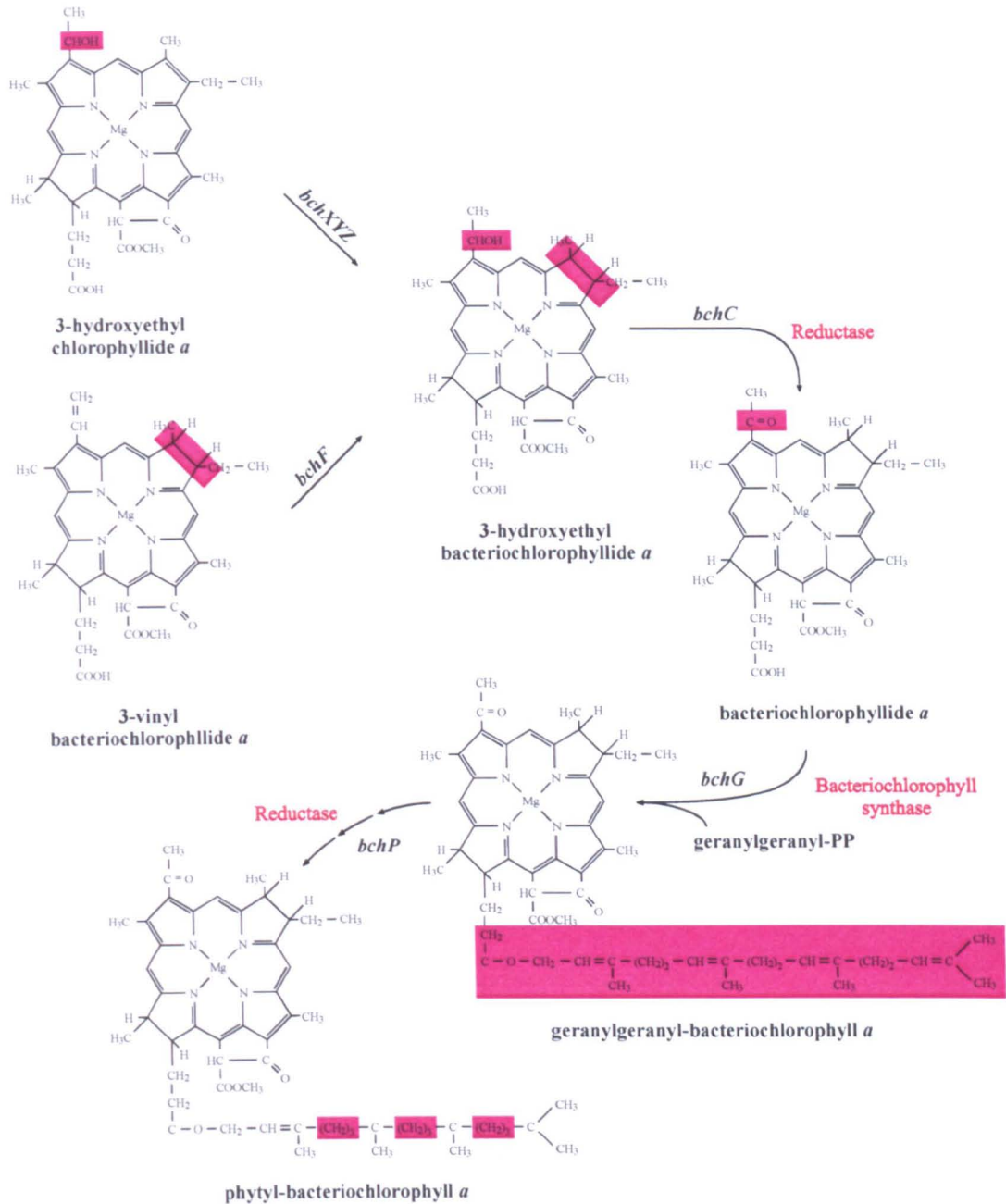


**Figure 1.2(b) The bacteriochlorophyll biosynthetic pathway**

The bacteriochlorophyll biosynthetic pathway from the interchangeable pathway catalysed by the *bchF* and *bchXYZ* gene products up to the formation of bacteriochlorophyll (adapted from Bollivar *et al.*, 1994b).

Analysis of mutants of the BChl biosynthesis pathway has enabled the identification of, and assignment of function, to many of the BChla biosynthetic enzymes of both *Rba. sphaeroides* and *Rba. capsulatus* (Coomber *et al.*, 1990; Taylor *et al.*, 1983; Biel and Marrs, 1983; Zsebo and Hearst, 1984; Addlesee and Hunter, 1999; Smith *et al.*, 1996; Suzuki and Bauer, 1995). In addition, *in vitro* assays have proved invaluable in the elucidation of the genetics and enzymology of several steps in the BChl biosynthesis pathway. These assays involve the heterologous overexpression of the genes in *E. coli* and have been used to study, for example, the methyltransferase step of the pathway (Gibson and Hunter, 1994; Bollivar *et al.*, 1994b), the reconstitution of *Rba. sphaeroides* magnesium-protoporphyrin chelatase activity *in vitro*, which requires the products of the *bchH*, *bchI* and *bchD* genes (Gibson *et al.*, 1995; Jensen *et al.*, 1998; Gibson *et al.*, 1999). Also the *in vitro* esterification reactions of bacteriochlorophyllide *a* with geranylgeranyl-PP (Oster *et al.*, 1997), and the hydrogenation reaction which generates phytyl-BChla (BChlaP) in *Rba. capsulatus* (Oster *et al.*, 1997) and *Rba. sphaeroides* (Addlesee and Hunter, 1999).

### 1.3.2 Carotenoid Biosynthesis

Carotenoids comprise a widely distributed class of structurally and functionally diverse natural pigments. These pigments are chemically classed as terpenoids, unsaturated hydrocarbons, derived from the general isoprenoid biosynthesis pathway, and typically consisting of eight linked isoprenoid units. Carotenoids are found in abundance in photosynthetic organisms and have two major functions in photosynthesis. First, as accessory light-harvesting pigments, they absorb light energy in the 450-600 nm range, and transfer it to neighbouring BChl molecules, thereby increasing the spectral range over which light energy can be absorbed beyond the limitations of BChl absorption. Second, as photoprotective agents, carotenoids play a vital role in preventing photooxidative damage (Figure 1.3) (Cogdell and Frank, 1987; Siefertmann-Harms, 1987; Cogdell *et al.*, 2000). The presence of excess light can lead to the generation of triplet excited BChl molecules (Figure 1.3b), which in turn can form highly reactive singlet oxygen, which is toxic to the cell (Figure 1.3c). Carotenoids can prevent the

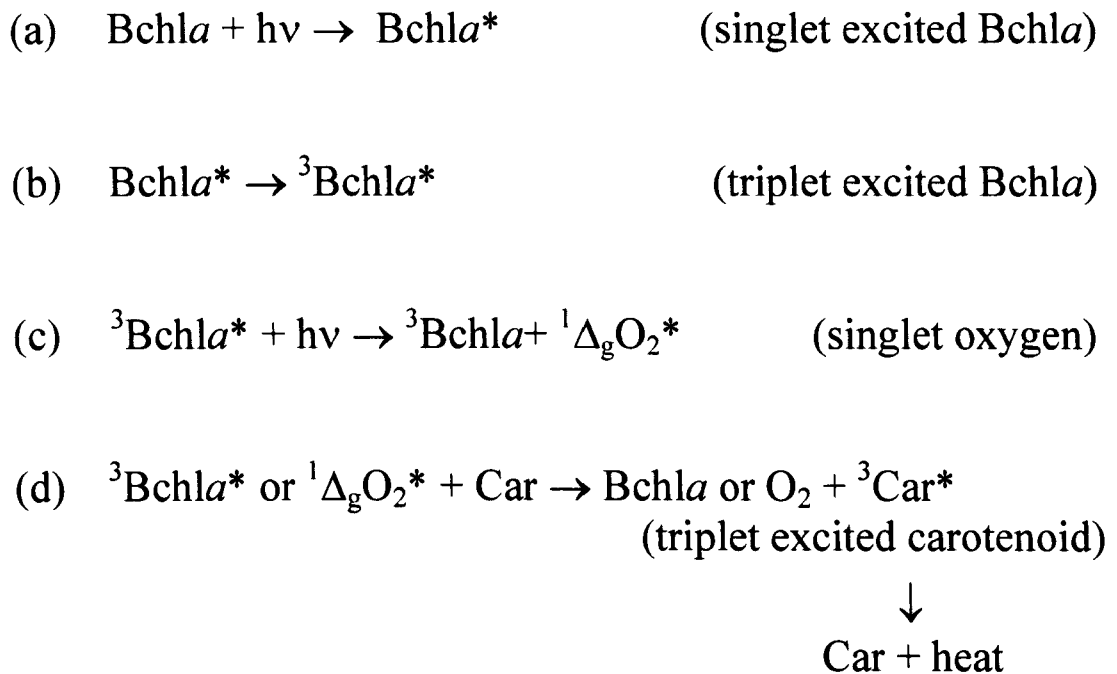


### Figure 1.3 The role of carotenoids in photoprotection

- (a) / (b) An excess of light can induce the formation of triplet excited Bchl molecules.
- (c) These triplet excited species can result in the formation of singlet oxygen, which is toxic to the cell.
- (d) Close contact of either  ${}^3\text{Bchl}^*$  or  ${}^1\Delta_g\text{O}_2^*$  with carotenoid molecules will result in this harmful species being quenched. Excited carotenoid molecules will dissipate energy in the form of heat to return to the ground state.

(Adapted from Cogdell *et al.*, 2000)

harmful effects of singlet oxygen in two ways: first, they can quench singlet oxygen directly (Foote and Denny, 1968), or they quench the triplet excited BChl ( $^3\text{BChl}a^*$ ) sensitiser, preventing the production of singlet oxygen (Borland *et al.*, 1988). *In vivo*, the major protective effect is the rapid quenching of  $^3\text{BChl}a^*$  so that no detectable singlet oxygen is produced (Cogdell and Frank, 1987). The energy transferred to the carotenoid molecules is then dissipated in the form of heat, and the carotenoid returns to the ground state (Figure 1.3d) (Frank and Cogdell, 1996). In addition, carotenoids dissipate excess radiant energy and help to preserve the structural integrity of the pigment-protein complexes with which they are non-covalently associated (reviewed by Armstrong, 1994).

Under normal conditions of anaerobic growth *Rba. sphaeroides* accumulates mainly spheroidene that confers a yellow-brown colour to the cells. In the presence of oxygen the cells produce the red pigments spheroidenone and hydroxyspheroidenone (Schmidt, 1978). In *Rba. sphaeroides*, as in the closely related bacterium *Rba. capsulatus*, the carotenoid (*crt*) genes, encoding the carotenoid biosynthesis enzymes, are clustered. The *crt* genes were mapped to a region of the *Rba. sphaeroides* 45.7 kb photosynthetic gene cluster by Tn5 mutagenesis (Coomber *et al.*, 1990) (Figure 1.12), and found to be flanked by the bacteriochlorophyll biosynthesis genes. The sequence of the *crt* gene cluster has been determined, and the functions of each gene product analysed by detailed examination of the carotenoids accumulated by Tn5 mutants (Lang *et al.*, 1995). The *Rba. sphaeroides* carotenoid biosynthesis pathway is shown in Figure 1.4.

Using insertional mutagenesis of *crt* genes in *Rba. capsulatus* the end products of the native carotenoid biosynthetic pathway have been altered from the normal spheroidene and spheroidenone. Mutations in *crtI*, *-C*, and *-D* led to the accumulation of phytoene, neurosporene and neurosporene derivatives respectively (Guiliano *et al.*, 1988). The availability of cloned genes encoding the biosynthesis of carotenoids not found in *Rhodobacter* species led to the possibility of introducing a wider range of foreign carotenoids into the bacterial photosynthetic apparatus than would normally be

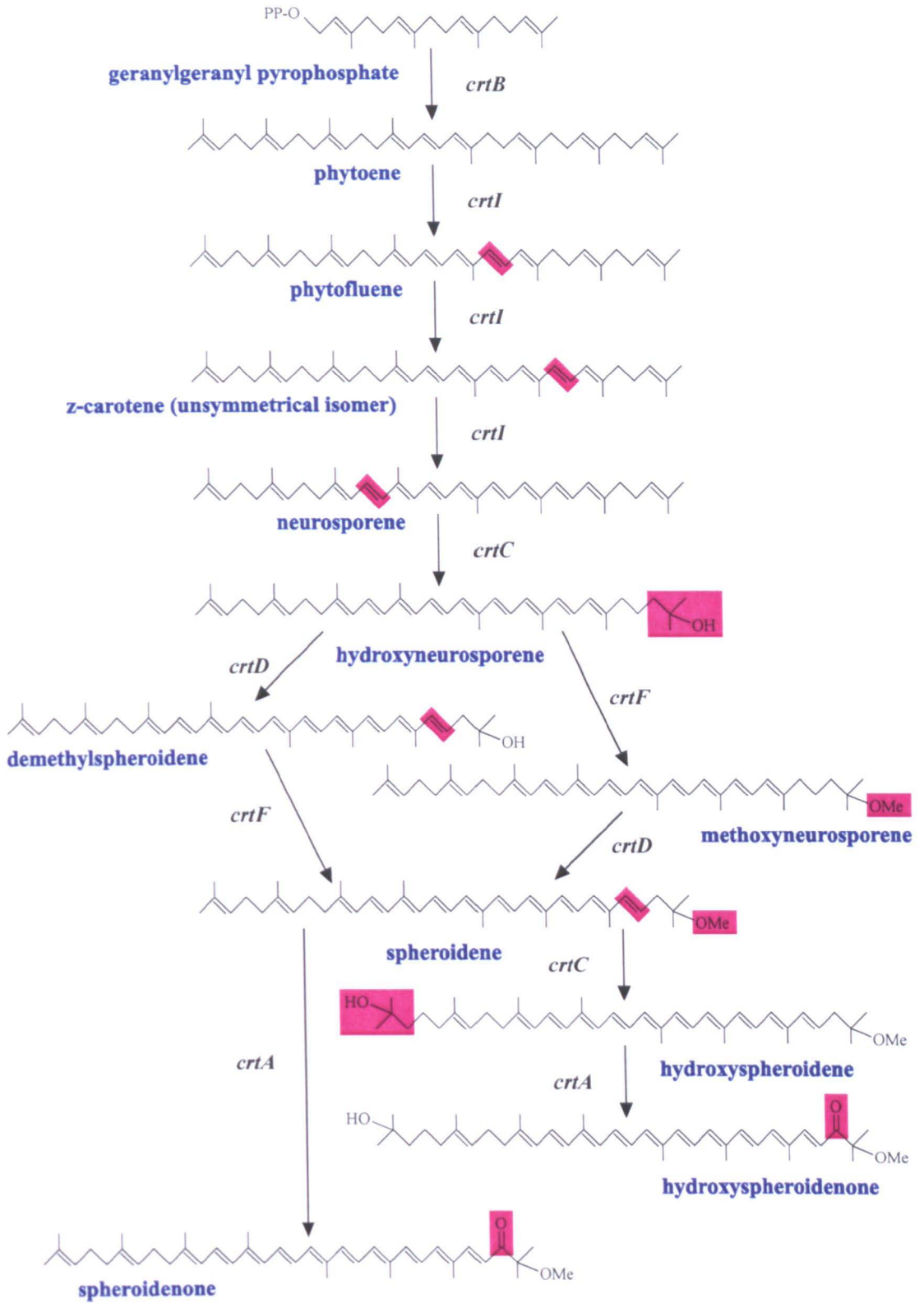


**Figure 1.4 The carotenoid biosynthetic pathway**

The pathway of carotenoid biosynthesis from geranylgeranyl pyrophosphate in *Rba. sphaeroides* is shown. The gene assigned to each enzymatic step is indicated and the groups modified in each step are coloured magenta (adapted from Garcia-Asua *et al.*, 2002).

available through standard mutagenesis of the native biosynthetic pathway. For example, part of the *Erwinia herbicola crt* cluster was expressed in various *crt* strains of *Rba. sphaeroides*. This led to the production of functioning light-harvesting complexes with a novel carotenoid composition, which included  $\beta$ -carotene and zeaxanthin (Hunter *et al.*, 1994). This experiment is of interest as it allows the convenient production of carotenoids, normally found in higher-plant photosynthesis, from a bacterial source.

The production of foreign carotenoids in *Rba. sphaeroides* was investigated further by the production of lycopene using an enzyme from *Er. herbicola* cloned into *Rba. sphaeroides* (Garcia-Asua *et al.*, 2002; Billsten *et al.*, 2002). The native 3-step phytoene desaturase (CrtI) from *Rba. sphaeroides*, which results in the production of neurosporene, was replaced with the 4-step phytoene desaturase enzyme from *Er. herbicola*, which results in the production of lycopene; this carotenoid contains two additional conjugated double bonds compared to neurosporene. When the cloned 4-step enzyme was introduced into a *crtIC* double mutant of *Rba. sphaeroides* lycopene accumulated in the cell and accounted for 93 % of the total carotenoid produced. Spectroscopic studies showed that the foreign carotenoid assembled into light-harvesting complexes and that it could transfer absorbed light energy to the BChl(s) at 54 % efficiency (Garcia-Asua *et al.*, 2002).

Carotenoid pigment accumulation in the *Rhodobacter* species clearly responds to environmental stimuli, particularly oxygen tension and light intensity (Cohen-Bazire *et al.*, 1957; Schumacher and Drews, 1978; Biel and Marrs, 1983; Armstrong *et al.*, 1993), and correlates with the presence and extent of the photosynthetic membrane. In particular, carotenoids are essential structural components of the LH2 complex (Lang and Hunter, 1994)

## 1.4 The light harvesting complexes of *Rba. sphaeroides*

The photosynthetic membrane of *Rba. sphaeroides* contains the BChl and carotenoid pigment molecules, which are non-covalently bound to proteins to form well organised pigment-protein complexes. *Rba. sphaeroides* contains three such complexes, the reaction centre (RC) and the light harvesting (LH) antenna complexes LH1 and LH2. The antenna complexes capture light energy and funnel excitation energy towards the RC. These complexes form the photosynthetic unit and are localised within the highly invaginated intracytoplasmic membrane (ICM). LH2 is present in variable amounts, depending upon incident light intensity. LH1 encircles RC in a fixed 1:1 stoichiometry (Aagaard and Sistrom., 1972), coming together to form dimeric core complexes in association with a third protein PufX (Aagaard and Sistrom., 1972) (Seibert *et al.*, 2004). In *Rba. sphaeroides* the LH complexes are sometimes referred to by their *in vivo* absorption maxima, B875 (LH1) and B800-850 (LH2). The composition of LH complexes in other photosynthetic bacteria differs somewhat. *Rs. rubrum* and *Rps. viridis* possess a single core antenna complex (Hawthorn and Cogdell, 1991; Zuber and Brunisholz, 1991). In contrast, *Rps. acidophila* contains a third light harvesting complex, LH3, which has a distinctive absorbance spectrum with peaks at 800 nm and 820 nm (Mccluskey *et al.*, 2001).

To date, all antenna complexes from purple bacteria comprise of two hydrophobic, membrane spanning polypeptides, between 50-60 amino acids in length. These helices are known as  $\alpha$  and  $\beta$  and exist in a 1:1 ratio, coming together to form a heterodimer (Brunisholz and Zuber, 1992). The heterodimer pairs are responsible for the orientation and local environment of the light harvesting pigments (BChl and carotenoids) within the complex. There is a high degree of homology between the  $\alpha$  and  $\beta$  polypeptides of LH1 and LH2, however there is little homology between the  $\alpha$  and  $\beta$  polypeptides themselves. An extensive analysis of the primary structure of light harvesting polypeptides from purple bacteria has allowed sequence homologies between species to be identified (Brunisholz and Zuber, 1992). A key discovery of

this work was the identification of a conserved histidine residue (His<sub>0</sub>), present in both  $\alpha$ - and  $\beta$ -polypeptides, which has been shown to form a ligand to the central magnesium ion of the BChl molecule (Robert and Lutz, 1985; McDermott *et al.*, 1995; Olsen *et al.*, 1997). The main absorbance peaks of the photosynthetic apparatus are due to the light harvesting pigments complexed with the LH antenna. Free BChl has absorbance maxima of 770 nm. It was suggested the red shift in absorbance was due to the local chemical environment (Zuber, 1985). For example, the H bonding of closely associated tryptophan and tyrosine residues 'tune' the BChl(s) (Fowler *et al.*, 1992; Fowler *et al.*, 1994; Sturgis *et al.*, 1997) In the case of *Rba. sphaeroides* the red shift extends to 800 nm and 850 nm for LH2 and 875nm for LH1.

#### 1.4.1 The peripheral light harvesting complex LH2

As already stated above the LH2 complex has two absorbance maxima, arising from BChl(s) that absorb maximally at 800 nm and 850 nm; therefore they are known as B800 and B850 respectively (Cogdell *et al.*, 1985). Each  $\alpha\beta$ -heterodimer in LH2 is non-covalently associated with three molecules of BChl, two of which absorb at 850 nm and a third at 800 nm (Clayton and Clayton, 1972).

##### 1.4.1.2 The structure of LH2

The structures of LH2 from *Rps. acidophila* and *Rhodovulum sulfidophilum* were determined by X-ray crystallography (McDermott *et al.*, 1995) and electron microscopy (Savage *et al.*, 1996) to be nonamers of  $\alpha\beta$ -heterodimers. Electron microscopy data demonstrate that LH2 from *Rba. sphaeroides* is also a nonamer (Walz *et al.*, 1998). The resolution obtained by X-ray crystallography for *Rps. acidophila* was 2.5 Å; this enabled detailed examination of the relationship between the structural information and the function of the complex for the first time. Now a more refined structure is available of *Rps. acidophila* LH2 at 2.0 Å (Papiz *et al.*, 2003). The atomic resolution images show that the *Rps. acidophila* LH2 complex consists of a ring of nine  $\alpha\beta$ -heterodimers, forming a hollow cylinder spanning the membrane (Figure 1.5).

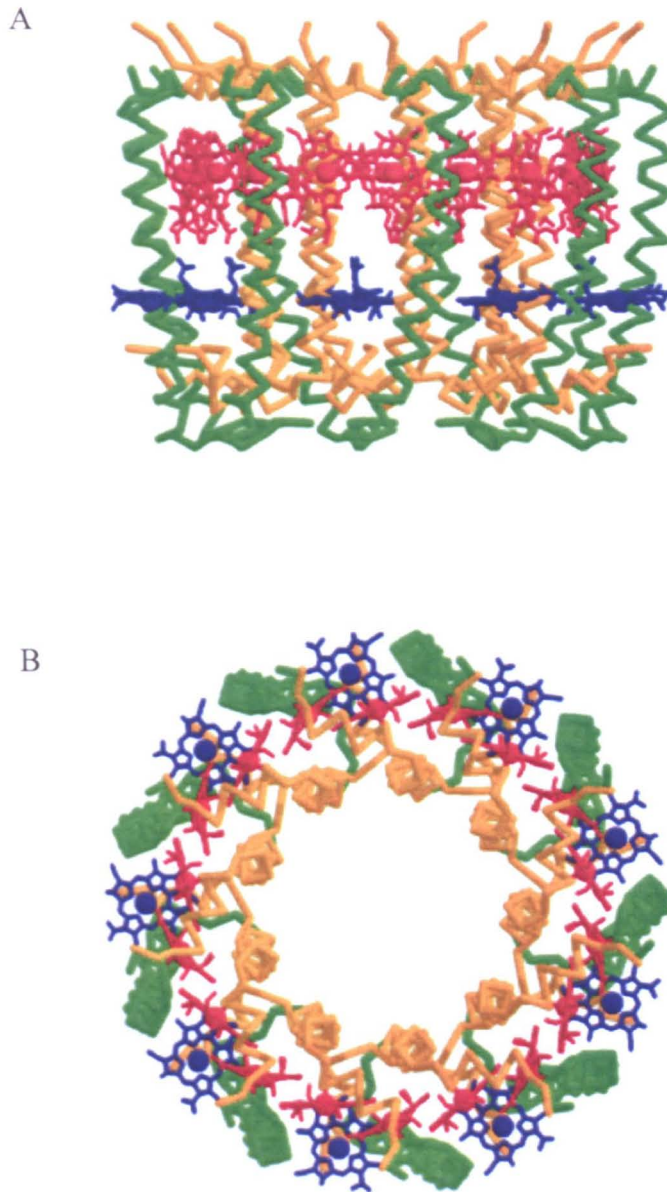


**Figure 1.5** The structure of the *Rps. acidophila* LH2 complex

**A** – shows a side-view of the complex, the concentric rings of polypeptides and BChl(s) can be seen. The  $\alpha$ -polypeptides (brown),  $\beta$ -polypeptides (green), B800 (blue) and B850 (red) BChl(s) are shown (McDermott *et al.*, 1995).

**B** – shows the projection view of the same structure. From this angle the circular shape of the complex is very apparent.

This ring consists of an inner ring of nine  $\alpha$ -polypeptides and an outer ring of nine  $\beta$ -polypeptides. The BChl molecules also form two rings, which are sandwiched between the  $\alpha$ - and  $\beta$ -polypeptides. The B850 BChl(s) form an eighteen-member ring of overlapping molecules coordinated to alternate  $\alpha$ - and  $\beta$ -polypeptides by a histidine ligand. These BChl(s) are positioned vertically with respect to the membrane plane and are situated toward the periplasmic face of the membrane. In contrast, the nine-member ring of B800 BChl(s) are relatively well separated, and positioned between the helices of the  $\beta$ -polypeptides in the outer ring. They lie toward the cytoplasmic face of the membrane and are almost parallel to it. The phytol chains of the  $\beta$  B850 and B800 pigments are intertwined within the structure. The nine membrane-spanning carotenoids are not associated with the polypeptides but are in close contact with both the B800 and B850 BChl(s) (Freer *et al.*, 1996). A second ring of carotenoids is present, the heads of which are located below the B850 BChl(s), however this ring was originally only partially resolved (McDermott *et al.*, 1995; Prince *et al.*, 1997). The refined 2.0 Å structure of LH2 (Papiz *et al.*, 2003) proposed a second rhodopin-glucoside carotenoid molecule, which lies on the outside of the complex between the  $\beta$ -polypeptides. New structural information was revealed at the N- and C-termini of the  $\alpha$ -peptide as a result of the improved resolution of the LH2 structure. At the N-terminus formyl- $\alpha$ -Met1 was originally postulated with the formyl oxygen atom ligating  $Mg^{2+}$  of the B800 BChl. From the high resolution structure the formyl group was refined from an acetyl to a carboxyl group; the surrounding residues donate several H-bonds to the oxygen atom of the COO- $\alpha$ Met1. It was suggested by Papiz *et al* that the presence of the COO- $\alpha$ Met1 may be a determining factor in the formation of LH2 rather than LH1. At the C-terminus of the  $\alpha$ -polypeptide the 2.5 Å structure terminates at  $\alpha$ -Gly48, but at a higher resolution the remaining five residues could be identified. Cherezov *et al.*, (2006) resolved the structure at 2.45 Å using swollen lipidic mesophases. It was possible to assign the region of density previously attributed to the RG2 molecule, as molecules of the detergents LDAO and  $\beta$ -DDM, which were used in the purification of the complex.

A similar cylindrical arrangement is seen for the crystal structure of LH2 from *Rs. molischianum* (Koepeke *et al.*, 1996), however the ring consists of eight  $\alpha\beta$ - heterodimers, with a sixteen-member ring of B850 BChl(s) and an eight-member ring of B800 BChl(s). The evidence suggests that LH complexes from different purple bacteria assume various ring sizes; however, the factors that control the oligomerisation state of these complexes are at present unknown.

Atomic force microscopy (AFM) has developed into a powerful tool to investigate membrane protein surfaces in a close-to-native environment. It allows information to be acquired at submolecular resolution on the membrane protruding structures of single proteins (Engel *et al.*, 1999; Engel and Muller, 2000; Scheuring *et al.*, 2001). AFM was used to report on the surface topography of *Rba. sphaeroides* LH2, reconstituted into 2D crystals (Scheuring *et al.*, 2003), which confirmed the electron microscopy data of Walz *et al.* (1998). The ring structure and organisation of LH2 from *Rps. acidophila* has also been analysed using AFM (Stamouli *et al.*, 2003).

#### 1.4.1.3 The B800 BChl(s) in LH2

The nine B800 BChl molecules in *Rps. acidophila* are well separated, with the planes of the bacteriochlorin rings parallel to the cytoplasmic membrane surface. The B800 molecules are sandwiched between the  $\beta$ -apoproteins, with the  $\beta$ Arg<sub>-10</sub> residue integral to their binding within the complex (Fowler *et al.*, 1997; Gall *et al.*, 1997). Site directed mutagenesis of  $\beta$ Arg<sub>-10</sub> has shown H-bonding provided by this residue, as well as the local electrostatic properties of the B800 binding site, to be responsible for the tuning of the B800 molecules. Fowler *et al.* (1997) replaced  $\beta$ Arg<sub>-10</sub> with a range of residues including Asn, Leu, His and Lys, each of which produced a blue shifted B800 peak, the most significant of which was the  $\beta$ Asn<sub>-10</sub> mutant, producing a B800 peak at 787 nm. Only the  $\beta$ Met<sub>-10</sub> mutant was seen to display no significant blue shift in absorbance, which is surprising due to its likely inability to form a hydrogen bond with the 2-acetyl carbonyl side group of the B800. The efficiency of internal energy

transfer within the LH2 molecule was not significantly impacted by the mutations, nor was the carotenoid to BChl transfer efficiency. However the decreased overlap between B800 and B850 peaks lead to a decrease in the rate of energy transfer. Shifts in the excitation spectra of the carotenoids were also observed.

#### 1.4.1.4 The B850 BChl(s) in LH2

The 18 B850 BChl(s) in LH2 are liganded to the conserved histidine residues on the  $\alpha$ - and  $\beta$ -polypeptides. An overlapping ring is formed, positioned vertically with respect to the membrane plane and situated toward the periplasmic face of the membrane. The B850 ring is responsible for accepting excitonic energy from the B800 BChl(s) and the complexed carotenoids, then transferring it to the B875 BChl(s) bound within an adjacent LH1 complex. The red shifted  $Q_y$  absorbance band of the B850 BChl is seen to be modulated by a Tyr-Tyr motif present on the  $\alpha$ -polypeptide (Tyr<sub>44</sub>-Tyr<sub>45</sub>) (Fowler *et al.*, 1992). Site directed mutagenesis studies by Fowler *et al.*, showed a progressive blue shift in the B850 BChl(s) when the absorbance spectra of the single mutant  $\alpha$ Tyr<sub>44</sub>→Phe (839 nm) and double mutant  $\alpha$ Tyr<sub>44-45</sub> →  $\alpha$ Phe<sub>44</sub>-Leu<sub>45</sub> (826 nm) were recorded at 77 K. These altered absorbance properties correlated with perturbed hydrogen bonding patterns when examined by resonance Raman spectroscopy (Fowler *et al.*, 1994). The Tyr<sub>44</sub>→Phe mutation results in the breakage of a hydrogen bond with the 2 acetyl carbonyl of the B850 BChl. The altered Raman signal resulting from the Tyr<sub>45</sub>→Leu mutation, may indicate the abolition of a hydrogen bond formed with the 2-acetyl carbonyl group of the BChl, or a perturbation of the H-bond pattern of the complex; in turn causing a change in the ability of other residues to form hydrogen bonds with the B850 BChl. The 3D structure of the B800-820 LH3 complex from *Rps. acidophila* showed that the 850 nm →820 nm shift in absorbance is associated with an out of plane distortion of the C2-acetyl carbonyl group, which could also contribute to the loss of Raman signal (Mccluskey *et al.*, 2001)

The carotenoid content of the LH2 complex in *Rba. sphaeroides* can also have a significant effect upon hydrogen bonding at the binding site of the B850 BChl(s).

Fourier Transform (FT) Raman spectroscopy has shown the strength of the hydrogen bond between the  $\alpha$ Tyr<sub>45</sub> residue and the B850 BChl is intrinsically linked to the chemical nature of the bound carotenoid (Gall *et al.*, 2003). These observations also have significance when evaluating the structural implications of carotenoid binding in *Rba. sphaeroides* LH2.

#### 1.4.1.5 The carotenoids of LH2

As previously discussed, the carotenoids complexed with antenna proteins in photosynthetic bacteria function as accessory light-harvesting pigments, as well as contributing to complex structure and reducing photo-oxidative stress (Cogdell and Frank, 1987; Siefermann-Harms, 1987; Cogdell *et al.*, 2000). Carotenoid biosynthesis is essential for the assembly of LH2 in *Rba. sphaeroides* (Lang and Hunter, 1994). Under normal conditions of anaerobic growth, *Rba. sphaeroides* LH2 accumulates mainly spheroidene, whereas in the presence of oxygen the red pigments spheroidenone and hydroxyspheroidenone are incorporated into the complex (Schmidt, 1978). Mutations in the carotenoid biosynthetic pathway can also lead to the incorporation of phytoene, neurosporene and neurosporene derivatives (Guiliano *et al.*, 1988). Carotenoid insertion in *Rba. sphaeroides* LH2 has a role in the binding of the B850 BChl, and is seen to be different to that seen in the 3D structure of LH2 in *Rps. acidophila* (Gall *et al.*, 2003). Gall *et al.* (2003) observed that the insertion of structurally different carotenoids resulted in no change in the Q<sub>y</sub> absorption of bound chlorophylls. However, insertion of neurosporene into the complex, in place of spheroidene or spheroidenone, evokes a weakening in the bond between  $\alpha$ Tyr<sub>45</sub> and the 2-acetyl carbonyl group of the B850 BChl. Neurosporene differs chemically from spheroidene and spheroidenone at one end of the molecule (by the presence of a CH<sub>3</sub>O group), while being chemically identical at the other end. Local structural changes at the B850 binding site caused by a change in the chemical properties of the bound carotenoid imply the insertion of the chemically different end of the molecule within the vicinity. If this is the case, carotenoid binding differs markedly in *Rba. sphaeroides* and *Rps. acidophila*, since the chemically conserved end of the carotenoid molecule is

inserted within the LH2 complex in *Rps. acidophila*. This shows that the structure and binding site of the carotenoid molecule in LH2 complexes is highly dependent upon species and the chemical nature of the considered molecule. Additionally, a feature of LH2 in *Rba. sphaeroides* as well as many other LH2-containing bacteria is the distinct electrochromic behaviour of some of the associated carotenoid molecules. It was shown that the carotenoids within the chromatophore responsible for the electrochromic signal associate exclusively with LH2 (Holmes *et al.*, 1980; Webster *et al.*, 1980; Crielaard *et al.*, 1992). Site directed mutagenesis of  $\beta\text{His}_{18} \rightarrow \text{Ser}$  abolished B800 binding, but was also seen to abolish the associated carotenoid band shift (Crielaard *et al.*, 1994). The mutant complexes were still able to bind carotenoid molecules and maintain energy transfer to the B850 BChl(s).

#### 1.4.2 The core light harvesting complex LH1

The LH1 core antenna has a single absorbance maximum of 875 nm, imparted by the B875 BChl(s) associated with a heterodimer of  $\alpha$ - and  $\beta$ -polypeptides. The LH1-RC-PufX complex of *Rba. sphaeroides* is seen in the membrane as a dimer (Jungas *et al.*, 1999; Seibert., *et al* 2004; Bahatyrova *et al.*, 2004). The dimeric LH1-RC-PufX core complex has been solved to a resolution of 8.5Å by cryo electron microscopy (Qian *et al.*, 2005). The only other dimeric core complex to date is found in *Rhodobacter blasticus*, with AFM studies being used to directly visualise it *in situ* within the membrane (Scheuring *et al.*, 2005). The study of monomeric LH1-RC core complexes by X-ray crystallography has yielded only one structure, that of the core complex of *Rps. palustris* at 4.8 Å (Figure 1.6) (Roszak *et al.*, 2003). An oval ring of 15  $\alpha\beta$  heterodimers and their associated BChl(s) surrounds the RC. However, closure of the ring is prevented by the presence of a single transmembrane helix that appears out of register with the array of inner LH1  $\alpha$ -apoproteins. This protein has been designated PufW, and forms a break in the ring, located next to the  $Q_B$  binding site of the RC, giving it the putative role of gating  $Q/QH_2$  flow between the RC and the cytochrome *bc<sub>1</sub>* complex.

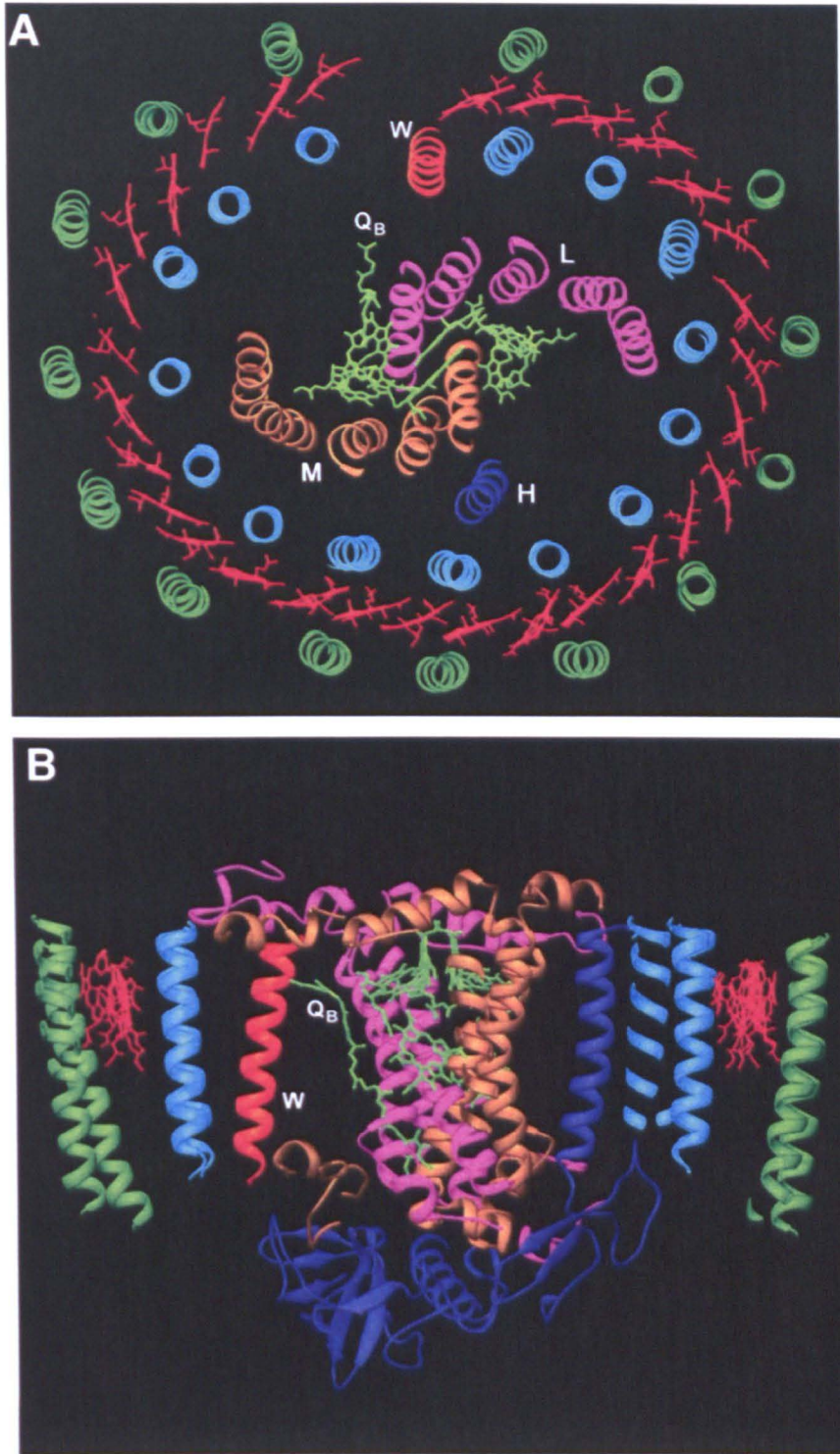


**Figure 1.6** The structure of the *Rps. palustris* LH1-RC-PufW complex

A schematic model of the core complex from *Rps. palustris* is shown (Roszak *et al.*, 2003).

**A.** A view of the complex perpendicular to the membrane.

**B.** The complex is viewed parallel to the membrane plane.  $\alpha$ -apoproteins are shown in cyan,  $\beta$ -apoproteins are shown in green. The reaction centre subunits and PufW are labelled within the model.

The most highly resolved structure of an RC-LH1 complex was reported by Jamieson *et al.*, (2002). Two two-dimensional crystal forms of *R. rubrum* RC-LH1 were analysed by electron cryomicroscopy, and the projection maps produced calculated to 8.5 Å. These maps revealed that in both crystal forms a single RC-LH1 unit is composed of 16  $\alpha\beta$ -heterodimers surrounding a single RC. The major difference between the crystal forms; as seen in the projection maps, is that one ring is circular and the other is ellipsoidal. This indicated that the LH1 ring is not rigid, which may have metabolic significance. Within the two crystal forms the RC adopted preferred orientations, suggesting specific interactions between the RC and LH1 subunits rather than a continuum of possible orientations. Cryo-EM of the LH1 complex from *Rs. rubrum* also suggested that it is organised into cylinders of 16  $\alpha\beta$ -heterodimers in a similar manner to the LH2 complex (Karrasch *et al.*, 1995). It was proposed that the BChl(s) of LH1 (which absorb at 880 nm) are arranged in an overlapping 32-member ring. It was noted that there is probably sufficient space for a single RC complex to reside within the ring of the *Rs. rubrum* LH1 complex (Karrasch *et al.*, 1995). The LH1 complex of *Rba. sphaeroides* has been modeled computationally as a hexadecamer of  $\alpha\beta$ -heterodimers, based on the close homology of the heterodimer of the *Rs. molischanum* LH2 complex (Hu *et al.*, 1998).

The solution structure of the *Rba. sphaeroides* LH1  $\beta$ -polypeptide by NMR (Conroy *et al.*, 2000) revealed a structure comprising two  $\alpha$ -helical regions joined by a more flexible 4 amino acid residue linker. The C-terminal helix forms the membrane-spanning region in the intact LH1 complex, whilst the N-terminus helix lies either in the lipid head groups or in the cytoplasm to form the basis of interaction with the  $\alpha$ -polypeptide. Overall the results proposed a modification of the existing models of the LH1 complex by replacing the continuous helix of the  $\beta$ -polypeptide with two helices, one of which lies at an acute angle to the membrane plane. It is suggested here that one of the key differences between LH1 and LH2 is that the  $\beta$ -subunit is more bent in LH1. This modification puts the N-terminus of LH1 $\beta$  close to the RC H-subunit and provides a rationale for the different ring sizes of LH1 and LH2 complexes.

Previous to Roszak *et al.*, (2003) in the absence of a high resolution atomic structure for LH1, information on the molecular arrangement of the LH1 BChl-binding sites was drawn from the crystal structure of *Rs. molischianum* LH2, which exhibits both sequence and BChl binding site similarities to those usually associated with LH1 (Germeroth *et al.*, 1993) Resonance-Raman spectroscopy has been successfully used in conjunction with site-directed mutagenesis to determine some of the amino acids involved in the BChl binding sites of LH1 (Olsen *et al.*, 1994, 1997; Sturgis *et al.*, 1997).

In the *Rba. sphaeroides* LH1 complex there are two hydrogen bonds, one to the C2-acetyl group, and one to the C9-keto group of each BChl molecule. Olsen *et al.* (1994) showed that the tryptophan residue at  $\alpha_{+11}$  ( $\alpha\text{Trp}_{+11}$ ) of *Rba. sphaeroides* LH1 formed part of the BChl binding pocket, H-bonding to one BChl C2-acetyl group within the basic heterodimeric subunit. Further studies were then conducted replacing this residue,  $\alpha\text{Trp}_{+11}$ , with a histidine residue, and altering the tryptophan residues  $\beta\text{Trp}_{+6}$  and  $\beta\text{Trp}_{+9}$ , conserved in the sequences of many LH1 antenna polypeptides, to each of the three other possible aromatic amino acids, phenylalanine, tyrosine and histidine (Sturgis *et al.*, 1997). The results of this work confirm that one BChl is H-bonded by  $\alpha\text{Trp}_{+11}$ , and provides evidence that the other BChl is H-bonded by  $\beta\text{Trp}_{+9}$ . Substitution of either of these residues by histidine resulted in the assembly of a complex with a slightly red-shifted BChl  $Q_y$  absorption maximum, which is proposed to be due to the strengthening of one of the H-bonds to a C2-acetyl group. In contrast, the effect of substituting either of these residues with tyrosine was determined by geometric constraints, which appear more severe for  $\beta\text{Trp}_{+9}$ ; substitution with phenylalanine resulted in a blue-shifted absorption maximum, due to the loss of one of the C2-acetyl H-bonds. Mutation of the  $\beta\text{Trp}_{+6}$  residue, located away from the pigment-binding site, was shown to cause a loss of binding site integrity and to destabilise the complex (Sturgis *et al.*, 1997).

Site-directed mutagenesis of the conserved His<sub>0</sub> residues of the core and peripheral light-harvesting  $\alpha$ - and  $\beta$ -polypeptides has enabled a model of the B880 binding site in

the LH1 complex of *Rba. sphaeroides* to be proposed (Olsen *et al.*, 1997). Site-directed modification of the  $\alpha$  and  $\beta$  His<sub>0</sub> residues has demonstrated that the B880 BChl binding site shows a high degree of specificity for the residue that provides the ligand to the BChl Mg<sup>2+</sup> ion. Substitution of  $\alpha$ His<sub>0</sub> resulted in no complex formation, while the mutation of  $\beta$ His<sub>0</sub> to Asn and Gln formed LH1 complexes, but in the case of  $\beta$ Gln<sub>0</sub> the complex was very unstable and present only at very low cellular levels. Olsen *et al.* (1997) proposed that the BChl molecules in the LH1 minimal unit are arranged in a head-to-head configuration, similar to that seen in the LH2 structures; but in a conformation that results in the C9-keto-carbonyl of the BChl being liganded to the  $\alpha$ -polypeptide approaching the protonated nitrogen of the His residue on the  $\beta$ -polypeptide, and *vice versa*. Hence, the BChl coordinating His<sub>0</sub> residue of the  $\alpha$  chain, hydrogen bonds to the C9-keto group of the BChl associated to the  $\beta$ -polypeptide, whereas the  $\beta$ His<sub>0</sub> residue hydrogen bonds to the C9-keto group of the  $\alpha$ His<sub>0</sub> coordinated BChl (Figure 1.7).

### 1.4.3 The Reaction Centre

*Rba. sphaeroides* is the only BChla-containing species for which a high-resolution crystal structure of the RC is known (Chang *et al.*, 1986, 1991; Allen *et al.*, 1987a,b; Ermler *et al.*, 1994; McAuley *et al.*, 2000; Katona *et al.*, 2003). The other known bacterial RC structure is from the BChlb-containing species *Rps. viridis* (Deisenhofer *et al.*, 1985; Deisenhofer *et al.*, 1995). The homologous nature of the amino acid sequences of both complexes is reflected in the strong similarity of the structures. However, one major difference is that the RC from *Rps. viridis* is associated with a peripheral, membrane-bound *c*-type cytochrome (cyt) subunit, whereas the *Rba. sphaeroides* RC interacts with a soluble, periplasmic cyt *c*<sub>2</sub>. The RC from *Rba. sphaeroides* contains three protein subunits (Figure 1.8A) known as L (light), M (medium) and H (heavy), named according to their apparent molecular weights determined by their electrophoretic mobility during SDS-PAGE (Clayton and

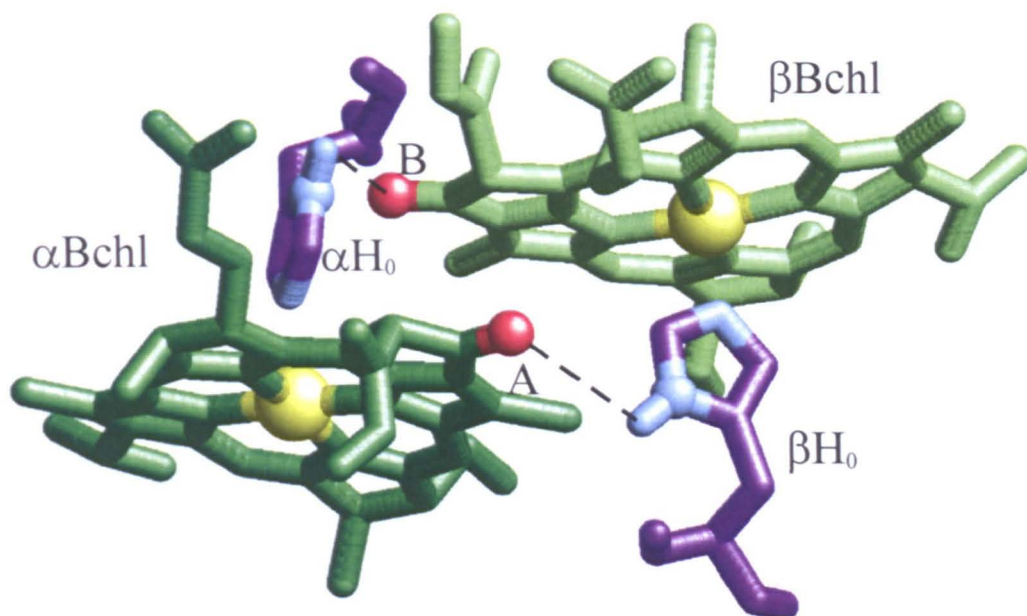


**Figure 1.7 Schematic model of B875 BChl(s) within the LH1 complex**

The His residues and the BChl orientations are based upon the *Rs. molischianum* structure. The proposed H-bonds are represented by the black dashed lines. The His residues belonging to the  $\alpha$ - and  $\beta$ -subunits are indicated on the diagram as  $\alpha\text{His}_0$  and  $\beta\text{His}_0$  respectively. The respective C9-keto carbonyl for each BChl is labelled A or B (Olsen *et al.*, 1997).

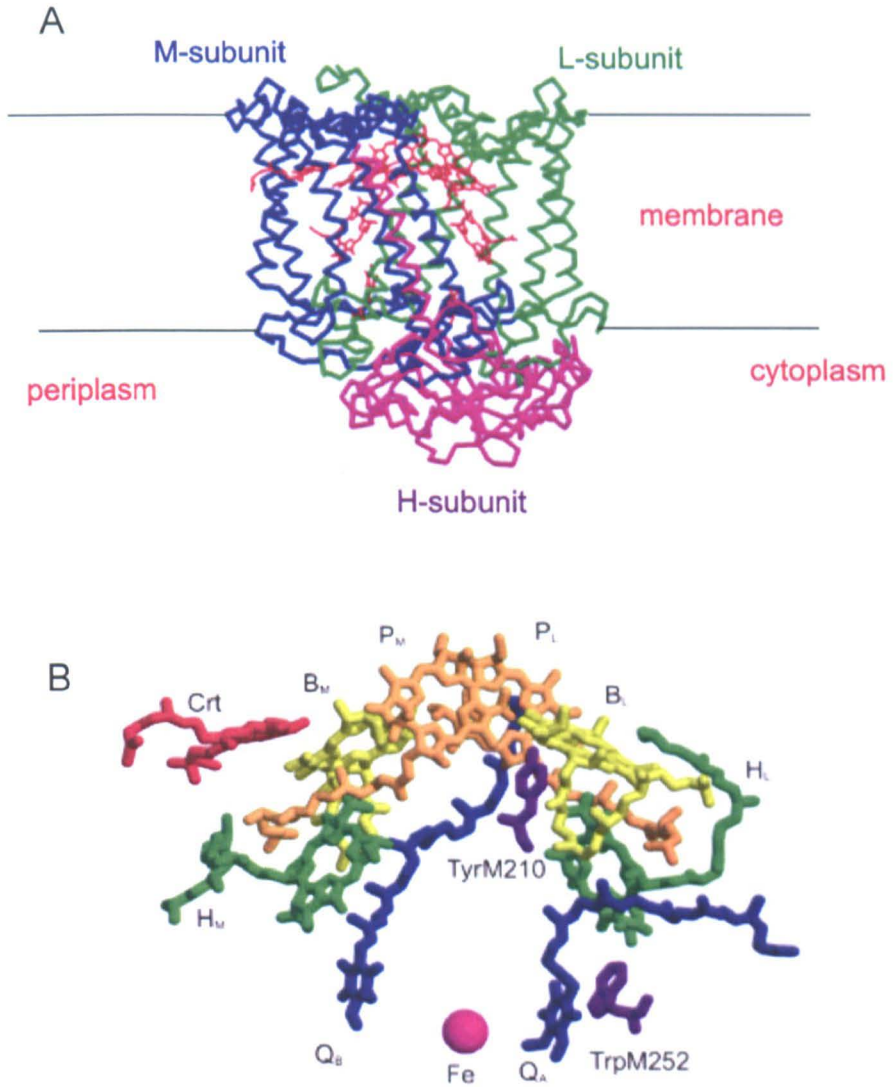


**Figure 1.8 Structure of the RC from *R. sphaeroides***

**A** – shows the protein subunits L, M and H of the RC in green, blue and purple respectively. The chromophores are shown in red, but are more easily seen in B

**B** – shows the chromophores RC special pair ( $P_L$ ,  $P_M$ , orange), accessory BChl(s) ( $B_L$ ,  $B_M$ , yellow), bacteriopheophytins ( $H_L$ ,  $H_M$ , green), quinones ( $Q_A$ ,  $Q_B$ , blue) and a carotenoid molecule (red).

Haselkorn, 1972; Okamura *et al.*, 1974). However, sequence analysis of the cloned genes encoding these proteins later revealed their true molecular weights to be 31, 34 and 28 kDa respectively (Williams *et al.*, 1983a, 1984, 1986). The L and M subunits are homologous and are related by a pseudo-twofold circular symmetry. Multiple pigment molecules (cofactors) are bound to the L and M subunits and are arranged accordingly in two symmetric branches, commonly referred to as the A and B branches: two BChl(s) which form a strongly interacting dimer and are known as the “special pair” ( $P_A$ ,  $P_B$ ), two accessory BChl(s) in close proximity to the “special pair” ( $B_A$ ,  $B_B$ ), two bacteriopheophytins ( $H_A$ ,  $H_B$ ) and a pair of quinones ( $Q_A$ ,  $Q_B$ ) (Chang *et al.*, 1986; Allen *et al.*, 1987b; Ermler *et al.*, 1994). Only the branch more closely associated with L-subunit is used in the light-driven electron transfer process and is accordingly termed the “active” branch (Zinth *et al.*, 1983; Michel and Deisenhofer, 1986) (Figure 1.8B). There is a carotenoid molecule that disrupts the two-fold symmetry of the complex and is within van der Waals contact with the accessory BChl of the inactive branch. There is also a non-heme iron atom located halfway between the two quinone molecules. The structure of several site-directed mutants of the *Rba. sphaeroides* RC have been determined, enabling the first correlations between spectroscopy, mutagenesis and structure (Jones *et al.*, 1992a,b; Jones *et al.*, 1994; McAuley *et al.*, 1999; McAuley *et al.*, 2000).

A lipidic cubic phase crystal structure of the RC from *Rba. sphaeroides* has been reported (Katona *et al.*, 2003). The crystals of the complex grown were 3D, the first type I crystal packing (where 3D crystals grow as multilayered 2D crystals) reported for a RC from a purple bacterium; the X-ray structure was refined to 2.35 Å resolution. The results revealed that the 2-fold pseudo-symmetry axis of the RC and the normal vector to the membrane plane are inclined at an angle of 11.5° relative to each other. An additional cardiolipin molecule was identified in addition to the one reported by McAuley *et al.* (1999), which contacts the membrane-exposed surfaces of the H and M subunits. The more recently identified cardiolipin molecule forms an additional interaction with a loop of the L subunit. A chloride-binding site was also identified and is located just within the membrane-spanning region of the RC within the M subunit. The chloride-binding site lies close to a water channel connecting the

quinone-binding site ( $Q_B$ ) with the protein's surface. Katona *et al.* (2003) have suggested that this chloride ion could provide specific sites for interaction with other integral membrane proteins.

The H-subunit has a single membrane spanning polypeptide, the majority of the protein forming a globular region at the cytoplasmic surface of the membrane. The function of the H-subunit is not well defined, although there is evidence to suggest that it is involved in the assembly of the RC (Chory *et al.*, 1984).

#### 1.4.4 The LH1-RC Core complex

The RC and LH1 complexes have been discussed individually in detail. The two molecules exist in a fixed 1:1 stoichiometry in the membrane, with a number of low resolution studies showing LH1 surrounding the RC (Stark *et al.*, 1984; Engelhardt *et al.*, 1986; Boonstra *et al.*, 1994; Walz *et al.*, 1998; Jungas *et al.*, 1999; Fotiadis *et al.*, 2004; Scheuring *et al.*, 2004; Seibert *et al.*, 2004; Roszak *et al.*, 2003). As previously discussed, the core complex in *Rba. sphaeroides* forms a dimer, when associated with a third protein PufX. The dimeric core complex structure has been solved to 8.5 Å by cryoEM (Qian *et al.*, 2005).

Work done by Roszak *et al.* (2003) reveals the crystal structure of the RC-LH1 core complex of *Rps. palustris* at 4.8 Å resolution. Initial phases were calculated by the molecular replacement method using the RC from *Rba. sphaeroides* as a model. The electron density map shows electron density is located around the outside of the RC, which is assigned to LH1. The LH1 protein  $\alpha$ -helices and BChl pigments were allocated to the density through a number of steps; after the first step, where the four inner-ring  $\alpha$ -helices were fitted into the best elongated stretches of the density surrounding the RC, one of the helices was substantially out of rank compared with the others. After all the inner-ring  $\alpha$ -helices had been assigned it was found there were 16

in total, which included the helix that appeared to be out of place, which is called helix W. The outer-ring  $\alpha$ -helices were then applied to specific stretches of density, but only 15  $\alpha$ -helices could be assigned; there was no density for the putative 16<sup>th</sup>  $\alpha$ -helix of the outer-ring and the position of this gap was opposite the helix W of the inner-ring. It therefore appears that the LH1 ring surrounding the RC is interrupted by another protein in much the same way that PufX does in *Rba. sphaeroides* (Figure 1.6). The crystal structure of the RC-LH1 core complex from *Rps. palustris* revealed that the LH1 complex appears to surround the RC in an elliptical shape with dimensions of  $\sim 110$  Å by  $\sim 95$  Å for the outer ring. The space within the LH1 complex is sufficiently large enough to accommodate the RC, the longest dimension of the inner LH1 ellipsoid is  $\sim 78$  Å (Roszak *et al.*, 2003).

Qian *et al.*, (2005) were able, for the first time, to unambiguously define the position and orientation of the RC within the dimeric core complex, with the planes of the BChl special pair lying at  $\sim 17.5^\circ$  relative to the long axis of the dimer. Surrounding the two RCs are two arcs of 14  $\alpha\beta$  heterodimer pairs, which can be identified in the projection map as doublets of clearly separated density peaks, with nearest neighbour  $\alpha$ - $\beta$  and  $\alpha$ - $\alpha$  distances ranging from 13.5 Å - 18.5 Å and 14.5 Å - 20.0 Å respectively (Figure 1.9a). 12 of the 14  $\alpha\beta$  pairs could be immediately and unambiguously identified within the arc of paired densities. At either end of the arc additional pairs of density are seen; a very strong density doublet is found close to the dimer interface, and a second area of weaker densities is seen at the end of the arc, indicating a fourteenth  $\alpha\beta$  pair. The densities ascribed to  $\alpha\beta$  pairs vary in strength throughout the arc, which may be consequence of the inherent flexibility of the dimer, a lower occupancy of certain  $\alpha\beta$  pairs or a tilt within the membrane plane. The weakness in density of the fourteenth  $\alpha\beta$  pair explains its absence in previous projections using negative stain (Jungas *et al.*, 1999; Seibert *et al.*, 2004; Scheuring *et al.*, 2004), however the  $\alpha$ - $\alpha$  spacing from the adjacent  $\alpha 13$  of 15.5 Å is close to the average of 16.5 Å for the whole complex. In contrast the  $\beta$ - $\beta$  spacing between  $\beta 13$  and  $\beta 14$  is 24.5 Å compared to the average of 22.0 Å, indicating a specific weakening in this region of the LH1 ring in the area associated with the  $Q_B$  site of the RC. As previously discussed, the LH1  $\beta$ -apoprotein

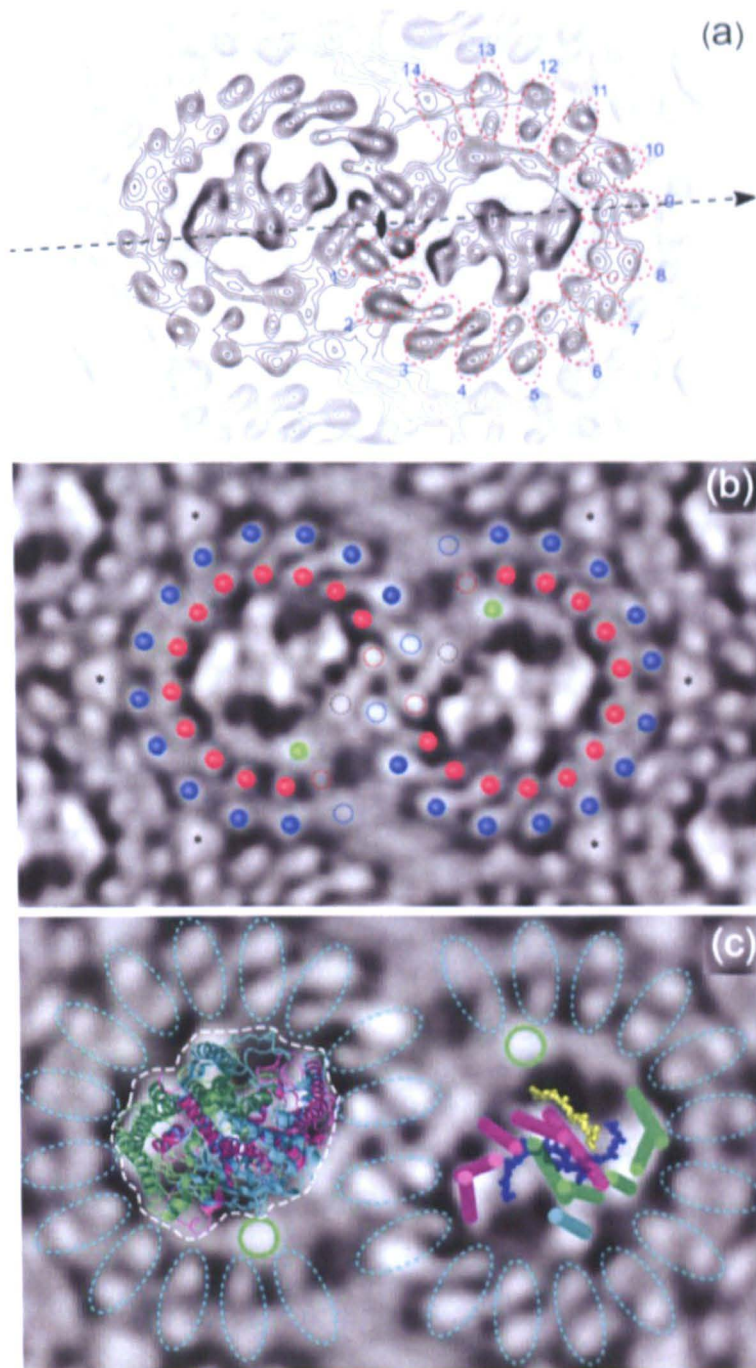


**Figure 1.9 The core complex dimer of *Rba. sphaeroides* resolved to 8.5 Å**

(a) Contour map of the averaged projection density of the core complex from *Rba. sphaeroides*. The axis of symmetry is marked by the lens symbol, with the long axis marked by the arrow. The 14  $\alpha\beta$  heterodimer pairs are numbered.

(b) Grey level representation of the density is shown.  $\alpha$  and  $\beta$  polypeptides are represented by red and blue circles respectively. PufX is shown as a green circle. The terminal subunits of LH1 are shown as open circles.

(c) The RC was fitted into the EM densities by translating and rotating the known RC structure. The position and orientation shown is the only one possible. The outline of the RC complex is denoted by a white dashed line. The area of diffuse electron density assigned to PufX is shown by an open green circle; it lies outside both the RC and LH1 densities.

has been shown to be inherently flexible (Conroy *et al.*, 2000) and the diffuse area of density associated with  $\beta 14$  reflects a highly mobile region of the LH1 assembly.

The electron density map also revealed an area of diffuse density outside of the envelope representing the RC, and clearly out of register with the arc representing the 14  $\alpha\beta$  heterodimers (Figure 1.9b). Qian *et al.*, attribute this density to PufX, as it lies adjacent to the  $Q_B$  site of the RC and within 12 Å of an LH1  $\alpha$ -apoprotein, with which PufX is known to interact (Parkes-Loach *et al.*, 2001). This proposed location fits with the notion that PufX acts as a gating protein, regulating the flow of quinone/quinol between the RC and the cytochrome *bc<sub>1</sub>* complex. The proposed location precludes PufX helix-helix interactions being responsible for the dimerisation of the core complex; however it does not exclude the possibility for PufX-PufX or PufX-LH1 interactions taking place via their N- or C-termini. This would fit with previous studies which showed truncations at the N-terminus of PufX caused the abolition of dimer formation (Francia *et al.*, 2002). The positioning of PufX between the RC  $Q_B$  site and the mobile LH1  $\beta 14$  subunit, coupled with inherent flexibility in the dimeric structure, plays a role in optimising quinone exchange during photosynthesis. It is worth mentioning that the superimposition of the core complex structure obtained by Roszak *et al.*, (2003) and that of dimer core complex which Qian *et al.*, (2005) resolved, places PufX and PufW within 12 Å of each other (Aleks Roszak, University of Glasgow, Data not shown).

The most up-to-date images of RC-LH1 core complexes from *Rs. rubrum* have been reported by Fotiadis *et al.* (2004). High-resolution AFM was used to image 2D-crystals, with topographs recorded of both the periplasmic and cytoplasmic side of the complex. These are the only AFM images to show two rings arising from the  $\alpha$ - and  $\beta$ -polypeptides. The images of the RC-LH1 complexes have extended previous ideas on the flexibility of the LH1 ring; elliptical rings of LH1 were found whether the RC was present or not and the ellipticity of the ring is conserved on the periplasmic and cytoplasmic sides of the complex. Upon closer inspection the LH1 complex is not perfectly elliptical, and is instead more 'D' shaped. Thus, the flexibility of LH1 is sufficiently pronounced to allow it to conform very closely to the real shape of the RC, which is also not perfectly elliptical in shape. Due to the nature of AFM, the relative

heights of the RC and LH1 complexes and their position in the membrane could be deduced. The data obtained showed that the highest part of the complex is the H-subunit of the RC and protrudes the membrane by 40 Å. The LH1 complex protrudes the membrane surface on the cytoplasmic side by 19 Å and it appears there is no height difference between the  $\alpha$ - (inner) and  $\beta$ - (outer) rings. On the periplasmic side, LH1 protrudes the membrane surface by 12 Å.

#### 1.4.5 PufX

The *pufX* gene is located at the end of the *puf* operon and is found in both *Rba. sphaeroides* and *Rba. capsulatus* (Youvan *et al.*, 1984; Zhu *et al.*, 1986; Lee *et al.*, 1989). The *Rba. sphaeroides* and *Rba. capsulatus* PufX proteins are 82 (9 kDa) and 78 (8.5 kDa) amino acids in length respectively. The *pufX* gene is essential for normal photosynthetic growth in *Rba. sphaeroides*, and its absence causes an increase in LH1 levels when compared with wild type (Farchaus *et al.* 1990; 1992). These authors have also shown that the PufX protein is contained within the ICM, on extraction of this fraction with 1 % OG (detergent) PufX co-purifies with RC-LH1. They concluded that PufX is part of the RC-LH1 core complex. PufX is oriented with its N-terminus exposed on the cytoplasmic side of the ICM (Pugh *et al.*, 1998). The deletion of *pufX* in *Rba. capsulatus* also produces mutants which are non-photosynthetic and have an increase in LH1 levels as compared with wild type (Klug and Cohen, 1988). Further investigations of these mutants by Lilburn *et al.* (1992) revealed that their ICM invaginations are approximately 50 % larger than WT and that individual complexes seemed fully functional but that electron transfer from the RC to the cytochrome *bc*<sub>1</sub> complex is impaired. This was the first indication that PufX has an important functional role in electron transfer. Westerhuis *et al.* (1993) demonstrated similar effects on electron transfer in *Rba. sphaeroides pufX* mutants and went on to show that the fluorescence excitation spectra of membrane fractions indicated a re-organisation of the functionally important aggregation state and supramolecular organisation of LH1.

When mutants of *Rba. sphaeroides* that contained RC and lacked LH complexes were studied in the presence and absence of the *pufX* gene it was evident that no significant difference between the two strains was seen when grown photosynthetically. This demonstrates that PufX is not an essential component of photochemistry at the RC or the transfer of electrons to the cytochrome *bc*<sub>1</sub> complex (McGlynn *et al.*, 1994). These same authors also found that when *pufX* is absent in strains deficient in LH2 the RC-LH1 complex size is increased by 1.16 fold, indicating that the overall increase in LH1 levels seen in *pufX* mutants is due to larger rather than more LH1 complexes. The main conclusion from McGlynn *et al.* (1994) was that the PufX protein interacts with the RC and prevents its total encirclement by LH1, which allows efficient electron transfer between the RC and *bc*<sub>1</sub> complex.

Purification of PufX from the native membranes of *Rba. sphaeroides* and *Rba. capsulatus* has been reported. The purified proteins were shown to inhibit the *in vitro* association of LH1  $\alpha$  and  $\beta$  subunits and pigments at low concentration, however only LH1  $\alpha$  was shown to bind to PufX. These results bolster further the idea that PufX prevents the encirclement of the RC (Recchia *et al.*, 1998). Parkes-Loach *et al.* (2001) showed that the C-terminus of PufX is processed in *Rba. sphaeroides* (12 C-terminal residues) and *Rba. capsulatus* (8 C-terminal residues). Francia *et al.* (2002) demonstrated a role for the C-terminus in the assembly / insertion of PufX into the ICM and a role for the N-terminus in dimerisation of core complexes through hydrophobic interactions, possibly with another PufX molecule. The stoichiometry of PufX with reference to the RC has been calculated by Francia *et al.* (1999), to be 1 PufX polypeptide to 1 RC complex. However these results should be viewed critically as the calculations were based on a method for detecting PufX which relies on its C-terminal segment that Parkes-Loach *et al.* (2001) have shown to be removed in the mature PufX protein.

Recent work by Tunnicliffe *et al.*, (2006) solved the solution structure of PufX by NMR (Figure 1.10). It was shown to be two hydrophobic helices flanked by two unstructured regions at the N- and C-termini. The two helices are connected by a

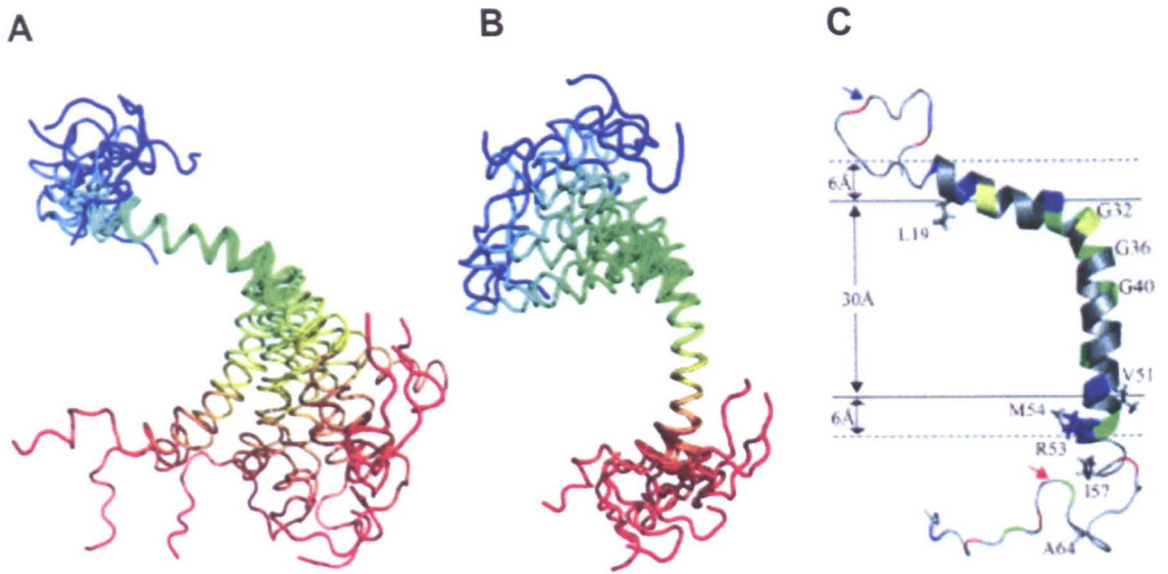


### Figure 1.10 The NMR structure of PufX

Structure of PufX. The structures are shown with the C-terminal (periplasmic) end at the bottom, in a possible 'side-on' orientation, as if viewed from within the membrane. Adapted from Tunnicliffe *et al.*, (2006)

**A.** Ensemble of 10 structures chosen at random from the 37 lowest energy structures, coloured from blue at the N-terminus to red at the C-terminus. The structures are aligned on residues 19–29. The C-terminal 12 residues are completely disordered and are not shown for clarity.

**B.** As (A), but aligned on residues 36–52.

**C.** Cartoon representation, showing the locations of the tryptophan sidechains (yellow), the glycines (green), lysines and arginines (blue) and aspartates and glutamates (red). The residues that shift most on addition of LH1 $\alpha$  are shown as wireframe and labelled. Glycines 32, 36 and 40, which encompass two successive GXXXG motifs, are labelled. A suggested position for the membrane is shown, with the solid lines marking the boundary of the hydrophobic core and the dashed lines showing the limit of the lipid headgroup region.

helical bend. The angle of the interhelical bend allows the N-terminal helix to lie within the lipid head group region or just outside it. The transmembrane helix spanning the hydrophobic core of the membrane lies between residues Gly30 and Gly52. The exposure of the C-terminus seen on the periplasmic side of the membrane is consistent with the post translation cleavage mentioned previously (Parkes-Loach *et al.*, 2001). The GXXXG motifs previously thought to drive dimerisation are in positions thought unlikely to be responsible for the direct coupling of RC-LH1 core complexes. The N-terminus of the polypeptide is predicted to extend  $\sim 40$  Å along the membrane interface, which would be sufficient to allow PufX-PufX interaction within a dimer complex.

#### **1.4.6 The function of bacteriochlorophyll in the light-harvesting complexes**

The absorption of light energy by pigment molecules is the first step in photosynthesis. In order to increase the efficiency with which excitation energy is utilised by the RC it is surrounded by an excess of pigment molecules held in position by the proteins of the LH complexes. The role of the LH complexes is to increase the surface area for the efficient absorption of incident light energy, and enable light in the 810 - 910 nm range to be utilised by the RC. Direct excitation of one of the BChl or carotenoid molecules of the ring in either LH1 or LH2 yields an excited state. It is proposed that the circular arrangement of the B850 and B800 BChl molecules of LH2, and the B875 BChl(s) of LH1 allows any excitation arising from incident light to become rapidly delocalised over a number of adjacent BChl(s), and to facilitate efficient energy transfer to an adjacent LH1, or LH2 complex (Cogdell *et al.*, 1996). Hence the organisation of the photosystem components enables captured light energy to be funnelled from the relatively high-energy pigments of the LH2 antenna to the lower energy pigments of the LH1 antenna and the RC. This process is energetically favourable as the delocalisation of energy around the LH2 B850 ring reduces the need for LH2 to be specifically orientated with respect to LH1. Furthermore, since the B850, B875 and RC special pair BChl(s) are at the same level in the membrane, the efficiency of

transfer between the rings is maximised by movement along a level plane (Hunter *et al.*, 1989; McDermott *et al.*, 1995; Fotiadis *et al.*, 2004).

There are many potential pathways for photons to be absorbed and for subsequent excitations to reach the RC. Absorption of an 800 nm photon by one of the LH2 B800 BChl(s) will require at least three sequential steps for the B800 excitation to be transferred to the RC: B800 (LH2) → B850 (LH2) → LH1 → RC. Time-resolved picosecond and femtosecond spectroscopy have been employed to determine the rate of excitation transfer between complexes and have revealed that the B800-B850 excitation transfer proceeds within approximately 700 fs (Shreve *et al.*, 1991; Pullerits and Sundström, 1996). Two-colour pump-probe femtosecond measurements revealed that the excitation transfer between B850 and LH1 takes place in 3-5 ps (Hess *et al.*, 1995). Finally, the slowest of the transfer steps and therefore the rate-limiting step, is that of transfer between LH1 and the RC, which requires approximately 35 ps (Visscher *et al.*, 1989; Beekman *et al.*, 1994). Hence, this suggests that the greatest distance for excitation transfer occurs between the LH1 BChl(s) and the RC special pair (reviewed by Hu *et al.*, 2002).

## **1.5 Electron flow and ATP synthesis in the photosynthetic membrane**

### **1.5.1 Light-driven electron flow in the RC**

Electron flow in the RC has been the subject of many reviews (Deisenhofer and Michel, 1991; Deisenhofer and Norris, 1993; Fleming and van Grondelle, 1994; Woodbury and Allen, 1995; Hoff and Deisenhofer, 1997; Bixon and Jortner, 1999). Following excitation transfer from the LH1 complex, an electron within the special pair ( $P_A$ ,  $P_B$ ) is promoted to an excited state. This electron is transferred, through the accessory BChl ( $B_A$ ), to the bacteriopheophytin ( $H_A$ ) in 2-3 ps. The reduced bacteriopheophytin ( $H_A^{-1}$ ) donates an electron to the adjacent quinone molecule ( $Q_A$ ) in about 200 ps. The  $Q_A$  in turn passes an electron to the  $Q_B$  molecule in 200  $\mu$ s, converting  $Q_B$  to a semiquinone radical. In the meantime, the positively charged

special pair is neutralised by the transfer of an electron from a reduced cytochrome  $c_2$  molecule located on the periplasmic side of the membrane. A second photon is then absorbed by the special pair and the flow of a second electron to  $Q_B$  takes place. The  $Q_B$  quinone molecule, now it has accepted two electrons, is reduced to the quinol form ( $QH_2$ ) by the simultaneous uptake of two protons from the cytoplasmic side of the membrane. It is at this point that the cycle leaves the RC by the release of the  $QH_2$  molecule into a mobile pool of quinones. A diagram of the RC cofactors is displayed in Figure 1.8B. The electron transfer cycle is completed by the oxidation of quinol by cytochrome  $bc_1$  complex; this results in the release of protons on the periplasmic side of the membrane and production of a reduced cytochrome  $c_2$ . The transfer of protons from the cytoplasmic side to the periplasmic side produces a proton gradient (PMF, proton-motive-force) that drives ATP synthesis at the ATP synthase (Abrahams *et al.*, 1994). A summary of the cyclic electron flow can be seen in Figure 1.11

### 1.5.2 The cytochrome $bc_1$ complex

The complexes of the cytochrome  $bc_1$  family are multisubunit complexes of integral membrane proteins that couple the redox energy of electron transfer reactions to proton translocation across the membranes of bacteria, mitochondria and chloroplasts. In doing so they conserve energy from the oxidation-reduction reactions in a form (the proton electrochemical gradient) that can be used to synthesize ATP. Electrons are transferred from a hydroquinone (ubiquinol, menaquinol or plastoquinol) to a small soluble redox protein such as cytochrome  $c$  or plastocyanin. The cytochrome  $bc_1$  complex, or ubiquinol-cytochrome  $c$  oxidoreductase, is present in mitochondria and  $\alpha$ -proteobacteria such as *Rba. sphaeroides*, where it functions in the electron transfer chain for both respiration and anaerobic photosynthesis (Crofts and Berry, 1998; Berry *et al.*, 2000). An X-ray crystallographic structure of the *Rba. capsulatus*  $bc_1$  was resolved to 3.8 Å (Berry *et al.*, 2004). It was shown to comprise of an intertwined homodimer with two monomers organised around a two-fold molecular axis. The Fe-S protein is found with the cyt  $b$  and cyt  $c_1$  subunits on one monomer, while its membrane anchor assembles with the same subunits on the other monomer.

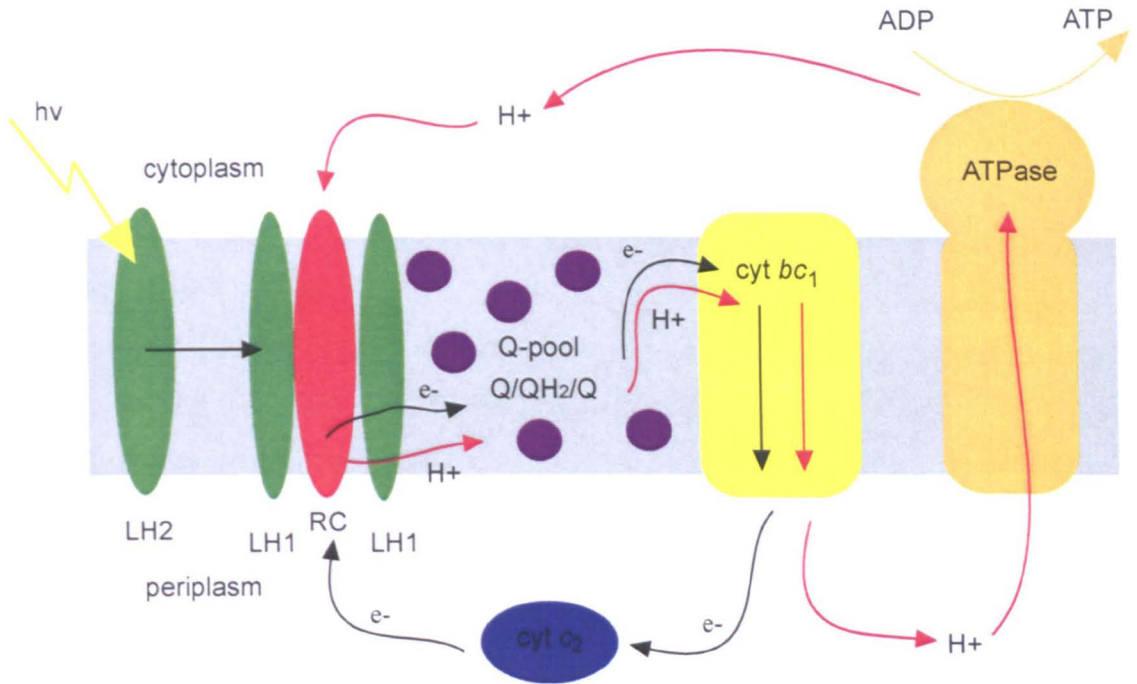


**Figure 1.11 Cyclic electron flow within the photosynthetic apparatus of *Rba. sphaeroides***

The subunits: LH2, LH1, RC, Q-pool, cytochrome  $bc_1$  complex, cytochrome  $c_2$  and ATPase are represented schematically. The RC (red) is surrounded by LH1 (green) to form the RC-LH1 core complex, which is surrounded by multiple LH2 (green) complexes. Photons are absorbed by LH complexes and excitation is transferred to the RC initiating a charge separation. Electrons are shuttled by the cytochrome  $c_2$  complex (blue) from the cytochrome  $bc_1$  complex (yellow) back to the RC. The electron transfer across the membrane produces a proton gradient that drives the synthesis of ATP from ADP by the ATPase (orange). Electron flow is represented by black arrows and proton flow by red arrows.

### 1.5.3 ATP synthase

In the light driven synthesis of ATP represents the movement of protons and electrons results in the formation of a proton-motive force and, according to the chemiosmotic hypothesis, synthesis of ATP is promoted by the backflow of protons via the enzyme ATPsynthase located in the membrane, which acts to redress the osmotic imbalance (Mitchell, 1968). Proton uptake is coupled to electron flow in the Q-cycle. The synthesis of ATP from ADP, Pi and protons is catalysed by a multiprotein complex, ATPase or ATP synthase, also known as the coupling factor as it couples electron (and proton) flow to phosphorylation (reviewed in McCarty *et al.*, 2000). ATP synthase is made up of two components. CF<sub>1</sub> is a hydrophilic 325 kDa multi-subunit factor which projects towards the cytoplasmic space; it is composed of three  $\alpha$  and three  $\beta$  subunits arranged as trimers and three other subunits called  $\gamma$ ,  $\delta$ , and  $\epsilon$ . CF<sub>0</sub> constitutes the hydrophobic membrane spanning component; it is composed of subunits I to IV, and is responsible for proton translocation. A structure at 2.8 Å resolution of the F<sub>1</sub>-ATPase from bovine heart mitochondria has been published (Abrahams *et al.*, 1994).

## 1.6 Photosynthetic gene clusters of *Rba. sphaeroides* and other purple bacteria

Following the detailed studies of the photosynthesis genes of *Rba. capsulatus* (Marrs, 1981; Taylor *et al.*, 1983; Zsebo and Hearst, 1984) analysis of the organisation of the *Rba. sphaeroides* genome revealed a high level of conservation between the two species. R-prime derivatives carrying large sections of genomic DNA were studied, and the subsequent isolation of two cosmid clones led to the generation of a linkage map of six *crt* and two *bch* loci (Pemberton and Bowen, 1981; Pemberton and Harding, 1986). The first physical map linking the *bch*, *puh* and *puf* genes of *Rba. sphaeroides* was determined using complementation of non-photosynthetic mutants, which facilitated the isolation of a number of overlapping clones and which represented a 45 kb region of the genome (Hunter and Coomber, 1988; Coomber and

Hunter, 1989). Localised transposon Tn5 mutagenesis was then used to characterise the cluster further, and enabled nine *bch* genes for BChl biosynthesis, and six *crt* genes to be mapped within the 45 kb region, flanked by the *puh* and *puf* operons (Coomber *et al.*, 1990).

The sequence of the *Rba. sphaeroides* gene cluster has now been determined (reviewed by Naylor *et al.*, 1999), with many more genes having been identified within it (Figure 1.12). Figure 1.12 also shows which photosynthetic components certain operons/genes encode for and the order in which they are assembled. The superoperonal organisation of the photosynthesis genes of both *Rba. sphaeroides* and *Rba. capsulatus* enables the organisms to respond rapidly to environmental change and closely regulate the expression levels of pigments and pigment-binding proteins (Bauer *et al.*, 1991; Wellington *et al.*, 1991).

The advent of whole genome sequencing has led to the publication of the *Rba. sphaeroides* 2.4.1. genome sequence ([www.rhodobacter.org](http://www.rhodobacter.org)). Analysis of this sequence has led to the discovery of another functionally significant operon, *puc2BA*, located outside of the PGC. The *puc2BA* operon will be discussed further in section 1.6.5 of this chapter.

### 1.6.1 The *puf* operon

The structural genes encoding the *Rba. sphaeroides* LH1 $\alpha$  and  $\beta$  polypeptides, *pufA* and *pufB*, and the RC L and M subunits, *pufL* and *pufM*, reside within the *puf* operon, which contains six genes transcribed in the order *pufQBALMX* (Williams *et al.*, 1983, 1984; Kiley *et al.*, 1987; Lee *et al.*, 1989; Hunter *et al.*, 1991; Naylor *et al.*, 1999). This arrangement is also conserved in *Rba. capsulatus* (Youvan *et al.*, 1984). The expression of the *puf* operon in *Rba. sphaeroides* and *Rba. capsulatus* involves regulation of both transcription and mRNA degradation. Two major *puf* operon transcripts have been identified, one of 2.7 kb which encodes the *pufBALMX* genes, and one of 0.5 kb which encodes the *pufBA* genes (Zhu and Kaplan, 1985; Belasco *et al.*, 1985).

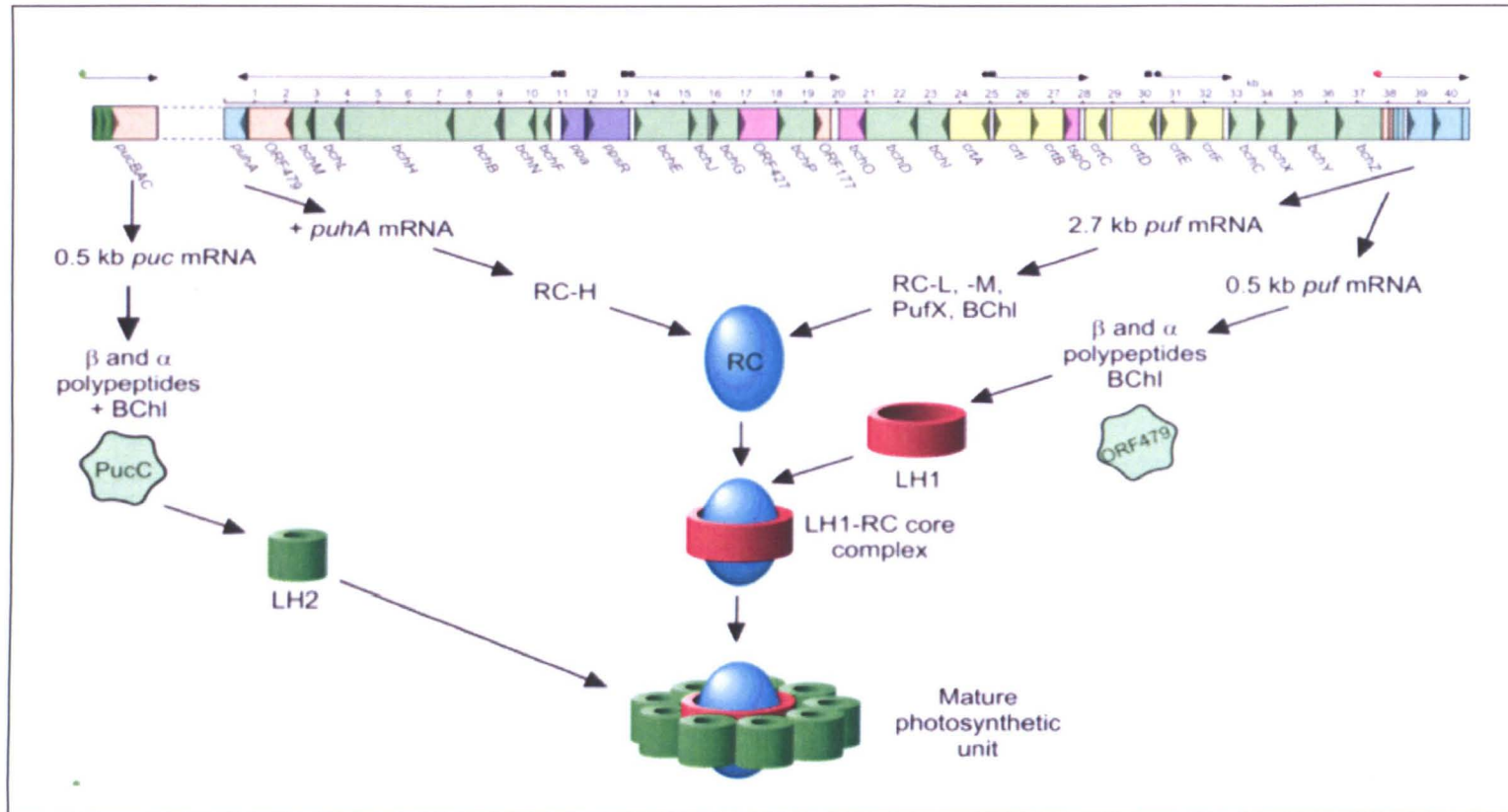


**Figure 1.12** The *Rba. sphaeroides* photosynthesis gene cluster

A physical map of the photosynthetic gene cluster from *Rba. sphaeroides* is shown as well as a model of the protein and pigments which the genes encode. The assembly factors PucC and ORF479 are shown in their respective assembly pathways.

The 0.5 kb mRNA transcript is 10-15 times more abundant than the 2.7 kb transcript. This molar excess of *pufBA*-specific mRNA over *pufLM* is the principal determinant of the 15:1 LH1:RC stoichiometry in the RC-LH1 core complex (Zhu and Kaplan, 1985; Belasco *et al.*, 1985). The levels of the *puf* operon transcripts have been shown to be regulated by oxygen and light. In response to a shift from high aeration to anaerobic growth both transcripts were shown to rise 10-30 fold, whereas shifting from high to low light photosynthetic growth conditions increased *puf* transcript levels approximately 3-fold (Zhu *et al.*, 1986a). The increased transcript levels, which have been shown to rise rapidly within the first hour of shifting from high aeration to low aeration growth (Hunter *et al.*, 1991), are not only due to increased *puf* operon transcription, but are in part the result of altered *puf* mRNA stability (Klug *et al.*, 1991). Hence, it is proposed that the oxygen- and light-regulated levels of *puf* transcripts directly account for the levels of LH1 and RC complexes in the ICM of *Rba. sphaeroides*.

The oxygen-regulated *puf* operon promoter has been functionally mapped to a region approximately 700 bp upstream of the *pufB* gene in both *Rba. sphaeroides* and *Rba. capsulatus* (Bauer *et al.*, 1988; Adams *et al.*, 1989; Hunter *et al.*, 1991). In both bacteria the promoter has been localised to a 37 bp region, which is highly conserved between the two species. This sequence contains a region of dyad symmetry and is located within the *bchZ* (formerly called *bchA*) structural gene that encodes a subunit of an enzyme involved in BChl biosynthesis (Bauer *et al.*, 1988; Hunter *et al.*, 1991).

In addition, it was discovered that this promoter was upstream of the *pufQ* gene, which led to the proposal that the operon was transcribed as *pufQBALMX*. There is strong evidence for the co-transcription of *pufQ* with the rest of the *puf* operon in *Rba. capsulatus* (Bauer *et al.*, 1988; Adams *et al.*, 1989), and it is likely that the inability to detect *pufQ* on Northern blots is due to the unstable nature of the mRNA, which rapidly degrades and gives rise to the 2.7 kb *pufBALMX* transcript. *In vitro* analysis of the *Rba. sphaeroides* *puf* operon transcripts revealed a separate *pufQ* transcript, and the absence of a transcript linking *pufQ* expression to the other *puf* genes. These findings led to the proposal that *pufBALMX* is transcribed independently

of *pufQ* in this organism (Gong *et al.*, 1994). However, in the absence of another identifiable promoter region, and in the light of the results of an *in vivo* analysis which showed that removal of the promoter upstream of *pufQ* effects the level of both *pufBALMX* and *pufQ* transcription (Hunter *et al.*, 1991), it remains feasible that the *puf* operon is transcribed as the *pufQBALMX* unit. The presence of sequences within or upstream of *pufQ* involved in regulating *puf* operon expression has not been ruled out, although it was demonstrated that the product of *pufQ* was not directly involved in the transcription of the *puf* operon (Gong *et al.*, 1994).

### 1.6.2 The function of *pufQ* and *pufK*

Genetic studies of *pufQ* in both *Rba. capsulatus* and *Rba. sphaeroides* have shown that there is a strong correlation between the amount of *pufQ* expression and the level of BChl synthesis (Bauer and Marrs, 1988; Hunter *et al.*, 1991). It is unlikely that *pufQ* itself encodes a BChl biosynthetic enzyme, as BChl is still produced in a *pufQ*-deletion mutant of *Rba. capsulatus*; but when *pufQ* is absent, the amount of BChl in the cell is greatly reduced. Levels of BChl are returned to normal levels upon introduction of a plasmid borne *pufQ* gene into the mutant cell. In addition, when deletions of the *pufQ* gene were introduced into mutants defective in *bch* genes, which accumulated BChl precursors, the production of these tetrapyrrole intermediates (of which ranged from protoporphyrin IX to bacteriochlorophyllide) was greatly reduced (Bauer and Marrs, 1988). It is proposed that the PufQ protein has a regulatory role in the BChl pathway; possibly to function as a carrier protein for intermediates of the magnesium branch of BChl biosynthesis, but does not affect the synthesis of hemes and cytochromes (Bauer and Marrs, 1988).

The effects of a series of mutations of the *Rba. sphaeroides pufQ* gene were analysed with respect to the spectral complexes of each mutant (Gong *et al.*, 1994). It was shown that, despite the presence of *puf* and *puc* transcripts at levels comparable to that of the WT, several of the mutants failed to assemble either one, or both, of the light-harvesting pigment-protein complexes. It was therefore proposed that PufQ was directly involved in the assembly of the photosynthetic complexes, specifically

interacting with complex-specific assembly factors at the point of BChl insertion (Gong *et al.*, 1994). This hypothesis could, therefore, explain the observed RC>LH1>LH2 order of preference for complex assembly when BChl is limiting. Conflicting evidence therefore exists to explain the role of PufQ; is it involved in the assembly of light-harvesting complexes or in the biosynthesis of BChl itself?

The PufQ protein of *Rba. capsulatus* was first detected *in vivo* by Western blot analysis of its chromatophore membranes (Fidai *et al.*, 1994). The protein could not be detected from a strain where the *puf* operon had been deleted, however, elevated amounts of PufQ were detected in a mutant strain defective in two *bch* genes and unable, therefore, to make BChl. When *Rba. capsulatus* was transferred from aerobic to semiaerobic growth, therefore inducing the production of BChl, an increase in the level of PufQ was observed after 3 hours. The extreme hydrophobic nature of the protein was also discovered as it was not solubilised by 3 % n-octyl- $\beta$ -D-glucopyranoside, a treatment that solubilises the RC-LH1 core complex (Fidai *et al.*, 1994b).

The gene designated *pufK* in *Rba. sphaeroides* by Gong and Kaplan, (1996) has no formal counterpart in *Rba. capsulatus*; however there is a region of DNA between *pufQ* and *pufB* that encodes a protein with 41.2 % similarity to *Rba. sphaeroides* PufK protein (Naylor *et al.*, 1999). *Rba. sphaeroides pufK* is a putative transcriptional regulator; the relatively rare codons in the gene may act as a 'ribosome gate', controlling differential translation of the large and small *puf* transcripts.

### 1.6.3 The *puhA* operon

The *puhA* operon, which is located 39 kb upstream of the *puf* operon at the 5' end of the photosynthetic gene cluster, is a monocistronic operon which encodes the RC-H subunit. *puhA* has been cloned and sequenced in both *Rba. sphaeroides* and *Rba. capsulatus* (Donohue *et al.*, 1986; Williams *et al.*, 1986; Youvan *et al.*, 1984).

#### 1.6.4 The *puc* operon

The *puc* operon consists of two structural genes, *pucB* and *pucA*, which encode the  $\beta$ - and  $\alpha$ -polypeptides of the LH2 complex, respectively and the assembly factor gene *pucC*. These *pucBA* genes have been cloned and sequenced in both *Rba. sphaeroides* and *Rba. capsulatus* (Ashby *et al.*, 1987; Kiley and Kaplan, 1987; Youvan and Ismail, 1985). The *pucC* gene of *Rba. sphaeroides* (Gibson *et al.*, 1992), identified in the region downstream of *pucBA*, shows extensive sequence homology to the *pucC* gene of *Rba. capsulatus* (Tichy *et al.*, 1989, 1991). However, the *pucDE* genes of *Rba. capsulatus* were not identified in *Rba. sphaeroides*, suggesting that the *puc* operon of this species is similar, but not identical.

When transcribed, the *puc* operon of *Rba. sphaeroides* yields a stable 0.5 kb *pucBA* transcript, and a less abundant 2.3 kb *puc*-specific transcript. Expression of both transcripts is highly regulated by both oxygen and light; the 0.5 kb transcript increases in abundance up to a hundred-fold in response to lowering of the oxygen tension, lowering the light-intensity results in a four to five-fold increase in the abundance of this mRNA (Kiley and Kaplan, 1987). In addition, the observed response to changes in the environmental conditions directly reflects the level of LH2 complex in the ICM under these conditions (Aagaard and Sistrom, 1972), which led to the proposal that transcription of *pucBA* regulates the abundance of the LH2 complex. The rate of increase in the level of *pucBA* mRNA in response to a shift from aerobic to anaerobic growth, was slower than that observed for the *puf* operon (Hunter *et al.*, 1987). This observation is consistent with that of Niederman *et al.*, (1976) who showed that in the hierarchy of assembly in the ICM, the LH2 complex is preceded by both the RC and LH1 complex. The similarly sized *pucBA* transcript of *Rba. capsulatus* was shown to respond to environmental changes in a similar fashion (Klug *et al.*, 1987; Zhu *et al.*, 1986b; Zhu and Hearst, 1986).

The 5' ends of both *Rba. sphaeroides pucBA* and *pucBAC* transcripts were mapped to 117 bp upstream of the *pucB* gene, therefore the 2.3 kb transcript runs to approximately 1.8 kb downstream of *pucA*, whereas the 3' end of the 0.5 kb transcript mapped to approximately 50 bp downstream of *pucA* (Lee *et al.*, 1989b). Complementation studies of a *pucBA* deletion mutant indicated that the sequences downstream of *pucBA* were required for LH2 assembly (Burgess *et al.*, 1989). Insertional disruption of this downstream region resulted in an LH2-minus phenotype, which was attributed to the loss of the 2.3 kb transcript in this mutant, and despite almost wild-type levels of the 0.5 kb transcript (Lee *et al.*, 1989b). Therefore it was suggested that the products of *pucC* and the additional open reading frames downstream of *pucA*, were involved in post-translational control of LH2 assembly (Lee *et al.*, 1989b; Tichy *et al.*, 1991).

Deletion analysis suggests that the *puc* operon promoter resides in the -84 to -66 bp region (Gibson *et al.*, 1992; Lee and Kaplan, 1992a,b), and enabled the 600 bp region of DNA upstream of the 5' end of the *puc* transcripts to be subdivided into two functionally separate regulatory domains. The upstream regulatory sequence and downstream regulatory sequence domains were proposed to be independently responsible for the enhanced and basal level transcriptional regulation of the *puc* operon, under aerobic and anaerobic conditions respectively (Lee and Kaplan, 1992a,b)

### 1.6.5 A second *puc* operon in *Rba. sphaeroides*

The genomes of *Rps. acidophila* and *Rps. palustris* have been observed to contain multiple copies of gene pairs encoding the  $\alpha$ - and  $\beta$ -apoproteins of LH2 (Tadros *et al.*, 1989; Tadros *et al.*, 1993; Gardiner *et al.*, 1996). All five gene pairs in *Rps. palustris* have been shown to be expressed and are subject to regulation according to light intensity. However, only two copies of the *puc* gene products have been detected in complexes purified from *Rps. palustris*.

Recent work on the *Rba. sphaeroides* 2.4.1. genome uncovered a second copy of the *pucBA* genes, which were designated *puc2BA* and given the gene numbers RSP1556 and RSP1557 respectively ([www.rhodobacter.org](http://www.rhodobacter.org)). The discovery of this gene pair has significant implications for any mutagenesis studies focused upon the manipulation of residues within the  $\beta$ -polypeptide of LH2 from *Rba. sphaeroides*. The role which the second gene pair plays in the genetic regulation of LH2 expression, and the function of the individually encoded polypeptides within the complex, has been explored by Samuel Kaplan's laboratory (Zeng *et al.*, 2003).

Zeng *et al.*, (2003) reported the mRNA transcript at the *puc2BA* locus to be 963 bp in length, which is substantially longer than that observed for *puc1BA* (337 bp). The Puc2B polypeptide shares 94 % identity and 95 % similarity with Puc1B, differing in only three amino acid residues, which are  $1\beta\text{Lys}_{-35} \rightarrow 2\beta\text{Pro}_{-35}$ ,  $1\beta\text{Asn}_{-34} \rightarrow 2\beta\text{Lys}_{-34}$  and  $1\beta\text{Val}_{-25} \rightarrow 2\beta\text{Ile}_{-25}$ . A comparison of Puc1A and the first 48 amino acids of Puc2A shows 58 % identity and 72 % similarity, however a long C-terminal extension beginning at the 49<sup>th</sup> amino acid of Puc2A is observed. The extension contains the repeating amino acid sequence PVAAAPAE EAAA or PV[A]EAAAPV[A]AEAAA. Transmembrane hidden Markov model 2.0 computer predictions suggest the presence of just one membrane spanning region for the Puc2B polypeptide, between residues Asn<sub>13</sub> and Thr<sub>37</sub>. A sequence comparison of the four Puc polypeptides is shown in Figure 1.13. Both Puc2B and 2A polypeptides retain the conserved  $\beta$ -His<sub>40</sub> and  $\alpha$ -His<sub>31</sub> residues which are presumed to ligand the central Mg<sup>2+</sup> of the B850 BChl(s) in *Rba. sphaeroides*. The Tyr<sub>44</sub> and Tyr<sub>45</sub> residues crucial in the binding of the B850 BChl are also conserved within the first 48 amino acids of Puc2A, as is the  $\beta$ Arg<sub>30</sub> residue, which forms an integral part of the B800 BChl binding site.

Zeng *et al.*, (2003) tagged the three polypeptides Puc2B, Puc2A, and Puc2AS (containing only the first 48 amino acids of Puc2A) with a Pho-A fusion protein in an effort to map their transcription and incorporation into the complex. Western blotting of extracted membrane fractions showed the presence of two fusion proteins 52 and 51 kDa in size, corresponding to Puc2B-PhoA and Puc2AS-PhoA respectively. The observed molecular mass of Puc2A was 75 kDa, compared to the calculated value of

```

1-----20-----40-----
RS 2.4.1. 1B MTDDLNKVWPSGLTVAEAEVHKQLILGTRVFGGMALIAHFLAAAATPWLG
RS 2.4.1. 2B MTDDPKKVWPSGLTIAEAEVHKQLILGTRVFGGMALIAHFLAAAATPWLG

1-----20-----40-----60-----
RS 2.4.1. 1A MTNGKIWLVVKPTVGVPLFLSAAVIASVVIHAAVLTTTWLPAYYQGSAAVAE-----
RS 2.4.1. 2A MNNSKMWLTVNPNLGVPLLLGSVAVASLVVHGAVLTTPWIANYYQGSEPWVAAAPAE
-----80-----100-----120
AAPVEAAAPADEAAAPVEEAAPVAEAAAPAEAAAPAAEAAPAEAAAPAEAAAPAEAA
-----140-----160-----180
APAAEAAAPAEAAAPAAEAAAPVEEAAPAAEAAAPAEAAAPVAEAAAPAEAAAPVAEPAA
-----200-----220-----240
EPAPAAEAAAPVAEVSAPAAELAAPVAMSLVDIAAKLNGLGYSVQSVTKTEGGYVVMNTD
-----260-----
ANGMPVAATLDPVTGLPFVPAAQ

```

**Figure 1.13 A sequence alignment of the polypeptides encoded by the two *puc* operons from *Rba. sphaeroides* 2.4.1.**

The three amino acid changes observed in Puc2B are highlighted in red. The long C-terminal extension is clearly seen in Puc2A. The transmembrane regions are shown in bold.

72 kDa, showing no significant processing of the polypeptide takes place. It is important to note that the three fusion proteins are not seen in the supernatant fraction, and so are all membrane associated. All three were expressed even when the chromosomal copies of the corresponding genes were deleted, but more importantly, deletion of the *puc1BAC* operon did not effect Puc2 polypeptide expression *in trans*; meaning transcription of *puc2BA* and expression of its encoded polypeptides is a process independent of control by *puc1BA* or *pucC*.

Immunoprecipitation of the Puc2BA-PhoA fusion proteins was carried out. Anti-PhoA antibodies and protein-A agarose beads were used to immunoprecipitate LH2 complexes containing the Puc2B, Puc2A, or Puc2AS-PhoA chimeric proteins. In the case of Puc2B-PhoA and Puc2AS-PhoA, an interaction between the  $\beta$ - and  $\alpha$ -apoproteins encoded by the *puc1BAC* operon was observed, with the resulting LH2 complexes displaying near wild type absorbance properties. Immunoprecipitated complexes containing the Puc2A-PhoA fusion protein displayed no absorption properties and did not form discernable LH2 complexes. To confirm the predicted topologies of the Puc2A and 2B polypeptides, alkaline phosphatase assays were carried out in cells of *Rba. sphaeroides* where different lengths of the *puc2B* or *puc2A* encoded polypeptides were fused with the PhoA protein. The results showed agreement with the predicted Markov models, with the N-terminal regions of both polypeptides being located on the cytoplasmic side of the membrane and the C-terminus on the periplasmic side. The entire extension at the C-terminus of Puc2A was observed present on the periplasmic side of the membrane.

#### **1.6.6 The role of the *puc2BA* operon in LH2 assembly**

Zeng *et al.*, (2003) produced a series of in-frame deletion mutants, in which *puc2B*, *puc2A* and *puc2BA* were removed. The amount of LH2 complex expression in the resulting mutants revealed a 30 % decrease in the absence of *puc2B*, whereas the absence of *puc2A* caused no obvious decline in LH2 abundance. The removal of both *puc2* genes resulted in LH2 levels similar to those observed upon removal of *puc2B* alone, with the levels of B875 and hence LH1 assembly apparently unaffected by the deletions made. These results indicate that the Puc2B polypeptide is exposed to the

same assembly pathway as the  $\beta$ - and  $\alpha$ -polypeptides encoded by *puc1BA*. The addition of extra copies of *puc1BA in trans* in the *puc2BA* deletion background failed to restore wild type levels of LH2 assembly, indicating levels of LH2 encoded by *puc1BAC* are under critical control and independent of transcript levels within the cell. The Puc2A polypeptide was seen to be translated and incorporated into the membrane, however it is not present in the LH2 complex itself, leaving ambiguity surrounding the role it plays.

A transcriptional fusion plasmid containing *puc2BA* upstream of a *lacZ* reporter gene was conjugated into *puc1BA*, *puc1C* and *puc2BA* deletion mutants. The  $\beta$ -galactosidase activity in these mutants was compared with the wild type at different light intensities in an attempt to establish whether the regulation *puc1B* exerts over *puc2BA* is at the level of transcription or is post transcriptional. The results showed the expression of *puc2BA* was regulated inversely with respect to the light intensity, and was independent of any mutations made to the *puc1BAC* operon. Translational fusions of *lacZ* and the *puc2B*, *puc2A* and *puc2BA* genes were introduced into wild type *Rba. sphaeroides* 2.4.1. and the three previously mentioned mutant backgrounds. No change in  $\beta$ -galactosidase activity was seen in any of the mutant backgrounds compared to wild type, indicating LH2 complex formation which incorporates Puc2B polypeptides is dependent upon the presence of a functioning *puc1BAC* operon and is regulated at a post translational level. Transcriptional fusion experiments also showed *puc1BA* expression was reduced by ~67 % in the absence of *puc1C*, showing a strong effect upon transcription which it is not exerted over *puc2BA*. In addition, it was noted that the *puc1BA* promoter was more active than its *puc2BA* counterpart.

## 1.7 The organisation of the photosynthetic membrane

Until 2004, the native architecture of the photosynthetic membrane was not known, and two opposing models for the organisation of the photosynthetic apparatus within the chromatophore existed. The first reported model was by Monger and Parson, (1977) who proposed the 'Lake' model. If a 'domain' in the antenna region is defined

as uniform with respect to the transfer of singlet excitations, does the RC trap excitations only within a relatively small and exclusive domain ('Puddle' model) or can 10-50 RCs in a chromatophore compete for a common pool of excitations in an extended domain ('Lake' model)? Their data indicated that singlet excitations could migrate over large domains in the antenna, and that the 'Lake' model was more likely.

Singlet-singlet annihilation studies of developing ICM vesicles showed that wild type membranes formed a domain of ~3000 BChl molecules involving 30 RCs (Hunter *et al.*, 1985). Further models of antenna organisation were reported in Hunter *et al.* (1989) where models were based on singlet-singlet quenching data reported in Vos *et al.* (1988). Their findings agreed with the qualitative 'Lake' model and reported that at least eight RC-LH1 core complexes were interconnected to form a single domain for energy transfer in a LH2 mutant strain of *Rba. sphaeroides*. For the WT this energy transfer domain is extended to include LH2 molecules. In the absence of the RC the energy transfer domain decreases in size suggesting the RC has a role in modifying the aggregation properties of LH1 in the membrane (Hunter *et al.*, 1989).

### **1.7.1 The native architecture of the photosynthetic membrane in *Rba. sphaeroides***

The advent of AFM as a biological tool enabled the possibility for the direct visualisation of the photosynthetic complexes within their native membrane. The native architecture of the photosynthetic apparatus of *Rba. sphaeroides* was visualised by Bahatyrova *et al.*, (2004). The multi-component membrane divides into specialised domains, each with a specific network organisation and with a particular pigment-protein complex predominating. LH2 exhibits two types of organisation; in the first, groups of 10 to 20 molecules form interconnecting 'energy conduits' between rows of dimeric core complexes, in the second; they are outside of these arrays in small clusters. The rows of dimeric core complexes form a highly efficient energy hub into which excitation energy can be funnelled and temporarily stored until it is passed on to the RC, with the possibility of the core complexes within the rows acting in a

cooperative manner as regards 'energy trapping'. If any particular RC is undergoing charge separation and thus is unable to accept excitation energy from its LH1 (a 'closed' state), this energy can migrate along a succession of dimer complexes until an 'open' RC is available. Images of the two separate LH2 domains and the associated core complex dimers are shown in Figure 1.14. The organisation seen in *Rba. sphaeroides* can be equated with the 'Lake' model proposed by Monger and Parson, with the RC's grouping together, utilising a common pool of excitons to facilitate charge separation. The images failed to identify the cytochrome  $bc_1$  complex or any ATP synthase molecules, this is a limitation of the work, but low numbers of these complexes within the membrane, and the lack of any recognisable features protruding from its cytoplasmic face make their identification a difficult task.

### 1.7.2 A comparison of photosynthetic membranes in purple bacteria

Work carried out previous to Bahatyrova *et al.*, (2004) paved the way for AFM imaging of native biological membranes from *Rba. sphaeroides*. It is now possible to compare the organisation of chromatophore membranes from six different species. *Blastochloris viridis* (previously *Rhodospseudomonas viridis*) membranes were visualised with high lateral (10 Å) and vertical (~1 Å) resolution in 2003 (Scheuring *et al.*, 2003). The study revealed single RCs surrounded by closed ellipsoidal LH1 complexes, each comprising of 16  $\alpha\beta$ -heterodimers. A technique termed nanodissection removed the tetraheme cytochrome subunit from the RC complex, caused by the lateral shearing forces of the tip across the surface of the membrane. This revealed the L and M subunits below, which show an asymmetric topography associated with the short ellipsis axis of the LH1 molecule. The LH1 molecules are seen to rearrange into a circular morphology after removal of the RC, perhaps indicating the elliptical shape of the RC-LH1 core complex confers specific energy transfer properties to the system (Figure 1.15a). *Blastochloris viridis* contains no peripheral light harvesting antenna complexes. The first images of membranes containing LH2 were taken from *Rba. sphaeroides* and *Rhodospirillum photometricum* (Bahatyrova *et al.*, 2004, Scheuring *et al.*, 2004) the membrane organisation in

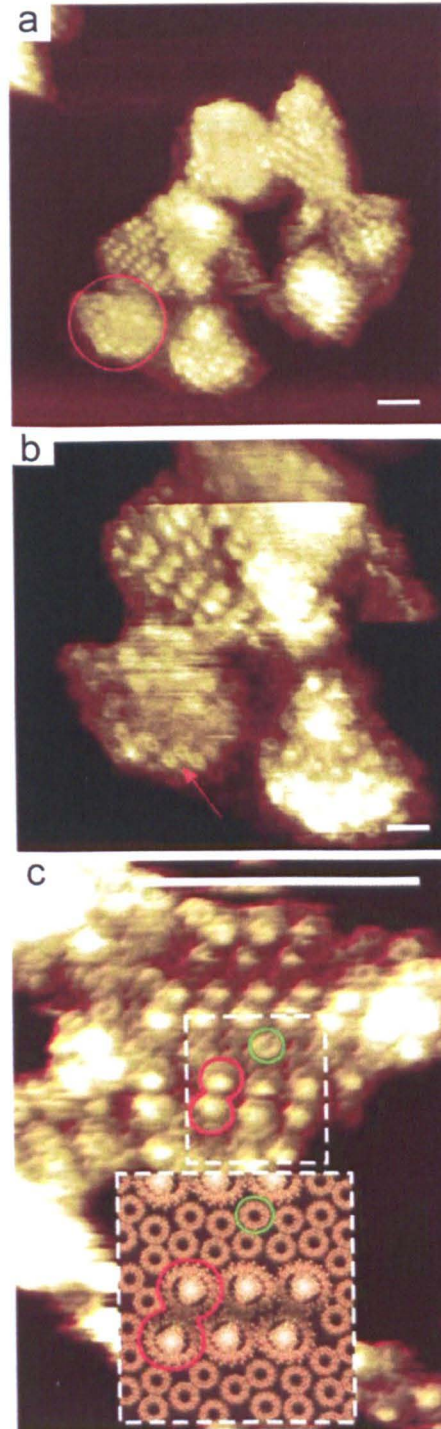


**Figure 1.14 AFM images of native membranes from *Rba. sphaeroides***

**a.** The circled region shows a domain comprising of mostly LH2.

**b.** A higher magnification image of the same region of membrane. The red arrow points at an individual LH2 complex within the highlighted domain.

**c.** A three dimensional view of a core complex array surrounded by LH2 complexes. The inset is a representation of the region denoted by the dashed box in the centre, using models derived from structural data.

(Bahatyrova *et al.*, 2004)

*Rba. sphaeroides* has been discussed previously, and is different to *Rps. photometricum*. Comparatively little is known about *Rsp. photometricum*, with no extensive genetic or biochemical analysis of the complexes comprising its photosynthetic unit having been carried out. The stoichiometry of LH2 to core complexes in its membrane was seen to vary (Figure 1.15c). Core complexes were seen to be monomeric and clustered together, segregating out of protein free lipid bilayers. A similar architecture is observed in *Phaeospirillum molischianum* (Goncalves *et al.*, 2005). The octomeric LH2 complexes of *Phsp molischianum* were found to arrange in a hexagonal lattice, forming large antenna domains. Monomeric core complexes were seen to cluster together (Figure 1.15d).

The membrane topology of a close relative of *Rba. sphaeroides*, *Rhodobacter blasticus* has been reported at high resolution (Scheuring *et al.*, 2004). The core complexes are seen to be dimeric as in *Rba. sphaeroides*, however their arrangement within the membrane is less ordered. The core complexes do not form rows of dimers; though the core dimers do form contacts, these appear to be random in orientation (Figure 1.15b). It is not possible to determine if this is a feature of the native membrane architecture in *Rba. blasticus*, since the imaged membranes have undergone a fusion process, which both disrupts the chromatophore structure and leads to membranes being bound to the mica in different orientations. The discreet arrays of LH2 are thus similarly disordered when compared to the membranes of *Rba. sphaeroides*.

The most recent work in this area has detailed the structure and organisation of the photosynthetic apparatus in *Rps. palustris* under varying light intensities (Scheuring *et al.*, 2006). The LH2 content of *Rps. palustris* is highly specific to the light levels in which it is grown. In low light conditions Low Light LH2 (LL-LH2) is produced, exhibiting a single Q<sub>y</sub> absorbance band at 800 nm (Evans *et al.*, 1990). In high light, ~50 % of LH2 are seen to absorb at both 800 and 850 nm. Comparison of highly resolved single LH2 complexes revealed an average difference in radius of 5 Å between LH2 and LL-LH2. LL-LH2 was seen to measure ~40 Å radially, and was predominantly octomeric in structure, while LH2 was seen to measure ~45 Å radially

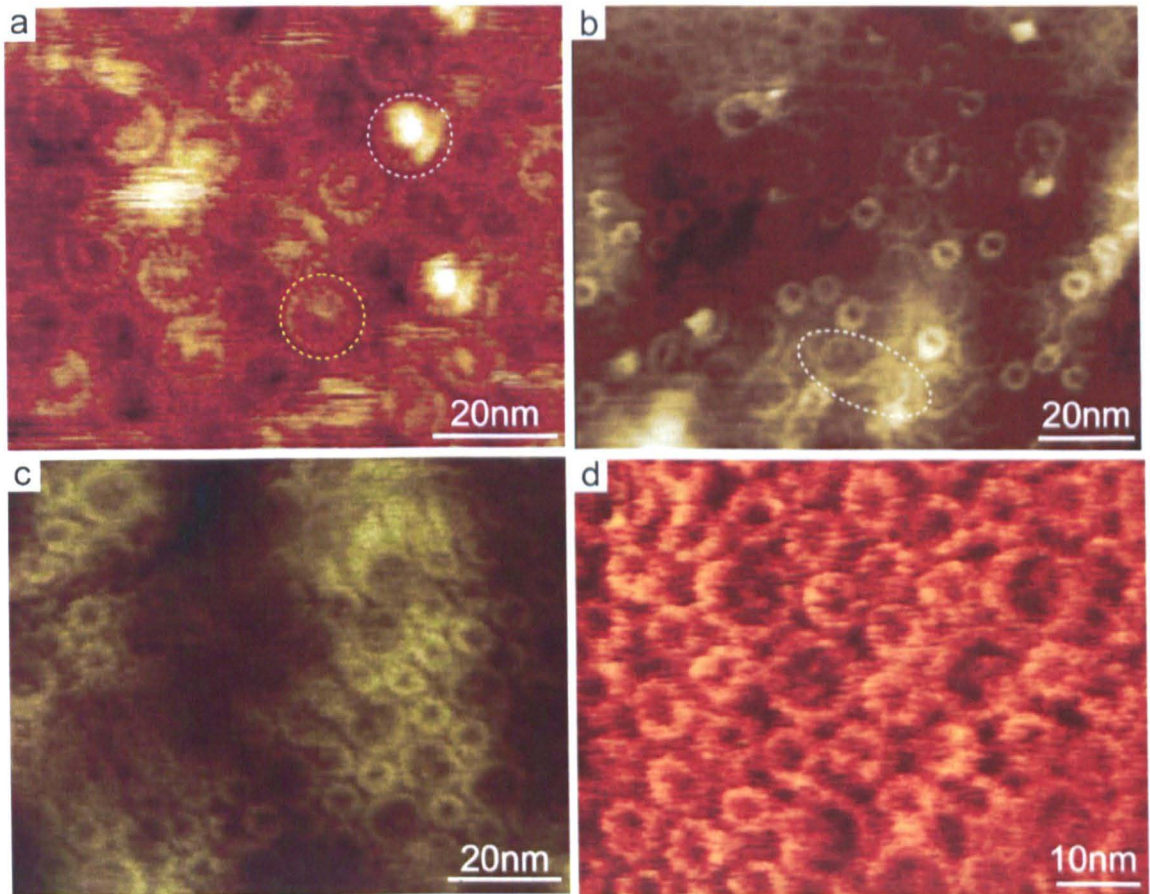


**Figure 1.15 A comparison of differing membrane architectures in purple photosynthetic bacteria**

- a. The membrane of *Rps. viridis* imaged using AFM. The tetraheme cytochrome can be seen attached to the reaction centre (white circle). Nanodissection of the tetraheme cytochrome reveals the L and M subunits beneath (yellow circle). (Scheuring *et al.*, 2003)
- b. The membrane of *R. blasticus* is seen by AFM. The dimeric core complex is highlighted by the dashed white oval. (Scheuring *et al.*, 2005)
- c. The membrane of *Rsp. photometricum* is imaged using AFM. Monomeric core complexes can be seen to cluster, surrounded by variable amounts of LH2 complex. (Schuering *et al.*, 2004)
- d. The membrane of *Phsp molischianum* imaged by AFM. Monomeric core complexes are seen to cluster together, surrounded by octomeric LH2 complexes. (Goncalves *et al.*, 2005)

and was predominantly nonameric (Figure 1.16c and 1.16d). Under low light growth conditions, membrane patches displayed different properties within discrete domains. Areas of membrane containing only para-crystalline core-complex were observed packing in a hexagonal fashion; these areas were seen to be adjacent to areas devoid of peripheral antenna complexes. However, mixed domains containing LL-LH2 and LH2 (~10 %) in close contact with core complexes predominated (Figure 1.16b). Under high light conditions, three types of membrane patches were observed. Type 1 membranes were densely packed with photosynthetic complexes, type 2 membranes showed areas of packed complexes adjoining areas of “pure” lipid. The third type of membrane patch displayed completely smooth surfaces, devoid of any complexes (Figure 1.16a). Core complexes were again seen to pack hexagonally, with low levels of disordered LH2 surrounding them. In this study, as in all carried out to date, the location of the cytochrome *bc*<sub>1</sub> complex was not elucidated.

## **1.8 Protein patterning utilising self assembled monolayers and photolithography**

The ability to pattern proteins at the nanoscale is of vast importance in producing biologically integrated devices for high throughput experiments in the field of proteomics. Several techniques are available for creating two dimensional arrays of proteins on surfaces (reviewed by Blawas and Reichert, 1998), including the use of photolithography and self assembled monolayers (SAMs). The field of protein patterning was originally conceived as a critical technology for the integration of biological molecules into miniature bio-electrical devices (Haddon and Lamola, 1985). The recent elucidation of the human genome sequence has increased in importance the ability to selectively immobilise proteins on the nanoscale, whilst retaining their function.

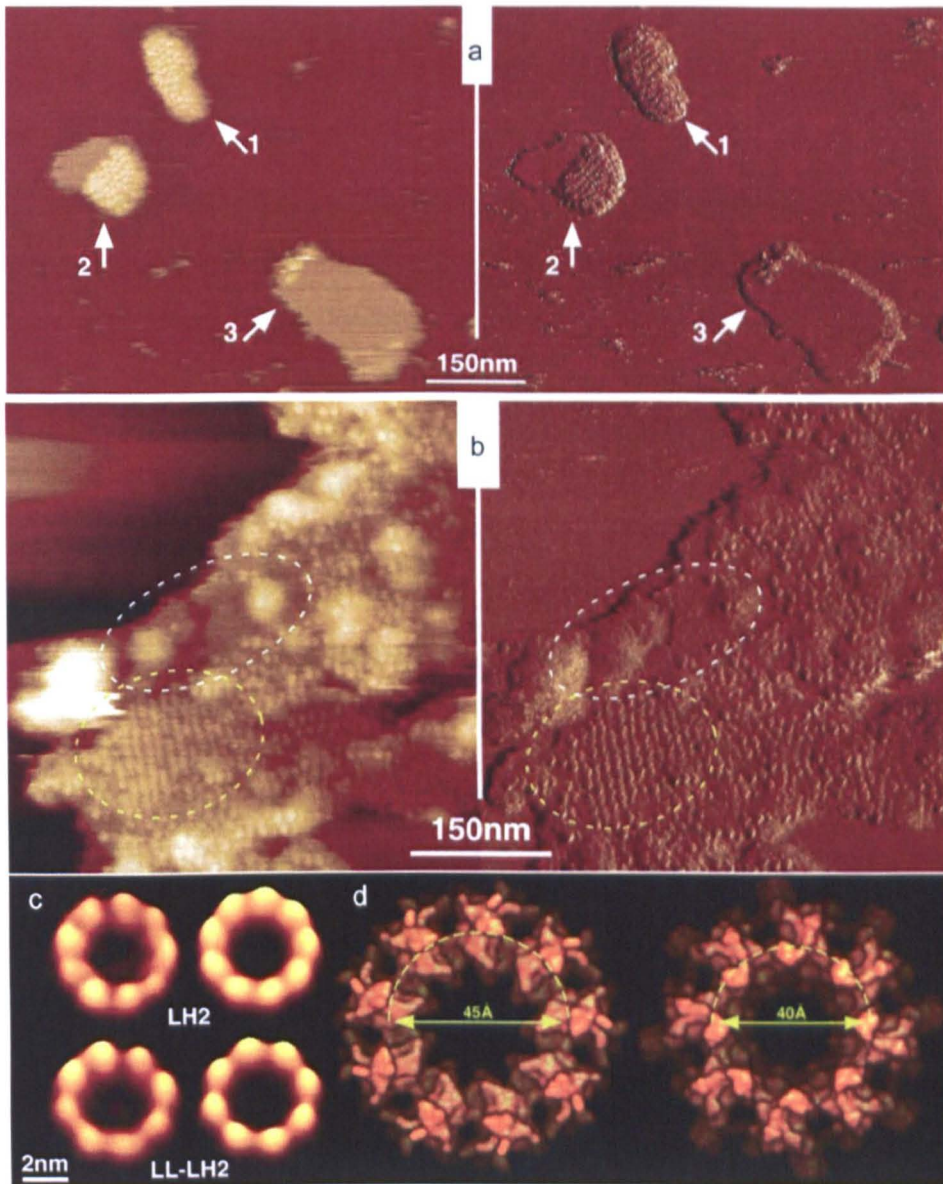


**Figure 1.16 Analysis of membrane organisation and its associated structures in *Rps. palustris* by AFM.**

**a.** The three different classes of membrane patches observed under high light conditions. 1. shows areas of densely packed complexes. 2. shows areas of complex segregating within large areas of protein free lipid. 3. shows areas of lipid devoid of protein. The image on the right depicts height, while the corresponding image on the left shows the measured deflection.

**b.** AFM Images of low light membranes are shown. Areas containing densely packed core complexes are seen (yellow dashed line). Areas of only LH2 are also observed (white dashed line)

**c.** LH2 and LL-LH2 are compared. The image shows averaged height images of many highly resolved complexes. LH2 are nonomeric. LL-LH2 are octomeric.

**d.** A comparison of the average radius of the LH2 and LL-LH2 complexes is shown. LH2 is seen to measure ~45 Å, while LL-LH2 measure ~40 Å.

Images were adapted from published data (Scheuring *et al.*, 2006)

### 1.8.1 Self assembled monolayers

SAMs are spontaneously formed regular arrays of organic molecules. These molecules are adsorbed onto solid surfaces (usually metals or metal oxides) from a solution (and sometimes gaseous) phase, resulting in the formation of thin crystalline or semi-crystalline films. The ligands that form SAMs possess a head group with a high affinity for the surface and a tail group which becomes the exposed surface of the SAM. The tail group can be specifically customized to introduce a wide range of surface chemistries to the exposed SAM.

SAMs make ideal candidates as the chosen substrate for the patterning of bio-molecules for a number of reasons. Their creation is simple and they remain stable at varying temperatures (up to ~70 °C). The well ordered surface of the SAM can be manipulated by changing the exposed tail group, allowing interactions with the bio-molecule to be modified to the user's specifications. The binding of linker molecules to the tail groups can also confer specificity, allowing attachment of the bio-molecule either electrostatically or covalently. The patterning of SAMs can be done using a variety of different techniques and can be carried out on a very small scale, with features below 100 nm in size being reported. Investigations into monolayer formation kinetics have utilised contact angle studies, infra-red spectroscopy, ellipsometry and X-ray photoelectron spectroscopy (Bain *et al.*, 1988). Evidence to date suggests the majority (90 %) of the monolayer is formed within 2 min, with the remaining 10 % forming in the following 18 hr. More recent work agrees with this premise, but claims the kinetics of adsorption are more complex than first thought (Huang and Hemminger, 1993; Pan *et al.*, 1996).

The most extensively studied class of SAMs are constructed using alkanethiols, which carry a thiol moiety as the head group and have a very high affinity for the noble metals. Their formation on gold, silver, copper, platinum and palladium has been extensively investigated (Laibinis *et al.*, 1991; Biebuyck *et al.*, 1994; Li *et al.*, 2003; Love *et al.*, 2003). The alkanethiol incorporates either an alkyl chain (which may be saturated) or an aryl group, with a tail group that can be tailored to give the exposed

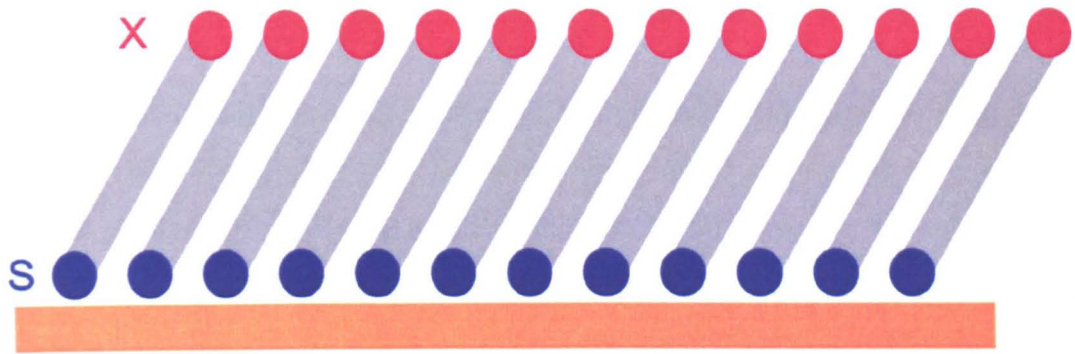
interface the required characteristics for further modification. The alkanethiols have a tilt angle of  $30^\circ$  and form a layer  $\sim 1\text{-}2$  nm thick (Figure 1.17A).

As previously mentioned, the exposed tail group of the alkanethiol monolayers can be tailored to further functionalise the monolayer. The bio-molecules can be attached directly to the tail group if its specific chemistry promotes protein adhesion. The use of electrostatic interactions to immobilise proteins is comparatively simple, and has the benefit of being easily reversible while the biological activity of the protein is often maintained (Topoglidis *et al.*, 2001). However, the interactions are non-specific and the orientation of the bio-molecules on the surface is difficult to control. Alternatively, the tail group can be used to attach a chemical linker to the surface which is capable of binding covalently to the surface exposed residues of proteins. Covalently attaching proteins is of use due to the high stability of the bond, and the ability to control protein orientation at the surface. One of the most studied methods of covalent protein tethering utilises a peptide bond, reacting a carbodiimide and N-hydroxysuccinimide (NHS) with a carboxylic acid tail group to form an active ester. This active ester can be further reacted with a protein solution and will form a covalent bond via any exposed amine groups (usually Lys residues) on the protein surface (Figure 1.17B). The creation of SAMs which poses a surface chemistry that repel proteins are also well characterised, with oligoethylene glycol linker molecules being used to create non-biofouling surfaces (Vanderah *et al.*, 2002)

## 1.8.2 Photolithography

There are numerous lithographic techniques available for the micro and nanofabrication of chemical surfaces. The most utilised methods are photolithography, particle beam lithography, and soft lithography. Photolithographic methods all share the same operational principle. That is to say an appropriate material is exposed to electromagnetic radiation at a selected wavelength, creating a set of chemical changes in the molecular structure of the material. A latent image is created on the regions of the material exposed to the radiation and this image is used as a template for the final

A



B

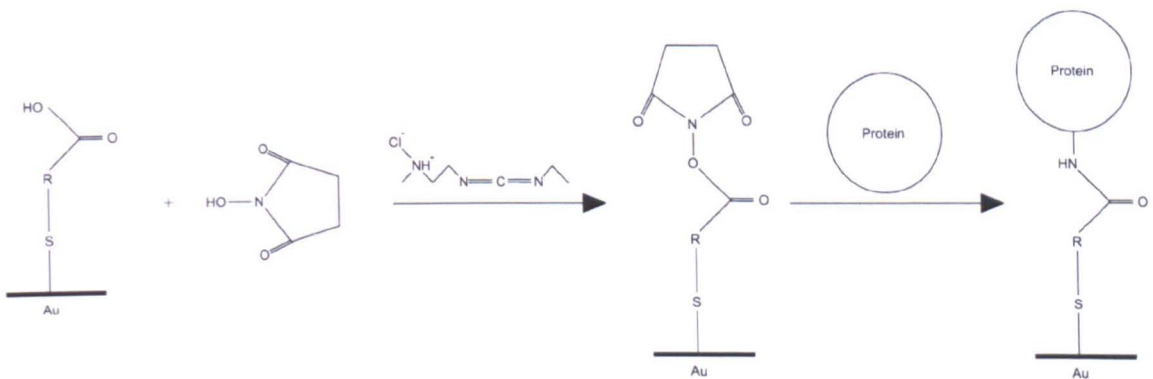


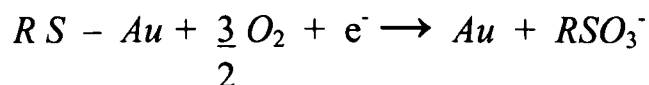
**Figure 1.17 Self Assembled Monolayers (SAMs)**

**A.** Alkanethiol monolayer on a gold surface is shown. Thiol moieties are shown in blue, the variable tail group is shown in red.

**B.** Mechanism of protein attachment via N(3-Dimethylaminopropyl)-N'-ethylcarbodiimide hydrochloride (EDC)/NHS crosslinking to a carboxylic acid terminated alkanethiol SAM.

patterning process. Many SAMs undergo chemical changes when exposed to UV radiation, making them ideal candidates for patterning by photolithography.

SAMs of alkanethiols on gold substrate undergo oxidation upon exposure to UV radiation in air, with the S-Au thiolate bond being converted to a more weakly bound sulfonate group ( $RSO_3^-$ ) (Huang and Hemminger, 1993), however this mechanism of oxidation is still not completely understood. It was initially thought the species responsible for thiolate oxidation is the ozone produced by UV photolysis of  $O_2$  (Norrod *et al.*, 1998. Zhang *et al.*, 1999), it is not known however if it is the ozone, or the singlet oxygen molecules generated by the degradation of the ozone at the metal surface, that are responsible for the oxidation. Recent work by Leggett *et al.*, (2004) reproduced the oxidation experiments in ozone free conditions and still found  $RSO_3^-$  to be present. It was proposed the reaction proceeds in the following way:



It is thought the reaction is initiated by 'hot electrons' being ejected from the metal surface upon irradiation with UV light. In order for the photo-oxidation to occur oxygen must penetrate the alkyl chain of the SAM, for this reason longer chain SAMs require increased exposure times to achieve complete oxidation (Cooper and Leggett, 1998).

After oxidation the sulfonates can be either washed away using a polar solvent such as water or ethanol, or alternatively they can be displaced by another alkanethiol. This mechanism of displacement can be utilised to pattern areas with contrasting surface chemistries. If a mask is placed over a SAM prior to photo-oxidation, the areas protected from the radiation will maintain their strong thiolate bond, while those exposed can be displaced by a new alkanethiol molecule. This technique is an inexpensive way of creating reliably patterned SAMs, which carry different properties with regards to protein adsorption. However, the size of the features possible to create

using this technique is limited by the size of the masks which can be easily manufactured.

## 1.9 Principles of atomic force microscopy

AFM (Binnig *et al.*, 1986) has evolved into a sensitive tool for the elucidation of membrane topology, capable of imaging the surface of fragile biological samples under physiologically relevant conditions with a lateral resolution of  $\sim 6 \text{ \AA}$  and a vertical resolution of  $1 \text{ \AA}$  (Müller *et al.*, 1995; Schabert *et al.*, 1995; Czajkowsky & Shao, 1998; Scheuring *et al.*, 1999; Fotiadis *et al.*, 2000; Scheuring *et al.*, 2003; Fotiadis *et al.*, 2003). Its ability to image biological samples directly at the nanometre scale has proved invaluable in answering questions regarding protein-protein interactions as well as native membrane architecture (Bahatyrova *et al.*, 2004; Schuering *et al.*, 2006).

In general, samples are scanned with a sharp probe (tip) which is mounted to the free end of a cantilever. Forces between the sample and the tip cause deflection in the cantilever. These forces are recorded by a reflected laser beam from the back of the cantilever onto a split photodiode array. This array measures both the vertical and horizontal deflections of the beam. The tip is moved using a piezoelectric scanner, which is controlled by a feedback loop with the photodiode.

As the cantilever approaches a surface, an attractive force is exerted upon it by the surface. This attraction reaches a maximum point, if the cantilever is brought still closer to the surface a strong repulsive force is exerted upon it. These effects are known as a force curve (Binnig *et al.*, 1986). Two modes of imaging are used primarily when imaging biological samples. Contact mode imaging maintains the tip in constant contact with the surface. Repulsive forces are recorded as the sample surface is scanned, providing the topological information. Tapping mode<sup>TM</sup> involves oscillating the cantilever at its resonant frequency, through the attractive and repulsive regions of the force curve, so that it is intermittently brought into contact with the

surface. This intermittent force applies less lateral force to a surface and so is ideally suited to imaging fragile samples such as biological membranes.

## Chapter 2: Materials and Methods

### 2.1 Materials

Unless otherwise stated, chemicals were obtained from Sigma Chemical Co. and were of analytical grade. All chemicals for SDS-PAGE were purchased from Invitrogen™ UK.

### 2.2 Standard buffers, reagents and media

All buffers and culture media were prepared as described in Sambrook *et al.* (1989), unless otherwise stated. Growth media were prepared using deionised water. Solutions for DNA work were prepared using distilled water which was further purified by passage through a Milli-Q system (Millipore) or NANOpure Diamond™ system. Analar-grade reagents were used for DNA work. Growth media and solutions used for DNA work were sterilised by autoclaving at 15 psi for at least 20 min, or by filtration through 0.45 µm filters. Heat-labile solutions, such as vitamins and antibiotics, were only added to culture media once it had cooled to below 50 °C.

### 2.3 *Escherichia coli* strains

All *E. coli* strains used in this work are listed in Appendix I. Strains were grown in Luria-Bertani (LB) medium (Sambrook *et al.*, 1989) with antibiotics added, when required, at the following concentrations (µg ml<sup>-1</sup>): neomycin, 30, or 20; streptomycin, 1000 (high); ampicillin, 200; tetracycline, 10. To select for insertion into the *lacZ* gene of pUC-derived plasmids, 5-bromo-4-chloro-3-indolyl-β-D-galactoside (X-gal) and isopropyl-β-D-thiogalactopyranoside (IPTG) were used at concentrations of 120 µg ml<sup>-1</sup> and 80 µg ml<sup>-1</sup>, respectively.

Stocks of *E. coli* strains were maintained at -70 °C in LB medium supplemented with 15% (v/v) glycerol.

## **2.4 Production of *E. coli* competent cells**

Various *E. coli* strains were treated as described by Hanahan (1985). The competent cells were stored as 200  $\mu$ l aliquots at  $-70^{\circ}\text{C}$ .

## **2.5 Transformation of *E. coli* competent cells**

An aliquot of competent *E. coli* cells (prepared as in section 2.4) was thawed on ice. 10-50 ng of plasmid DNA in TE buffer (1 mM EDTA, 10 mM Tris, pH 8.0) were added to 100  $\mu$ l of the cell suspension in a 1.5 ml microcentrifuge tube. After incubation on ice for 30 min, the cells were heat-shocked at  $42^{\circ}\text{C}$  for 45 sec and then placed on ice for 5 min. Subsequently, 1 ml of SOC medium (2% (w/v) tryptone, 0.5% (w/v) yeast extract, 20 mM glucose, 10 mM NaCl, 2.5 mM KCl, 10 mM  $\text{MgCl}_2$ , 10 mM  $\text{MgSO}_4$ , at a final pH of 6.8-7.0) were added to the suspension, the cells were incubated at  $37^{\circ}\text{C}$  for 1 hr, and then spread on an LB agar plate with appropriate selection. Colonies were grown overnight at  $37^{\circ}\text{C}$ .

## **2.6 Nucleic acid manipulation**

### **2.6.1 Small-scale preparation of plasmid DNA (mini-prep)**

Small quantities of plasmid DNA were prepared using the FastPlasmid™ Miniprep DNA purification system (Eppendorf), according to the manufacturer's instructions, a copy of which can be downloaded from [www.eppendorf.com](http://www.eppendorf.com). Transformed *E. coli* cultures were grown overnight in sterile plastic 7 ml universals containing 3 ml of LB medium with the appropriate antibiotic selection at  $37^{\circ}\text{C}$  in an orbital shaker (180 rpm). The DNA pellets were resuspended in 30  $\mu$ l of TE buffer and stored at  $-20^{\circ}\text{C}$ . The yield was typically about 5  $\mu$ g of plasmid DNA per mini-prep.

### 2.6.2 Larger-scale preparation of plasmid DNA (midi-prep)

Larger quantities of plasmid DNA were prepared using the Plasmid Midi Kit (Qiagen), according to the manufacturer's instructions, a copy of which can be downloaded from [www.qiagen.com](http://www.qiagen.com). Transformed *E. coli* cultures were grown overnight in 250 ml conical flasks containing 100 ml of LB medium with the appropriate antibiotic selection at 37 °C in an orbital shaker (180 rpm). The DNA pellets were resuspended in 300 µl of TE buffer and stored at -20 °C. The yield was typically about 50 µg of plasmid DNA per midi-prep.

### 2.6.3 Polymerase chain reaction (PCR)

Site-directed mutagenesis of DNA fragments by the polymerase chain reaction (PCR) was performed by the Quikchange® method (Stratagene). Reactions were performed in a total volume of 50 µl containing 5 µl of 10x reaction buffer, 125 ng of each primer (Appendix I), 2 mM dNTPs and 2.5 units of ACCUZYME™ (Bioline). Primers were produced by MWG Biotech and resuspended in water to 100 ng µl<sup>-1</sup>. Reactions were carried out using conditions appropriate to the T<sub>m</sub> of the primers and the length of the fragment to be amplified, as specified in the Quikchange® Site-Directed Mutagenesis Kit instruction manual, a copy of which can be downloaded from [www.stratagene.com](http://www.stratagene.com). Primers were denatured for 30 sec at 95 °C followed by 20 cycles of amplification (95 °C, 30 sec; 55 °C, 1 min; 68 °C, 2.5 min) and a final extension for 5 min at 68 °C in a PHC-3 Thermal Cycler (Techne). Following amplification, PCR reactions were cleaned up *via* gel purification (section 2.6.7).

### 2.6.4 Restriction enzyme digestions

Restriction enzymes were purchased from New England Biolabs (USA) or Promega (UK), and the suppliers' instructions followed with regard to reaction buffers and incubation temperatures. All resulting Quikchange® PCR reactions had the addition of *DpnI* as stated in the Quikchange® Site-Directed Mutagenesis Kit instruction manual (Stratagene). The DNA was then gel-purified (section 2.6.7).

### 2.6.5 Dephosphorylation of DNA

The 5'-phosphate groups were removed from the ends of DNA fragments, where necessary, by the addition of 1 unit of calf intestinal phosphatase (Boehringer Mannheim) to a restriction digest at the end of the digestion period. Incubation was continued for a further 30 min at 37 °C. The reaction was then incubated at 65 °C for 10 min prior to DNA gel purification (section 2.6.7).

### 2.6.6 Agarose gel electrophoresis of DNA

Restriction enzyme digests, PCR reactions and purified DNA fragments were routinely analysed by electrophoresis through 0.8 % agarose gels in 1 x TAE (40mM Tris-acetate, 1mM EDTA) running buffer containing 0.5 µg ml<sup>-1</sup> ethidium bromide (Sambrook *et al.*, 1989). 6 x gel loading buffer (0.03 % bromophenol blue, 0.03 % xylene cyanol, 60 % glycerol, 60 mM EDTA in 10 mM Tris-HCl, pH 7.6) was added to DNA samples, and 10-500 ng of DNA were typically loaded per lane; 200 ng of 1 kb DNA ladder (Fermentas) was run as a marker alongside the samples in order to estimate the sizes of DNA fragments. DNA was visualised by exposure to a source of 254 nm ultraviolet light.

### 2.6.7 Recovery of DNA from agarose gels

DNA fragments requiring purification were electrophoresed through low-melting-point agarose gels in 1 x TAE. The desired fragment was excised from the gel and the gel slice incubated at 65 °C for 5-10 min. The DNA was extracted from the melted agarose using the QiaQuick Gel Extraction Kit (Qiagen), according to the manufacturer's instructions, a copy of which can be downloaded from [www.qiagen.com](http://www.qiagen.com).

### 2.6.8 Ligation of DNA fragments

Typically 10 ng of vector DNA and three molar equivalents of the desired insert fragment were ligated together in a total volume of 10 µl, containing 1 unit of T4 DNA ligase (Gibco BRL) and 1 x ligation buffer (50 mM Tris/HCl, pH 7.6, 10 mM MgCl<sub>2</sub>, 5 % (w/v) PEG 8000, 1 mM ATP, 1 mM DTT; King and Blakesley, 1986). Ligation mixtures were left at 12 °C overnight and then transformed into *E. coli* DH5-α cells as described in section 2.5.

## **2.7 DNA sequencing**

Plasmid DNA required for sequencing was transformed into *E. coli* DH5- $\alpha$  cells (sections 2.4 and 2.5). After overnight incubation at 37 °C colonies were stabbed into 1 ml LB medium with appropriate antibiotic selection contained in a 1.5 ml screw top microfuge tube. Samples were sent to Lark Technologies Inc. for sequencing. Results were returned by email and sequences analysed using DNA Star software programme

## **2.8 Protein Manipulation**

### **2.8.1 SDS-polyacrylamide gel electrophoresis (SDS-PAGE)**

Protein samples were separated by SDS-polyacrylamide gel electrophoresis using the NuPAGE™ pre-cast gel system produced by Invitrogen™ life technologies. The MES buffer system was used according to the manufacturer's instructions. A 12 % Bis-Tris polyacrylamide gel was used in all cases. All samples were heated at 37 °C for 30min prior to loading; 10-20  $\mu$ l were loaded per well. Protein bands were visualised by staining gels with Coomassie Brilliant Blue R250. The protein standards used were SeeBlue molecular weight markers (Invitrogen™).

### **2.8.2 Purification of proteins featured in this thesis**

The purification of proteins carried out as part of this study is detailed in Chapter 4.

### **2.8.3 Quantification of LH2 complex**

Absorbance units are used in this thesis to quantify amounts of light harvesting complex, rather than for example protein concentration. 1.0 Absorbance Unit (AU) of membrane sample or light harvesting complex is defined as 1 ml of material having an

absorbance of 1.0 with a pathlength of 1 cm. For example 50 ml of LH2 complex having  $A = 1.0$  is 50 AU, as is 500 ml of  $A = 0.1$ .

#### **2.8.4 Crystallisation trials of purified LH2**

LH2 was purified as in section 4.3.2. For crystallisation, the protein was concentrated to an absorbance of 100 at 850nm and stored at 4 °C prior to trials. The sitting drop method of vapour diffusion was used for each trial. Typically 1 ml of ammonium sulphate solution was added to the well of the crystallisation tray (Hampton Research) to form the reservoir. Initial screens saw 20  $\mu$ l of protein solution containing 0.1% LDAO, 3.5 % Benzamidine Hydrochloride, with varying concentrations of phosphate buffer and NaCl, being added to the sitting drop. Crystal trays were sealed and stored at 17 °C. Later screens utilised the Innovadyne Screenmaker 96+8 at Daresbury SRS. The sitting drop containing the protein solution was 400 nl in volume. A full list of all the crystallisation conditions that were screened is available in Appendix II .

#### **2.8.5 Screening of LH2 crystals**

The screening of crystals for their diffraction properties was carried out by Dr. Miroslav Papiz at Daresbury SRS. This was carried out at station 9.6, which was set at a wavelength of 0.92 Å. It has a single crystal Si(111) monochromator 20 m from the source, a vertical focusing 1.2 m mirror at 11 m from the source and a vertically microfocussing mirror (0.28 m long) 0.5 m from the sample. The beam used was 130 micron vertical x 150 micron horizontal in dimension. The detector is a Quantum 4 CCD detector (ADSC, California, U.S.A.). Crystals were screened within Free Mounting System (FMS) humidifier (Proteros Gmb, Germany)

#### **2.8.6 N-terminal sequencing of proteins**

Purified LH2 samples were denatured and the individual polypeptides were separated using SDS-PAGE. N-terminal sequencing of light harvesting polypeptides and of RSP6124 was carried out by Dr Arthur Moir at the Krebs Institute sequencing and synthesis facility.

#### **2.8.7 Mass spectroscopy of light harvesting polypeptides**

All mass spectroscopy was carried out by Dr Mark Dickman at the Chemical & Process Engineering Department, University of Sheffield. Purified light harvesting

complexes were mixed with Switchos solvent (3 % acetonitrile, 0.1 % formic acid) working in a total volume of ~ 7 $\mu$ l. Separation of the peptide mixture was carried out on an LC Packings Ultimate Nano-LC system with a flow rate of 300 nL min<sup>-1</sup> using the following buffers along a 0-70 gradient : Ultimate Solvent A: 5 % ACN, 0.1 % FA, Ultimate Solvent B: 95 % ACN, 0.1 % FA. The system is controlled by Chromeleon software (Dionex). Samples were passed through a pre-column for filtering and de-salting before the analytical C18 column (reverse phase material PepMAP<sup>TM</sup> 100 C18 silica, 100 Å pore size). The Nano-LC system is directly coupled to an Applied Systems QStarXL Hybrid ESI Q-ToF MS/MS. The range of the mass detector was limited to 300 to 2000 m/z and all data were collected with Analyst software (Applied Biosystems) settings in positive ion mode.

Identification of RSP6124 was carried out after tryptic digest of the purified LH2 sample was carried out. The enzymatically cleaved samples were then subjected to the same process as described previously in this section.

## **2.9 *Rhodobacter sphaeroides* strains**

*Rba. sphaeroides* strains used in this study are listed in Appendix I. Strains were grown in M22+ medium (Hunter and Turner, 1988); liquid cultures were supplemented with 0.1 % casamino acids. Antibiotics were used at the following concentrations ( $\mu$ g ml<sup>-1</sup>): tetracycline, 1.0; neomycin, 20; streptomycin, 5. Stocks of strains were maintained as for *E. coli*.

## **2.10 Growth of *Rba. sphaeroides***

### **2.10.1 Semi-aerobic growth**

*Rba. sphaeroides* cultures were grown semi-aerobically in the dark, conditions which induce maximal pigment synthesis (Niederman *et al.*, 1976). Single colonies were inoculated into 10 ml of M22+ and grown overnight at 34 °C with 180 r.p.m. shaking. The following day, each 10 ml culture was added to 70 ml of M22+ in a 100 ml conical flask. This was shaken overnight at 180 rpm at 34 °C, after which time the

cells were suitable for spectral analysis. The culture could be further increased by transferring into a 2 litre flask containing a total volume of 1.6 litres of M22+.

### **2.10.2 Photosynthetic growth**

For growth under photosynthetic conditions, 2 litre semi-aerobic cultures were used to inoculate a 20 litre culture flask completely filled with M22+ media. This was capped tightly with a rubber bung and placed under low light intensity (5 W/m<sup>2</sup>) at room-temperature. The internal temperature of the culture was regulated by a water cooled element immersed within the culture flask.

## **2.11 Conjugative transfer of plasmid DNA from *E. coli* to *Rba. sphaeroides***

A simplified form of the method of Hunter and Turner (1988) was used to transfer pRK derivatives from *E. coli* strain S17-1 into *Rba. sphaeroides*. 10 ml of *Rba. sphaeroides* cells, grown overnight in semi-aerobic culture, were pelleted and resuspended in 1 ml of LB medium. To 100 µl of this suspension, a single fresh *E. coli* colony was added, and the cells mixed by vortexing. The mixture was pipetted onto well-dried LB agar, allowed to dry into the medium, and incubated for 6-8 hours at 34 °C. The dried patch of cells was then scraped off the plate and resuspended in 1 ml of M22+ medium. 100 µl of resuspended cells was spread onto each of several M22+ agar plates with appropriate antibiotic selection. Transconjugant *Rba. sphaeroides* colonies appeared after 4-6 days incubation at 34 °C.

## **2.12 Membrane preparation from *Rba. sphaeroides***

### **2.12.1 Intracytoplasmic membrane preparation**

Unless otherwise stated, all intracytoplasmic membranes (ICMs) were prepared as described in Jones *et al.* (1994) and stored at -20 °C until required. All steps were

performed, as far as possible, at 4 °C. Harvested cells were resuspended in 10 ml of membrane buffer (1 mM Tris-HCl, 1 mM EDTA, pH 7.5), a few grains of DNase I were added, and the cells disrupted in a French pressure cell at 18,000 psi. The broken cells were layered onto a discontinuous (15-40 % w/v) sucrose gradient, and the gradient centrifuged in a Beckmann Ti45 rotor at 27,000 rpm (57000 x g) for 16 hr. The ICM fraction formed a band just above the 15 % - 40 % interface, and was collected with a micropipette.

### **2.12.2 ICM partial solubilisation and fractionation**

ICM prepared as described in section 2.11.1 was pelleted by ultracentrifugation at 100,000 x g for 4 hr and resuspended with gentle homogenisation in 50 mM HEPES buffer at pH 8.0 containing 0.03 %  $\beta$  DDM (Buffer A) to A=16 at 850 nm in a total volume of 200  $\mu$ l. When required membranes were solubilised by the addition of  $\beta$ -DDM dropwise from a 10 % w/v stock in buffer B. Samples were incubated on ice in the dark for 15 min with occasional gentle mixing 250  $\mu$ l of sample per gradient was loaded onto a 20/25/30/35/40/50 % w/w sucrose density step gradient in buffer A and centrifuged for 20 hr at 200000 x g. Pigmented fractions were harvested using a sterile, blunted hypodermic syringe and frozen at -20 °C until required.  $\beta$ -DDM of  $\geq$  99.5 % purity was sourced from Glycon Biochemicals, TGZ, Zapfholzweg, 1 D-14943 Luckenwalde, Germany

## **2.13 Spectroscopy**

### **2.13.1 Room temperature absorbance spectra**

Absorbance spectra of purified LH2 complexes and membrane fractions were recorded on a Cary 50 UV-Vis spectrophotometer between 250-950 nm. Baselines were corrected and spectra were processed with Datamax/Grams 32 software as required (Jobin Yvon Ltd. U.S.A.).

### **2.13.2 Low temperature absorbance spectra**

Absorbance spectra were recorded as described in section 2.13.1. Samples were cooled to 77 K in a OptistatDN-V optical cryostat made by Oxford Instruments. Samples were

suspended in a cryo-stable buffer comprising of 50 mM Tris, 55 % glycerol (v/v) 25 % sucrose (w/v).

### **2.13.3 Fluorescence spectroscopy**

All emission and excitation fluorescence spectra were recorded in a cryo-stable buffer comprising of 50 mM Tris, 55 % glycerol (v/v) 25 % sucrose (w/v). Samples were cooled to 77 K in a OptistatDN-V optical cryostat made by Oxford Instruments. Measurements were recorded on a SPEX FluoroLog spectrofluorimeter (SPEX Industries Inc.). Excitation was provided from a Tungsten light source in the visible-IR region of the spectrum.

## **2.14 Electron microscopy**

Samples were applied to glow discharged carbon coated copper grids and negatively stained with 0.75 % w/v uranyl formate. Images were recorded at 100 kV on a Philips CM100 microscope equipped with a Gatan Ultrascan 667 CCD camera at magnifications between X 5000 and X 52,000. Images were recorded by Dr Pu Qian at the Robert Hill Institute, Department of Molecular Biology and Biotechnology, University of Sheffield.

## **2.15 Self Assembled Monolayers**

### **2.15.1 Formation of evaporated gold surfaces**

Gold surfaces were prepared on glass slides by evaporation. This was done by Stefan Janusz and Nick Reynolds in the Department of Chemistry, University of Sheffield. Gold deposition was achieved using an Edwards Auto 306 evaporator system at a base pressure of  $1 \times 10^{-7}$  mbar. After deposition of the evaporated film, surfaces were left to cool in the evaporator then immediately placed into the alkane thiol solution to facilitate SAM formation.

### **2.15.2 Self Assembled Monolayer formation**

All SAMs were formed on the surface of freshly evaporated gold surfaces. The gold surface was placed in a HPLC grade ethanol solution containing 1 mM alkane thiol. Degassing of this solution by sparging with oxygen free N<sub>2</sub> gas for 20 min had taken place before insertion of the gold surface. The samples were left for 18 hr to ensure optimum monolayer coverage. After SAM formation, samples were sonicated to remove any aggregated material.

### **2.15.3 Photopatterning of SAMs**

The photopatterning of SAMs was carried out by Nick Reynolds and Stefan Janusz (Department of Chemistry, University of Sheffield). A Coherent Innova 300 C frequency doubled argon ion laser emitting light at 244 nm was used to photopattern SAMs of 1H,1H,2H,2H-Perfluorooctanethiol. An electron microscope square patterned grid (Agar Scientific, UK) was placed over the nitrogen dried SAM and held in place with a (UV transparent) quartz disk. The sample was then exposed to the beam (100 mW) via focusing lenses for a period of 12 min. After exposure, the patterned SAM was immediately placed in a solution of 1 mM mercaptoundecanoic acid and left for 2 hr to ensure the complete displacement of the sulfonates generated by the photopatterning.

## **2.16 Atomic force microscopy**

### **2.16.1 AFM of membrane fragments**

Membrane samples were prepared as described in section 2.11. A 1 in 20 dilution of sample solution (10 mM Hepes, pH 7.5) was adsorbed to the surface of freshly cleaved mica (Ted Pella, Redding, CA, USA). A small drop of adsorption buffer (10 mM Tris-HCl, pH 7.5, 150 mM KCl, 25 mM MgCl<sub>2</sub>) was applied to the mica surface to ensure a firm attachment of the membranes. At the same time 1 µl of the sample was injected into the thin film of adsorption buffer and left for 1-1.5 hr. The sample was then gently washed with the recording buffer (10 mM Tris-HCl, pH 7.5, 150 mM KCl) and placed onto the AFM stage, where 100 µl of recording buffer was added to the liquid cell.

Images were recorded on a Digital Instruments Nanoscope 4.0. NSP-20 Si<sub>3</sub>N<sub>4</sub> cantilevers (Veeco Instruments Ltd, UK) had a spring constant of 0.06 Nm<sup>-1</sup> and operating frequencies 7-10 kHz in liquid. AFM topographs were obtained using Tapping mode™ in liquid. The images with the highest resolution could be achieved when the free tapping amplitude was 1-2 nm and the amplitude setpoint was adjusted to minimal forces, resulting in the damping of the free amplitude by only 5-10 %. Images were recorded as 512 x 512 pixel arrays at a typical scanning frequency of 1-3 Hz. Quantitative analysis of the AFM topographs, was done using Scanning Probe Image Processor program (Image Metrology ApS, Lyngby, Denmark).

### **2.16.2 Atomic force fluorescence microscopy (AFFM)**

AFFM images were recorded using a custom built Atomic Force Fluorescence Microscope (Kassies, Thesis 2005). This machine combines an AFM with a confocal microscope, allowing for the simultaneous capture of both optical and topographic details of the sample being imaged. The confocal microscope used a diode laser (RLT80010MG,  $\lambda = 800$  nm, Roithner Laser Technik, Vienna, Austria) as the excitation source. The fluorescent light was captured using either a single photon counting avalanche photo diode (APD) (SPCM-AQR-14, Perkin Elmer Optoelectronics) or by a Charge Coupled Device (CCD) camera (Spec-10:100B, Princeton Instruments). AFFM images were recorded by Nick Reynolds, Chemistry Department, University of Sheffield and Mariana Escalantarium at the Biophysical Techniques Group, Department of Science & Technology, BMTI, MESA, University of Twente, Enschede, The Netherlands.

### **2.16.3 Friction Force Microscopy**

Friction force microscopy was carried out by Nick Reynolds at the chemistry Department, University of Sheffield. Friction images were generated in contact mode by scanning the tip across the sample surface at 90 ° to the sample normal. Scans were performed at a scan speed of 3 Hz over an area of 40µm. NSP-20 Si<sub>3</sub>N<sub>4</sub> cantilevers with a spring constant of 0.06 Nm<sup>-1</sup> were used for imaging (Veeco Instruments Ltd).

## 2.17 Surface Plasmon Resonance

All surface plasmon resonance studies were carried out using a Biacore3000 instrument (Biacore Life Sciences, GE Healthcare, UK). The LH2 complexes were purified as detailed in section 4.2.2. Purified LH2 complex ( $A = 12.5$ ) was injected onto the sensor chip at a rate of  $10 \mu\text{l min}^{-1}$  for a period of 10 min. The LH2 were exposed to a modified biacore sensor chip, possessing various SAM surface chemistries. The SAMs were adsorbed onto gold chips as described in section 2.15.1. Washing of the chip was carried out at a rate of  $30 \mu\text{l min}^{-1}$  for a period of 30 sec with a solution of 1 % sodium dodecyl sulphate (SDS). All spectra were analysed using Datamax/Grams 32 software (Jobin Yvon Ltd. U.S.A.).

## **Chapter 3:      The role of the Puc2B polypeptide in the LH2 complex of *Rhodobacter sphaeroides*.**

### **3.1    Summary**

The spectroscopic properties of the LH2 complex from *Rba. sphaeroides* have been extensively characterised. The elucidation of the genome sequence of this organism has provided new insight into the genetic components which are expressed to comprise the polypeptides that assemble to form this pigment-protein complex. The second *puc* operon encodes two polypeptides, Puc2B and Puc2A, which are transcribed and translated. Puc2B is assembled into LH2 complexes whilst Puc2A is found in ICM but not incorporated into LH2 complexes.

The work in this chapter details the attempts to assign any contribution which Puc2B makes to the binding of BChl(s) within the LH2 complex, and thus measure any effect it has on the spectroscopic properties of the complex. Mass spectroscopy has allowed the incorporation of Puc2B within the LH2 complex to be observed for the first time in native complexes.

The effect the second *puc* operon has on the ability of the cell to adapt to high light conditions is measured, with this gene pair being shown to be crucial in modulating LH2 complex levels under these conditions.

Initial attempts to analyse any effects the second *puc* operon has upon the membrane architecture were attempted using AFM. Images of *Rba. sphaeroides* 2.4.1.  $\Delta 2BA$  were obtained, with the regular hexagonal packing of LH2 complexes in large scale arrays being observed for the first time.

## 3.2 Introduction

The existence of multiple operons encoding polypeptides that assemble into the LH2 complexes of photosynthetic organisms has been known for some time, this being the case for both *Rps. acidophila* and *Rps palustris* (Tadros and Waterkamp., 1989; Tadros *et al.*, 1993; Gardiner *et al.*, 1996). Before publication of the genome sequence of *Rba. sphaeroides* ([www.rhodobacter.org](http://www.rhodobacter.org)) it had been thought the organism possessed only one *puc* operon (*puc1BAC*). However, it is now known that the  $\beta$ -polypeptides comprising the LH2 complexes in *Rba. sphaeroides* are comprised of two populations, designated Puc1B and Puc2B (Zeng *et al.*, 2003). Several mutagenesis studies were previously carried out under the assumption that only Puc1B was present within the LH2 complex. For example, Fowler *et al.*, (1997) produced a series of site directed mutants designed to replace the  $\beta$ Arg<sub>10</sub> residue of the LH2 complex. These mutants assembled LH2 complexes which displayed a range of blue shifted B800 peaks.

The mutagenesis studies above were carried out under the assumption that the genes encoding the LH2 apoproteins had been removed by the insertion of a streptomycin resistance cassette replacing the *puc 1BAC* operon (Jones *et al.*, 1992). However, as stated previously, genome sequencing ([www.rhodobacter.org](http://www.rhodobacter.org)) has revealed the presence of a second *puc* operon, designated *puc2BA* (Zeng *et al.*, 2003). It has been demonstrated that *puc2B* is transcribed and translated, forming Puc2B, with three amino acid changes when compared to Puc1B; these are  $\beta$ Lys<sub>35</sub>→Pro,  $\beta$ Asn<sub>34</sub>→Lys and  $\beta$ Val<sub>25</sub>→Ile (Zeng *et al.*, 2003).

The work carried out by Zeng *et al.*, (2003) also established that the incorporation of Puc2B into the LH2 complex occurs in *Rba. sphaeroides*. Results also demonstrated that the B800 and B850 absorbance properties of complexes in which the  $\beta$ -polypeptide was either Puc1B, or a mixture of Puc1B and Puc2B, are unchanged. However, these measurements were carried out at room temperature on immunoprecipitated LH2 complexes. These complexes were made up of chimeric  $\alpha$ - and  $\beta$ - apoproteins which had been combined with PhoA fusion proteins. This chapter endeavours to build on this work, attempting to analyse the spectroscopic contribution

Puc2B makes within the LH2 complex more stringently and to quantify the contribution of Puc2B to the complex previously assumed to be Puc1B1A. Zeng *et al.*, (2003) measured the absorbance of immunoprecipitated LH2 derived from PhoA fusion proteins. This work characterises the spectroscopic properties of LH2 complexes solubilised from native membranes and purified to homogeneity.

The extent to which the Puc2B polypeptide is incorporated within LH2 in wild type complexes is currently unknown, as is the role of this polypeptide within the LH2 complex, or within the context of the photosynthetic membrane. This chapter presents results which analyse the low temperature absorbance and fluorescence properties of LH2 complexes containing, in addition to Puc1A, exclusively Puc1B, exclusively Puc2B, or a mixture of both polypeptides (wild type). Attempts have been made to assess the level of contribution Puc2B makes to the ring of nine  $\beta$ -polypeptides present in the LH2 complex. The phenotype of a *puc2BA* deletion mutant is explored under differing light conditions and AFM is used to assess the ICM architecture in the same deletion mutant.

### 3.3 Results

#### 3.3.1 The creation of the strain *Rba. sphaeroides* 2.4.1. $\Delta 1BA-\Delta 2BA$ (pRKCBC1-2B1AC), which has an LH2 complex comprising Puc2B1A.

##### 3.3.1.1 Site directed mutagenesis of *puc1B*

The plasmid pUCHS27 (Appendix I) was used to create a pseudo *puc* operon, containing the genes *puc2B1AC*. Site directed mutagenesis was performed using two rounds of QuikChange<sup>TM</sup>PCR on the wild type *puc1B* gene contained within pUCHS27, producing the plasmid pUCHS27-2B1A. The conditions used in these PCR reactions are detailed in section 2.6.3. The first round produced the residue changes  $\beta\text{Lys}_{.35}\rightarrow\text{Pro}$ ,  $\beta\text{Asn}_{.34}\rightarrow\text{Lys}$ , using the primers P1-2B and P2-2B; the sequences of these primers can be found in Appendix I. The second round of PCR produced the residue change  $\beta\text{Val}_{.25}\rightarrow\beta\text{Ile}_{.25}$ . The primers used in this reaction were P3-2B and P4-2B; the sequences of these primers can be found in Appendix I. The resulting plasmid

was isolated and the modified gene sequence was confirmed using sequencing reactions carried out by Lark Technologies Ltd, UK (Figure 3.1, Figure 3.2A and B).

### **3.3.1.2 Subcloning of the *puc2B1A* genes and conjugation into the deletion mutant *Rba. sphaeroides* $\Delta 1BA-\Delta 2BA$**

The *puc2B1A* genes were sub-cloned from the plasmid pUCHS27-2B1A, into the plasmid pRKCBC1, creating the plasmid pRKCBC1-2B1AC (Figure 3.2D). pUCHS27-2B1A underwent digestion using the restriction enzymes *KpnI* and *BamHI*. The ~350bp fragment was ligated with linearised pRKCBC1, which had also undergone digestion using restriction enzymes *KpnI* and *BamHI*. The resulting plasmid was isolated and designated pRKCBC1-2B1A. The sequence of the cloned genes was again confirmed by sequencing reactions carried out by Lark Technologies Ltd, UK.

The pRKCBC1-2B1AC vector was transformed into *E.coli* *S17-1*, for conjugative transfer of pRKCBC1-2B1AC into the strain *Rba. sphaeroides* 2.4.1.  $\Delta 1BA-\Delta 2BA$  by the method described in section 2.11. This strain was received from Professor Samuel Kaplan's laboratory (University of Texas, U.S.A.). *Rba. sphaeroides* 2.4.1.  $\Delta 1BA-\Delta 2BA$  carries in-frame deletions of the *puc1BA* and *puc2BA* genes (Zeng *et al.*, 2003), creating a null LH2 background for observing expression from the pRKCBC-2B1AC plasmid. Cell growth was controlled by tetracycline resistance conferred by pRKCBC-2B1AC and whole cell spectra were recorded of the resulting colonies using a Guided Wave Model 260 spectrophotometer; the expression of the LH2 complex within these strains, as well as the acquired antibiotic resistance, confirmed successful complementation with the *puc2B1A* genes (Figure 3.2E and F).

## pUCHS27-2B1A

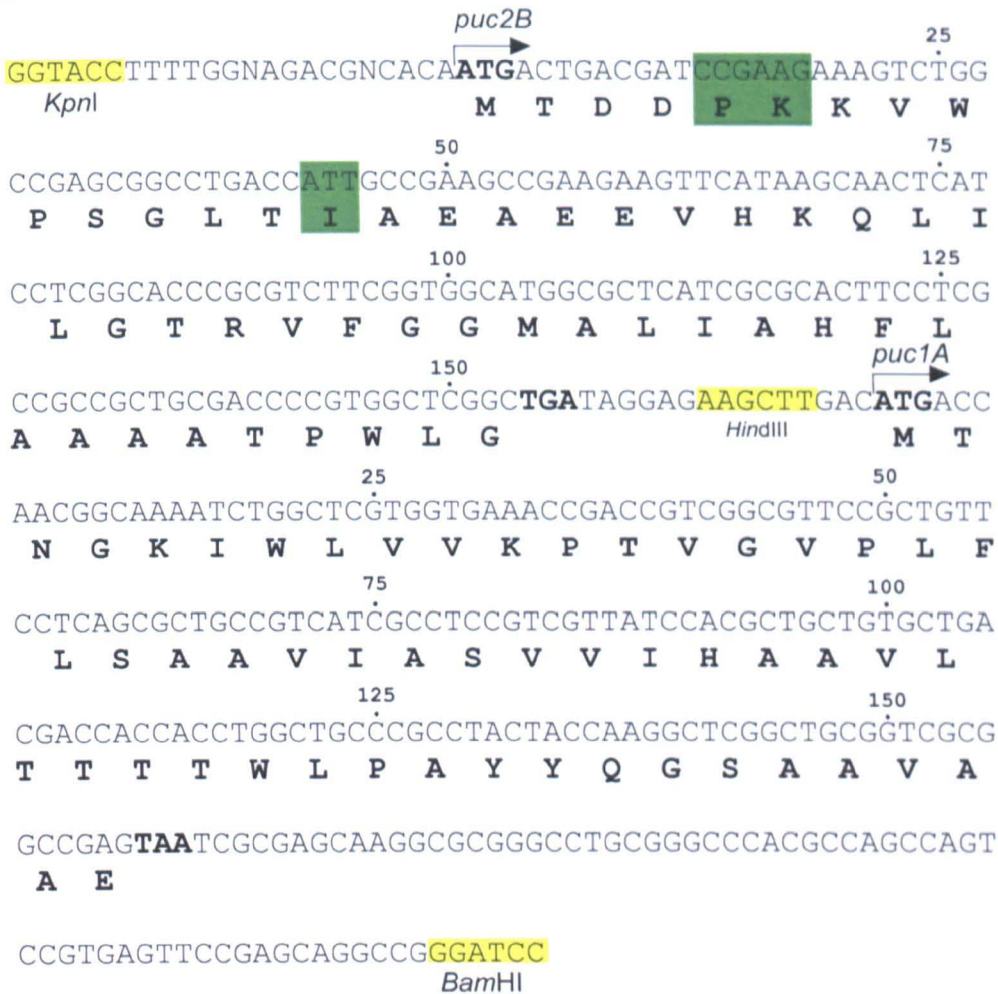


**Figure 3.1** A *puc2B1A* gene pair created by site directed mutagenesis

The sequence data obtained for pUCHS27-2B1A are shown. The mutated residues following conversion from 1B to 2B are highlighted in green. The restriction sites used during the cloning process are highlighted in yellow. Start and stop codons are shown in bold. Sequencing was carried out by Lark Technologies Ltd, UK.

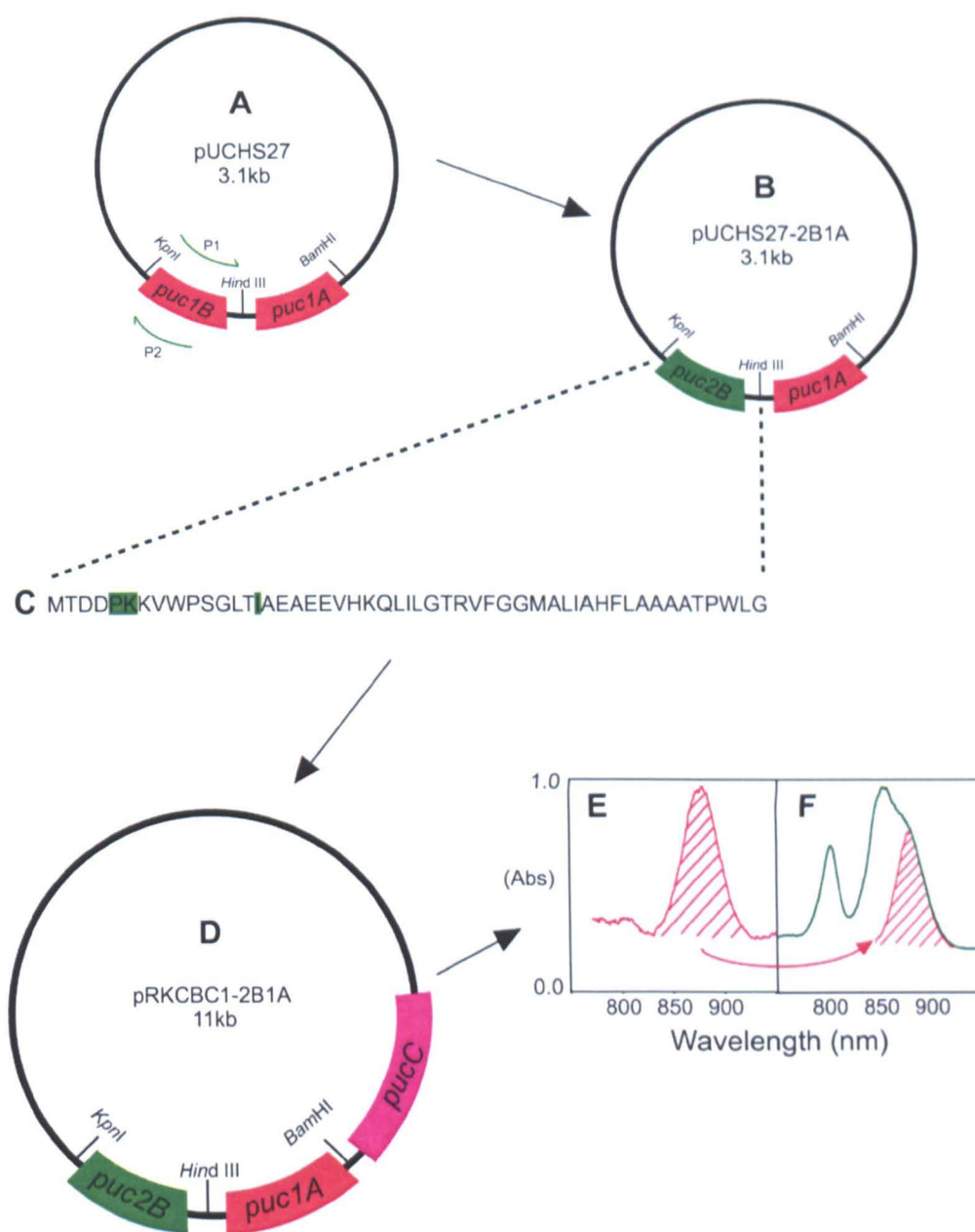


**Figure 3.2 Creation of transconjugant strain *Rba. sphaeroides*  $\Delta 1BA-\Delta 2BA(pRKCBC1-2B1AC)$**

- A. pUCHS27 vector used for the QuikChange mutagenesis *puc1B*. Primers P1 and P2 used to carry out the mutagenesis are detailed in Appendix I.
- B. pUCHS27-2B1A vector carries *puc2B* with *puc1A*.
- C. The Puc2B protein sequence obtained from pUCHS27-2B is shown.
- D. pRKCBC1-2B1A was created after insertion of the *puc2B-puc1A* genes into the multiple cloning site of pRKCBC1
- E. The absorbance spectrum of *R. sphaeroides* 2.4.1. $\Delta 1BA-\Delta 2BA$  is shown before complementation with pRKCBC1-2B1AC.
- F. The absorbance spectrum of *R. sphaeroides* 2.4.1. $\Delta 1BA-\Delta 2BA(pRKCBC1-2B1AC)$  is shown after complementation.

All spectra have been normalised to an absorbance of 1.0 at peak maxima for comparison

### 3.3.2 Spectroscopic comparison of purified LH2 complexes containing differing $\beta$ -polypeptide compositions.

Detailed in this section are the spectroscopic properties of three different LH2 complexes, purified from the strains *Rba. sphaeroides* 2.4.1., *Rba. sphaeroides* 2.4.1. $\Delta$ 2BA (which were provided by Professor Samuel Kaplan, University of Texas, U.S.A.), and *Rba. sphaeroides* 2.4.1. $\Delta$ 1BA- $\Delta$ 2BA (pRKCBC1-2B1AC) (section 3.3.1.2) (Appendix I). The only observable difference between the LH2 complexes in these three strains is the  $\beta$ -polypeptide composition of the LH2 complex they assemble. *Rba. sphaeroides* 2.4.1. produces a wild type complex, containing Puc1B, Puc2B and Puc1A, which is referred to in this study as WT-LH2. *Rba. sphaeroides* 2.4.1. $\Delta$ 2BA carries an in-frame deletion of the *puc2BA* operon, the LH2 complex assembled in this strain contains only the Puc1B  $\beta$ -polypeptide and is referred to in this study as LH2-1B1A. *Rba. sphaeroides*  $\Delta$ 1BA- $\Delta$ 2BA(pRKCBC1-2B1AC) assembles LH2 containing exclusively Puc2B, which is referred to in this study as LH2-2B1A. All the spectroscopic values of the complexes purified from these strains compared in sections 3.3.2.2, 3.3.2.3 and 3.3.2.4 are summarised in Table 3.1.

#### 3.3.2.1 Purification of the LH2 complexes.

All three strains described in section 3.3.2 were grown photosynthetically with an incident light level of  $5 \text{ W m}^{-2}$  as detailed in section 2.10.2. The purifications of the LH2 complexes from the three different cell stocks produced were carried out using the method detailed in section 4.3.2. The final purification product from each strain is shown by SDS-PAGE in Figure 3.3A. The purification procedure produces monodisperse complexes, as exemplified by the negative stain electron micrograph of purified LH2-1B1A (Figure 3.3B).

#### 3.3.2.2 LH2 absorbance properties

Absorbance spectra of WT-LH2, LH2-1B1A and LH2-2B1A were recorded at 77 K. Figure 3.4A shows that WT-LH2 absorbs maximally at 800 nm and 851nm. The B800:B850 peak height ratio is 0.96. The  $Q_x$  absorbance peak occurs at 588 nm. The carotenoid absorbance maxima occur at 453 nm, 479 nm, and

Complex	Absorbance maxima (nm)		Fluorescence excitation maxima (nm)		Fluorescence emission maxima (nm)			Fluorescence emission fwhm (nm)		
	B800	B850	B800	B850	Ex479	Ex590	Ex800	Ex479	Ex590	Ex800
WT-LH2(1B2B1A)	800	851	802	856	871	871	868	32	32	36
LH2-1B1A	800	851	801	855	871	871	870	32	32	33
LH2-2B1A	798	851	802	859	872	872	871	30	30	30

Complex	Carotenoid absorbance maxima (nm)			Q <sub>x</sub> absorbance maxima (nm)	Carotenoid fluorescence excitation maxima (nm)			Q <sub>x</sub> fluorescence excitation maxima (nm)
WT-LH2(1B2B1A)	453	479	515	588	457	483	518	593
LH2-1B1A	453	479	515	587	453	480	517	590
LH2-2B1A	453	479	515	585	458	485	520	592

**Table 3.1 The spectroscopic properties of WT-LH2, LH2-1B1A and LH2-2B1A**

A summary of the spectroscopic data detailed in Chapter 3 of this thesis is shown. The values quoted are derived from the spectra recorded at 77 K displayed in Figures 3.4, 3.5 and 3.6.

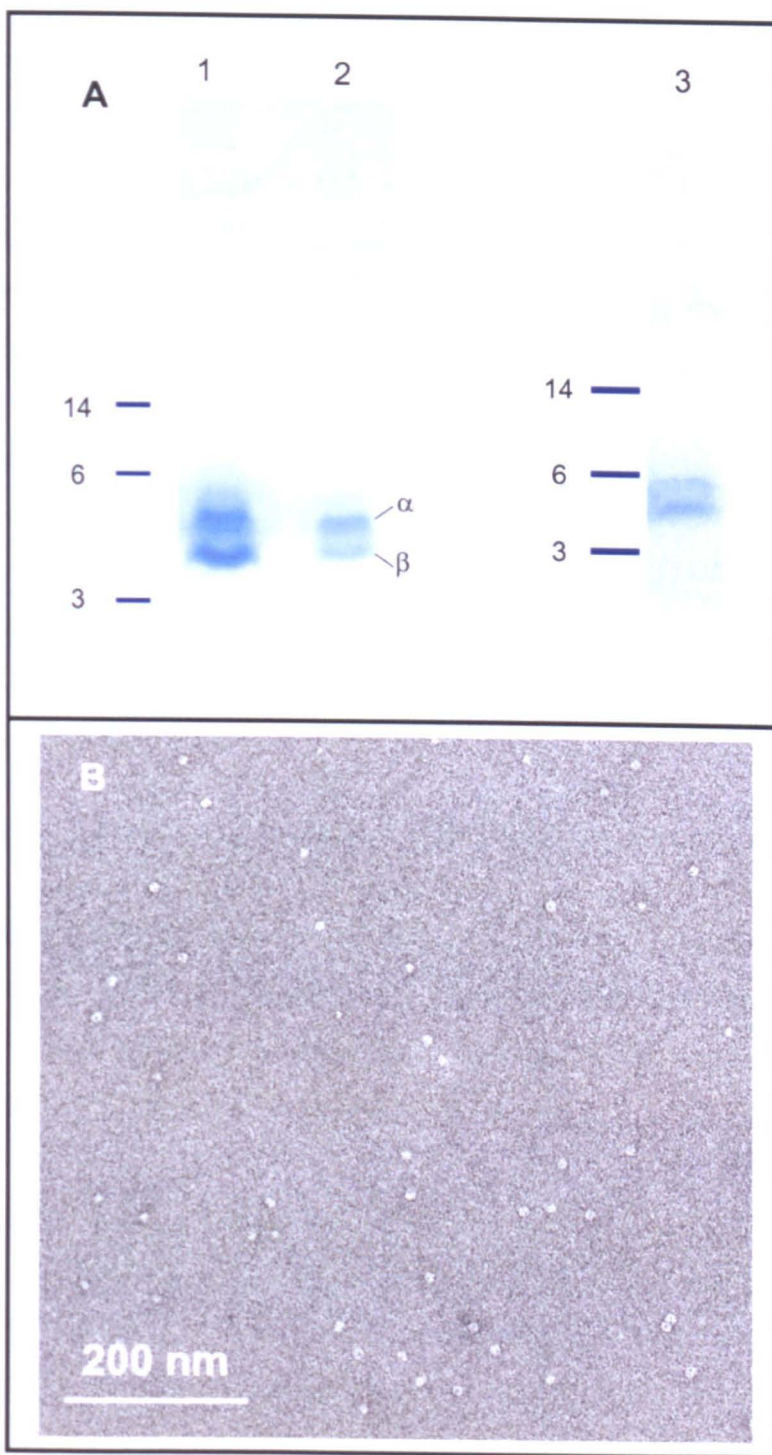


**Figure 3.3 Purification of WT-LH2, LH2-1B1A and LH2-2B1A**

A. A 12% SDS-PAGE of the final purification products of all three LH2 complexes

1. WT-LH2
2. LH2-2B1A
3. LH2-1B1A

Invitrogen SeeBlue™ MW markers are represented by blue lines

B. A negative stain electron micrograph showing purified monodispersed LH2. The sample was stained with 0.75% uranyl acetate. Electron microscopy was carried out by Dr Pu Qian (University of Sheffield).

515 nm, indicating the presence of spheroidene as the predominant form of bound carotenoid.

Figure 3.5A shows that LH2-1B1A also absorbs maximally at 800 nm and 851 nm, with a peak height ratio of 0.92. The  $Q_x$  absorbance peak occurs at 587 nm, a blue shift of 1 nm compared to WT-LH2. The carotenoid absorbance maxima are identical to those of WT-LH2.

The absorbance spectrum of the purified LH2-2B1A complex is shown in Figure 3.6A. The B800 absorbance peak at 798 nm is blue shifted by 2 nm with respect to WT-LH2, but the absorbance maximum at 851 nm is identical to that of the WT-LH2 complex. The B800:B850 peak height ratio is 0.95. The  $Q_x$  absorbance peak displays a blue shift of 3 nm, occurring at 585 nm. The carotenoid absorbance maxima are identical to those of WT-LH2.

### **3.3.2.3 Fluorescence excitation properties of WT and mutant LH2 complexes.**

The fluorescence excitation properties of each complex were compared at 77 K. The recorded spectra are shown in Figures 3.4B, 3.5B and 3.6B. Each spectra shown are the average of four separate scans. Excitation wavelengths between 400 nm and 870 nm were monitored at an emission wavelength of 890 nm.

Figure 3.4B shows the fluorescence excitation spectrum of WT-LH2. The B800 and B850 fluorescence peak maxima occur at 802 nm and 856 nm respectively. The  $Q_x$  fluorescence peak occurs at 593 nm, while the carotenoid fluorescence maxima occur at 457, 483 and 518 nm. Two small excitation peaks are seen at 730 and 753 nm.

Figure 3.5B shows the fluorescence excitation spectrum of LH2-1B1A, with maxima occurring at 801 nm and 855 nm (a red shift of 1 nm) respectively. The  $Q_x$  maximum is at 590 nm (a blue shift of 3 nm), while the carotenoid excitation maxima (453, 480, and 517 nm) all occur within 4 nm of those seen in WT-LH2.

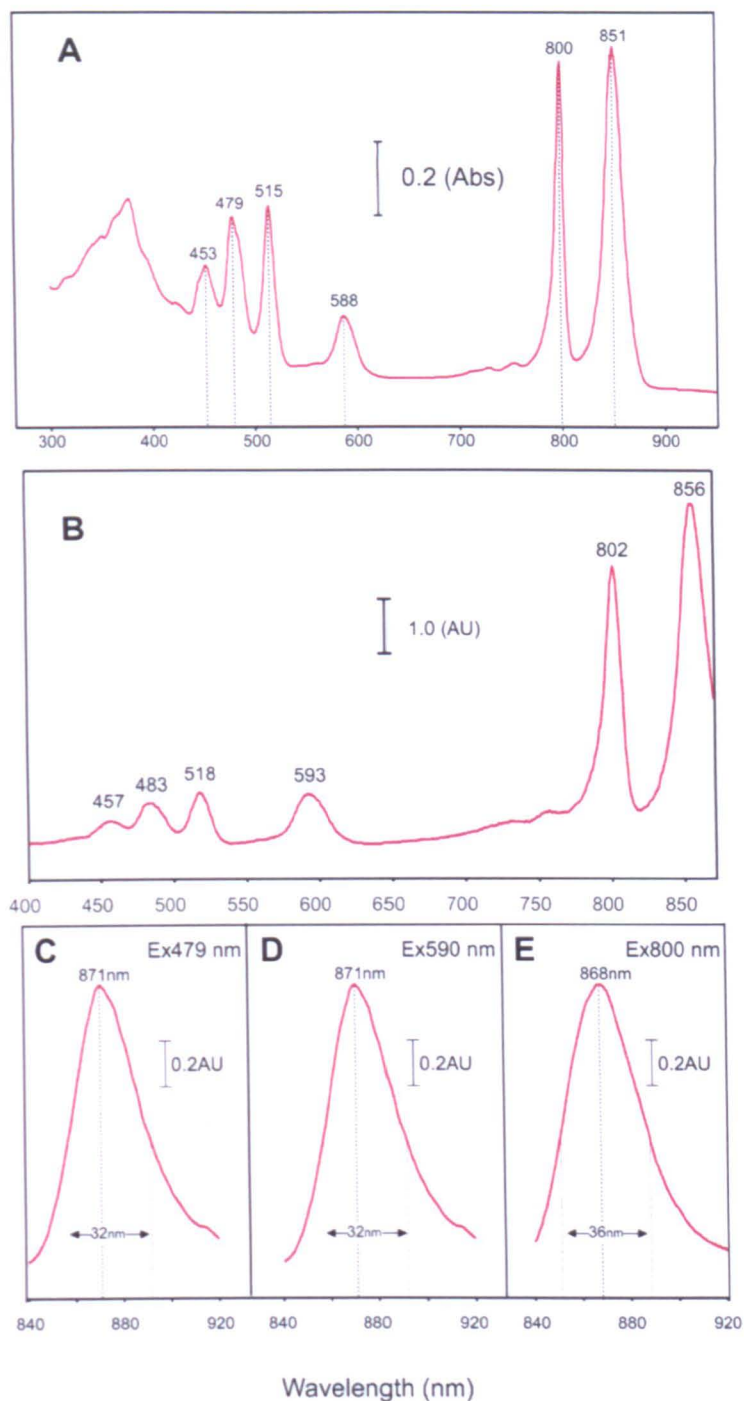


**Figure 3.4 Spectroscopic analysis of WT-LH2 at 77 K**

- A. Absorbance spectrum. Data have been normalised to an absorbance of 1.0 at 850nm
- B. Fluorescence excitation spectrum. Data have been normalised to 1.0 AU at  $Q_x$  maxima. Excitation slit widths of 1.25 mm and emission slit widths of 5 mm were used.
- C. Fluorescence emission spectrum with an excitation wavelength of 479nm.
- D. Fluorescence emission spectrum with an excitation wavelength of 590nm.
- E. Fluorescence emission spectrum with an excitation wavelength of 800nm

All fluorescence emission spectra have their peak maxima and full width half maxima labelled. The spectra have been normalised to 1 AU at peak maxima. Excitation slit widths of 2.5 mm and emission slit widths of 2.5 mm were used.

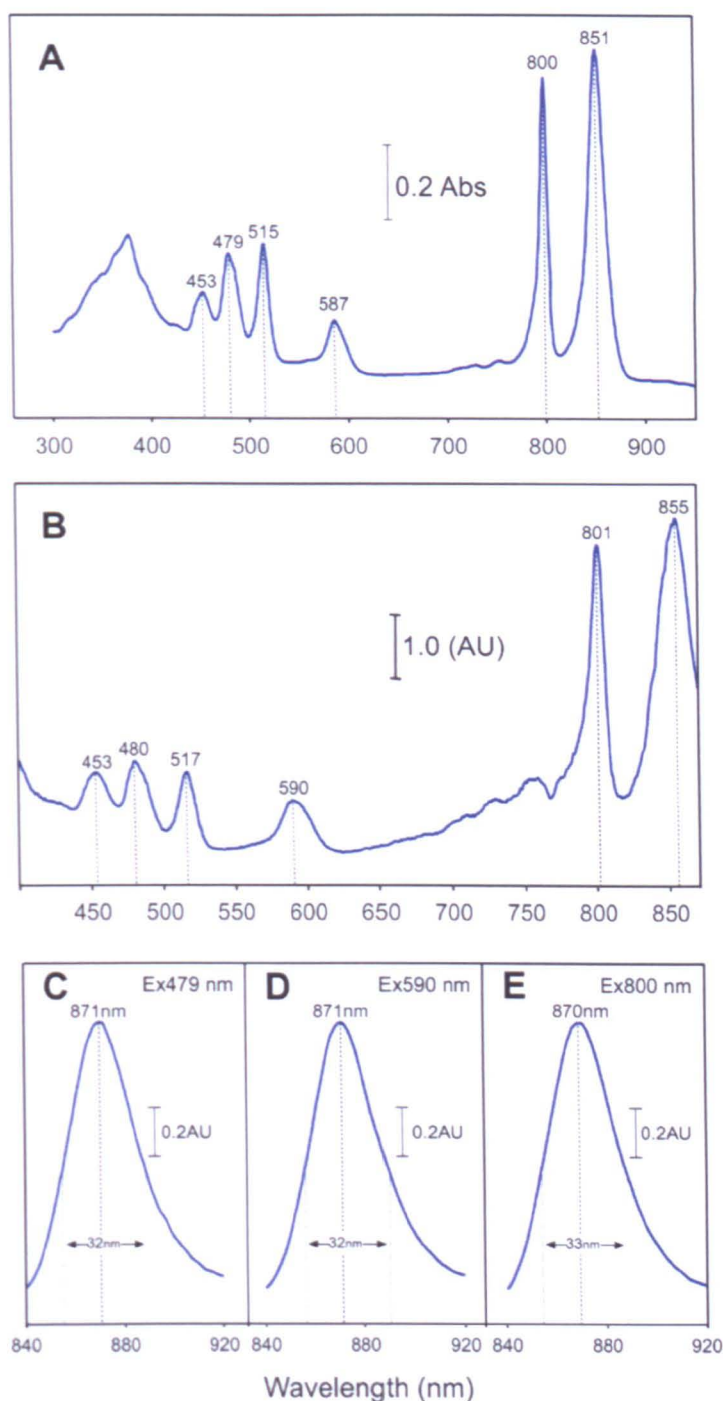


**Figure 3.5 Spectroscopic analysis of LH2-1B1A at 77 K**

- A. Absorbance spectrum. Data have been normalised to an absorbance of 1.0 at 850nm
- B. Fluorescence excitation spectrum. Data have been normalised to 1 AU at  $Q_x$  maxima for clarity with excitation slit widths of 1.25 mm and emission slit widths of 5 mm.
- C. Fluorescence emission spectrum with an excitation wavelength of 479nm.
- D. Fluorescence emission spectrum with an excitation wavelength of 590nm.
- E. Fluorescence emission spectrum with an excitation wavelength of 800nm

All fluorescence emission spectra have their peak maxima and full width half maxima labelled. The spectra has been normalised to 1 AU at peak maxima. Excitation slit widths of 2.5 mm and emission slit widths of 2.5 mm were used.

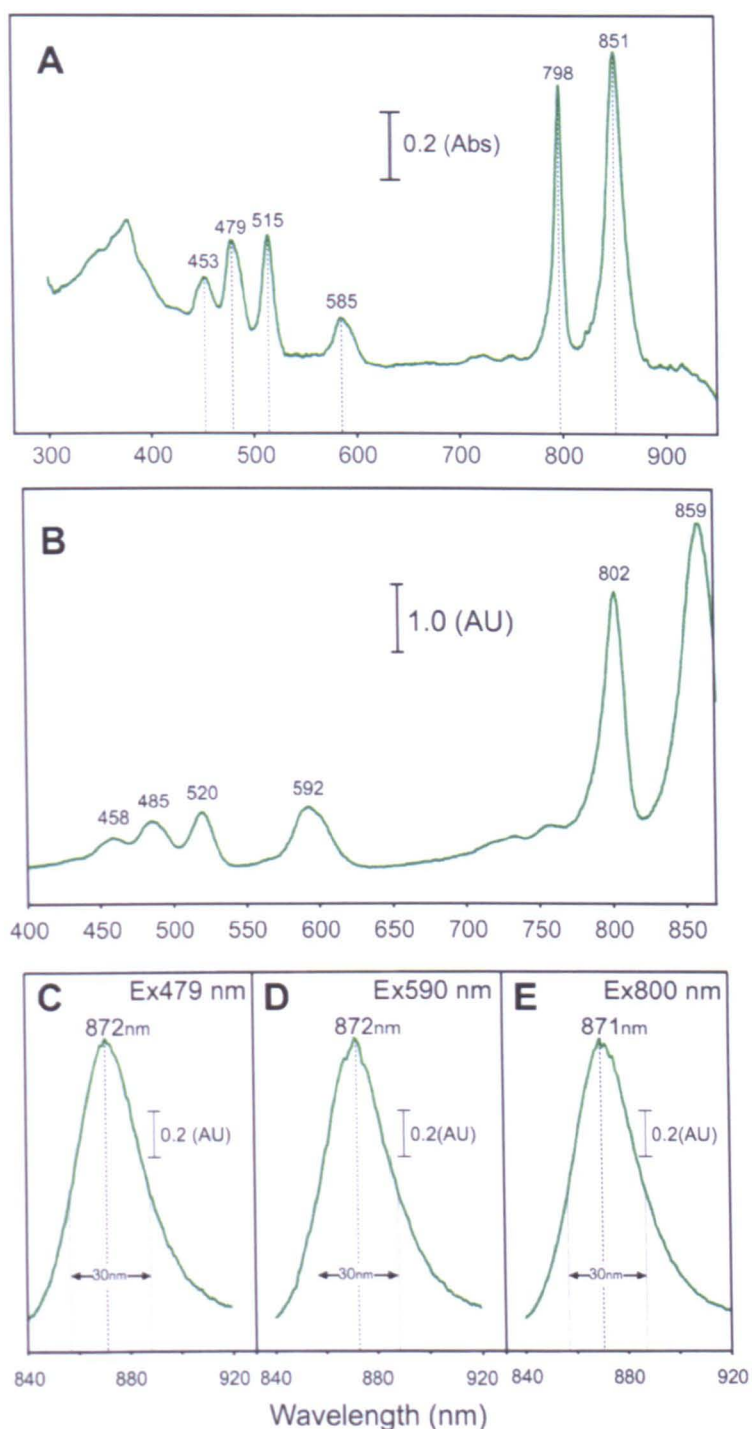


**Figure 3.6 Spectroscopic analysis of LH2-2B1A at 77 K**

- A. Absorbance spectrum. Data have been normalised to an absorbance of 1.0 at 850nm.
- B. Fluorescence excitation spectrum. Data have been normalised to 1 AU at  $Q_x$  maxima for clarity, with excitation slit widths of 1.25 mm and emission slit widths of 5 mm.
- C. Fluorescence emission spectrum with an excitation wavelength of 479nm.
- D. Fluorescence emission spectrum with an excitation wavelength of 590nm.
- E. Fluorescence emission spectrum with an excitation wavelength of 800nm

All fluorescence emission spectra have their peak maxima and full width half maxima labelled. The spectra has been normalised to 1 AU at peak maxima. Excitation slit widths of 2.5 mm and emission slit widths of 2.5 mm were used.

LH2-2B1A (Figure 3.6B) displays near-IR peak maxima at 802 and 859 nm respectively, the latter being a red shift of 3 nm compared with WT. The  $Q_x$  excitation peak occurs at 592 nm (a blue shift of 1 nm), while the carotenoid fluorescence maxima are all within 2 nm of the WT-LH2 complex. Both LH2-2B1A and LH2-1B1A display the same small excitation peaks at 730 and 753 nm seen in the WT-LH2 complex.

### 3.3.2.4 Fluorescence emission properties of WT and mutant LH2 complexes

The fluorescence emission properties of all three complexes were measured at 77 K (Figures 3.4, 3.5 and 3.6). All three complexes were excited at wavelengths of either 479 nm (carotenoid), 590 nm ( $Q_x$ ) or 800 nm (B800 BChl). Each spectrum shown is the average of 4 separate scans.

Figures 3.4C, D and E display the fluorescence emission spectra of WT-LH2 upon excitation at 479, 590 and 800 nm respectively. The fluorescence emission maximum is at 871 nm when the complex is excited at 479 and 590 nm although there is a 3 nm blue shift to 868 nm when the B800 BChl(s) are excited directly. The full width half maxima (fwhm) at each excitation wavelength were calculated using Datamax/Grams 32 software (Jobin Yvon Ltd. U.S.A.). A value of 32 nm was seen upon excitation at 479 and 590 nm, with an increase to 36 nm when the B800 BChl(s) were excited directly.

The fluorescence peak maxima of the LH2-1B1A complex seen upon excitation at 479 and 590 nm are identical to those of WT-LH2 (Figures 3.5C and D). However a 2 nm red shift in the emission maximum compared to WT-LH2 is seen upon excitation at 800 nm (Figure 3.5E). This 870 nm maximum is blue shifted by 1 nm with respect to the emission peaks of the same complex at excitation wavelengths of 479 and 590 nm. The fwhm is identical upon excitation at 479 and 590 nm, with a value of 32 nm. An increase in fwhm of 1 nm is seen when the B800 BChl(s) are excited directly. This is in contrast with the 4 nm fwhm increase seen in WT-LH2 upon excitation at 800 nm, with respect to excitation at 479 and 590 nm.

The fluorescence emission maxima of LH2-2B1A (Figure 3.6C, D and E) with 479 and 590 nm excitation are red shifted by 1 nm when compared to those of WT-LH2 and red are shifted by 3 nm with 800 nm excitation. This 871 nm emission maximum is blue shifted by 1 nm with respect to excitation wavelengths of 479 and 590 nm. The fwhm of 30 nm is identical at all three excitation wavelengths and is in contrast with the 4 nm increase seen in WT-LH2 when excited at 800 nm. 30 nm is the narrowest fwhm at all wavelengths for all three complexes examined.

### **3.3.3 Analysis of the contribution of the Puc2B polypeptide to wild type LH2 complexes.**

This section details the attempts made to analyse the contribution of the second *puc* operon, and its resulting polypeptides, upon the phenotype of *Rba. sphaeroides* 2.4.1. and to assess their direct contribution to the assembled WT-LH2 complex. The strains used in this section are *Rba. sphaeroides* 2.4.1. and *Rba. sphaeroides* 2.4.1.Δ2BA. The complexes analysed were obtained from the same purifications as those characterised in section 3.2.2.

#### **3.3.3.1 Growth curve comparison of *Rba. sphaeroides* 2.4.1. and *Rba. sphaeroides* 2.4.1. Δ2BA**

Comparison of the growth rates of *Rba. sphaeroides* 2.4.1. and *Rba. sphaeroides* 2.4.1. Δ2BA under both low and high light conditions were carried out. A 10 ml inoculum of semi-aerobically grown cells with an A<sub>650</sub> of 1.5 was added to a total culture volume of 600 ml. Low light cells were grown at 30 °C under 5 Wm<sup>-2</sup> illumination. High light cells were grown at 30 °C under 25 Wm<sup>-2</sup> illumination. The optical densities of the cell cultures were measured at 650 nm. The growth curves of both strains at low and high light are displayed in Figure 3.7.

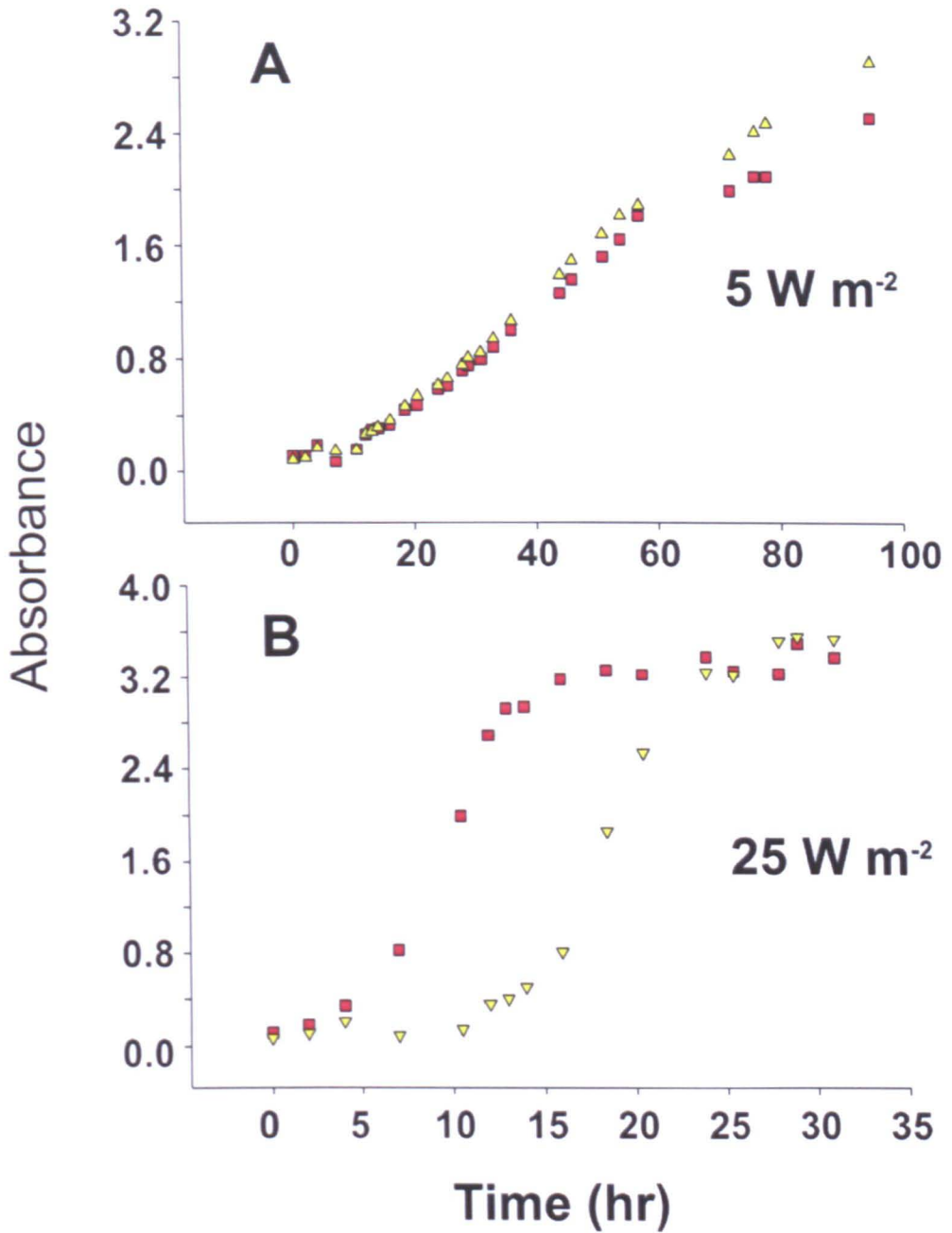


**Figure 3.7 Growth curve comparison**

The growth curves for *Rba. sphaeroides* 2.4.1. (red squares) and *Rba. sphaeroides* 2.4.1.  $\Delta 2BA$  (yellow triangles) are shown. The cultures were grown at 30°C. Cultures were inoculated with cells previously grown semi-aerobically in the dark, to an A650 of 0.1. Cell density was measured at 650 nm.

- A Low light culture
- B High light culture.

Under low light conditions both strains display almost identical phenotypes. There is a slight difference in the final  $A_{650}$  achieved after 100 hrs, with that of *Rba. sphaeroides* 2.4.1. being ~2.4, while *Rba. sphaeroides* 2.4.1.  $\Delta 2BA$  reached 2.8 (Figure 3.7A).

Under high light conditions there is a contrasting difference in the lag phase exhibited by the two strains. This lag phase is present due to the need for the semi-aerobically grown cells to adapt to photosynthetic growth conditions. Figure 3.7B shows that the lag phase displayed by *Rba. sphaeroides* 2.4.1. lasts for ~4 hrs, whereas that of *Rba. sphaeroides* 2.4.1.  $\Delta 2BA$  lasts for ~11hrs. With the exception of the lag phase, the growth curves of both strains are almost identical, reaching a final cell density ( $A_{650}$ ) of 3.6. Figure 3.8 compares the near-IR spectra recorded for the high light cell cultures of *Rba. sphaeroides* 2.4.1. and *Rba. sphaeroides* 2.4.1.  $\Delta 2BA$ . The levels of LH1 and LH2 in the wild-type display the typical 1:1 ratio expected in high light cultures much earlier in the experiment than in the mutant lacking the second *puc* operon. The retardation in LH2 assembly in the wild-type occurs within the first 7 hr(s) of growth, whereas it is not until the 24 hr stage that a similar reduction in LH2 levels is seen in the mutant, as it adapts to the high light conditions.

### **3.3.3.2 Electrospray mass spectroscopy analysis of purified WT-LH2 and LH2-1B1A complexes**

The  $\beta$ -polypeptides of the purified WT-LH2 and LH2-1B1A complexes were compared by electrospray mass spectroscopy. The purified complexes were prepared as described in section 2.8.7 before being injected into an Applied Systems QStarXL Hybrid ESI Q-ToF MS/MS. All mass spectroscopy was carried out by Dr Mark Dickman in the Department of Chemical and Process Engineering, University of Sheffield. The  $\beta$ -polypeptide component of each complex was identified, and the amino acid sequence confirming the identity of both Puc1B and Puc2B was obtained by tandem mass spectroscopy (MS/MS).

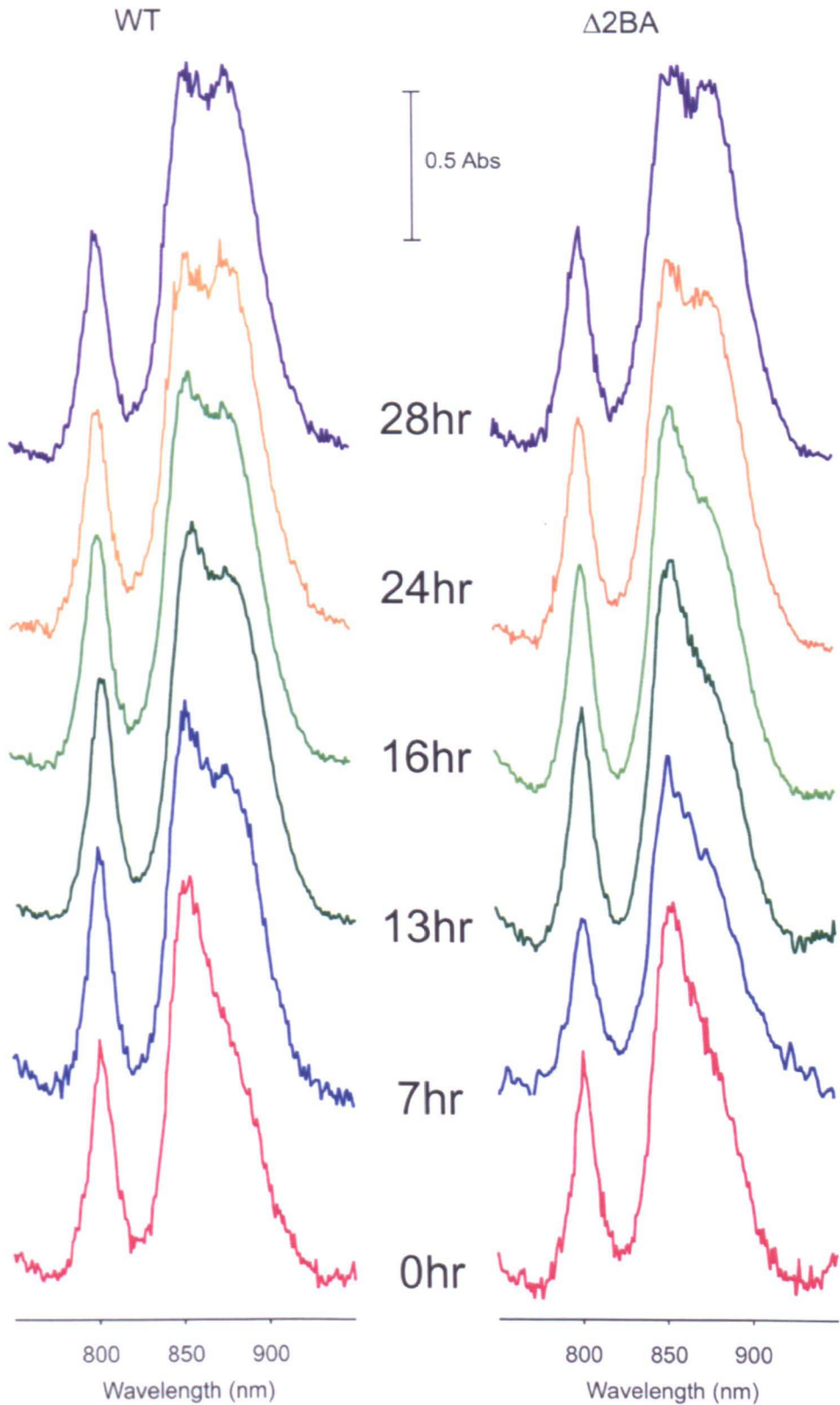


**Figure 3.8 A comparison of light harvesting complex expression under high light conditions.**

Whole cell spectra of *Rba. sphaeroides* 2.4.1.(WT) and *Rba. sphaeroides* 2.4.1. $\Delta$ 2BA are shown. Cells were grown with an illumination of  $25 \text{ Wm}^{-2}$ . Spectra have been normalised to an absorbance of 1.0 with a manual baseline applied for clarity.

WT-LH2 complexes comprised both Puc1B and Puc2B. Figure 3.9A shows the electrospray ionisation (ESI) spectrum obtained for Puc1B in WT-LH2. The peaks corresponding to the three charged species of the peptide are labelled. The MS/MS data obtained allowed the peptide sequence to be elucidated, confirming the identification of Puc1B (Figure 3.9B). The b series ion values obtained for Puc1B are displayed in Appendix I. The same identification of Puc1B was made in the LH2-1B1A complex (data not shown).

The presence of Puc2B in the WT-LH2 complex was confirmed. The ESI spectrum for the peptide is shown in Figure 3.10A, and the three charged species observed are labelled. The peptide sequence was confirmed by MS/MS (Figure 3.10B), and the b series ion values obtained are displayed Appendix I. No identification of Puc2B was made in LH2-1B1A, confirming its absence from this complex.

It should be noted that successful identification of the  $\alpha$ -polypeptide encoded by Puc1A in both complexes was made using both ESI and MS/MS. This polypeptide was shown to be identical in both complexes and corresponds in amino acid sequence to that identified by Zuber *et al.*, 1985 (data not shown).

### **3.3.3.3 AFM analysis of low light membranes from *Rba. sphaeroides* 2.4.1. $\Delta$ 2BA**

An initial analysis of the ICM architecture of *Rba. sphaeroides* 2.4.1.  $\Delta$ 2BA was carried out using AFM. ICM fragments were prepared (as described in 2.12.2) from *Rba. sphaeroides* 2.4.1.  $\Delta$ 2BA cells grown at 30 °C with 5 Wm<sup>-2</sup> illumination. Membranes fragmented by treatment with 0.001 %  $\beta$ -DDM were harvested from a 20/25/30/35/40 % sucrose step gradient (Figure 3.11A) and firmly adhered to a freshly cleaved mica surface as described in section 2.16.1. AFM images were recorded with help gratefully received from Dr. Jaimey Tucker (University of Sheffield). All AFM images shown in this section were recorded with a scan rate of 2.0 kHz, with 512 x 512 sample lines, as described in section 2.16.

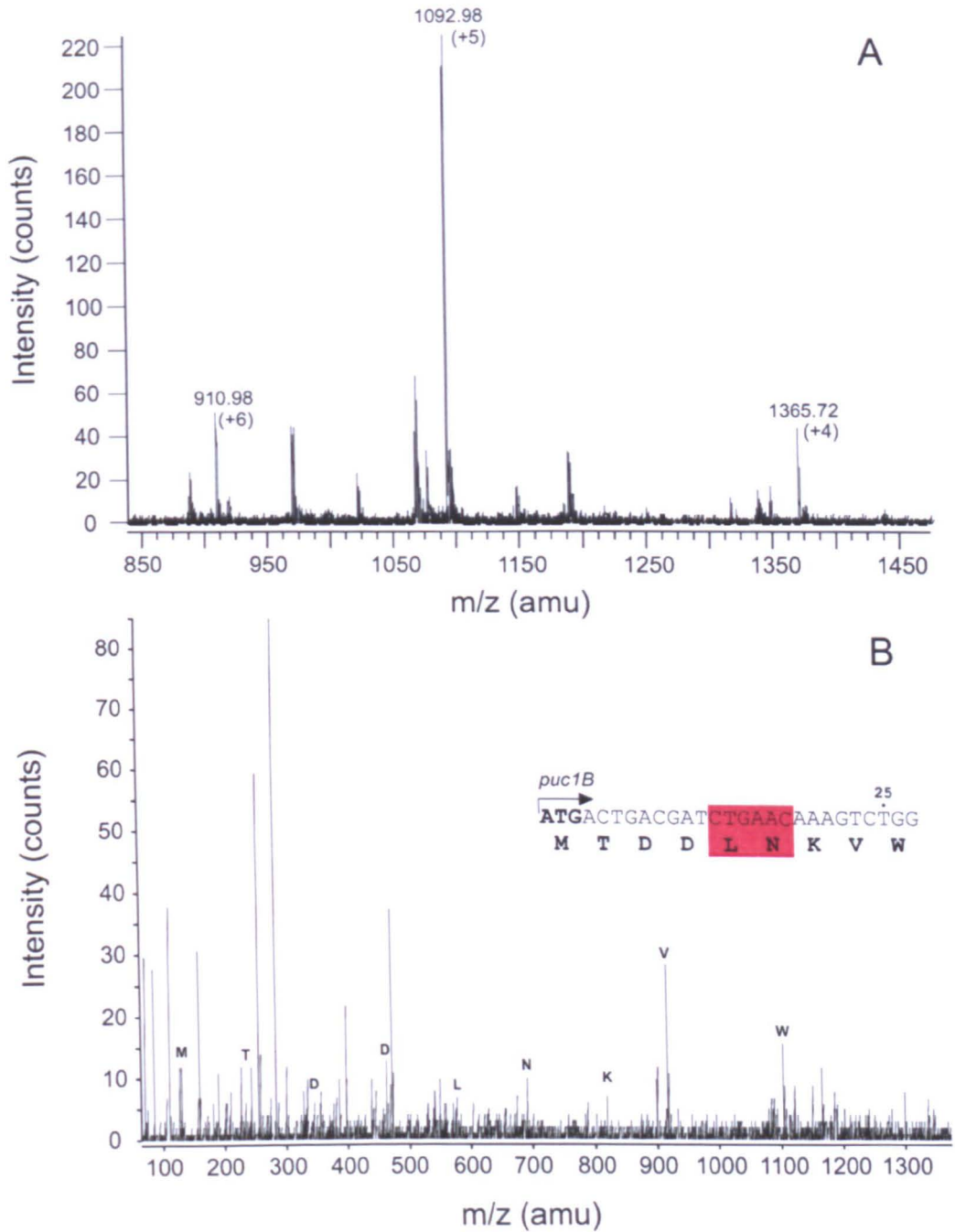


**Figure 3.9 Identification of Puc1B in purified WT LH2 complexes by mass spectrometry**

**A** Positive ESI-MS  $m/z$  spectrum showing three charged species of the Puc1B polypeptide. The sample was analysed in 95% acetonitrile, 0.1% formic acid.

**B** Peptide sequencing by tandem mass spectrometry. The b series ions corresponding to the N-terminal sequence of Puc1B are shown. Inset is the corresponding gene sequence for *puc1B*. The variable residues are highlighted in red.

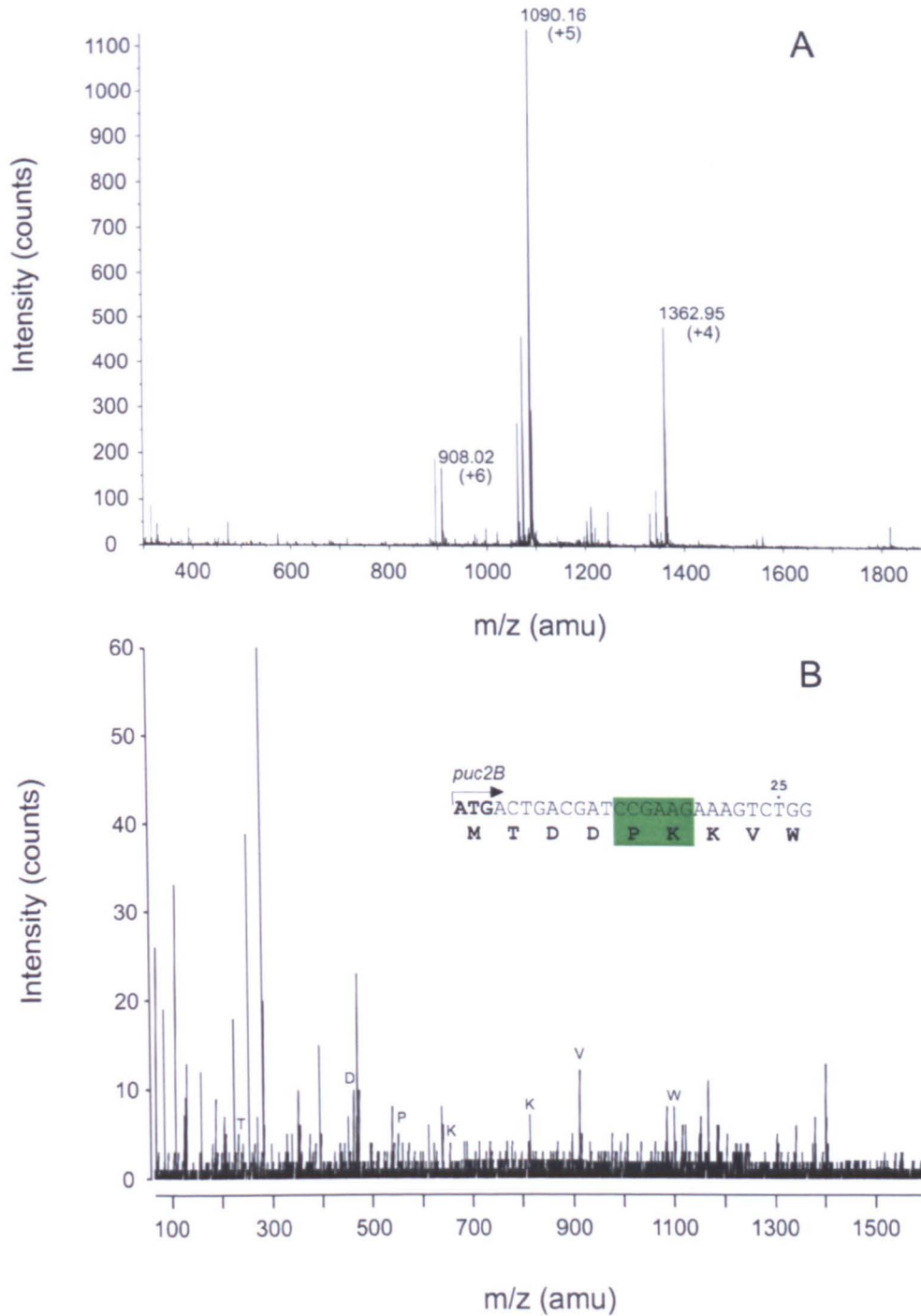


**Figure 3.10 Identification of Puc2B in purified WT LH2 complexes by mass spectrometry**

**A** Positive ESI-MS *m/z* spectra showing three charged species of the Puc2B polypeptide. The sample was analysed in 95% acetonitrile, 0.1% formic acid.

**B** Peptide sequencing by tandem mass spectrometry. The b series ions corresponding to the N-terminal sequence of Puc2B are shown. Inset is the corresponding gene sequence for *puc2B*. The variable residues are highlighted in green.

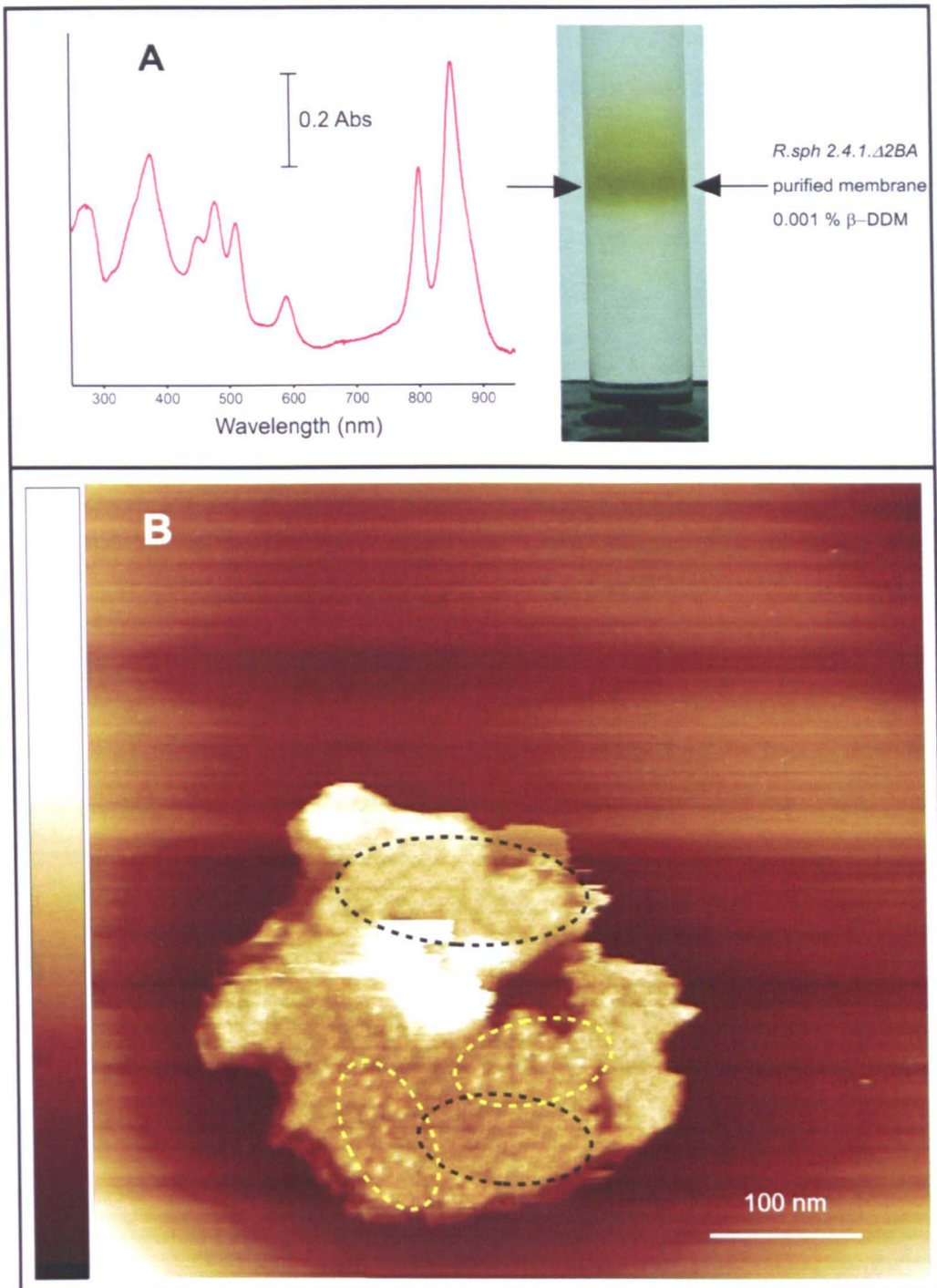


**Figure 3.11 Sucrose gradient purification of ICM fragments from *Rba. sphaeroides* 2.4.1.Δ2BA.**

- A.** A 20/25/30/35/40 % sucrose step gradient containing 0.001% β-DDM used for purifying ICM fragments from *Rba. sphaeroides* 2.4.1.Δ2BA. Cells were grown photosynthetically with  $5 \text{ Wm}^{-2}$  illumination. A room temperature absorbance spectrum of the harvested membrane fragments is shown.
- B.** An AFM topograph of a membrane patch isolated in Figure 3.10A is shown. A height scale of 30 nm is shown. Domains containing dimeric core complexes are highlighted by dashed yellow ovals, domains containing only LH2 complexes are highlighted by dashed black ovals.

Figure 3.11B shows an AFM topograph of a membrane fragment isolated by sucrose gradient fractionation. At this low magnification it is possible to discern ordered regions within the membrane. The areas highlighted by dashed yellow ovals in Figure 3.11B contain arrays of core complex dimers. The dashed black ovals highlight regions of highly ordered LH2 arrays. The core complexes are not evenly dispersed among the LH2 complexes. Instead the LH2 only domains pack in a hexagonal lattice and the cores tend to aggregate.

The LH2-only domains within the *Rba. sphaeroides* 2.4.1.  $\Delta 2BA$  membrane patches were analysed in more detail. Figure 3.12C shows a high magnification image of the LH2 only domains typical of this sample. The angle between the lowest point within three adjacent LH2 complexes was calculated to be  $125.0 \pm 4.1^\circ$  ( $n = 25$ ). This is in approximate agreement with an angle of  $122.1 \pm 4.8^\circ$  ( $n = 26$  Figure 3.12B) calculated for LH2-only membranes purified from the strain DPF2-R (Appendix I), which were previously imaged by Bahatyrova., (2005). The LH2 complexes form an array of rows each exhibiting this angle, which are arranged in a 'high-low' orientation. This lattice order is maintained in all the membrane patches imaged from the *Rba. sphaeroides* 2.4.1.  $\Delta 2BA$  sample. The height difference between the 'high' and 'low' rows of LH2 was shown to be  $1.0 \pm 0.2$  nm ( $n = 28$ ). A graphical representation of the height profile taken along a line perpendicular to several rows of LH2 is displayed in Figure 3.13B. The average horizontal distance from the centre of a 'high' LH2 complex to the centre of a complex in an adjacent 'high' row is  $16.4 \pm 1.7$  nm ( $n = 16$ ).

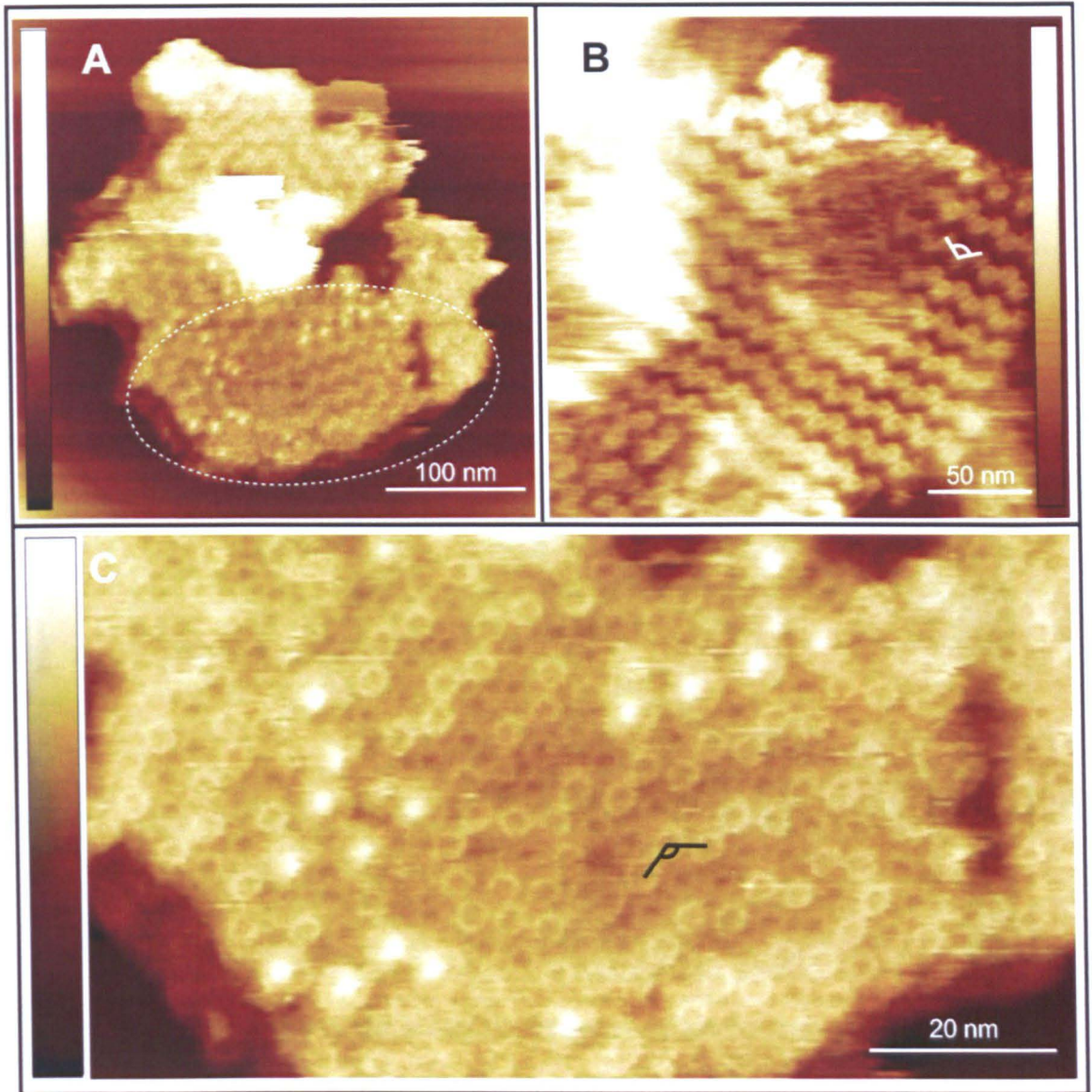


**Figure 3.12 A comparison of LH2 arrangement in LH2-only and *Rba. sphaeroides*  $\Delta 2BA$  membranes.**

- A. An AFM topograph of a membrane fragment purified from *Rba. sphaeroides* 2.4.1.  $\Delta 2BA$  grown under  $5 \text{ W m}^{-2}$  illumination. A height scale of 30 nm is shown. The area highlighted by a white dashed oval is displayed in Figure 3.12C.
- B. An AFM topograph of a membrane fragment purified from *DPF2-R* grown under semi aerobic conditions. A height scale of 6 nm is shown. The marked angle between LH2 rings is  $\sim 122.1 \pm 4.8^\circ$  ( $n = 25$ ).
- C. A high magnification AFM topograph of the area marked by a dashed white oval in Figure 3.12A. A height scale of 11 nm is shown. The marked angle between LH2 rings is  $\sim 125.0 \pm 4.5^\circ$  ( $n = 25$ ).

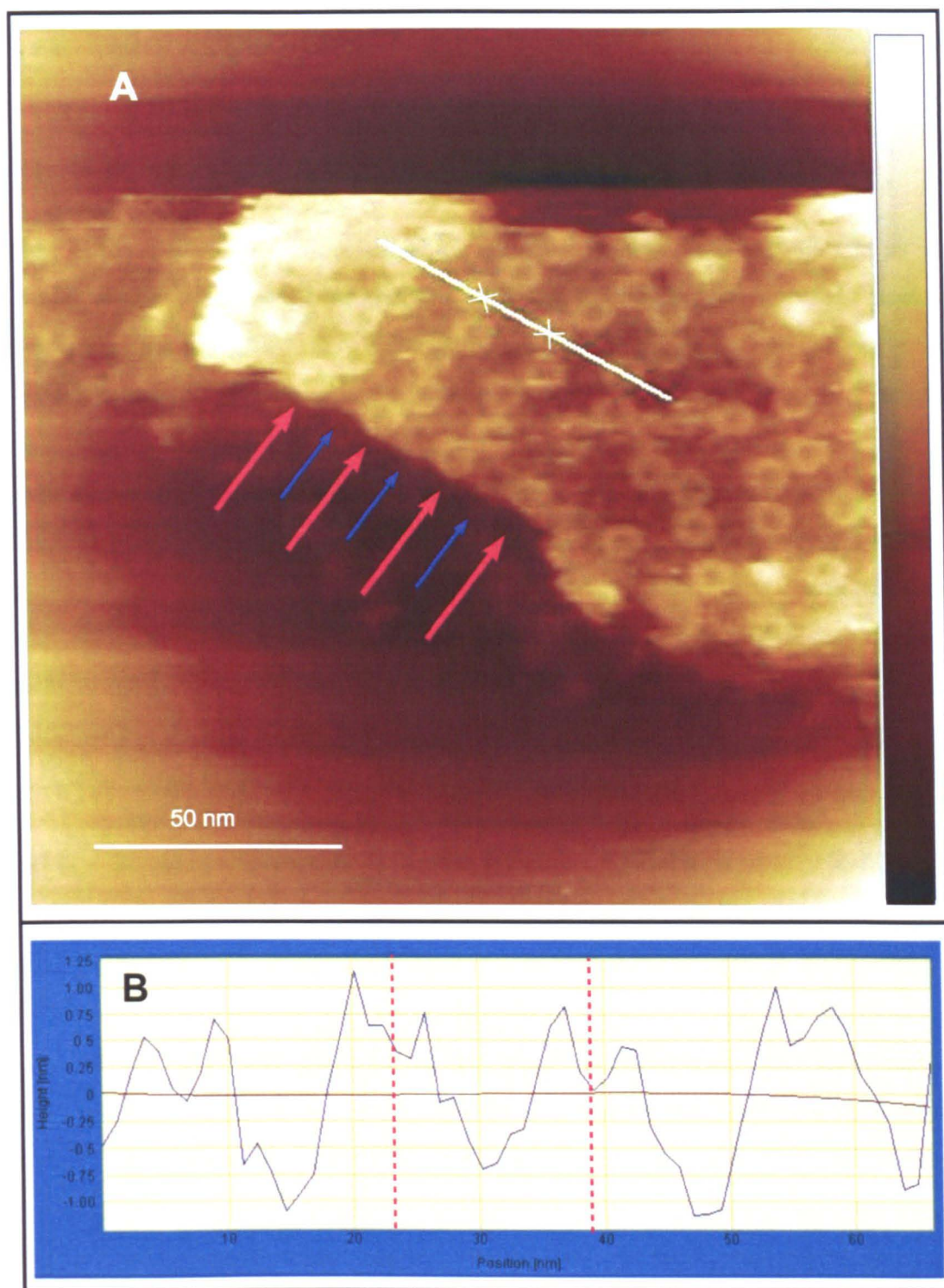


**Figure 3.13** An AFM topograph and height profile of ordered LH2 arrays within the membrane

- A. An ICM patch from *Rba. sphaeroides* 2.4.1. $\Delta$ 2BA grown photosynthetically with  $5 \text{ W m}^{-2}$  illumination. A height scale of 13 nm is shown. Red arrows indicate rows of 'high' LH2 complexes, blue arrows indicate rows of 'low' LH2 complexes.
- B. A height profile recorded along the white line drawn in panel A is shown. The red lines mark the positions of the two white crosses shown in panel A.

## 3.4 Discussion

### 3.4.1 Context

The existence of multiple operons which encode polypeptides that assemble into LH2 complexes has been known for some time, this being the case for both *Rps. acidophila* and *Rps. palustris* (Tadros and Waterkamp., 1989; Tadros *et al.*, 1993; Gardiner *et al.*, 1996). Since the discovery of the second *puc* operon in *Rba. sphaeroides* (Zeng *et al.*, 2003), the  $\beta$ -polypeptide composition of the LH2 complex in this organism has been unclear. An understanding of the structural, and hence spectroscopic contribution, that Puc2B makes within the complex is required to place into context the considerable amount of previous work carried out. This work has often focused on mutagenesis of the LH2 apoproteins, with subsequent analysis of the spectroscopic contributions that their amino acid side chains confer to the bound pigments. It is also important to elucidate any role the polypeptides play in LH2 assembly or the regulation of complex assembly within the membrane.

### 3.4.2 The spectroscopic properties of WT-LH2, LH2-1B1A and LH2-2B1A

The B800 and B850 absorbance peaks of LH2 can be used to discern the local environment in which the complexed BChl(s) are housed. Shifts in these peaks often indicate the structural perturbation of these environments. The  $Q_y$  maxima in LH2-1B1A are identical to those of WT-LH2. However the 2 nm blue shift observed in the B800 peak of LH2-2B1A, although small, indicates that the change in  $\beta$ -polypeptide composition has slightly disturbed the B800 BChl binding site. The amino acid alterations which convert the original *puc1B1A* gene pair into *puc2B1A* (Figure 3.1) are all present in the N-terminal region of the  $\beta$ -polypeptide. This region has been shown to be proximal to the B800 binding site in *Rps. acidophila* LH2; the B800 molecules are positioned between the  $\beta$ -polypeptides within the outer ring of the complex (McDermott *et al.*, 1995; Papiz *et al.*, 2003). The N-terminal region of the  $\beta$ -polypeptide in *Rba. sphaeroides* LH2 is 10 amino acids longer than that of *Rps. acidophila*. Changes in this region could cause the small shift observed in the

B800 peak. It is also possible the changes at the N-terminus could have an effect on the global structure of the  $\beta$ -polypeptide and thus affect a shift in absorbance. The 3 nm blue shift in the  $Q_x$  absorbance band of LH2-2B1A in comparison to WT-LH2 is further evidence that the binding of the B800 BChl(s) has been perturbed in some way. For further discussion of B800 binding in relation to the  $\beta$ -polypeptide see Chapter 5. The absorbance spectra shown in Figures 3.4A, 3.5A and 3.6A indicate that the carotenoid composition of WT-LH2, LH2-1B1A, and LH2-2B1A appear to be identical.

A comparison of the fluorescence excitation spectra of the three different complexes shows the presence of a red shift in the B850 excitation peaks of LH2-2B1A. It is apparent there is a population of 'red' B850 BChl(s) where the complex is comprised of a homogenous Puc2B  $\beta$ -polypeptide ring, and these BChl(s) are the terminal emitters. This homogeneity is associated with a narrowing of the B850 emission band and an accompanying red shift.

There are no significant differences in the peak maxima of the fluorescence emission spectra of the three complexes when excited at 479 and 590 nm. The fwhm of B850 fluorescence emission in WT-LH2 and LH2-1B1A at these wavelengths are identical. However, the reduction of LH2-2B1A fwhm by 2 nm in comparison with WT-LH2 for 479 and 590 nm excitation may again be indicative of the loss of heterogeneity conferred by the homogenous ring of the Puc2B polypeptide reducing the number of differing environments in which the BChl(s) are housed. The 3 nm blue shift observed in WT-LH2 upon excitation at 800 nm is significant, compared with carotenoid and  $Q_x$  excitation and does not occur in LH2-1B1A or LH2-2B1A (though a blue shift of 1 nm does occur in both complexes). The appearance of an emission maximum of 868 nm with 800 nm excitation is accompanied by a 4 nm increase in fwhm for the emission band. These two results indicate a group of 'blue' B850 BChl(s) in the WT complex accepting excitation energy specifically from B800 BChl(s), which are not present in either mutant complex, and which widen the B850 emission band. The less pronounced blue shifts seen in LH2-1B1A and LH2-2B1A, as well as the conservation of their smaller fwhm values, indicate a reduction in the number of different

environments in which the B850 BChl(s) are housed in the homogenous  $\beta$ -polypeptide mutants. This could be attributed to the elimination of heterogeneity in the N-terminal region having an effect upon the global structure of the  $\beta$ -polypeptide. Thus any slight heterogeneity in B850 binding in the WT-LH2 complex which favours a population of 'blue' environments is removed in the mutants. The lack of this effect upon excitation at 479 nm may be due to the energy transfer from the carotenoids being preferential towards the same type of 'red' chlorophylls. Excitation at 590 nm would excite all BChl(s) simultaneously, masking small variations between the three complexes in the energy transfer from the B800 BChl(s).

The fact that LH2-2B1A displayed the largest shifts in absorbance and fluorescence with respect to WT-LH2 may indicate that Puc2B could play a role in modulating the tuning of the BChl(s) housed within LH2 in WT-LH2. The spectroscopic contribution the Puc2B polypeptide makes, although not large, is significant. Previous spectroscopic data which has come from complexes subjected to mutagenesis of the  $\beta$ -polypeptide must now be evaluated in the knowledge that a significant number of the polypeptides in the complex have not been mutated. The fact that changes in the spectroscopic properties of these previously studied complexes were still seen even though they were only partial mutants may indicate that the contribution the residues investigated have on pigment binding has been underestimated.

Further work should focus on low temperature CD, in an attempt to detect the small changes in the BChl environments which may be causing the peak maxima and fwhm shifts observed so far.

### **3.4.3 Analysis of the contribution the second *puc* operon and its resulting polypeptides makes to the phenotype of *Rba. sphaeroides* 2.4.1.**

The two cultures were inoculated with dark grown cells and subjected to either low ( $5 \text{ Wm}^{-2}$ ) or high ( $25 \text{ Wm}^{-2}$ ) light intensity. The growth curve presented in section 3.3.3.1 also provides the first evidence of a significant phenotypic effect attributable to the second *puc* operon. Under low light both the wild type and mutant ( $\Delta puc2BA$ )

behaved identically. The increase of ~7 hr in the lag phase observed in the absence of *puc2BA* when grown under high light is of great interest. It appears counter intuitive, since under high light conditions there is significantly less LH2 produced by the organism, so any *puc* mutation would be expected to influence low light, not high light growth.

The cause of this phenotypic effect could be a result of factors other than the absence of Puc2B. Zeng *et al.*, (2003) have already demonstrated the complex regulatory relationship which exists between the two *puc* operons. The deletion of *puc2BA* may interrupt an important transcriptional or post-translational regulatory pathway and be responsible for the extended lag phase observed. In addition, Puc2A is incorporated into the ICM (Zeng *et al.*, 2003); its absence in the mutant analysed may also contribute to the observed phenotype. The second *puc* operon appears to be necessary for rapid adaptation to high light conditions.

It is apparent from the spectra presented in Figure 3.8 that this lag in adaptation involves LH2 assembly; cells lacking both Puc2B and Puc2A are unable to down regulate the production of LH2 when the incident light levels are increased. In other words, the  $\Delta 2BA$  mutant assembles too much LH2 when its environmental conditions are considered. This inability to adapt means the photosynthetic membrane of *Rba. sphaeroides* 2.4.1. $\Delta 2BA$  absorbs a potentially damaging amount of light, to the point where the onset of the log phase of the culture is delayed by up to 9 hr(s). It is possible that Puc2B or Puc2A have the effect of retarding the assembly of LH2 in high light conditions when the presence of large amounts of this complex is not required. A large pool of LH2 in the *Rba. sphaeroides* 2.4.1.  $\Delta 2BA$  mutant increases the amount of excitation energy being funnelled into the RC complexes which will shift the equilibrium between reduced and oxidised ubiquinone that shuttles between the RC and the cytochrome *bc*<sub>1</sub> complex. The ideal state of the quinone pool is one where there is a roughly equal proportion of oxidised and reduced species, with a membrane potential of +150 mV (Verméglio and Joliot., 2002 ). The extended lag phase displayed by *Rba. sphaeroides* 2.4.1.  $\Delta 2BA$  could be due to the poor efficiency in energy production causing an imbalance in the redox poise of the quinone pool, which has

resulted from the overproduction of QH2 by the RC. The hypothesis that Puc2B or Puc2A somehow retards the production of LH2 and maintains Q/QH2 equilibrium is similar in principle to mechanisms in other photosynthetic organisms, in which they can reduce the size of their light harvesting antenna systems when light levels increase. This type of photoacclimation is demonstrated in *Denaliella tertiolecta*, where the light-intensity-dependent changes in LHCII are due to changes in *cab* gene expression (Escoubas *et al.*, 1995).

#### **3.4.4 The analysis of the LH2 complex by electrospray mass spectroscopy**

The identification of Puc2B in the WT-LH2 complex by mass spectroscopy is the first direct evidence that this polypeptide is incorporated into the native LH2 complex. The level to which the incorporation occurs cannot be discerned from the data obtained, since the method used does not allow quantitative analysis. The confirmation of the presence of both 'PucB' polypeptides in WT-LH2 does further support the supposition that the heterogenous nature of the  $\beta$ -polypeptide ring dictates some of its spectroscopic properties. A study investigating the level of contribution Puc2B makes to the complex should be undertaken. The labelling of the polypeptides in WT-LH2 with N<sup>15</sup> would allow for the quantitative analysis of the composition of the  $\beta$ -polypeptide ring by electrospray mass spectroscopy. This should be carried out for complexes purified from cells grown at varying light levels, thus allowing any variation in the amount of Puc2B in complexes grown under high light to be linked to the observed phenotype. This quantitative analysis could also be used on complexes isolated specifically from UPB and ICM, allowing the possibility of any role for Puc2B in complex assembly to be investigated.

#### **3.4.4 AFM analysis of the ICM from *Rba. sphaeroides* 2.4.1. $\Delta 2BA$**

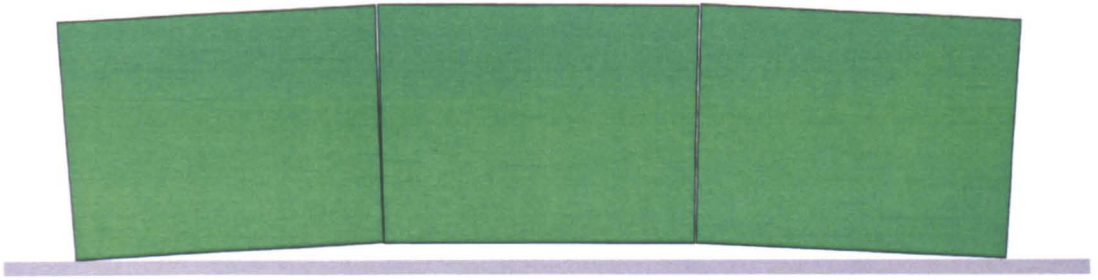
The AFM images presented in this chapter are part of the initial attempts which were made to characterise the membrane architecture of mutants lacking in genes which constitute the two *puc* operons. Although time constraints meant it was only possible to image the membrane of *Rba. sphaeroides* 2.4.1. $\Delta 2BA$  grown in low light conditions,

and no comparison with wild type has been made, the results are highly significant and so are presented in this chapter.

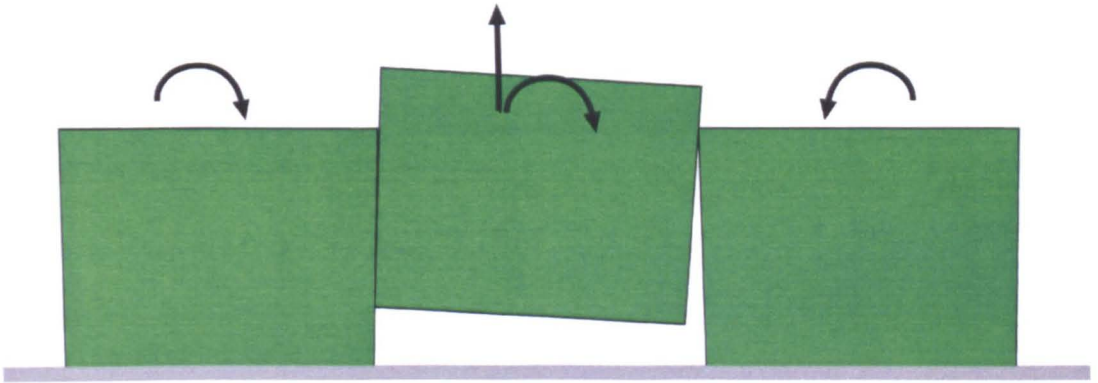
For the first time it has been possible to visualise large scale LH2-only domains from *Rba. sphaeroides*. This kind of information was missing from the original report of membrane architecture in this bacterium (Bahatyrova *et al.*, 2004) The LH2 antenna is arranged in highly ordered arrays, packing within a para-crystalline hexagonal lattice. This arrangement has not been seen before in native membranes of any wild-type purple bacteria. However, it is almost identical to that seen in membranes purified from the LH2-only mutant DPF2R (Figure 3.12B) (Bahatyrova., 2005). The angles between adjacent LH2 complexes in the *Rba. sphaeroides* 2.4.1.  $\Delta 2BA$  membranes and the LH2-only membranes purified from DPF2R are in approximate agreement. The small increase in angle seen in the membranes imaged in this study ( $\sim 3^\circ$ ) could be caused by interruptions in the LH2 arrays by the core complexes, or perhaps the absence of Puc2B and Puc2A has slightly affected packing of the complexes. To clarify this it is necessary to image comparable wild-type membranes. However it should be recognised this is the first evidence of the regular arrangement of LH2 in this fashion in pseudo-wild type membranes.

It has been previously hypothesised (Bahatyrova., 2005) that the observed 'high-low' packing arrangement with alternating height levels is due to the shape of the LH2 complex, which is either inherently slightly conical in cross-section, or which acquires this shape due to tight binding of lipids on one side of the complex. It has been suggested the deposition of a curved membrane patch onto a flat mica surface induces lateral pressures, which are responsible for forcing alternate rows of LH2 to move in both their vertical and possibly horizontal position, thus causing the 'high-low' arrangement observed (Bahatyrova., 2005). The images obtained in the present work support this hypothesis. A schematic representation of a possible cause for the rows of 'high' and 'low' LH2 complexes is shown in Figure 3.14A, B and C. A full analysis of the packing arrangement of LH2 domains should be carried out when images of the wild-type membranes have been obtained.

A



B



C

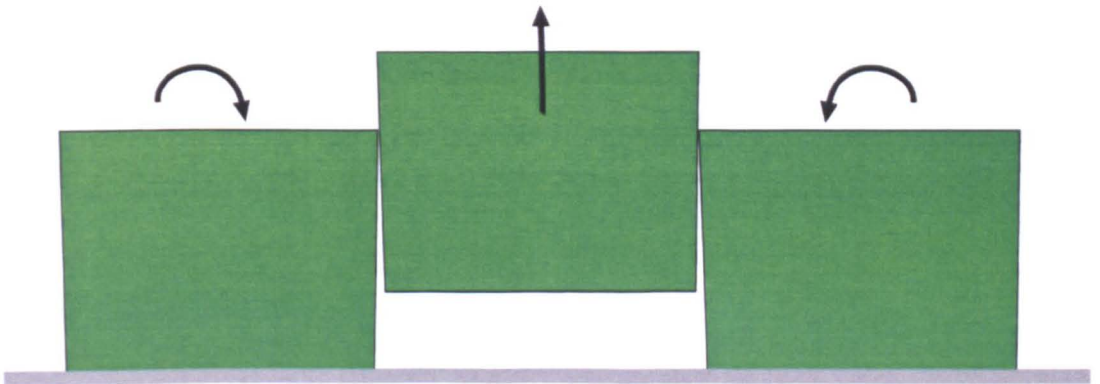


**Figure 3.14 Modelling the movement of LH2 on mica**

A model of the possible translations forced upon the 'high' rows of LH2 after deposition on a mica surface is shown. This figure is displayed courtesy of Dr John Olsen (University of Sheffield).

The dimeric core complexes imaged are associated spatially, forming contacts with each other. Only one membrane patch imaged provided data which clearly showed core complexes interacting with each other. Previous images of wild-type membranes (Bahatyrova *et al.*, 2004) showed dimeric core-complexes arranged in discrete rows, which were separated by LH2 acting as conduits that deliver excitation energy to the LH1-RC-PufX assemblies. This is not the case in the image presented here; the core complexes cluster at the edges of the LH2 arrays, contacting each other in either an 'end on end' or 'side by side' fashion. The fact that core complexes cluster and are not dispersed throughout the membrane supports the conclusions drawn by Bahatyrova *et al.*, (2004), that excitation energy is able to be delocalised throughout a matrix of core complexes. Thus if an RC is in a 'closed' state, the excitation energy is able to transfer to a closely associated 'open' RC.

The AFM topographs presented in this chapter are highly significant. The areas of LH2-only membrane imaged are extensive and much greater than any seen before. The images have provided further insight into the way in which *Rba. sphaeroides* arranges its multi-complex antenna system. It should now be possible to study the properties which the four different Puc polypeptides confer upon membrane structure by directly imaging the ICM of selected mutants. It is of particular interest to elucidate the ways in which they may affect the formation and arrangement of not only the LH2 domains, but also the core complex arrays within the membrane.

From the spectroscopic whole cell data in Figure 3.8 it would appear that the  $\Delta 2BA$  mutation produces larger amounts of LH2 than those expected under high light growth conditions. The AFM data shown in Figure 3.12 demonstrate that these unwanted LH2 form large ordered assemblies that are connected to regions containing core complexes. Thus it is likely in the  $\Delta 2BA$  mutant that the high light intensity is harvested and transmitted to the RCs, over-reducing the quinone pool and stalling growth.

## **Chapter 4: The purification and crystallisation of LH2-1B1A, and the identification of the novel protein RSP6124 from *Rhodobacter sphaeroides*.**

### **4.1 Summary**

The structural characteristics of bacterial light harvesting complexes have been elucidated over the last two decades using a variety of techniques. However, as yet no atomic resolution structure exists for the peripheral light harvesting complex of *Rba. sphaeroides*. The recent discovery of a second *puc* operon in this organism encoding  $\alpha$ - and  $\beta$ -apoproteins of the LH2 complex has provided insights into the heterogeneous nature of its  $\beta$ -polypeptide ring. The deletion of the second *puc* operon removes this heterogeneity and may provide an opportunity to crystallise the LH2 complex from *Rba. sphaeroides* and elucidate its 3D structure to atomic resolution.

This chapter describes the development of a purification protocol for the LH2-1B1A complex. This complex possesses a  $\beta$ -polypeptide ring comprised exclusively of Puc1B. The crystallisation of LH2 complexes purified using this protocol is detailed, along with the unsuccessful attempts to obtain structural data from the resulting crystals by X-ray crystallography.

A previously undescribed protein, RSP6124, was identified during the purification of LH2-1B1A. A bio-informatic analysis of this protein is presented. Although its role within the organism is still unclear, there is evidence which suggests that strong electrostatic interactions between RSP6124 and the extrinsic regions of the LH2 complex may exist. RSP6124 contamination of the purified LH2-1B1A sample provides an alternative explanation for current failures to obtain high resolution diffraction data from 3D crystals.

## 4.2 Introduction

The structures of the bacterial light harvesting complexes have been extensively studied using EM, AFM, NMR, and X-ray crystallography, elucidating their key structural features (Miller 1982; Stark *et al.*, 1984; Engelhardt *et al.*, 1986; Boonstra *et al.*, 1994; McDermott *et al.*, 1995; Walz *et al.*, 1998; Jungas *et al.*, 1999; Jamieson *et al.*, 2002; Papiz *et al.*, 2003., Scheuring *et al.*, 2004); in the case of the *Rba. sphaeroides* RC, structural information is available at atomic resolution (Deisenhofer *et al.*, 1985; Deisenhofer *et al.*, 1995; Chang *et al.*, 1986, 1991; Allen *et al.*, 1987a and b; Ermler *et al.*, 1994; McAuley *et al.*, 2000; Katona *et al.*, 2003). It is known that LH2 acts as the peripheral antenna complex within the light harvesting array of the photosynthetic membrane. Depending upon incident light levels it is present in variable stoichiometry to the RC-LH1-PufX core complex; its expression is tightly regulated at the transcriptional, translational and post-translational levels (Kiley and Kaplan, 1987; Zeng *et al.*, 2003). LH2 harvests solar energy from the photons which excite its bound pigment molecules, transferring this excitation energy with high efficiency to the LH1-RC-PufX core complex (Hunter *et al.*, 1989; McDermott *et al.*, 1995; Bahatyrova *et al.*, 2004). The structural and functional role of the LH2 complex has been discussed extensively in section 1.4 and 1.6 of this thesis.

The two structural genes, *puc1B* and *puc1A*, encode the  $\beta$ - and  $\alpha$ -polypeptides of the LH2 complex respectively, with the LH2 assembly factor PucC encoded by *pucC* (Gibson *et al.*, 1992). Recent work sequencing the *Rba. sphaeroides* 2.4.1. genome ([www.rhodobacter.org](http://www.rhodobacter.org)) uncovered a second copy of the *pucBA* genes, which was designated *puc2BA*. Zeng *et al.*, (2003) demonstrated that the Puc2B polypeptide plays a significant role in complex assembly, showing that LH2 levels are 30% lower in its absence. Puc2A was not observed to be incorporated into the LH2 complex, and to date its function is still unclear. An excess of *puc1B* transcript did not rescue LH2 expression levels in *puc2B* null mutants (Zeng *et al.*, 2003)

LH2 from *Rba. sphaeroides* has been extensively studied for many years and despite attempts no atomic resolution structure yet exists. In the light of the extensive body of

biophysical data on this complex it is important that its structure is solved to atomic resolution. The discovery of the second  $\beta$ -polypeptide indicates that the population of LH2 rings is structurally heterogeneous (See also Chapter 5). This offers a plausible hypothesis for the lack of a 3D structure of the *Rba. sphaeroides* LH2 complex, as heterogeneity within or between rings could disrupt the lattice contacts required to form a regular crystal structure possessing high diffraction properties. This chapter details attempts to crystallise the purified LH2-1B1A complex using a new protocol. The discovery of the previously unknown protein RSP6124, which co-purifies with LH2-1B1A, is also discussed. The presence of RSP6124 is proposed as one possible reason for the an atomic structure of LH2 in *Rba. sphaeroides*.

## 4.3 Results

### 4.3.1 Mutant strains of *Rba. sphaeroides*

The mutant strain *Rba. sphaeroides* 2.4.1.  $\Delta puc2BA$  was kindly provided by Professor Samuel Kaplan (University of Texas, USA). The strain carries an in-frame deletion of the *puc2BA* operon. The *puc1BAC* operon is unchanged, as are all the other genes encoded within the PGC. The LH2 complex purified from this strain contains only  $\alpha$ - and  $\beta$ -polypeptides encoded by the *puc1BAC* operon (Zeng *et al.*, 2003) and will be referred to in this study as LH2-1B1A.

### 4.3.2 The purification of LH2-1B1A

The LH2-1B1A complex studied in this chapter was purified from *Rba. sphaeroides* 2.4.1.  $\Delta puc2BA$ , which was grown photosynthetically as described in section 2.10.2. Cells were disrupted in a French press cell at 18,000 psi. The lysate was centrifuged at 20,000 rpm for 30 min in the Beckman JA-20 rotor and the supernatant containing the crude membrane fraction was collected for concentration. The crude membranes were centrifuged at 40,000 rpm for 2hr in a Beckman Ti45 rotor. The membrane pellet obtained was homogenised in membrane buffer (20mM Tris, pH 8.0 at 4 °C) to a concentration of 200  $A_{850}$  units  $ml^{-1}$ . LDAO at stock concentration of 30 % was added to the homogenised membranes to a final concentration of 3 %. The

membranes were then allowed to solubilise with stirring for 1hr at room temperature in the dark. After solubilisation, the detergent extract was passed through a 0.25  $\mu\text{m}$  syringe filter to remove any particulate matter. The filtered membranes were then applied to a DEAE-Sepharose anion exchange column. After washing with purification Buffer A (20mM Tris, 0.1 % LDAO, pH 8.0), a gradient with an increasing NaCl concentration of 5mM  $\text{ml}^{-1}\text{min}^{-1}$  was applied to the column (using high salt buffer B comprising 20mM Tris, 0.1 % LDAO, pH 8, 1M NaCl). The bound protein eluted at a NaCl concentration of  $\sim 150$  mM.

The ratio of absorbance of the purified sample at 850 and 280 nm gives an indication of the ratio of LH2 present compared to bulk protein. Absorbance at 280nm gives a measure of absolute absorbance by the aromatic residues of all proteins within the sample, whereas the 850 nm absorbance is specific to LH2 B850 BChl(s). This ratio allows an approximate assessment of the purity of the sample throughout the various stages of the purification. After the first DEAE-Sepharose column, fractions with an 850:280 ratio greater than 2.2 were collected and pooled. This pooled fraction was buffer exchanged into Buffer A using a Centriprep spin concentrator (Millipore, Bedford, USA) and applied to a second DEAE-Sepharose column. The same washing and elution protocol was applied to the bound protein as with the first DEAE-Sepharose column. After elution, fractions possessing a ratio greater than 2.7 were pooled.

The second pooled fraction was then applied to a Source 15Q ion exchange column. The bound protein was washed with Buffer A then eluted from the column using an increasing NaCl gradient of 6mM  $\text{ml}^{-1}\text{min}^{-1}$ . The main elution peak eluted from the column at a NaCl concentration of  $\sim 350$  mM. This peak was multi-component in nature, and the elution profile changed depending upon the amount of protein that was loaded onto the column. The different elution patterns observed with differing protein loading are described in more detail in section 4.3.3. Eluted fractions with an 850:280 ratio greater than 3.0 were pooled for further purification.

Pooled fractions were concentrated using a Centriprep™ spin concentrator, to a volume of 500  $\mu\text{l}$ . This sample was then loaded onto a Superdex 200 preparation grade gel filtration column (GE Healthcare, UK) pre-equilibrated with Buffer A at a flow rate of 0.3  $\text{ml min}^{-1}$ . At this stage, the fractions with an 850:280 nm ratio greater than 3.3 were pooled and spin concentrated to a final concentration of 100  $\text{A}_{850}$  units  $\text{ml}^{-1}$ . Typically a total yield of  $\sim 6 - 8\%$  can be expected for a purification of this type. Over 90 % of LH2 from the starting membranes is lost during the purification process.

An SDS-PAGE gel showing the pooled fractions at each step of the purification is shown in Figure 4.1. The  $\alpha$ - and  $\beta$ -polypeptides have been labelled and they are the major protein bands following purification. The H, M and L subunits of the RC can also be seen in the lanes 1-4, but these are absent in the later stages of the purification (lanes 5-8). Figure 4.2 shows the absorbance spectra of the pooled fractions at each stage of the purification. An increasing 850:280 nm ratio is observed, and this can be clearly tallied with the increasing purity of the LH2 sample, as seen by SDS-PAGE in Figure 4.1. The purified complexes were visualised by electron microscopy using negative stain. They are seen to be monodisperse, as required for 3D crystal trials (Figure 4.3).

#### **4.3.3 Identification of different populations of LH2-1B1A by Source 15Q ion exchange chromatography**

The elution profile of the LH2-1B1A complex from the Source 15Q ion exchange column contains multiple components. When LH2-1B1A samples containing  $\sim 200$  AU were applied to a column with a 1ml bed volume, the elution profile was seen as a single peak with two distinct shoulders on the ascending side occurring at  $\sim 300$  mM and  $\sim 325$  mM NaCl. A third shoulder is seen on the descending side of the elution peak at a NaCl concentration of  $\sim 360$  mM (Figure 4.4).

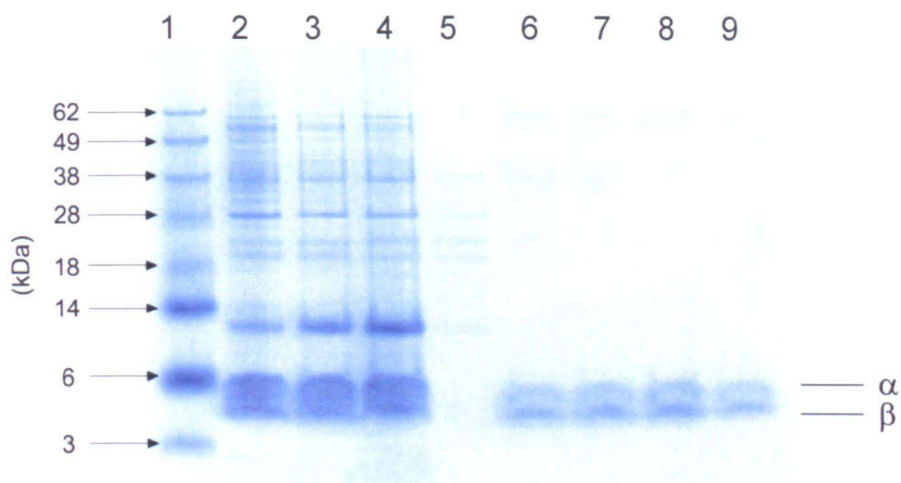


### Figure 4.1 Purification of LH2-1B1A

A 12% SDS-PAGE of samples taken at each stage of a LH2-1B1A purification.

- Lane 1 – Invitrogen SeeBlue™ MW markers
- Lane 2 – *Rba. sphaeroides*  $\Delta$ 2BA cell lysate
- Lane 3 – ICM pre-solubilisation
- Lane 4 – ICM post-solubilisation with 3 % LDAO
- Lane 5 – Flow through of first DEAE Sepharose column
- Lane 6 – Sample post first DEAE Sepharose column
- Lane 7 – Sample post second DEAE Sepharose column
- Lane 8 – Sample post Resource-Q™ column
- Lane 9 – Sample post Superdex-200™ gel filtration column

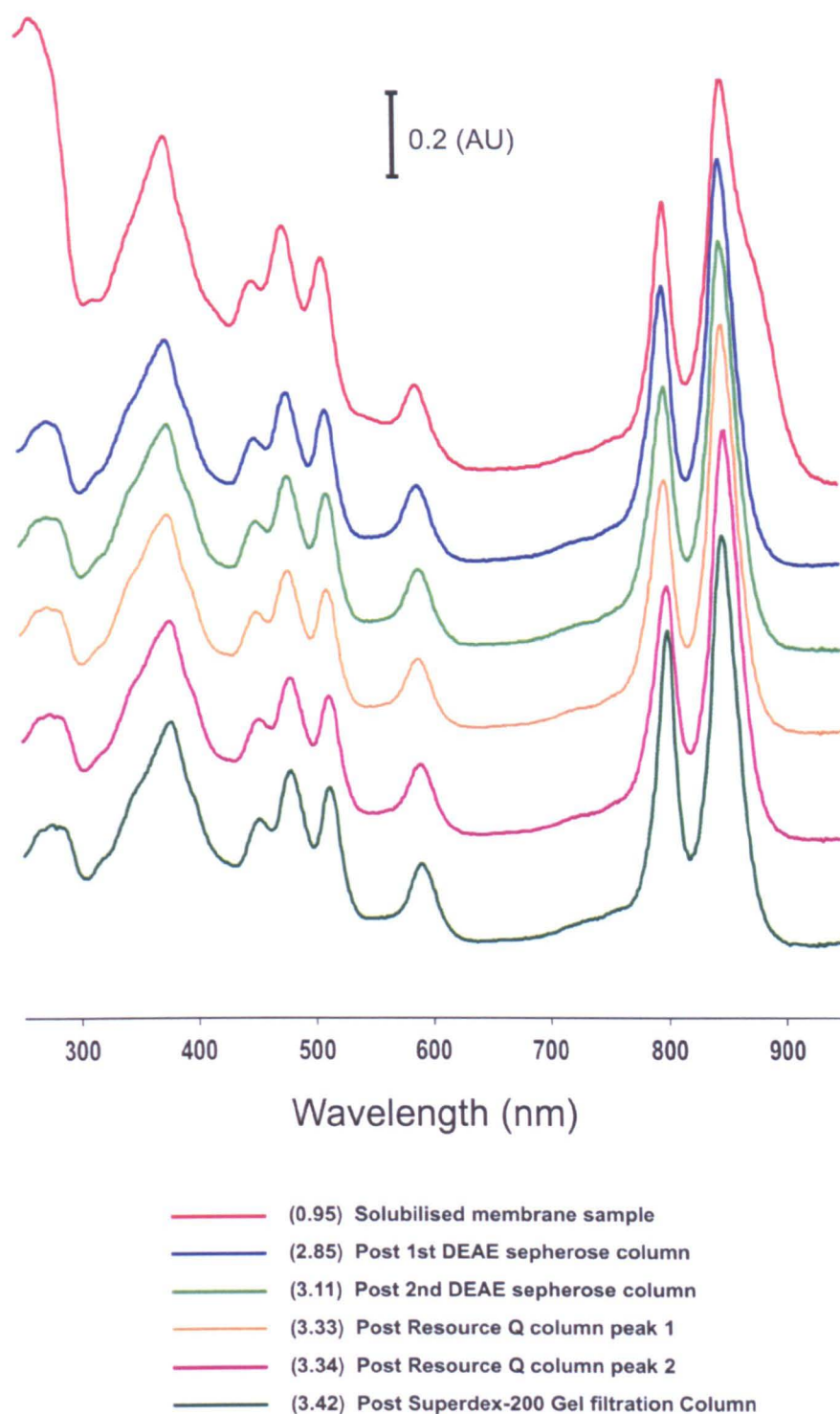


**Figure 4.2 Absorbance spectra of LH2-1B1A throughout purification**

The absorbance spectra of LH2 samples at each stage of purification are shown. Spectra have been normalised to a value of 1 AU at 850nm and stacked for clarity. Measurements were taken at room temperature. 850:280 nm ratios are shown in brackets in the figure key.

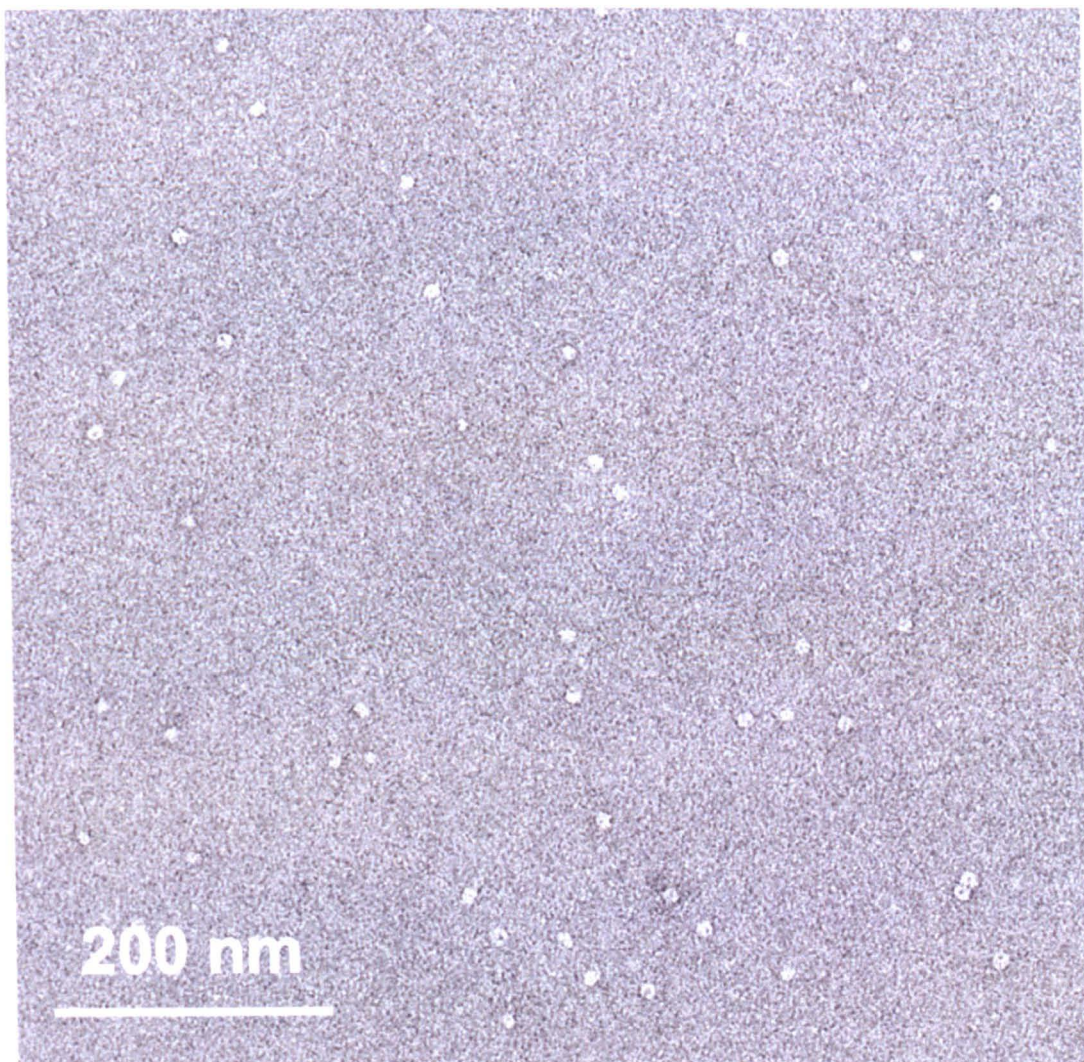


**Figure 4.3 Monodisperse LH2 for crystallisation**

A negative stain electron micrograph showing purified monodispersed LH2. The sample was stained with 0.75% uranyl acetate. Electron microscopy was carried out by Dr Pu Qian (University of Sheffield).

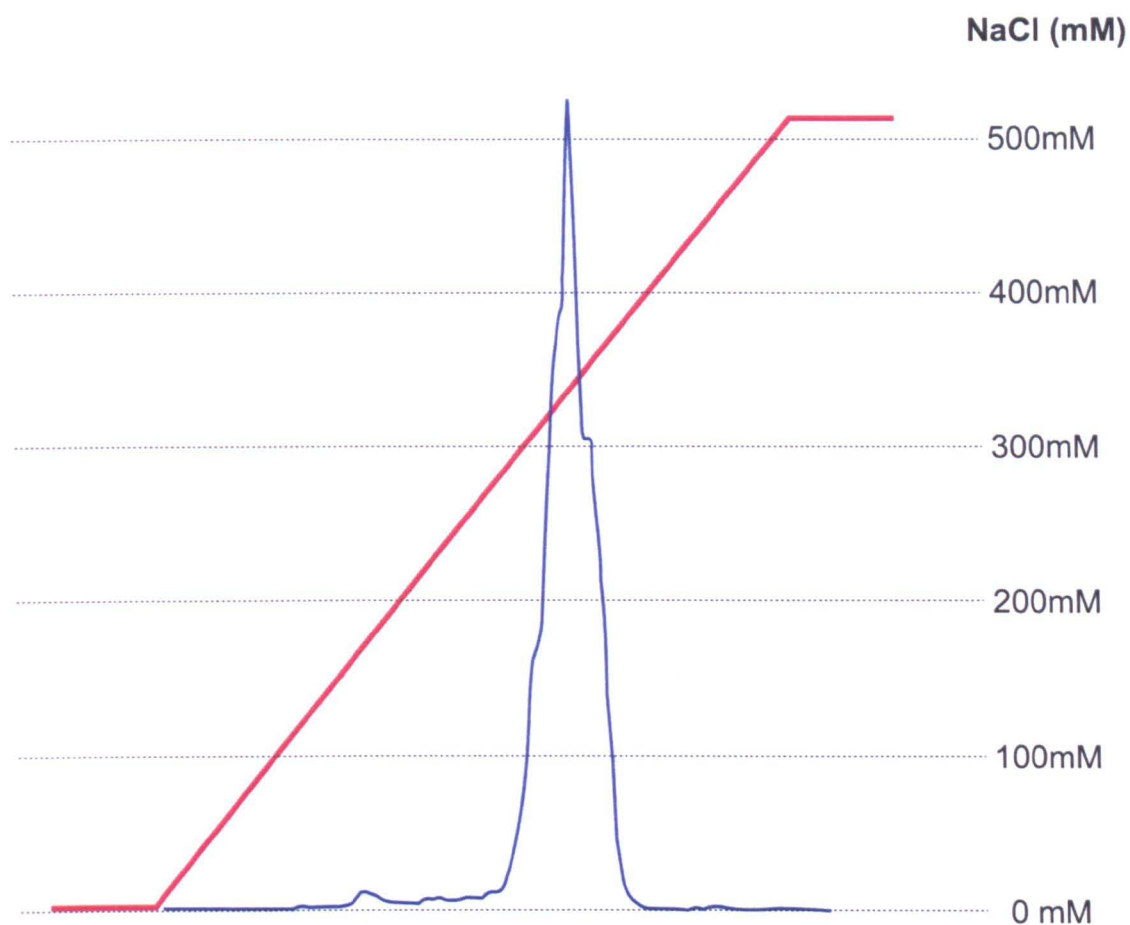


**Figure 4.4 Source 15-Q column elution profile with low sample loading**

The elution profile of LH2-1B1A from a Source 15-Q ion exchange column is shown. The column was loaded with  $A_{850} = \sim 200$  LH2-1B1A. The concentration of NaCl was increased along a gradient of  $6 \text{ mM ml}^{-1}$ . The NaCl gradient is shown in red; sample absorbance was measured at 280nm and is shown in blue.

When the amount of LH2-1B1A added to a column with an identical bed volume totalled ~600 AU, the elution profile changed markedly. 600 AU of LH2-1B1A was seen to saturate the column's binding capacity. When eluted along an increasing NaCl gradient at 6 mM min<sup>-1</sup>, the elution profile changed from one single multi-component peak, into two distinct major peaks, and one minor peak. The first peak eluted at a NaCl concentration of ~300 mM, with the second eluting at ~390 mM. The minor peak eluted between the two major peaks, at a NaCl concentration of ~360 mM (Figure 4.5). LH2-1B1A from the two major peaks was isolated for further analysis, which included the B800-B850 absorbance spectra recorded at 77 K. These were identical for both major elution peaks, with absorbance maxima at 799.5 nm and 850 nm (Figure 4.6).

#### 4.3.4 N-terminal sequencing analysis of purified LH2-1B1A

The two major populations of LH2-1B1A that eluted from the Source 15Q ion exchange column underwent further purification separately by gel filtration as described in section 4.3.1. Each purification product was then N-terminally sequenced as described in section 2.8.6 N-terminal sequence data was obtained from the SDS-PAGE gel bands corresponding to the  $\alpha$ - and  $\beta$ - polypeptides of LH2. The blotting membrane onto which the polypeptides were transferred and isolated from is shown in Figure 4.7A. The N-terminal sequence of the  $\beta$ -polypeptide agreed with previously published data (Zuber *et al* 1985). The  $\alpha$ -polypeptide sequence also agreed with Zuber *et al.*, (1985), however the  $\alpha$ -polypeptide gel band was seen to contain a significant contribution from a previously undescribed peptide. The N-terminal sequence obtained for this peptide is SDMEXAMSQM.

A BLAST search was carried out using the sequence SDMEXAMSQM, and the peptide was shown to be hypothetical protein RSP6124, which has been putatively identified after genome analysis of *Rba. sphaeroides* 2.4.1. The gene encoding RSP6124 has been assigned the accession number CP000143 ([www.rhodobacter.org](http://www.rhodobacter.org)); CP000143 will be referred to in this study as *rsp6124*. RSP6124 is predicted to be 103 amino acids in length. The LH2  $\alpha$  bands for peaks 1 and 2 of the Source 15Q purification were composed of 46 % and 32 % of RSP6124 respectively (Figure 4.7B).

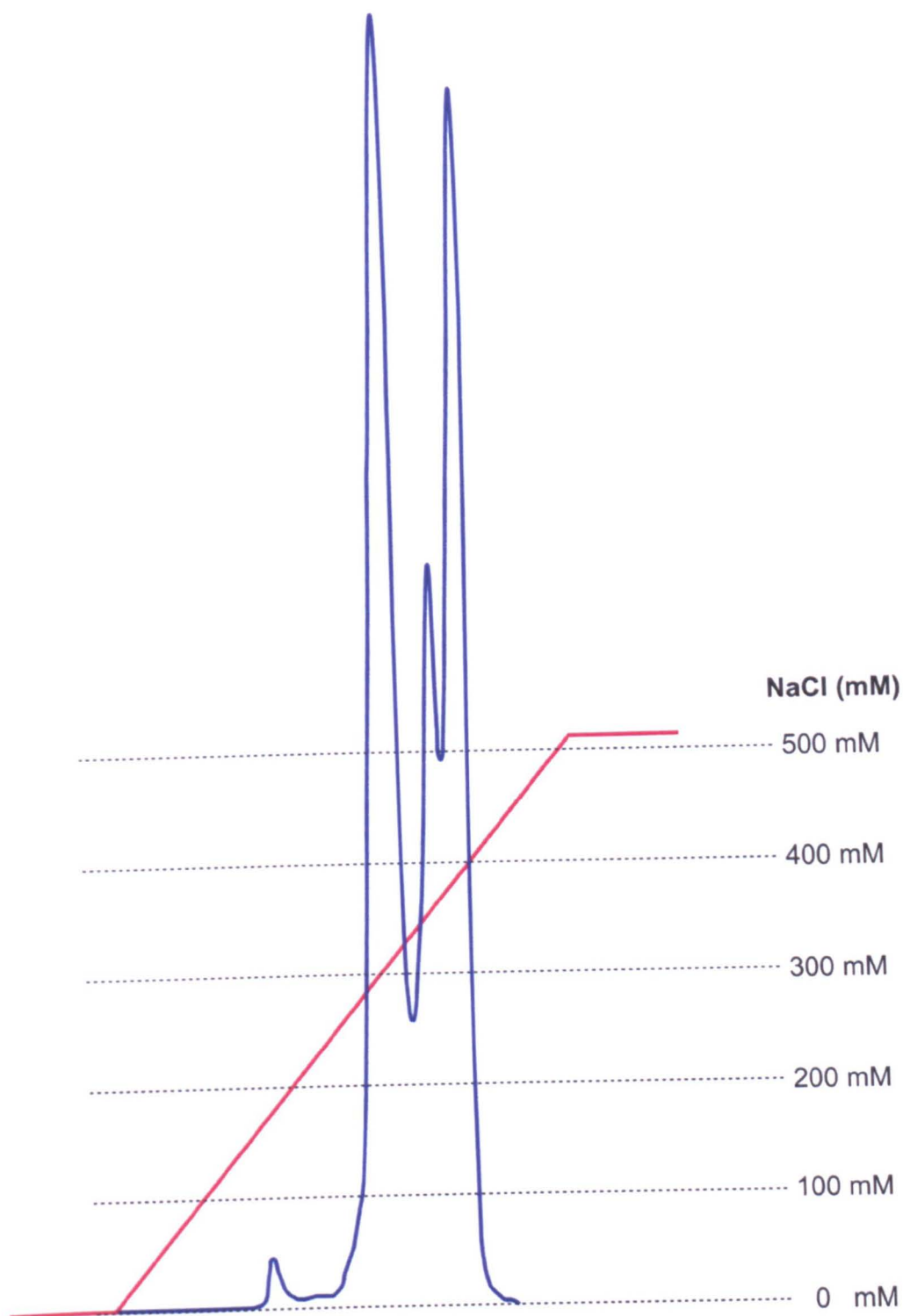


**Figure 4.5 Source 15-Q column elution profile with high sample loading**

The elution profile of LH2-1B2A from a Resource Q ion exchange column is shown. The column was loaded with  $A_{850} = \sim 600$  LH2-1B1A. The concentration of NaCl was increased along a gradient of  $6 \text{ mM ml}^{-1}$ . The NaCl gradient is shown in red; sample absorbance was measured at 280nm and is shown in blue.

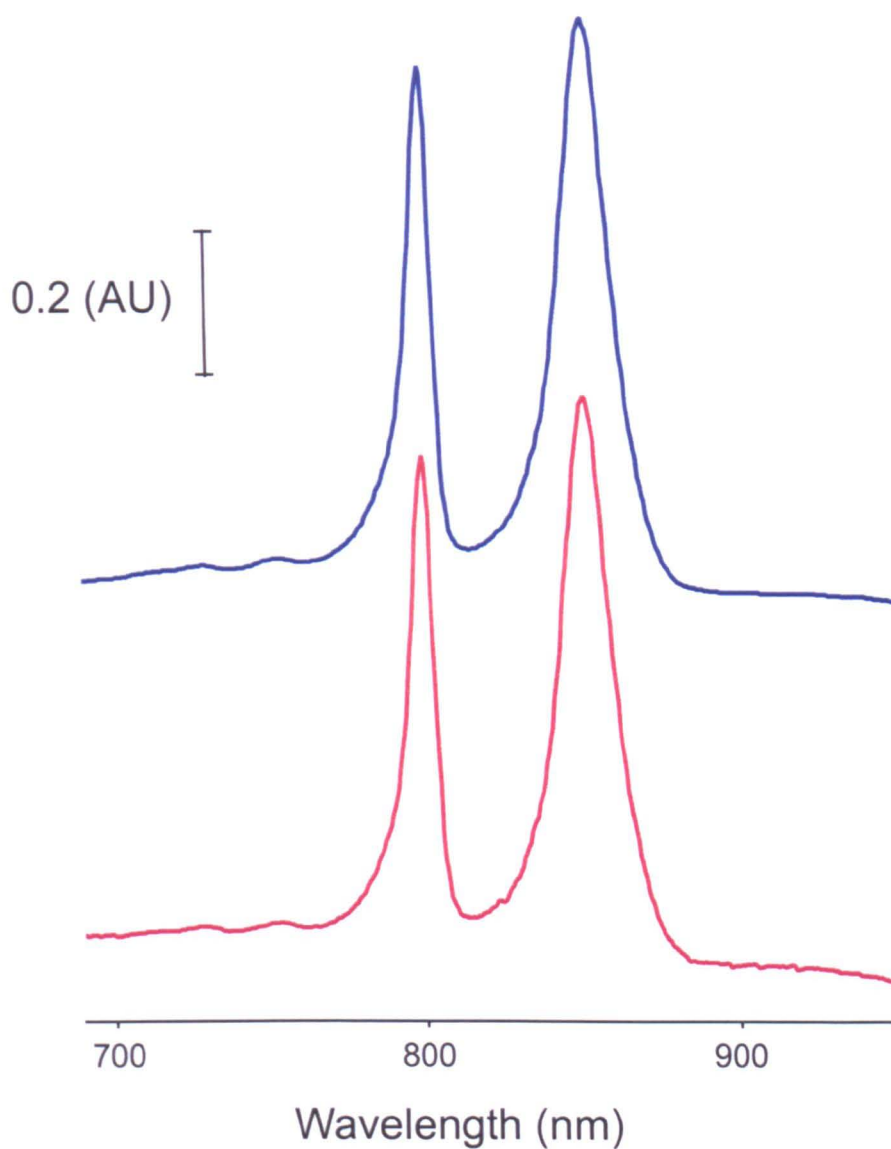
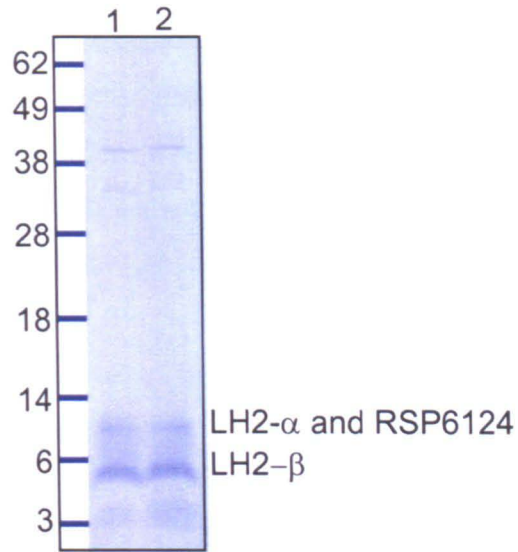


**Figure 4.6 Comparison of Q<sub>y</sub> absorbance maxima between elution peaks**

The Q<sub>y</sub> absorbance maxima of purified LH2 after elution from a Source15Q column are shown. LH2 from the first major elution peak is shown in blue, LH2 from the second major elution peak is shown in red. Data collection was carried out at 77K. Spectra have been normalised to 1AU at 850nm and stacked for clarity.

A



B

Source 15Q column peak 1				Source 15Q column peak 2			
Residue (LH2- $\alpha$ )	aa (pM)	Residue (RSP6124)	aa (pM)	Residue (LH2- $\alpha$ )	aa (pM)	Residue (RSP6124)	aa (pM)
Met	<b>xx</b>	Ser	<b>xx</b>	Met	31.8	Ser	15.4
Thr	140.9	Asp	52	Thr	51.2	Asp	5.8
Asn	128.2	Met	59	Asn	30	Met	4.7
Gly	106.5	Glu	49.8	Gly	17.8	Glu	10.9
Lys	<b>x</b>	Lys	<b>x</b>	Lys	<b>x</b>	Lys	<b>x</b>
Ile	110.9	Ala	48.8	Ile	20.5	Ala	5.8
Trp	14.3	Met	48.5	Trp	1.8	Met	3.6
Leu	88	Ser	33.8	Leu	14.7	Ser	6.8
Val	85.6	Gln	34.3	Val	<b>xx</b>	Gln	<b>xx</b>
Val	110.5	Met	34.3	Val	<b>xx</b>	Met	<b>xx</b>
<b>Total</b>	<b>784.9</b>		<b>360.5</b>		<b>167.8</b>		<b>53</b>
<b>RSP6124</b>		<b>45.92 %</b>				<b>31.85 %</b>	

### Figure 4.7 N-terminal sequence analysis of purified LH2-1B1A

**A** The blotting membrane from which protein bands were extracted and sequenced is shown. The  $\alpha$ - and  $\beta$ -polypeptide are labelled. Lane 1 shows elution peak 1, Lane 2 shows elution peak 2. An indication of the Invitrogen SeeBlue™ markers used is shown.

**B** The amount of LH2- $\alpha$  and RSP6124 in the ' $\alpha$ ' gel band is shown. A comparison of relative concentrations, and the percentage contribution of RSP6124 to the gel band is shown.

#### 4.3.5 Electrospray mass spectroscopy analysis of purified LH2-1B1A

In an attempt to further understand the contribution of RSP6124 to the purified LH2-1B1A sample, electrospray mass spectroscopy was carried out on samples isolated from both major elution peaks from the Source 15Q column. Both samples underwent trypsin cleavage before analysis. The results were analysed using the Mascot search engine (Perkins *et al.*, 1999) and the first half of the RSP6124 peptide was identified (amino acids 2-51), with the ion scores corresponding to the peptide fragments suggesting a high level of significance. No peptide fragments were observed for the second half of the peptide (amino acids 52-104). However, peptide fragments from residues 52-97 of a homologous hypothetical protein in *Rba. sphaeroides* ATCC 17029 were observed. The peptide fragments identified, along with their ion scores are displayed in Figure 4.8

#### 4.3.6 Bioinformatic analysis of RSP6124

The amino acid sequence of RSP6124 is shown in Figure 4.8. The protein has been probed using a range of different bioinformatic tools in order to characterise any primary, secondary or tertiary structural domains present. BLAST searches using the primary amino acid sequence of RSP6124 showed no significant homology with any known protein. Homology was identified with two hypothetical proteins which were putatively assigned after analysis of the draft genome sequences of the related strains *Rba. sphaeroides* ATCC 17025 and *Rba. sphaeroides* ATCC 17029 ([www.genome.jgi-psf.org](http://www.genome.jgi-psf.org)). Sequence alignments of *rsp6124* and RSP6124 have been carried out with the corresponding hypothetical gene and protein sequences of the two related strains and are displayed in Figure 4.9. The homologous protein, hypothetical protein rsph17025\_3142, from *Rba. sphaeroides* ATCC 1725 will be referred to as RSP3142 in this study. Hypothetical protein rsph17029\_1843, from *Rba. sphaeroides* ATCC 17029 will be referred to as RSP1843 in this study.

RSP3142 and RSP1843 share 100% and 98.5% sequence identity respectively with RSP6124, between residues Met<sub>1</sub> and Thr<sub>69</sub>. Between residues Gly<sub>70</sub> and Arg<sub>103</sub>, RSP6124 shares no identity with either hypothetical protein.

Residue number (start-end)	Expected molecular mass	Observed molecular mass	Peptide sequence	Ion score
7 - 18	1322.5897	1322.6032	K.AMSQMLADMTPK.K	71
7 - 18	1338.5856	1338.5982	K.AMSQMLADMTPK.K (oxidation M)	74
19 - 29	1274.6811	1274.6870	K.KLPTNEEIFGK.G	51
19 - 37	2015.0603	2015.0687	K.KLPTNEEIFGKGAQLGDAK.A	36
38 - 51	1525.7087	1525.7156	K.AMGFTDILDSMTPK.K	58
52 - 81	3404.7552	3404.7867	K.KLPTNEEIFGQLAELDTTAFDALDLFRPK.K	44
82 - 91	1182.5838	1182.5954	K.KLMSYDELGK.M	85
92 - 97	711.3368	711.3447	K.MVGMKF.-	38

#### Amino acid sequence for RSP6124

1 **MSDMEKAMSQMLADMTPKKLPTNEEIFGKGAQLGDAK**

38 **AMGFTDILDSMTPK**KLPTNEEIFGQLAELDTTGLRR

74 **AARSLPAEEADELRRARQDGRDEVLIDKGRM**

#### Amino acid sequence for RSP1843

1           - -+               - ++           -- +           - +  
**MSDMEKAMSQMLADMTPKKLPTNEEIFGKGAQLGDAK**

38               - -           ++           --           - -           -  
**AMGFTDILDSMTPKKLPTNEEIFGQLAELDTTAFDAL**

74           - + ++           -- +           +  
**DLFRPKKLMSYDELGKMVGMKF**

**Figure 4.8 Identification of RSP6124 by electrospray mass spectroscopy**

The purified LH2 sample underwent trypsin cleavage. The peptide fragments of RSP6124 were identified by mass spectroscopy. Matched peptides are shown in red. Regions of RSP1843 from *Rba. sphaeroides* ATCC 17029 were also identified; these are shown in blue. Charged residues have been highlighted within the RSP1843 sequence.

**A**

Rsph 241	ATGTCTGATA	TGGAAAAGGC	GATGTCGCAG	ATGCTGGCCG	ACATGACGCC	50
Rsph 17029	ATGTCTGATA	TGGAAAAGGC	GATGTCGCAG	ATGCTGGCCG	ACATGACGCC	50
Rsph 17025	ATGTCTGATA	TGGAAAAGGC	GATGTCGCAG	ATGCTG <b>A</b> CCG	ACATGACGCC	50
Rsph 241	GAAGAAGCTG	CCCACCAATG	AGGAAATCTT	CGGCAAGGGC	GCCCAGCTGG	100
Rsph 17029	GAAGAAGCTG	CCCACCAATG	AGGAAATCTT	CGGCAAGGGC	GCCCAGCTGG	100
Rsph 17025	GAAGA <b>A</b> ACTG	CCCACCA <b>A</b> CG	<b>A</b> AGAGATCTT	CGGCAAGGGC	GCCCAGCTGG	100
Rsph 241	GCGACGCCAA	GGCGATGGGC	TTCACCGACA	TCCTCGACTC	<b>G</b> ATGACGCCG	150
Rsph 17029	GCGACGCCAA	GGCGATGGGC	TTCACCGACA	TCCTCGACTC	CATGACGCCG	150
Rsph 17025	GCGACG <b>G</b> GAA	GGCGATGGGC	TTCACCGACA	TCCTCGA <b>T</b> TC	CATGACGCCG	150
Rsph 241	<b>A</b> AGAA <b>A</b> CTGC	CGACCAACGA	AGAGATCTTC	GGCCAGCTCG	CCGAGCTCGA	200
Rsph 17029	AAGAAGCTGC	CGACCAACGA	AGAGATCTTC	GGCCAGCTCG	CCGAGCTCGA	200
Rsph 17025	AAGAAGCTGC	CGACCAACGA	AGAGATCTTC	GGCC <b>A</b> ACTCG	CCG <b>A</b> ACTCGA	200
Rsph 241	CACGACGGGC	CTTCGACGCG	CTGCTCGATC	TCTTCCGGCC	GAAGAAGCTG	250
Rsph 17029	CACGACGG <b>.</b> C	CTTCGACGCG	CTGCTCGATC	TCTTCCGGCC	GAAGAAGCTG	250
Rsph 17025	CACGACGG <b>.</b> C	CTTCGACGCG	CTGCTCGA <b>G</b> C	TCTT <b>C</b> ACCC	GAAGAAGCTG	250
Rsph 241	ATGAGCTACG	ACGAGCTCGG	CAAGATGGTC	GGGATGAAGT	TCTGATCGAC	300
Rsph 17029	ATGAGCTACG	ACGAGCTCGG	CAAGATGGTC	GGGATGAAGT	TCTGA.....	300
Rsph 17025	ATGAGCTACG	ACGA <b>A</b> CTCGG	<b>G</b> AAAAGCCTC	<b>GG</b> CCTC <b>A</b> AGC	TCTGA.....	300
Rsph 241	<b>A</b> AGGGACGCT	<b>GA</b>				
Rsph 17029	.....	..				
Rsph 17025	.....	..				

**B**

RSP6124	MSDMEKAMSQ	MLADMTPKKL	PTNEEIFGKG	AQLGDAKAMG	FTDILDSMTF	50
RSP1843	MSDMEKAMSQ	MLADMTPKKL	PTNEEIFGKG	AQLGDAKAMG	FTDILDSMTF	50
RSP3142	MSDMEKAMSQ	ML <b>T</b> DMTPKKL	PTNEEIFGKG	AQLGDAKAMG	FTDILDSMTF	50
RSP6124	KKLPTNEEIF	GQLAELDTTG	LRRAARSLPA	EEADELRRAR	QDGRDEVLLID	100
RSP1843	KKLPTNEEIF	GQLAELDTTA	FDALLDLFRE	KKLMSYDELG	KMVMKMF...	100
RSP3142	KKLPTNEEIF	GQLAELDTTA	FDALLE <b>L</b> FTF	KKLMSYDELG	KSLGLKL...	100
RSP6124	<b>KGR</b>					
RSP1843	...					
RSP3142	...					

**Figure 4.9 DNA and protein sequence alignments**

The DNA sequences which encode the hypothetical proteins RSP6124, RSP1843 and RSP3142 are aligned for comparison. The organisms in which these proteins are found are *Rba. sphaeroides* 2.4.1., *Rba. sphaeroides* ATTC17029 and *Rba. sphaeroides* ATTC 17025 respectively. Protein sequence alignments are also shown.

**A** – DNA sequence alignment  
**B** – Protein sequence alignment

RSP3142 and RSP1843 comprise 97 amino acids, and share 80% sequence identity and 92% similarity between residues 70 and 97. The stark contrast in the C-terminal region of RSP6124 in comparison to the two hypothetical proteins can be explained when the DNA alignments are analysed, with a frame shift being observed between base pairs 208 and 209 (Figure 4.9). This observation explains the discrepancy in the C-terminal sequence of peptide fragments observed in section 4.3.5, and this is discussed further in section 4.4.3. It should be noted that all bioinformatic analyses on RSP6124 were carried out using the amino acid sequence obtained by electrospray mass spectroscopy, not the sequence proposed after analysis of the *Rba. sphaeroides* 2.4.1. genome ([www.rhodobacter.org](http://www.rhodobacter.org)).

The 1D secondary structure of RSP6124 was predicted using the PROFsec programme at [www.predictprotein.org](http://www.predictprotein.org). The analysis was not conclusive, but a stretch of 11 amino acids at the N-terminus is predicted to form an helical structure, with the 8 residues immediately following forming a loop region. The probabilities for these regions of secondary structure as well as other less well defined regions are shown in Figure 4.10A.

The amino acid motif LXXMTPKKLPTNEEIFGXXAXL is repeated within the primary sequence of RSP6124 between residues Leu<sub>12</sub> - Leu<sub>33</sub> and Leu<sub>45</sub> - Leu<sub>66</sub> (Figure 4.10B). This motif has been subjected to a BLAST search, but no homology was found to any other protein sequence.

Transmembrane hidden Markov model 2.0 analysis predicted RSP6124 to be completely extramembranous, with no transmembrane or membrane associated domains being recognised. In addition, no homology with any 3D domains of known proteins was found by the SWISS MODEL comparative modelling programme ([swissmodel.expasy.org](http://swissmodel.expasy.org)). 28 of the 97 amino acids in this sequence are charged polar side chains, almost equally proportioned between positive charges (12) and negative charges (16).

## A

```

1 MSDMEKAMSQMLADMTPKKLPTNEEIFGKGAQLGDAKAMGFTDILDSMTPKKLPTNEEIFGQLAELDTT 69
2 .. HHHHHHHHHHHH..... HHH..... HHHHHHH.....
3 |..... LLLLLLL..... LLLLLLL..... |..
4 947889888887505888799817          6888688827887778

```

```

1 AFDALLDLFRPKKLMSYDELGKMVGMKF 97
2 .... HHH.....
3 . LLL.....
4 8888863

```

## B

```

7  AMSQMLADMT  PKKLPTNEEI  FGKGAQLGDA  36
   |  |  |  |  |  |  |  |  |  |  |  |  |  |  |
40 GFTDILDSMT  PKKLPTNEEI  FGQLAELDTT  69

```

### Figure 4.10 Predict protein analysis of RSP6124

A. The results of a PredictProtein analysis of RSP6124 are shown.

1. The amino acid sequence of RSP6124 is shown
2. Predicted regions of alpha helix are shown in red
3. Predicted loop regions within the protein are shown in green.
4. The probability for each prediction is scored out of 9 (0=low, 9=high). Predictions with scores higher than 6 are highlighted in yellow

B. A repeated motif LXXMTPKKLPTNEEIFGXXAXL is observed within the primary amino acid sequence of RSP6124

The region of DNA containing *rsp6124* was identified using the genome sequence for *Rba. sphaeroides* 2.4.1. published online ([www.rhodobacter.org](http://www.rhodobacter.org)). Sequence alignments of the 1000 bp region of DNA directly upstream of *rsp6124*, and the known sequences of the oxygen regulated promoters of the *puf* and *puc1BAC* operons were carried out using the T-coffee alignment software (Notredame *et al.*, 2000). Figure 4.11 highlights regions 1 and 2 showing 43 and 50 % identity respectively to the *puc* promoter. Regions 3, 4, and 5 share 41, 31, and 37 % sequence identity with the *puf* promoter respectively.

#### 4.3.7 Crystallisation trials of LH2-1B1A

The screening of crystallisation conditions for LH2-1B1A was carried out in three stages. Firstly, the conditions at which LH2 from *Rps. acidophila* formed crystals were initially used as a template for LH2-1B1A crystallisation. As described in section 2.8.4, the sitting drop method was used, with ammonium sulphate at concentrations ranging from 2.4 - 3.2 M present as the reservoir solution. The drop solution initially contained a combination of phosphate buffer (at 0.8 M or 0.9 M concentration), LH2-1B1A (at 100 A<sub>850</sub> units ml<sup>-1</sup>) and the amphiphile benzimidazole hydrochloride (at 3.5 % w/v). The screens applied are all listed in Appendix II; this work was carried out in Professor Richard Cogdell's laboratory at Glasgow University. The initial screens yielded clustered crystals, which are shown in Figures 4.12A and 4.12B.

Secondary screens narrowed the range of crystallisation conditions attempted. Varying concentrations of MgCl or NaCl were added to the protein solution in the sitting drop. These screens are also detailed in Appendix II. The crystals obtained are displayed in Figures. 4.12C and 4.12D. The addition of MgCl<sub>2</sub> yielded no crystals, however, varying the concentration of NaCl altered the morphology of the crystals which formed. Crystal formation occurred on a 2 – 3 week timescale.

Finally, tertiary screens were designed around the results obtained in the first two screens. Duplicate tertiary screens were set up, with the two distinct populations of



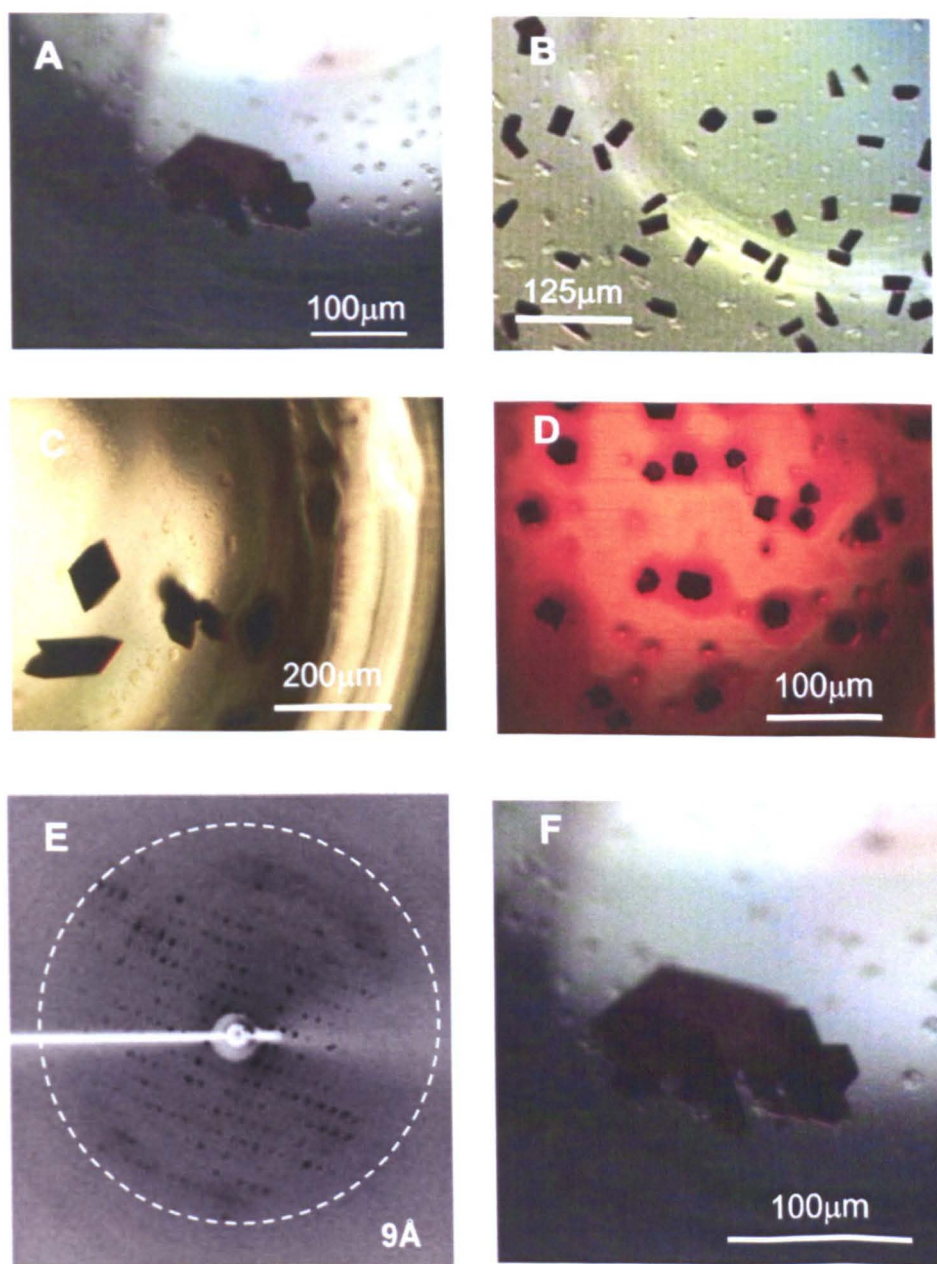


**Figure 4.12 Crystallisation of the purified LH2-1B1A**

- A. Clustered crystals grown at Glasgow University during first phase trials.
- B. Smaller monoclinic crystals grown at Glasgow University during first phase trials.
- C. Crystals grown in the absence of NaCl during second phase trials at the University of Sheffield.
- D. Crystals grown in the presence of NaCl during second phase trials at the University of Sheffield.
- E. A diffraction pattern obtained from the crystal cluster shown in panel F.
- F. An enlarged image of the crystal cluster seen in panel A, which is seen to diffract in panel E

All the conditions at which the crystals shown are seen to form are detailed in Appendix II

LH2-1B1A separated during the Source15Q ion exchange purification process, being crystallised independently of each other. The final screens were carried out at Daresbury-SRS laboratories. The Innovadyne Screenmaker 96+8 crystallisation robot was used to screen 576 different crystallisation conditions. Crystals grew at 130 of these conditions, taking ~3 weeks to form. For each crystal trial, identical crystal morphology was observed for both populations of LH2-1B1A. A full description of all the conditions trialled and a summary of the crystals formed are shown in Figures 4.13, 4.14 and 4.15.

#### **4.3.8 Diffraction of LH2-1B1A crystals**

Of the crystals produced in the laboratory of Professor Richard Cogdell, the most highly diffracting showed diffraction to 9Å resolution, using the X-ray source located at Glasgow University. The resulting diffraction data could not yield any structural details as there was too high a degree of mosaic spread (Figure 4.12E).

Large scale screening of the crystals for their diffraction properties was performed by Dr Miroslav Papiz at the Daresbury-SRS facility. This was carried out by the method described in section 2.8.5. No changes were observed in diffraction when the humidity of the crystal environment was altered. The intrinsic humidity of the crystal's phosphate buffer was 92%, which was established using the Free Mounting System (FMS) (Proteros Gmb). All screenings were subsequently carried out at this relative humidity. The most highly diffracting crystals formed in well B-V displayed in Figure 4.13A, with resolution achieved at the 10Å level (Figure 4.13B).

**A**

	I	II	III	IV	V	VI	VII	VIII	IX	X	XI	XII	XIII	XIV	XV	XVI	
A	◆	◆	◆	◆	◆	◆	◆	◆	◆	◆							0
B			◆	◆	◆	◆	◆	◆	◆	◆	◆	◆	◆	◆			0.091
C							◆	◆	◆	◆	◆	◆	◆	◆			0.182
D	◆	◆															0.273
E																	0.364
F																	0.455
G					◆	◆											0.545
H																	0.636
I																	0.727
J																	0.818
K																	0.909
L																	1
	2.40		2.57		2.74		2.91		3.09		3.26		3.43		3.60		
	$[(\text{NH}_4)_2\text{SO}_4] \text{ (M)}$																

$[\text{NaCl}] \text{ (M)}$

**B**

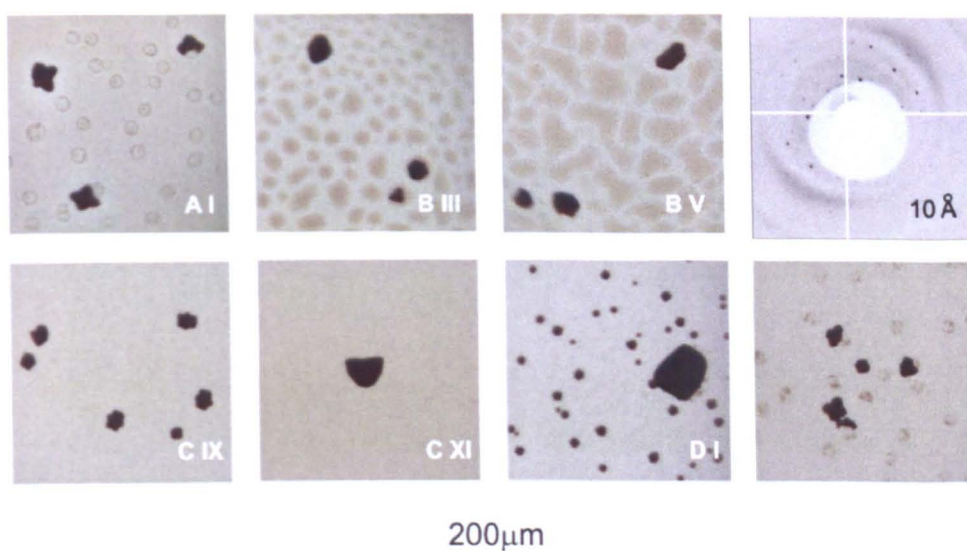


**Figure 4.13 Crystal growth and screening at Daresbury SRS ( i )**

**A** The crystal trial conditions carried out upon the Innovadyne Screenmaker 96+8 are summarised. A blue diamond indicates crystal formation. The protein solution crystallised contained 0.8 M Phosphate buffer (pH 8.0), 0.1% LDAO, LH2-1B1A ( $A_{850} 100 \text{ ml}^{-1}$ ), 3.5 % benzamidine hydrochloride and the NaCl concentration was varied as shown. The  $(\text{NH}_4)_2\text{SO}_4$  (pH 9.0) reservoir concentrations were varied and are shown. Both elution peaks from the Source 15Q ion exchange column were crystallised separately. Panels denoted by odd numbers were from Peak 1, panels denoted by even numbers were from Peak 2.

**B** A representative sample of the crystals which were later screened for diffraction at Daresbury SRS. The diffraction pattern obtained for the crystals displayed in panel B-V is shown.

**A**

	I	II	III	IV	V	VI	VII	VIII	IX	X	XI	XII	XIII	XIV	XV	XVI	
A					◆	◆	◆	◆	◆	◆	◆	◆	◆	◆	◆	◆	0
B							◆	◆	◆	◆	◆	◆	◆	◆			0.091
C										◆	◆	◆	◆	◆	◆	◆	0.182
D													◆	◆	◆	◆	0.273
E													◆	◆	◆	◆	0.364
F																	0.455
G											◆	◆			◆	◆	0.545
H											◆	◆			◆	◆	0.636
I																	0.727
J																	0.818
K																	0.909
L																	1
	2.40		2.57		2.74		2.91		3.09		3.26		3.43		3.60		

[(NH<sub>4</sub>)<sub>2</sub>SO<sub>4</sub>] (M)

[NaCl] (M)

**B**

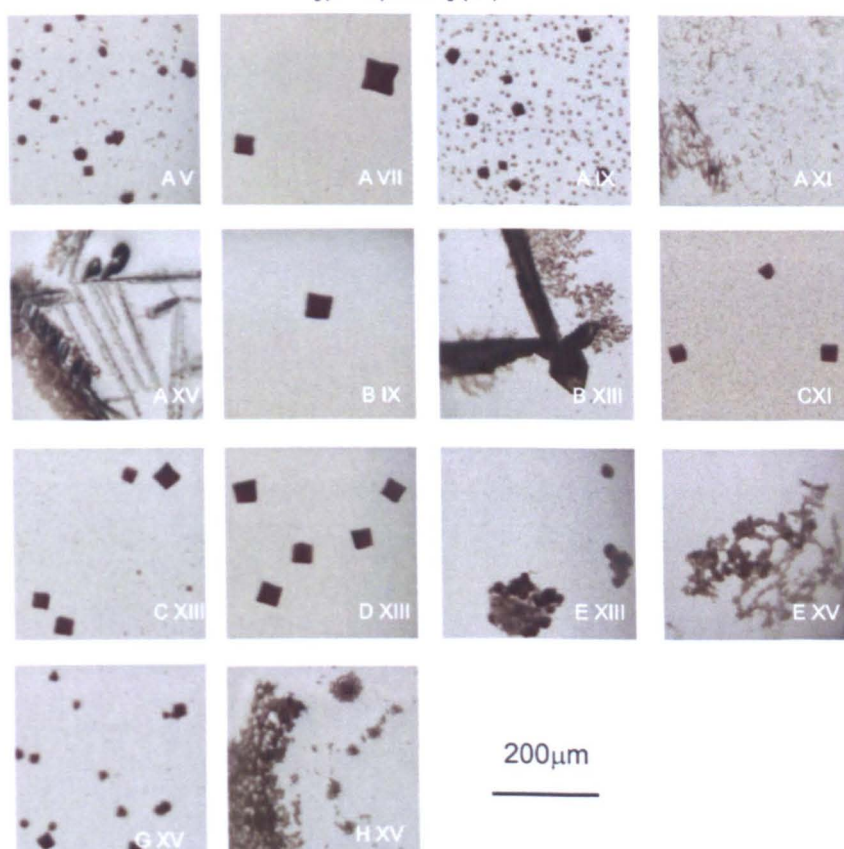


**Figure 4.14 Crystal growth and screening at Daresbury SRS ( ii )**

**A** The crystal trial conditions carried out upon the Innovadyne Screenmaker 96+8 are summarised. A blue diamond indicates crystal formation. The protein solution crystallised contained 0.8M phosphate buffer (pH 8.0), 0.1% LDAO, LH2-1B1A ( $A_{850}$  100 ml<sup>-1</sup>), 3.5 % benzamidine hydrochloride, 0.2% n-undecyl-β-D-maltoside and the NaCl concentration was varied as shown. The (NH<sub>4</sub>)<sub>2</sub>SO<sub>4</sub> (pH 9.0) reservoir concentrations were varied and are shown. Both elution peaks from the Source 15Q ion exchange column were crystallised separately. Panels denoted by odd numbers were from Peak 1, panels denoted by even numbers were from Peak 2.

**B** A representative sample of the crystals which were later screened for diffraction at Daresbury SRS.

A

	I	II	III	IV	V	VI	VII	VIII	IX	X	XI	XII	XIII	XIV	XV	XVI	
A	◆	◆	◆	◆	◆	◆	◆	◆	◆	◆					◆	◆	0
B			◆	◆	◆	◆	◆	◆	◆	◆	◆	◆	◆	◆	◆	◆	0.091
C									◆	◆	◆	◆	◆	◆	◆	◆	0.182
D											◆	◆	◆	◆	◆	◆	0.273
E													◆	◆	◆	◆	0.364
F																	0.455
G							◆	◆					◆	◆			0.545
H																	0.636
I													◆	◆			0.727
J																	0.818
K																	0.909
L																	1
	2.40		2.57		2.74		2.91		3.09		3.26		3.43		3.60		

[[NH<sub>4</sub>]<sub>2</sub>SO<sub>4</sub>] (M)

[NaCl] (M)

B

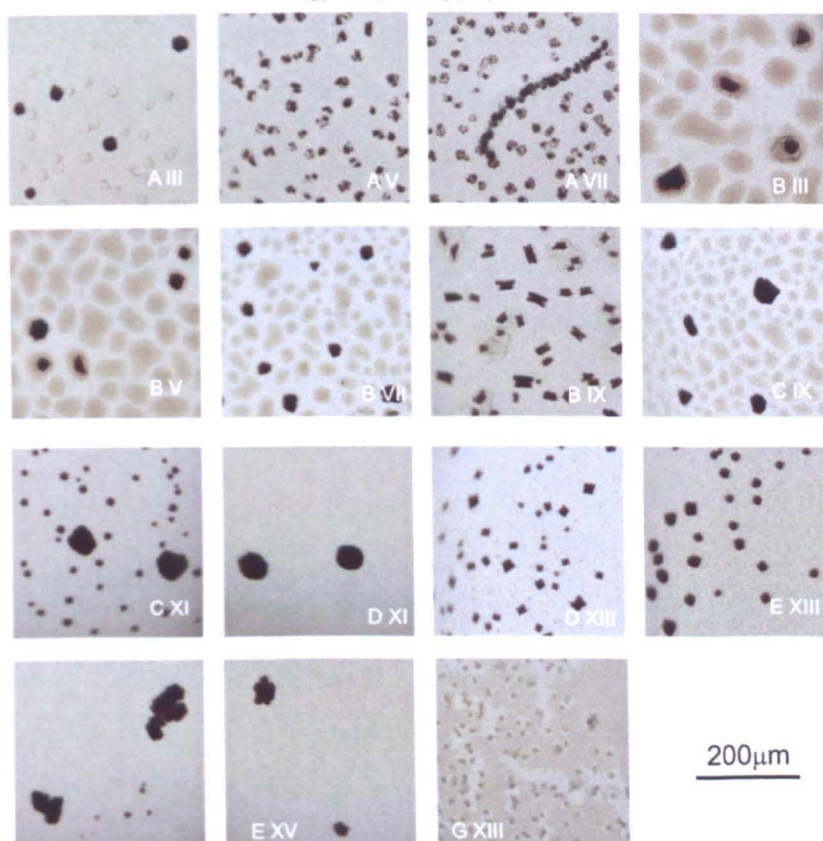


**Figure 4.15 Crystal growth and screening at Daresbury SRS ( iii )**

**A** The crystal trial conditions carried out upon the Innovadyne Screenmaker 96+8 are summarised. A blue diamond indicates crystal formation. The protein solution crystallised contained 0.9M phosphate buffer (pH 8.0), 0.1% LDAO, LH2-1B1A ( $A_{850}$  100 ml<sup>-1</sup>), 3.5 % benzamidine hydrochloride and the NaCl concentration was varied as shown. The (NH<sub>4</sub>)<sub>2</sub>SO<sub>4</sub> (pH 9.0) reservoir concentrations were varied and are shown. Both elution peaks from the Source 15Q ion exchange column were crystallised separately. Panels denoted by odd numbers were from Peak 1, panels denoted by even numbers were from Peak 2.

**B** A representative sample of the crystals which were later screened for diffraction at Daresbury SRS.

## 4.4 Discussion

### 4.4.1 Context

The discovery of the second *puc* operon in *Rba. sphaeroides*, and the revelation that the LH2 ring is heterologous in nature with regard to the  $\beta$ -polypeptide (Zeng *et al.*, 2003), placed a new emphasis on not only the mutagenesis work previously carried out on the complex, but also provided the possibility of a new avenue for investigating its 3D structure. It is postulated that a reason behind the failure of previous 3D structural investigations could be the heterogeneity introduced into the complex by the presence of the second  $\beta$ -polypeptide, with the regular lattice contacts required in the third plane of the crystal being interrupted by the variations in the extramembranous regions of the  $\beta$ -polypeptides. The deletion of *puc2BA* provides the opportunity to purify and crystallise a homogenous LH2 complex. The results presented in this chapter detail attempts to crystallise the protein for 3D structural analysis. During this process a novel protein, RSP6124, co-purifies with LH2, suggesting an alternative explanation for previous failures to elucidate the 3D structure of the LH2 complex in *Rba. sphaeroides*.

### 4.4.2 The purification of LH2-1B1A

The purification described in section 4.3.2 was adapted from a method developed at the University of Glasgow. Stringent purification of the LH2-1B1A complex was required to obtain monodisperse protein for crystallisation (Figures 4.1, 4.2, 4.3). There are clearly different populations of LH2-1B1A present in the purified sample. The different peaks that eluted from the Source15Q ion exchange column (Figure 4.5) cannot be attributed to complexes differing markedly in their structure, as the spectral properties of the two peaks are identical (Figure 4.6). The difference in the contribution of RSP6124 to each peak may explain the elution pattern. The putative association of RSP6124 may affect the binding of LH2-1B1A to the ion exchange matrix, with higher concentrations of RSP6124 seen in the first peak than the second (Figure 4.7). The possibility of using a higher resolution binding resin, such as

monoQ™, should be explored in future to explore the possibility of separating the different populations completely.

At 10.8 kDa, RSP6124 is ~10 times smaller than an intact LH2 complex, but is seen to elute with LH2 after gel filtration. Co-purification of the two proteins after selection for their size and charge properties indicates a significant interaction between them. It seems likely that RSP6124 adheres very strongly to extrinsic regions of LH2, with almost 1 in 3 amino acid residues of RSP6124 carrying a charge (Figure 4.8). The C-terminus of LH2 has a total of 9 negative charges; in contrast the N-terminus of the complex has 54 negative and 45 positive charges. The extent of contamination of the  $\alpha$ -polypeptide band with RSP6124 is consistent with between 2-3 RSP6124 molecules per LH2 ring balancing out the charges and possibly adhering electrostatically to the extrinsic N-terminus. Such is the strength of these interactions that not even 400 mM NaCl can separate the two proteins.

#### 4.4.3 RSP6124: a novel protein in *Rba. sphaeroides*

The role RSP6124 plays within the cell is currently unknown. Its co-purification with LH2-1B1A after such a stringent series of purification steps is certainly significant. The fact electrospray mass spectroscopy of samples purified from *Rba. sphaeroides* 2.4.1. uncovered peptide fragments identical to the second half of RSP1843 from *Rba. sphaeroides* ATTC\_17029 indicates the frame shift observed in Figure. 4.9 is in fact a genome sequencing error; the C-terminal sequence of RSP6124 is actually identical to that of RSP1843. Unfortunately, bioinformatic tools have not yielded any compelling information that could assign a putative role to RSP6124. The Transmembrane hidden Markov model 2.0 analysis, which showed no membrane associated regions within the protein, indicates any association with LH2 would likely be at the cytoplasmic or periplasmic interface of the complex. The lack of any homology with any known 3D protein domains shown by SWISS MODEL means the nature of any interactions RSP6124 shares with other proteins cannot be speculated upon. The repeated motif, LXXMTPKKLPTNEEIFGXXAXL, may be of significance in a structural or interaction recognition role, but the lack of homology this motif

shares with any other known sequence does not allow any further conjecture. The PredPlot analysis shows RSP6124 is likely to be soluble, comprising predominantly  $\alpha$ -helical and loop regions, but again the level of significance which can be placed upon this conclusion is not high.

The region of DNA upstream of *rsp6124* shares two regions of sequence homology with the *puc* promoter (Lee and Kaplan, 1992); one is ~400 bp more distal to the start of *rsp6124* than the *puc* promoter is to the *puc* operon, so this may be too far upstream to be implicated in RSP6124 expression. The second observed homology is with the *puf* promoter, with regions between ~500 and ~100 bp upstream of the start codon; these are more proximal to the start of *rsp6124* (Figure 4.11) than those seen for the regions of *puc* homology. These alignments suggest oxygen regulated expression could be acting upon *rsp6124*. If *rsp6124* does possess an oxygen regulated promoter, its transcription would be concomitant with that of light harvesting polypeptides. This coupled with the co-purification of RSP6124 with LH2-1B1A means that it is possible to propose a role in the assembly or function of the light harvesting complexes, particularly LH2 for example. However it should be noted that RSP6124 has never been identified in any AFM studies of *Rba. sphaeroides* membranes, so the procedures used to prepare these membrane patches appear to remove RSP6124.

In work carried out by Dr Jaimey Tucker, RSP6124 has been shown to be present within the Upper Pigmented Band (UPB) precursor fraction of purified membranes from *Rba. sphaeroides* 2.4.1. The UPB is the biosynthetic precursor of the mature ICM (Niederman *et al.*, 1979). The presence of RSP6124 was determined by electrospray mass spectroscopy, but it was absent from the ICM fraction of the same sample (data not shown). This result adds support to the hypothesis that RSP6124 is involved in either assembly of the LH2 complex, or that it directs its arrangement within the developing photosynthetic membrane.

Unfortunately the discovery of RSP6124 was made at a late stage within the lifetime of this project. Future work should focus on the creation of a *rsp6124* null mutant, to probe any phenotypic effects upon LH2 complex assembly. It is also of fundamental

importance to remove the protein from purified samples intended for crystallisation studies as its presence in such high quantities could have a deleterious effect upon the order of the crystal lattice being formed. Once *rsp6124* has been isolated genetically, the protein can be tagged and expressed, allowing the production of antibodies, which can be used to track its assembly and location during membrane development.

#### 4.4.4 Crystallisation of LH2-1B1A

To date the highest resolution structural data obtained pertaining to LH2 from *Rba. sphaeroides* has been achieved by EM, with a 6Å projection structure (Waltz *et al.*, 1998). Attempts to achieve atomic resolution by 3D x-ray crystallography have, to date, all been unsuccessful. Atomic resolution data will increase understanding of carotenoid binding within the complex, which has been shown to be different to that of *Rps. acidophila* (Gall *et al.*, 2003). It will also raise the possibility that site directed apoprotein and carotenoid mutants can be analysed structurally. The work presented in this chapter achieved resolution to ~10 Å regularly with crystals screened at Daresbury-SRS. These data does not provide any structural information. The original hypothesis, which supposes the reduction in  $\beta$ -polypeptide heterogeneity gained from the  $\Delta 2BA$  deletion, would increase the regularity of lattice contacts within the crystal, must be modified after the discovery of RSP6124. It is thought that contamination of the purified samples by RSP6124 is a causative factor in unsuccessful attempts to obtain an atomic resolution structure of *Rba. sphaeroides* LH2, since it introduces irregularity into the crystals which form. The genetic deletion of *rsp6124* would be the quickest and most effective way of removing the contaminating protein from the purified LH2-1B1A sample. In addition to this, further crystallisation conditions should be explored, using the successful screens detailed in this chapter as a template. Recent work manipulating the phospholipid (PL) content during crystallisation of lactose permease (LacY) showed three different crystal forms, of increasingly better resolution, occurred as the concentration of co-purified *E. coli* PL was increased (Guan *et al.*, 2006). Further screens should expand the addition of

secondary detergents, along with exploring the inclusion of lipids native to *Rba. sphaeroides* in the trial conditions.

Alternative methodologies that have proven successful for membrane protein crystallisation could also be attempted. Lipidic cubic phase crystallisation of LH2-1B1A has begun in collaboration with Professor Martin Caffrey at the University of Limerick, Ireland. This work is still very early in its development and so has not been detailed in this chapter. This method was recently used to clarify ambiguity surrounding the carotenoid content of LH2 in *Rps. acidophila* (Cherezov *et al.*, 2006), the 3D structure obtained identified regions of electron density previously assigned to a 'bent' carotenoid molecule and showed that they are in fact detergent molecules. Lipidic sponge phase crystallisation has recently been shown to provide practical advantages when working with membrane proteins. Wadsten *et al.*, (2006) used the sponge phase to crystallise the RC from *Rba. sphaeroides* allowing them to build and refine the mobile ubiquinone, in contrast with their previous lipidic cubic phase RC structure. Sponge phases allow membrane protein crystallisation in a native like lipid environment.

## **Chapter 5: The creation of the *Rba. sphaeroides* deletion mutants $\Delta 3$ and $\Delta 4$ , and the comparison of LH2-only membranes containing WT- LH2, LH2-1B1A and LH2-2B1A**

### **5.1 Summary**

The spectroscopic properties of the LH2 complex from *Rba. sphaeroides* have been extensively characterised. The elucidation of the genome sequence of this organism has provided new insight into the genetic components which are expressed to comprise the polypeptides that assemble to form this pigment-protein complex. The second *puc* operon encodes two polypeptides, Puc2B and Puc2A, which are transcribed and translated. Puc2B is assembled into LH2 complexes whilst Puc2A is found in ICM but not incorporated into LH2 complexes.

This chapter details the creation of two new deletion strains of *Rba. sphaeroides* 2.4.1. which lack the ability to assemble any LH2, LH1 or RC. The expression of *puc* genes *in trans* is carried out, and the assembly levels of the LH2 complex in the deletion strains lacking both *puc* operons is shown to be markedly lower than in a deletion strain which carries *puc2BA* on its genome.

The spectroscopic characteristics of LH2 complexes comprising exclusively Puc1B, Puc2B or a mixture of both are analysed whilst bound within the membrane. Puc2B is shown to be integral to B800 BChl binding within the LH2 complex of *Rba. sphaeroides* 2.4.1. A hypothesis for the cause of the reduction of B800 BChl binding in the absence of Puc2B is proposed.

## 5.2 Introduction

The elucidation of the *Rba. sphaeroides* genome sequence ([www.rhodobacter.org](http://www.rhodobacter.org)) has added to an already extensive understanding of the genetic properties of this organism. Of the mutants created those seen to halt the expression of light harvesting complexes are of most interest to this study. The creation of the *Rba. sphaeroides* strain DD13 (Jones *et al.*, 1992) saw the deletion of *puc1BA* by the insertion of a streptomycin resistance cassette ( $\text{Sm}^r$ ), coupled with the insertion of a kanamycin resistance cassette ( $\text{Km}^r$ ) knocking out the *pufBALMX* genes. The loss of all LH2 assembly, as displayed by absorbance spectroscopy, was consistent with the removal of all the genes encoding the LH2 apoproteins. However, Zeng *et al.*, (2003) discovered a second *puc* operon, *puc2BA*, which is now thought to contribute significantly to the levels of LH2 assembly.

The discovery of this gene pair has had significant implications on previous mutagenesis studies, which have focused on the manipulation of  $\beta$ -polypeptide residues in the *Rba. sphaeroides* LH2 complex. The role which this second gene pair plays in the genetic regulation of LH2 expression, as well as the function of the individually encoded polypeptides within the complex, has been explored by Samuel Kaplan's laboratory (Zeng *et al.*, 2003). Zeng *et al.*, (2003) produced a series of in-frame deletion mutants, which included the removal of *puc2B*, *puc2A* and *puc2BA*. The amount of LH2 complex assembly in the resulting mutants in comparison with wild type revealed a 30% decrease in the absence of *puc2B*, whereas the absence of *puc2A* caused no obvious decline in LH2 abundance. The removal of both *puc2* genes resulted in LH2 levels similar to those observed upon removal of *puc2B* alone, with the levels of B875 and hence LH1 assembly apparently unaffected by the deletions made.

These results indicate that the Puc2B polypeptide is exposed to the same assembly pathway as the  $\beta$ - and  $\alpha$ -polypeptides encoded by *puc1BA*. The addition of extra copies of *puc1BA* *in trans* in the *puc2BA* deletion background failed to restore wild type levels of LH2 assembly, indicating that levels of LH2 encoded by *puc1BAC* are

independent of transcript levels within the cell and that heterogeneity of *puc* expression is important in some way. The Puc2A polypeptide is translated and incorporated into the membrane, however it is not present in the LH2 complex itself, leaving ambiguity surrounding the role it plays.

This recent work has implications for results obtained from mutagenesis of *puc1B* using existing LH2 deletion backgrounds, since there are two  $\beta$ -polypeptides to consider rather than the presumed one. This chapter details the creation of two new deletion backgrounds, which are completely lacking in LH2, LH1 and RC encoding genes. The levels of LH2 assembly within these mutants upon complementation *in trans* with *puc* genes are evaluated and compared to those seen in DD13. The contribution of the second  $\beta$ -polypeptide is examined in LH2-only membranes, comparing the spectroscopic properties of LH2 complexes comprising exclusively Puc1B, Puc2B or a mixture of the two polypeptides.

## 5.3 Results

### 5.3.1 Creation of the *Rba. sphaeroides* deletion strains $\Delta 3$ and $\Delta 4$

The creation of the deletion strains  $\Delta 3$  and  $\Delta 4$  is detailed in this section. The suicide vector pSUP202- $\Delta$ BALM was gratefully received from Dr Emma Radcliffe (University of Sheffield). The kanamycin antibiotic resistance cassette carried by this plasmid, derived from the transposon Tn5, is flanked by two regions of DNA homologous to regions  $\sim 1.6$  kb upstream of *pufB* and  $\sim 3$  kb downstream of *pufM*. A representation of this plasmid can be seen in Figure 5.1A. A double homologous recombination event occurring between these regions and those located on the genome

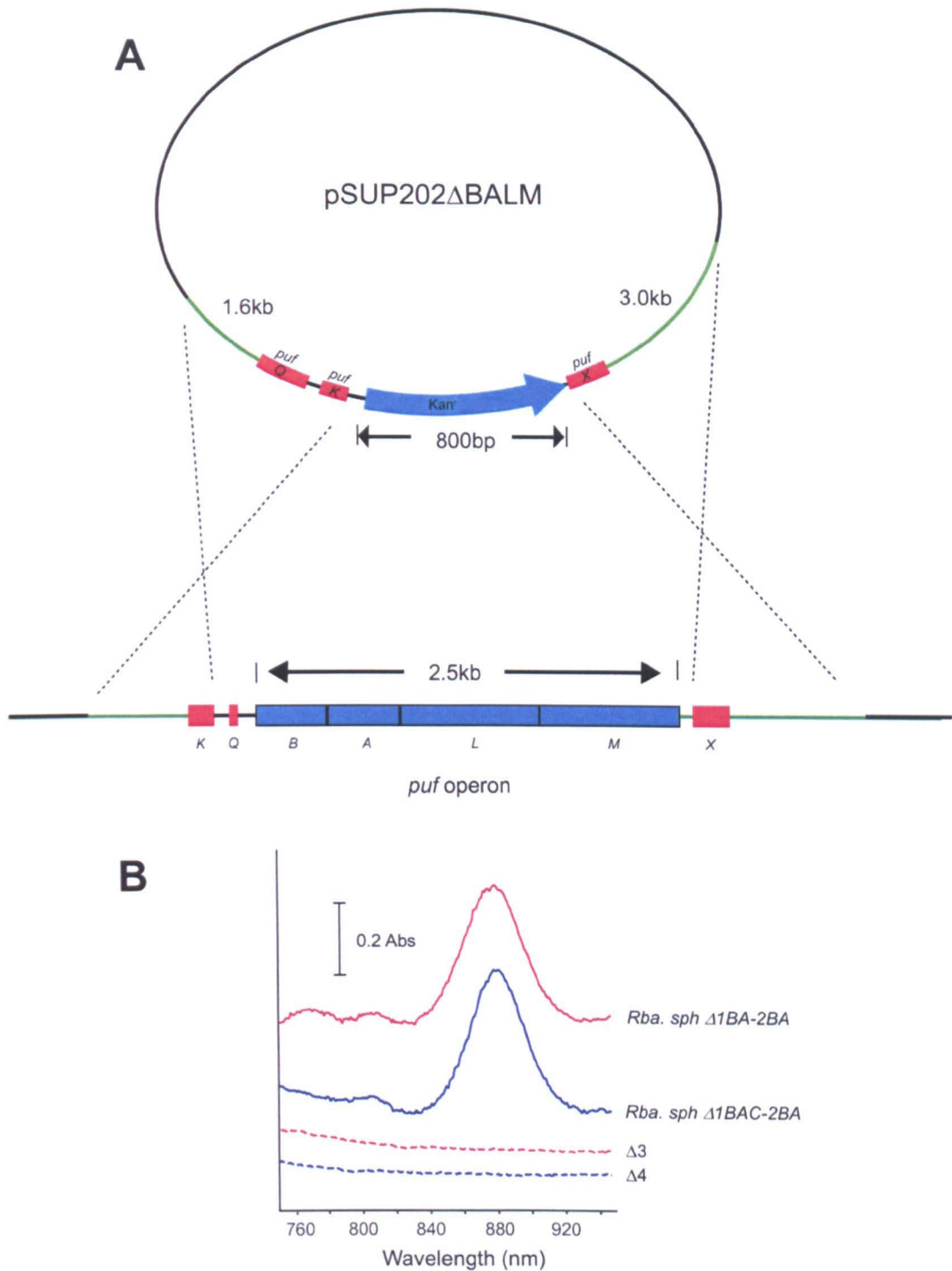


**Figure 5.1 The creation of deletion mutants  $\Delta$ 3 and  $\Delta$ 4**

**A** The pSUP202- $\Delta$ BALM vector is shown. The double homologous event knocking out the *pufBALM* genes is depicted. Homologous regions are depicted in green.

**B** The whole cell absorbance spectra of *Rba. sphaeroides*  $\Delta$ 1BA-2BA and *Rba. sphaeroides*  $\Delta$ 1BAC-2BA were recorded at room temperature. The loss of all light harvesting complex expression is seen in the resulting mutant background  $\Delta$ 3 and  $\Delta$ 4. Spectra have been stacked and corrected for light scattering for clarity.

of a strain of *Rba. sphaeroides* would result in the abolition of the genes *pufBALM* and its replacement with the Kan<sup>r</sup> cassette. In this chapter the strains of *Rba. sphaeroides* into which the antibiotic resistance cassette was incorporated are *Rba. sphaeroides*  $\Delta 1BA-\Delta 2BA$  and *Rba. sphaeroides*  $\Delta 1BAC-\Delta 2BA$  (Appendix I). These strains were gratefully received from Professor Samuel Kaplan (University of Texas, USA). The conjugative transfer and homologous recombination of pSUP202- $\Delta$ BALM into *Rba. sphaeroides*  $\Delta 1BA-\Delta 2BA$  and *Rba. sphaeroides*  $\Delta 1BAC-\Delta 2BA$  created the strains  $\Delta 3$  and  $\Delta 4$  respectively (Figure 5.1).

### 5.3.1.2 Conjugative transfer of the suicide plasmid pSUP202 $\Delta$ BALM

The conjugative transfer of pSUP202- $\Delta$ BALM into the strains *Rba. sphaeroides*  $\Delta 1BA-\Delta 2BA$  and *Rba. sphaeroides*  $\Delta 1BAC-\Delta 2BA$  was carried out using the method described in section 2.11 (Figure 5.1). Selection for recombinant colonies was carried out on M22+ medium agar plates containing neomycin (0.02 mg ml<sup>-1</sup>). The recombinant colonies were isolated and their whole cell spectra were recorded using the Guided Wave Model 260 spectrophotometer. Those colonies displaying the abolition of an absorbance peak at 875 nm were replica plated onto identical grids on M22+ medium agar plates containing either neomycin (0.02 mg ml<sup>-1</sup>), or both neomycin (0.02 mg ml<sup>-1</sup>) and carbenicillin (0.02 mg ml<sup>-1</sup>). This double selection method discriminates between colonies which have undergone single and double recombination events, as a single homologous recombination event would incorporate the entire length of the plasmid DNA into the genome of the host, including the carbenicillin resistance gene found on pSUP202- $\Delta$ BALM. Double recombination events give neomycin resistant colonies but not carbenicillin resistance. Colonies that grew on M22+ media supplemented with neomycin and carbenicillin were assumed to have undergone single homologous recombination events and were discarded. One of the neomycin resistant colonies derived from *Rba. sphaeroides*  $\Delta 1BA-\Delta 2BA$  was isolated and named  $\Delta 3$ . One of the colonies that grew on neomycin only which was originally derived from *Rba. sphaeroides*  $\Delta 1BAC-\Delta 2BA$  was isolated and named  $\Delta 4$ . Absorbance spectra showing the abolition of light harvesting complex assembly in these deletion strains is shown in Figure 5.1B. A comparison of the

genetic backgrounds of the three deletion mutants presented in this chapter is shown in Figure 5.2

### 5.3.2 Analysis of LH2 assembly within *Rba. sphaeroides* $\Delta 3$ and $\Delta 4$

Conjugative transfer of the plasmid pRKCBC1 (Appendix I), which encodes *puc1BAC*, into the strains DD13,  $\Delta 3$  and  $\Delta 4$  was carried out as described in section 2.11. Whole cell absorbance spectra were recorded of the resulting tetracycline resistant colonies using a Guided Wave Model 260 spectrophotometer; the assembly of LH2 within these strains, as well as the acquired antibiotic resistance, confirmed successful complementation with the *puc1BAC* genes.

A comparison of the levels of LH2 assembly within the resulting transconjugate strains was carried out. Cultures of  $\Delta 3$ -pRKCBC1,  $\Delta 4$ -pRKCBC1 and DD13-pRKCBC1 were grown to late log phase semi-aerobically in the dark as described in section 2.10.1. The whole cell absorbance spectra of these cultures were recorded at a normalised cell density of 2.0 at 650 nm. The resulting spectra are shown in Figure 5.3. The levels of LH2 assembly in  $\Delta 3$ (pRKCBC1) and  $\Delta 4$ (pRKCBC1) were ~53 % and ~69 % lower respectively when compared to that of DD13(pRKCBC1).

### 5.3.3 A comparison of LH2-only membranes comprising WT-LH2, LH2-1B1A and LH2-2B1A.

The availability of these new deletion strains provides the opportunity to compare the complexes WT-LH2, LH2-1B1A and LH2-2B1A in the membrane environment. WT-LH2 complexes have a  $\beta$ -polypeptide complement comprised of both Puc1B and Puc2B. The LH2-1B1A complex is comprised of a  $\beta$ -polypeptide ring containing exclusively Puc1B. The LH2-2B1A complex was created by mutation of the *puc1BA* gene pair to encode *puc2B1A* (see Chapter 3), and thus possesses a  $\beta$ -polypeptide ring containing only Puc2B. This section details the absorbance and fluorescence spectral properties of these complexes in isolated ICM. This type of analysis avoids any potential problems associated with differential effects of detergent on the structure or

Strain	Genome		Plasmid	
	<i>puc</i>	<i>puf</i>	<i>puc</i>	<i>puf</i>
Wild-Type	1B 1A C 2B 2A	B A L M X	-- -- -- --	-- -- -- --
DD13	-- -- C 2B 2A	-- -- -- --	-- -- -- --	-- -- -- --
Δ3	-- -- C -- --	-- -- -- X	-- -- -- --	-- -- -- --
Δ4	-- -- -- -- --	-- -- -- X	-- -- -- --	-- -- -- --
DD13(pRKCBC1)	-- -- C 2B 2A	-- -- -- --	1B 1A C -- --	-- -- -- --
Δ3 (pRKCBC1)	-- -- C -- --	-- -- -- X	1B 1A C -- --	-- -- -- --
Δ4 (pRKCBC1)	-- -- -- -- --	-- -- -- X	1B 1A C -- --	-- -- -- --
DD13(pRKCBC-2B1A)	-- -- C 2B 2A	-- -- -- --	-- 1A C 2B --	-- -- -- --

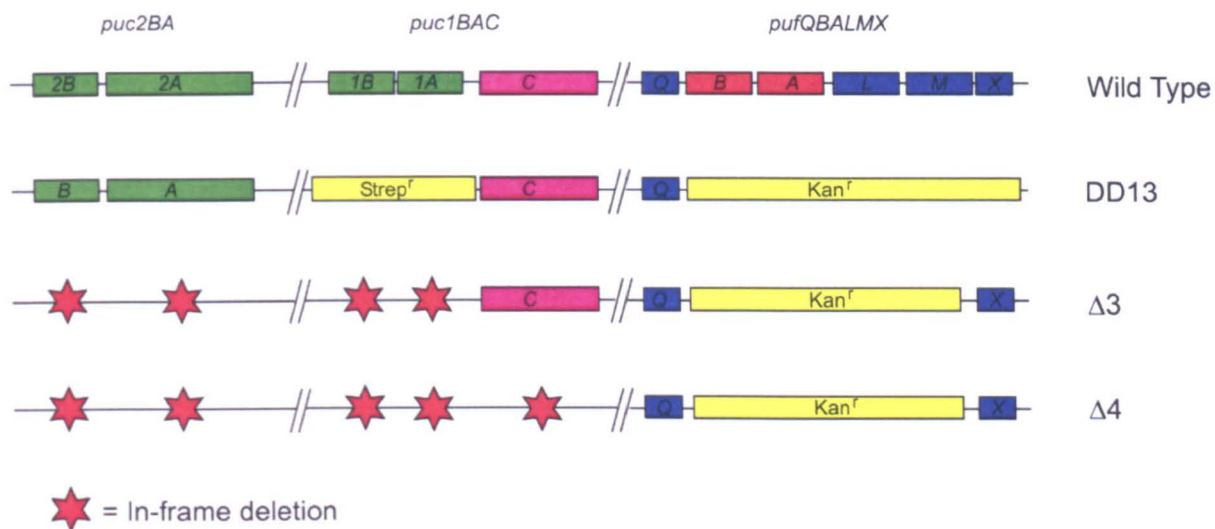


**Figure 5.2** *Rba. sphaeroides* deletion backgrounds

A comparison of the three deletion backgrounds and their transconjugant derivatives used in this chapter is presented. DD13 was first described by Jones *et al.*, (1992). The creation of Δ3 and Δ4 are detailed in this chapter.

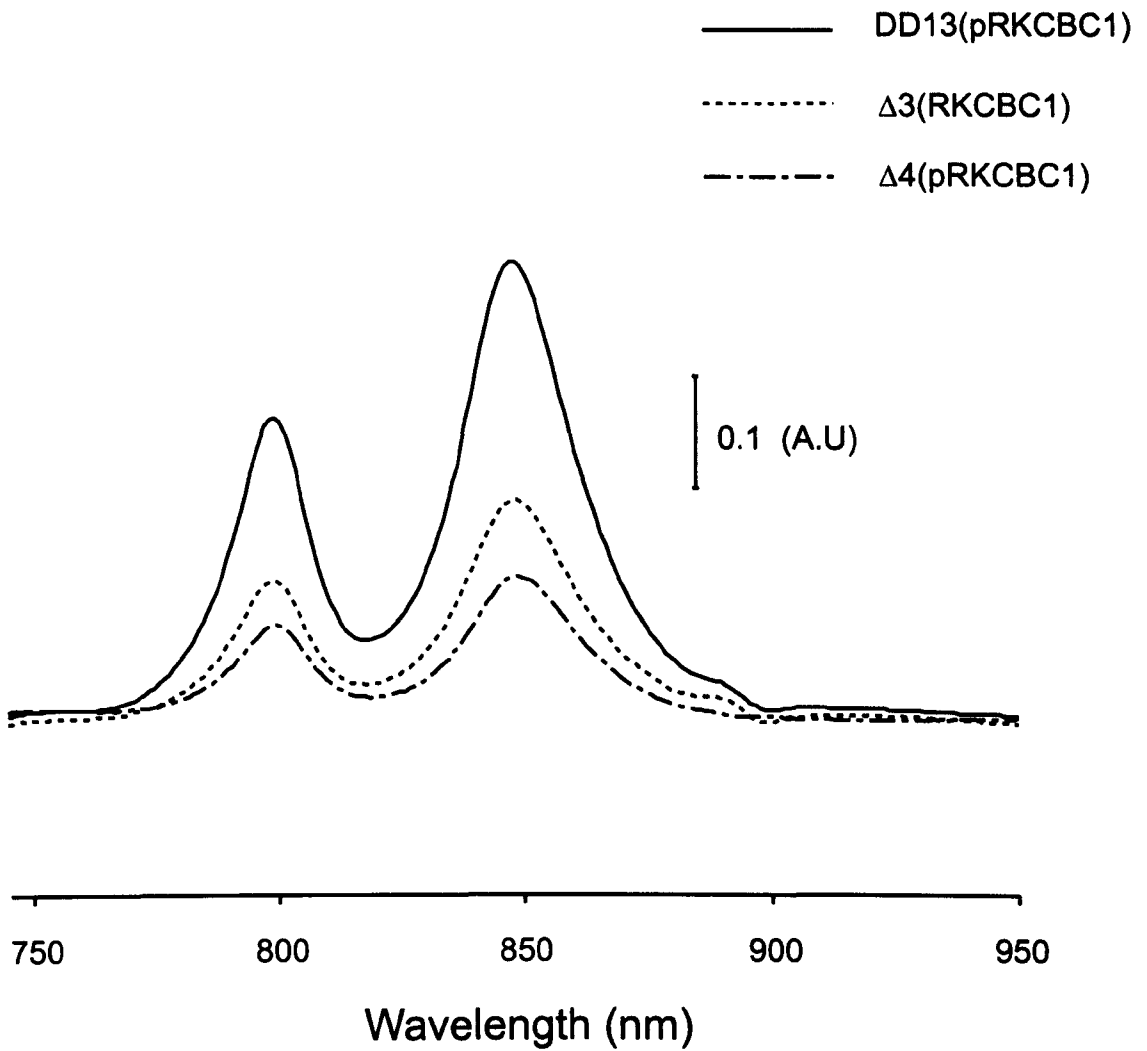


**Figure 5.3 LH2 complex assembly in DD13,  $\Delta 3$  and  $\Delta 4$**

The expression of *puc1BAC* genes in the three deletion strains is compared. Whole cell spectra were recorded in late log phase at a cell culture absorbance of 2.0 at 650 nm. Spectra have been corrected for light scattering and are stacked for clarity. LH2 complexes assembled in both  $\Delta 3$  and  $\Delta 4$  are LH2-1B1A, LH2 complexes assembled in DD13 are WT-LH2.

aggregation states of the complexes. These ICM were isolated from the strains DD13(pRKCBC1),  $\Delta 3$ (pRKCBC1) and DD13(pRKCBC-2B1A) respectively, using the method described in section 2.12.1. The strain DD13(pRKCBC-2B1A) was created using the conjugative transfer methods detailed in sections 2.11 and 5.3.1.2. The *puc* genetic complement of all three strains is detailed in Figure 5.2. In this chapter, the membranes isolated from these strains will be referred to according to their LH2 complex  $\beta$ -polypeptide content for clarity. Thus WT- LH2, LH2-1B1A and LH2-2B1A have been analysed.

A comparison of LH2-1B1A and LH2-2B1A yields information on the relative function of Puc1B versus Puc2B. A comparison of WT-LH2 with either LH2-1B1A or LH2-2B1A provides an insight into the role of heterogeneity within the ring.

### **5.3.3.1 Low temperature (77 K) absorbance properties of WT-LH2, LH2-1B1A and LH2-2B1A.**

The absorbance spectra of the membrane samples were recorded at 77 K as described in section 2.13.1. The WT-LH2 B800 and B850 absorbance maxima are compared in Figure 5.4. WT-LH2 membranes display absorbance peaks at 799 and 854 nm (Figure 5.4A). The position of the B800 maximum of LH2-1B1A is identical to that of WT-LH2, however a 2 nm red shift is observed in the B850 peak, occurring at 856 nm (Figure 5.4B). The position of the peak maxima of LH2-2B1A are identical to those of the wild type complex (Figure 5.4C).

The B800:B850 peak height ratios of the three membrane samples were calculated and are compared in Figure 5.4. WT-LH2 membranes display a ratio of 0.94. A marked reduction is seen in LH2-1B1A membranes, which have a ratio of 0.51. The ratio of 0.88 displayed by LH2-2B1A membranes is similar to that seen in WT-LH2.

The absorbance spectra of all three membrane samples were recorded between 300 and 920 nm and are displayed in Figure 5.5. These spectra show that the

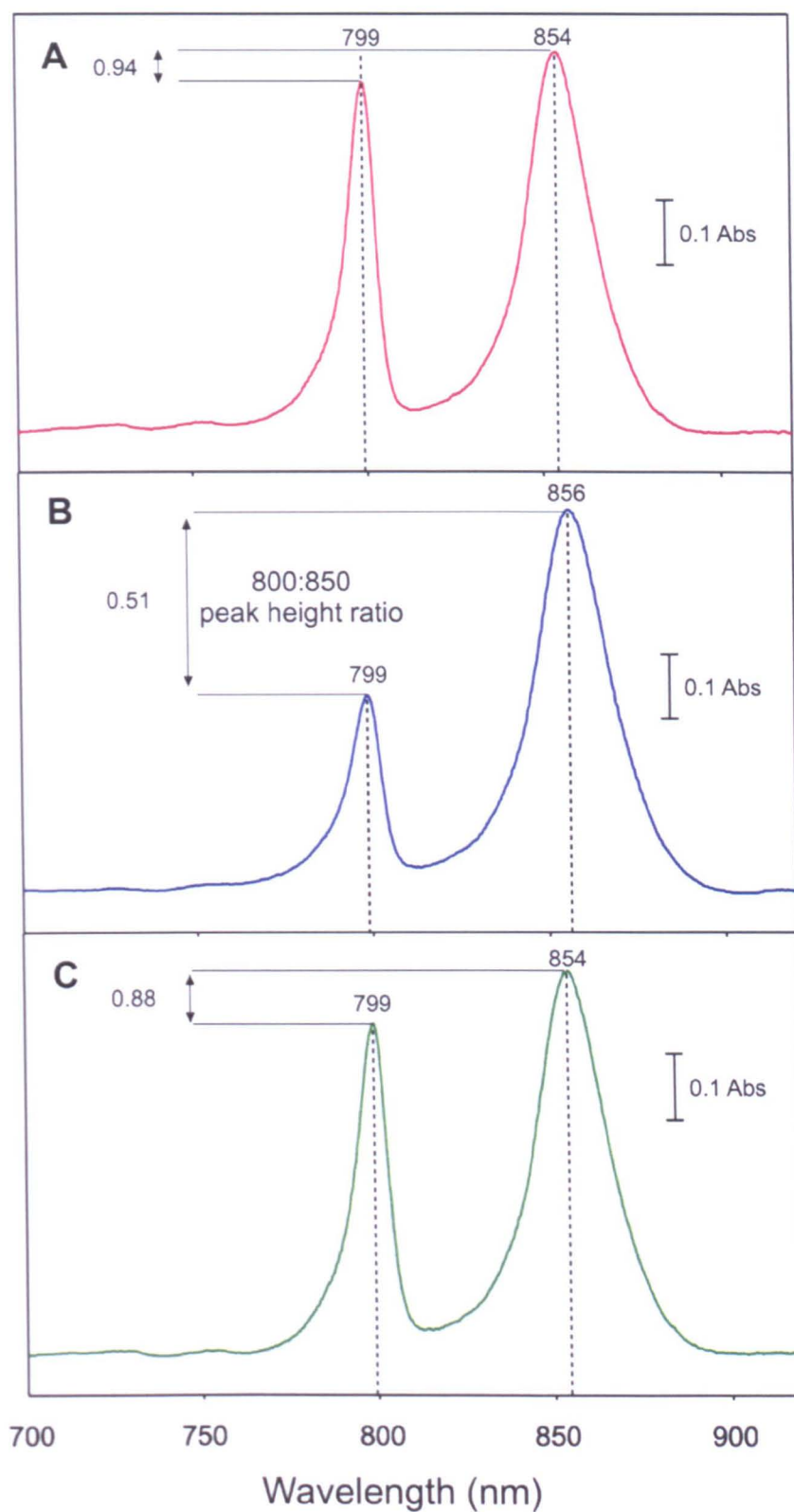


**Figure 5.4 Absorbance spectra at low temperature (77 K)**

Spectra of the membranes purified from the three different strains are shown. Spectra have been normalised to an absorbance value of one and corrected for light scattering for clarity.

- A. WT-LH2
- B. LH2-1B1A
- C. LH2-2B1A

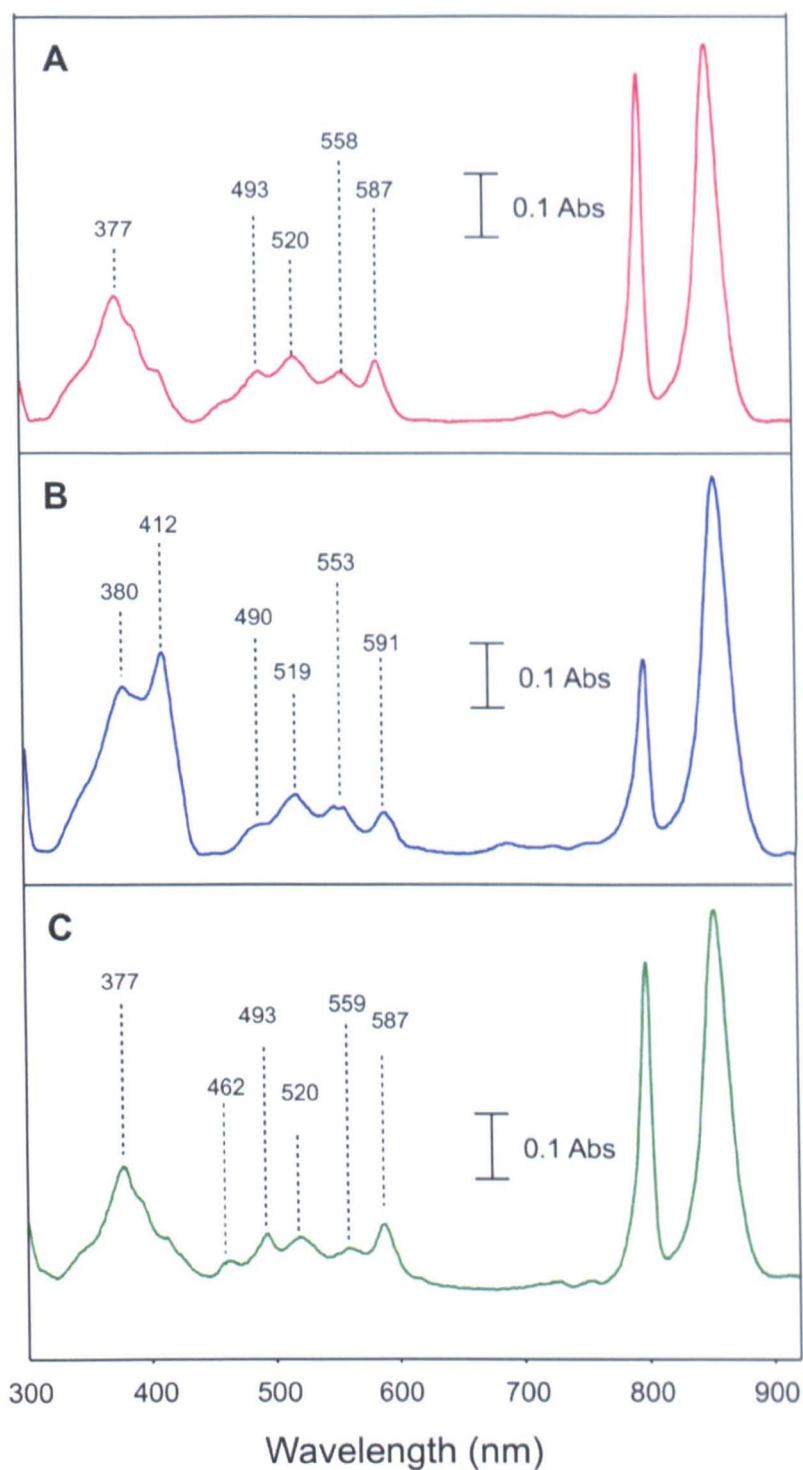


**Figure 5.5 Absorbance spectra in the carotenoid and near IR regions at 77 K**

Spectra of the extracted membranes from the three different strains are shown. Spectra have been normalised to an absorbance value of 1.0 at 850 nm and are corrected for light scattering for clarity.

- A. WT-LH2
- B. LH2-1B1A
- C. LH2-2B1A

WT-LH2 and LH2-2B1A complex closely resemble each other, but that LH2-1B1A is distinguished by the lower B800:B850 absorbance ratio, as noted above, as well as the differing carotenoid absorbance maxima. The position of the  $Q_x$  maxima of WT-LH2 and LH2-2B1A are identical. A red shift of 4 nm is seen in the  $Q_x$  peak of LH2-1B1A compared to WT-LH2, occurring at 591 nm. The peak maxima of all three carotenoid regions are labelled in Figure(s) 5.5A, B and C. The most significant differences occur in LH2-1B1A membranes when compared to WT-LH2, with an extra peak being seen at 412 nm. A double peak is also observed centred at 553 nm which is not seen in WT-LH2.

### **5.3.3.2 Low temperature (77 K) fluorescence excitation properties of WT-LH2, LH2-1B1A and LH2-2B1A.**

Fluorescence excitation spectra of each of the three purified membrane samples were recorded at 77 K as described in section 2.13.3. The acquired spectra displayed in Figure 5.6 are the average resulting from 4 separate scans. The peak maxima of the BChl(s) occur at 590, 801 and 860 nm in the WT-LH2 LH2 complex. The  $Q_x$  maximum displayed by LH2-1B1A membranes is red shifted by 2 nm compared to the WT-LH2, while the B800 and B850 maxima are identical. All the BChl peak maxima seen in LH2-2B1A are red shifted, occurring at 591, 803 and 861 nm. Excitation spectra of the carotenoid region of all three membrane samples were poorly resolved and so are not displayed.

### **5.3.3.3 Fluorescence emission properties**

The fluorescence emission properties of each of the three samples were recorded at 77 K as described in section 2.13.3. Each spectrum shown in Figure 5.7 are the averages resulting from three separate scans. The peak maxima and fwhm for each sample have been labelled. All three membrane samples were excited at 520, 590 and 800 nm.

The peak maxima of WT-LH2 membranes when excited at 520, 590 and 800 nm occurred at 887, 890 and 890 nm respectively. The fwhm values for the three

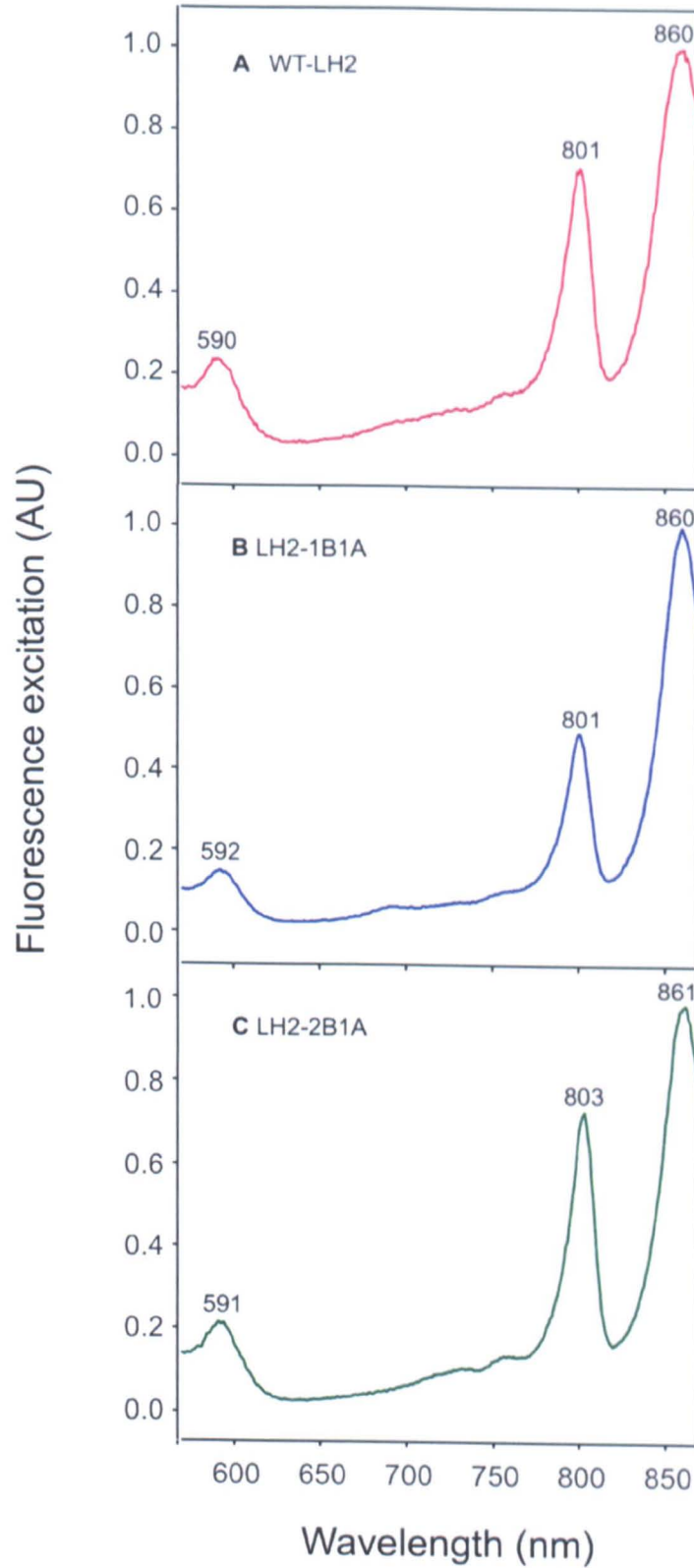


**Figure 5.6 Fluorescence excitation at low temperature (77 K)**

Excitation spectra of the membrane fraction purified from the three strains are shown. Fluorescence emission was measured at 900 nm. Excitation slit widths of 2.5 mm, and emission slit widths of 5 mm were used. All spectra have been normalised to a value of 1 A.U. at the B850 maxima for clarity.

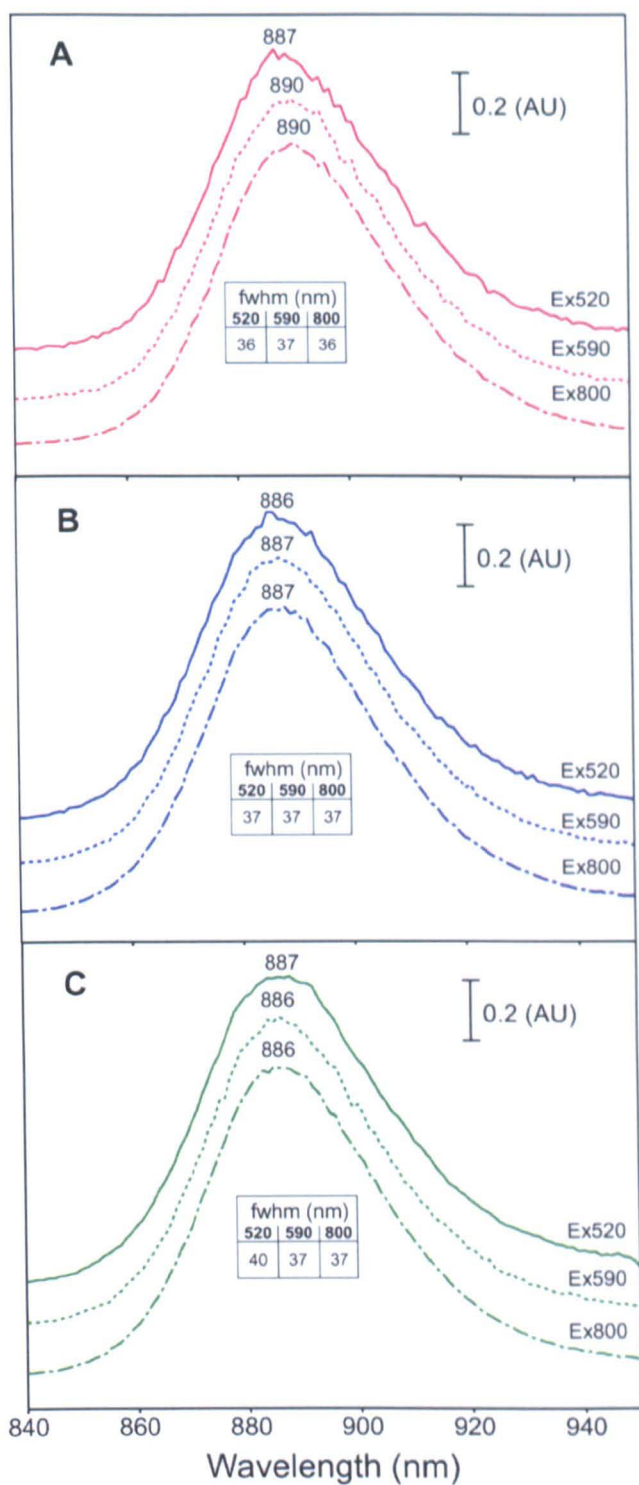


**Figure 5.7 Fluorescence emission spectra at low temperature (77 K)**

The fluorescence emission spectra of membranes purified from the three strains are shown. Spectra were recorded with excitation slit widths of 5 mm, and emission slit widths of 2.5 mm. The spectra have been normalised to a value of 1 AU at peak maxima and stacked for clarity. Peak maxima have been labelled.

- A. WT-LH2
- B. LH2-1B1A
- C. LH2-2B1A

spectra were 36, 37 and 36 nm respectively. The 3 nm red shift in emission maximum observed in the WT-LH2 upon excitation at 590 and 800 nm when compared with 520 nm excitation is not seen in either LH2-1B1A or LH2-2B1A. In samples comprised of homogenous  $\beta$ -polypeptide rings (either LH2-1B1A or LH2-2B1A), all three peak maxima lie within 1 nm of each other, occurring at either 886 or 887 nm. The fwhm of all three peaks displayed by LH2-1B1A is 37 nm and the fwhm of LH2-2B1A are 40, 37 and 37 nm upon excitation at 520, 590 and 800 nm respectively. The large difference in fwhm upon carotenoid excitation is only seen in this mutant, and is an increase of 4 nm when compared to WT-LH2.

## 5.4 Discussion.

### 5.4.1 Context

The creation of a new deletion background lacking the second *puc* operon in which LH2 mutagenesis studies can be carried out is important. The previous mutagenesis studies using DD13 (Jones *et al*, 1992; Fowler *et al.*, 1997) must now be viewed with the caveat that not all the  $\beta$ -polypeptides contained the desired mutation. The fact that the sometimes large spectroscopic effects of the mutations were observed in these studies may indicate that a system in which all  $\beta$ -polypeptides undergo change could demonstrate further, more dramatic shifts in the spectral properties of its bound BChl(s).

The spectroscopic characteristics of the different solubilised and purified LH2 complexes previously described in this thesis (Chapter 3) were collected from monodisperse single particles. In contrast this chapter details the spectroscopic properties of the complexes in their natural membrane environment, which includes a highly aggregated state. It is important to understand their behaviour in this environment since any roles of the different  $\beta$ -polypeptides within the membrane system may become apparent. Unfortunately the systems used in this chapter cannot be analysed after photosynthetic growth because the *puf* operon has been removed.

However, a direct comparison can be made between the spectroscopic properties of membrane bound (this chapter) and detergent solubilised complexes (Chapter 3) as long as the carotenoid background and aggregation state are borne in mind.

In addition, the AFM results in section 3.3.3 of this thesis have already shown that LH2 comprised of a homogenous  $\beta$ -polypeptide complement (LH2-1B1A) displays long range arrangements in the membrane which have not been seen previously in WT-LH2. The study of the effects the different  $\beta$ -polypeptides have upon purely LH2 arrangement within the membrane can be studied most effectively in an LH2-only system, free of any effects from the RC-LH1-PufX core complexes.

#### **5.4.2 Analysis of LH2 assembly in $\Delta 3$ and $\Delta 4$**

There is a much larger loss of LH2 assembly when only *puc1B1A* genes are expressed *in trans* in  $\Delta 3$  and  $\Delta 4$  when compared with a genetic background which also contains LH1-RC-PufX complexes. In such a background, a loss of 30 % of assembled LH2 was recorded upon removal of the second *puc* operon (Zeng *et al.*, 2003). Losses of LH2 increase to 53 % ( $\Delta 3$  background) and 69 % ( $\Delta 4$  background) when the *puf* operon is removed. Regulatory effects conferred by the *puf* operon or its encoded complexes, cannot be discounted as being responsible for this further reduction in LH2 assembly. It is likely the 16 % reduction seen in  $\Delta 4$  compared to  $\Delta 3$  is due to the absence of *pucC* on the host genome. Although this assembly factor gene is present on all the plasmids which are used in these complementation studies, it is apparent the extra copy carried on the genome  $\Delta 3$  increases the levels of LH2 complex when compared with  $\Delta 4$ .

The low level of LH2 complex expression in these mutants hinders their usefulness when considering them as vehicles for large-scale LH2 overexpression. This problem was first identified when undertaking the crystal trials detailed in Chapter 4 of this thesis. This work required large amounts of highly pure LH2, which is not practicably feasible using  $\Delta 3$  or  $\Delta 4$  as hosts for complex expression. However, these mutants do provide a suitable null background for LH2-only studies where the spectroscopic properties of the complexes in the membrane environment are to be analysed.

### 5.4.3 The spectroscopic properties of WT-LH2, LH2-1B1A and LH2-2B1A

#### 5.4.3.1 Absorbance properties

A 2 nm red shift in the B850 peak position observed in LH2-1B1A is coupled with a significant reduction in 800:850 peak height ratio compared to WT-LH2. The second of these observations represents an important phenotypic difference. The reduction in B800 binding can be tallied with a similar but smaller reduction in the B800:B850 peak height ratio exhibited by purified LH2 complexes comprised solely of Puc1B1A (Chapter 3 of this thesis). The relative B800:B850 peak height ratios of the purified complexes from Chapter 3 and their respective membrane fragments purified in this chapter are compared in Figure 5.8. The reductions observed indicate a significant lessening in the ability of an LH2 ring assembled with only the Puc1B  $\beta$ -polypeptide to bind B800 BChl. The reduction in B800 absorbance observed both in membrane bound and purified complexes when Puc2B is absent means it is likely this polypeptide is responsible for the stabilisation of the B800 binding site. A comparison of the relative areas underneath the B850 and B800 absorbance peaks confirms that the reduction in peak height ratio for LH2-1B1A complexes (Figure 5.8) is due to a significant loss in the amount of bound B800 BChl and not simply the broadening of the B800 absorbance peak possibly caused by changes in the B800 binding environment.

An analysis of the carotenoid absorbance bands shows that two classes of complex exist. Firstly, WT-LH2 and LH2-2B1A show identical patterns of absorbance. The second class contains only LH2-1B1A, which exhibits a wide variation in carotenoid absorbance peaks when compared to WT-LH2. This observation, in conjunction with the reduced B800:B850 peak height ratio in this mutant allows the conclusion that it is specific interactions brought by residues in the N-terminal region of the  $\beta$ -polypeptide, and not the heterogenous nature of the  $\beta$ -polypeptide ring, which are important in

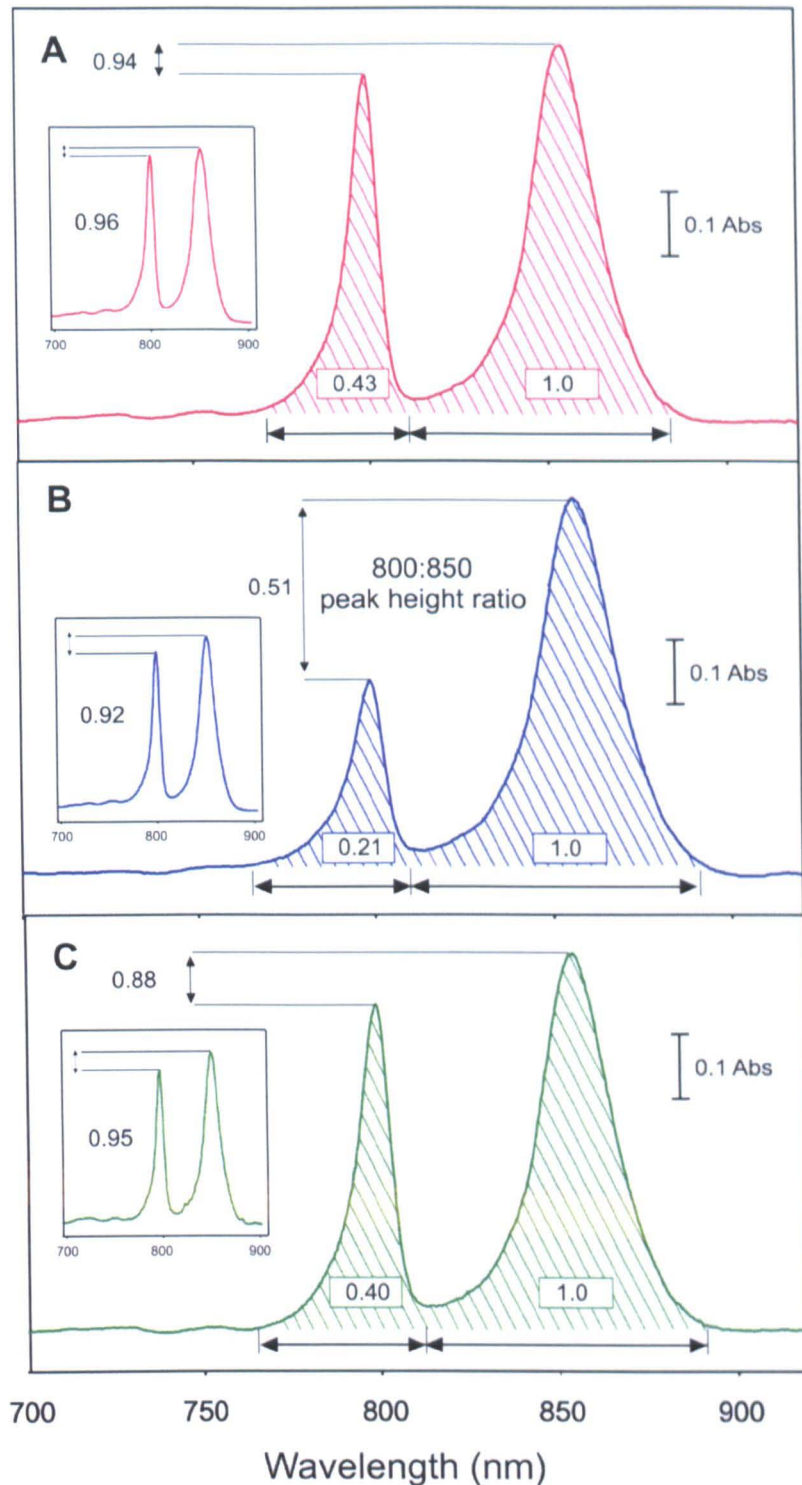


**Figure 5.8 B800:B850 absorbance comparison at 77 K**

Absorbance spectra of the purified membranes are shown. Spectra have been normalised to an  $A_{850}$  of 1.0 and corrected for light scattering for clarity. The area of each BChl peak has been calculated. For comparison all B850 areas have been normalised to 1.0 with respect to the wild-type for comparison. Inset in each panel is the 77 K absorbance spectra of the purified complex (Chapter 3) containing an identical  $\beta$ -polypeptide composition to their respective membranes. All purified complex spectra have been normalised to an  $A_{850}$  of 1.0

- A. WT-LH2(1B2B1A)
- B. LH2-1B1A
- C. LH2-2B1A

determining the stability and spectroscopic properties of the B800 BChl(s) bound within the LH2 complex in *Rba. sphaeroides*.

#### 5.4.3.2 Fluorescence excitation properties

A comparison of the B800 and B850 peak positions of LH2-1B1A and LH2-2B1A with WT-LH2 uncovers red shifted pigments in LH2-2B1A membranes. LH2-2B1A membranes exhibited peaks which occur at 803 and 861 nm, whilst  $Q_y$  maxima in WT-LH2 and LH2-1B1A occurred at 801 and 860 nm. These shifts are indicative of a small variation in the B800 BChl(s) of LH2-2B1A, with some red-shifted molecules being involved in preferentially transferring energy to the B850 BChl(s). However, these peak shifts, although more pronounced upon energy transfer from B800 BChls, are small in nature. The presence of an exclusively Puc2B N-terminal region of the  $\beta$ -polypeptide apparently causes the observed red shifts, and thus is likely to slightly alter the binding of B850 BChl within the complex due to minor long range changes in its structure.

Of more significance than the observed  $Q_y$  peak shifts in LH2-2B1A membranes, is the decrease in fluorescence energy transfer seen upon excitation of the B800 BChl(s) in LH2-1B1A membranes. The excitation spectra presented in Figure 5.6 were normalised at their B850 excitation maxima for comparison. This was necessary due to the poor resolution obtained in the carotenoid and  $Q_x$  excitation regions. Consequently a quantitative analysis comparing all three membrane samples for their energy transfer properties is not possible. However a qualitative assessment can conclude that the consequence of the previously observed reduction in B800 absorbance in LH2-1B1A membranes corresponds with a reduction in energy transfer from B800 to B850. This is further evidence that it is the Puc2B polypeptide which is responsible for the stabilisation of the B800 binding site within the WT-LH2 complex.

The results presented in this chapter cannot conclusively explain the decrease in B800 binding observed in membrane bound LH2-1B1A complexes, when compared to the smaller losses in the respective purified complexes. A comparison of these losses is

made in Figure 5.8. It is possible the purification process used to isolate the complexes analysed in Chapter 3 preferentially selects for LH2 complexes of higher structural integrity. Thus the observed reduction in B800 absorbance is not as pronounced, but may not represent the true reduction in B800 binding.

### 5.4.3.3 Fluorescence emission properties

Upon excitation at 590 and 800nm the fluorescence emission maxima of LH2-1B1A and LH2-2B1A are blue shifted by 3 and 4 nm respectively. This suggests that a homogenous  $\beta$ -polypeptide ring modifies the B850 BChl(s) in membrane bound LH2 complexes so that they fluoresce at shorter wavelengths. This shift in fluorescence does not occur upon excitation at 520 nm, indicating that energy transfer from the carotenoids to the B850 ring is not influenced by the specific  $\beta$ -polypeptide present (even though their absorbance properties are altered).

A blue shift in B850 emission is not seen in purified LH2 complexes (Chapter 3 of this thesis). Also, the membrane bound WT-LH2 complexes do not exhibit the marked increase in fwhm upon B800 excitation that is seen in purified WT-LH2 complexes. It is possible that the structural constraints imposed by the lipid bilayer, as well as intercomplex interactions within the membrane, remove the variability in the number of distinct environments which the B850 BChl(s) can occupy. However, the carotenoid content of the purified complexes (mostly spheroidene) is not the same as those in the membrane bound complexes (mostly spheroidenone) analysed in this section, so a direct comparison is not completely legitimate.

Future work should focus upon repeating the spectroscopic analyses put forward in this thesis, in a consistent carotenoid background. This would facilitate not only a clearer understanding of any role the  $\beta$ -polypeptide has in carotenoid binding, but would also allow for the direct comparison of spectroscopic data obtained for the bound BChl(s) within the solubilised monomeric and membrane bound complexes.

#### 5.4.3.4 The role of the $\beta$ -polypeptide in the LH2 complex

The differences which occur between Puc1B and Puc2B are all in the N-terminal region. An amino acid sequence alignment comparing the  $\beta$ -polypeptide seen in the *Rps. acidophila* LH2 3D structure (McDermott *et al.*, 1995) with Puc1B and Puc2B from *Rba. sphaeroides* is shown in Figure 5.9D. It is clear from this comparison that the major difference between the two species' polypeptides is their length at the N-terminus, with those belonging to *Rba. sphaeroides* being 10 amino acid residues longer in this region. A representation of the 3D structure of LH2 from *Rps. acidophila* is shown in Figures 5.9A and B. The location of the variable residue  $\beta X_{-25}$  from *Rba. sphaeroides* has been highlighted in red, whilst the four amino acids which precede it at the N-terminus are highlighted in blue.  $\beta X_{-25}$  was the only position of the three variable residues seen in *Rba. sphaeroides* PucB polypeptides which is present in *Rps. acidophila*. The other two,  $\beta X_{-34}$  and  $\beta X_{-35}$ , are found in the extended N-terminal region possessed by Puc1B and Puc2B so their locations could not be mapped on the *Rps. acidophila* LH2 structure.

The position of the  $\beta Ala_{-25}$  residue is of interest, since it lies at the N-terminal end of the transmembrane helix. If this remains true in *Rba. sphaeroides* LH2, it may provide an explanation for the variability of B800 binding observed upon alteration of the amounts of Puc1B and Puc2B within the complex.  $\beta X_{-25}$  is in close proximity to  $\alpha Lys_{-32}$ , which is highlighted in purple at the N-terminal region of the  $\alpha$ -polypeptide in Figure 5.9C.  $\alpha Lys_{-32}$ , which is also present in *Rba. sphaeroides*, lies close to the position at which the  $\alpha$ -polypeptide re-enters the membrane and thus facilitates the H-bonding of the B800  $Mg^{2+}$  by COO- $\alpha Met_{-36}$  (Papiz *et al.*, 2003). Variability in the size of the residue located at  $\beta X_{-25}$  may confer different steric effects upon the membrane re-entry of the  $\alpha$ -polypeptide at  $\alpha Lys_{-32}$ , hence affecting the binding site of the B800 BChl(s). It is possible that a  $\beta$ -polypeptide ring composed solely of Puc1B places unfavourable constraints upon the  $\alpha$ -polypeptide when it re-enters the membrane, which is reflected in the significant loss of B800 BChl binding.



Alternatively, an explanation for the variability in B800 binding in these mutants may be found by considering the length of the  $\beta$ -polypeptide N-terminal region. Puc1B and Puc2B of *Rba. sphaeroides* possess a significantly larger N-terminal region than that found in the  $\beta$ -polypeptide of *Rps. acidophila* LH2. If the structure is considered as a whole, this means an extra 90 amino acid residues need to be accommodated within the LH2 ring in this region. The accommodation of a large number of residues at the N-terminus of *Rba. sphaeroides* LH2 may confer long range constraints upon the  $\alpha$ - and  $\beta$ -polypeptides. Even small changes at the N-terminal region may have significant effects upon the binding of the B800 BChl(s) within the complex.

It is also possible that interactions between Puc1B and Puc2B at the N-terminus confer specific structural characteristics in this region which stabilise the complex. It is potentially the loss of these stabilising interactions which is reflected by the marked reduction in B800 binding in the absence of Puc2B. Coincidentally,  $\beta$ Lys<sub>34</sub> from Puc2B carries a positive charge which is not found in its counterpart in Puc1B ( $\beta$ Asn<sub>34</sub>), adding weight to the previous supposition, since Puc2B could potentially form electrostatic interactions with neighbouring  $\beta$ - and  $\alpha$ -polypeptides which Puc1B could not. However, it is important to mention that the nature of  $\beta$ -polypeptide heterogeneity within the LH2 population in WT-LH2 is not properly understood. It is possible that Puc1B and Puc2B are incorporated within the same LH2 ring. Alternatively there may be two populations of LH2 in wild type organisms, comprising a homogenous  $\beta$ -polypeptide ring containing either Puc1B or Puc2B.

The long N-terminal extension present in the *Rba. sphaeroides*  $\beta$ -polypeptides but absent from *Rps. acidophila*  $\beta$ -polypeptides may be explained by the carotenoids which they bind. *Rps. acidophila* LH2 binds exclusively rhodopin-glucoside, which possess a large glucoside head group located next to the N-terminus of the  $\beta$ -polypeptide, as shown in Figure 5.10 (McDermott *et al.*, 1995). However, *Rba. sphaeroides* binds carotenoids from the spheroidene or neurosporene family. These do not carry large head groups such as glucoside, and in fact there is evidence

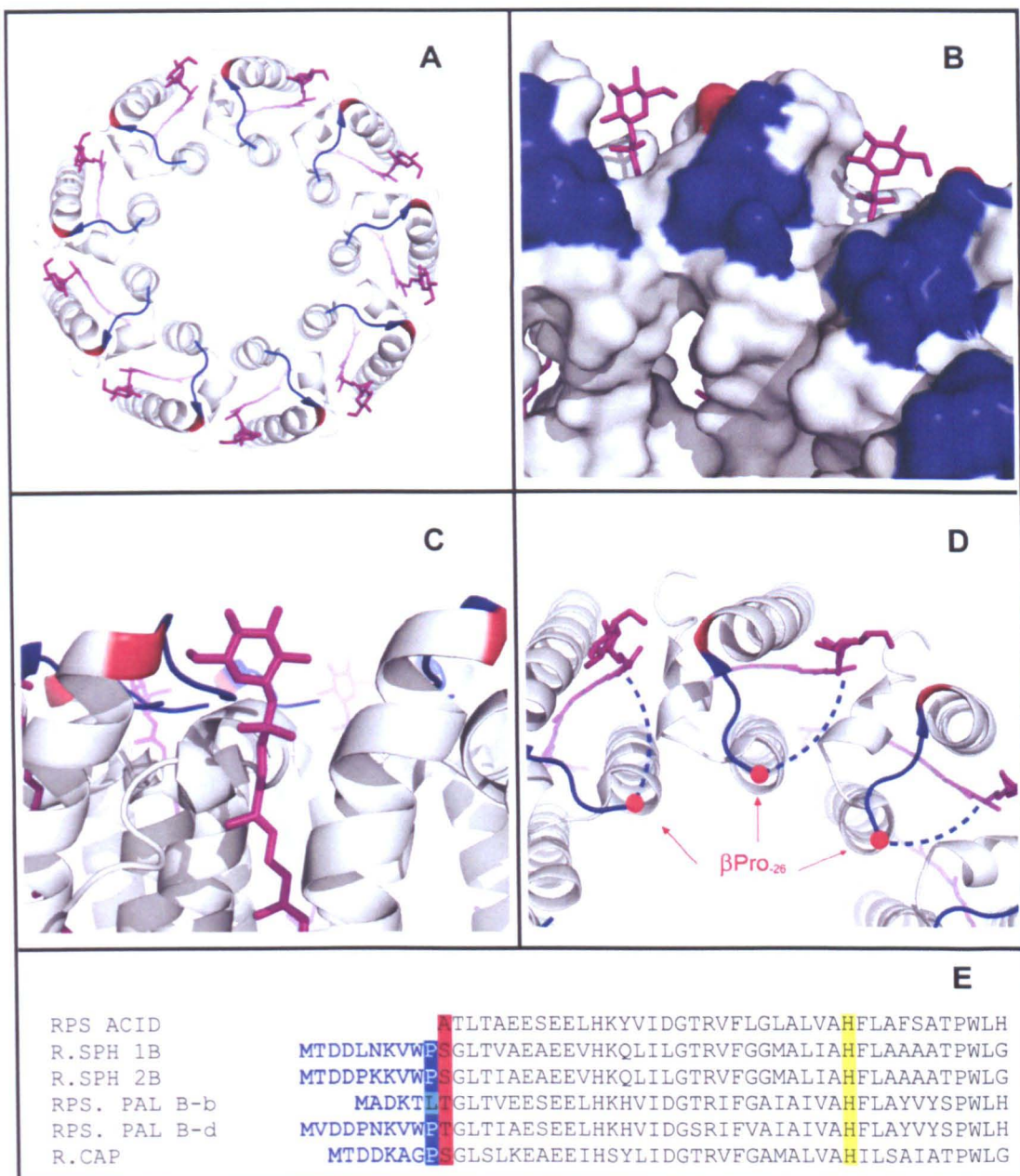


**Figure 5.10 Rhodopin-glucoside within the LH2 structure (McDermott *et al.*, 1995)**

Four views of rhodopin-glucoside bound within LH2 from *Rps. acidophila* are presented in panels A-D. In all cases the first four residues at the N-terminus of the  $\beta$ -polypeptide are highlighted in blue, the  $\beta$ Ala<sub>25</sub> residue is shown in red. Rhodopin-glucoside is coloured purple. Panel D depicts the possible orientation of the long N-terminus of the  $\beta$ -polypeptide in *Rba. sphaeroides*, which is represented by the dashed blue line. The conserved  $\beta$ Pro<sub>26</sub> has been highlighted by a red circle.

Panel E presents a sequence alignment of the  $\beta$ -polypeptides from *Rps. acidophila*, *Rba. sphaeroides* 2.4.1, *Rps. palustris* and *Rba. capsulatus*. All sequences have been aligned to the conserved His<sub>0</sub> residue for clarity. The N-termini belonging to polypeptides which extend beyond that seen in *Rps. acidophila* are denoted by blue text. A conserved proline residue which immediately precedes the start of the *Rps. acidophila*  $\beta$ -polypeptide is highlighted.

that carotenoids are inserted in the *Rba. sphaeroides* LH2 complex in the opposite orientation to that seen in *Rps. acidophila*, with the head group being located proximal to the B850 binding site (Gall *et al.*, 2003).

It is possible that during the evolution of the *Rps. acidophila* LH2 complex a portion of the  $\beta$ -polypeptide N-terminus was removed. This removal may have allowed the binding of a carotenoid with a large head group at membrane interface, such as rhodopin-glucoside, consequently forming a more stable complex. An analysis of the N-terminal amino acid sequence of  $\beta$ -polypeptides from other organisms which assemble LH2 (Figure 5.10E) uncovers two significant facts. Firstly, all species analysed in Figure 5.10 possess a  $\beta$ -polypeptide with an N-terminus at least six amino acids longer than that of *Rps. acidophila*, and none of them synthesise rhodopin-glucoside. Secondly, a conserved proline residue can be seen, occurring in the  $\beta X_{26}$  position. It is possible that a turn in the coil at the N-terminus caused by this residue means that the binding site where the glucoside head group is located in *Rps. acidophila* is occupied by the large N-terminus of the  $\beta$ -polypeptide in these organisms (Figure 5.10E). Despite the lack of a comparable head group, it is possible that the Puc1B or Puc2B polypeptide interacts differently with the native carotenoid, producing the effects seen on both the carotenoid absorbance maxima (Figure 5.5) as well as the intensity of the B800 absorbance (Figure 5.8)

## **Chapter 6: Micron patterning of functional light harvesting 2 complexes by specific covalent attachment to N-hydroxysuccimide ester self-assembled monolayers.**

### **6.1 Summary**

The field of bio-nanotechnology is rapidly expanding. The ability to sequence whole genomes has brought with it the necessity to further understand their accompanying proteomes. The patterning of proteins at the micron and nano-scale could allow for the development of protein arrays similar to the DNA micro-arrays currently available. The attachment of light harvesting complexes to surfaces is also a field of growing interest. There exists a marked difference in energy conversion efficiency between biological light harvesting systems and conventional man-made photovoltaic cells. The incorporation of highly efficient light harvesting complexes from nature to these photovoltaic cells may help bridge the existing gap.

The use of Self Assembled Monolayers (SAMs) to provide surfaces possessing specific surface chemistries has been extensively studied in recent years. The modification of these SAMs using UV illumination is known as photolithography. This technique provides the opportunity to pattern SAMs, imparting specific features at the surface on the micron scale.

This chapter details the specific attachment of purified LH2 complexes from *Rba. sphaeroides* to micron patterned SAMs. Surface plasmon resonance studies have been used to select SAMs possessing tail groups with specific chemical properties. Two surfaces that have contrasting attractive and repulsive responses to membrane protein adsorption have been identified. The functionality of the purified LH2 complexes is shown by confocal microscopy to be maintained whilst they are covalently attached to the surface.

## 6.2 Introduction

The ability to pattern proteins on the micron and nano scales is of vast importance in producing biologically integrated devices for high throughput experiments in the field of proteomics. Several techniques are available for creating two dimensional arrays of proteins on surfaces (reviewed by Blawas and Reichert., 1998), including the use of photolithography and self assembled monolayers (SAMs). The field of protein patterning was originally conceived as a critical technology for the integration of biological molecules into miniature bio-electrical devices (Haddon and Lamola., 1985). The recent elucidation of the human genome sequence has increased in importance the ability to selectively immobilise proteins on the nanoscale, whilst retaining their function.

Light harvesting complexes are an ideal candidate as a test protein for developing this technology. They are a membrane proteins, which is also true of many of the proteins of interest to which a patterning technology could be applied. For instance drug targets are often cell receptor proteins which bind extrinsically or intrinsically to the membranes in mammalian cells. In addition, a protocol is in existence for the isolation of LH2 to a high degree of purity (Chapter 4 of this thesis), which is important, since the patterning of specific proteins is dependent upon sample homogeneity. LH2 also possess its own chromophore system, which allows the functionality of the protein to be probed easily. This can be done whilst it is covalently attached to the patterned surface by using fluorescence based microscopy. Assessing the fitness of the protein is important, since it is necessary to show that the patterning techniques do not dramatically change or reduce its function.

The attachment of light harvesting complexes themselves to surfaces is a field of growing interest. There exists a marked difference in energy conversion between biological light harvesting systems and conventional man-made photovoltaic cells (~60 % versus 10-20 %) (Frolo *et al.*, 2005) This dichotomy has led to the evolution of a growing body of work, probing the usefulness and practicalities of increasing the

efficiency of existing photovoltaic cells by incorporating light harvesting molecules within them (Ogawa *et al.*, 2002; Trammel *et al.*, 2004; Lebedev *et al.*, 2006).

Self-Assembled Monolayers are ideal templates for the patterning of protein molecules (Ostuni *et al.*, 2003; Deckert *et al.*, 2004; Senaratne *et al.*, 2005). Their creation is simple and they remain stable at varying temperatures (up to  $\sim 70$  °C). The well ordered surface of the SAM can be manipulated by changing the exposed tail group, allowing interactions with the bio-molecule to be modified to the user's specifications. The binding of linker molecules to the tail groups can also confer specificity, allowing attachment of the bio-molecule either electrostatically or covalently. The photopatterning of SAMs relies on the fact that many types of SAM undergo chemical changes when exposed to UV radiation, thus making them ideal candidates for patterning by photolithography. The mechanisms by which SAMs are photo-patterned are explored in section 1.8.2.

The work in this chapter involves the micron scale photo-patterning of alkanethiol self-assembled monolayers. The properties of the patterned SAMs were manipulated by changing the chemical nature of their exposed tail group. The patterning of purified LH2 complexes onto these features is explored using a combination of techniques, including SPR, AFM and confocal microscopy.

The results detailed in this Chapter represent a collaborative piece of work, involving Professor Graham Leggett (Department of Chemistry, University of Sheffield), Dr Cees Otto (University of Twente, Enschede, The Netherlands.) and my laboratory. The AFM, fabrication of SAMs and their subsequent patterning were carried out by Nick Reynolds and Stefan Janusz in the Department of Chemistry (University of Sheffield). Confocal microscopy using an AFFM was carried out at the University of Twente by Nick Reynolds and Maryana Escalantarum.

## 6.3 Results

### 6.3.1 Purification of WT-LH2

The LH2 used in this chapter was purified from wild-type *Rba. sphaeroides* 2.4.1., which was photosynthetically grown under low light ( $5 \text{ Wm}^{-2}$ ) illumination as described in section 2.10.2. The purification of the LH2 complex from this strain was carried out as described in section 4.3.2. An SDS-PAGE analysis of the WT-LH2 purity throughout the purification process is shown in Figure 6.1. The spectroscopic properties of the purified complex were characterised using low temperature (77 K) absorbance and fluorescence microscopy. The absorbance maxima of the B800 and B850 BChl(s) occurred at 800 and 851 nm respectively, with fluorescence excitation maxima of 802 and 856 nm. The absorbance, fluorescence excitation and fluorescence emission spectra for the complex are shown in Figure 6.2. For a full analysis and discussion of the purified complexes spectroscopic properties see Chapter 3.

### 6.3.2 The creation of SAMs

The fabrication of the SAMs used for protein patterning was carried out as described in section 2.15.2. Four specific SAMs were created, each possessing different chemical properties at their tail groups thus allowing for the functionalisation of the exposed surface. The four SAMs probed were mercaptoundecanoic acid (MUA), oligo ethylene glycol (OEG), 1H,1H,2H,2H-Perfluorooctanethiol (PfoT) and N-hydroxysuccinimide (NHS) ester. The creation of the NHS tail group was carried out via N-(3-Dimethylaminopropyl)-N'-ethylcarbodiimide hydrochloride (EDC)/NHS

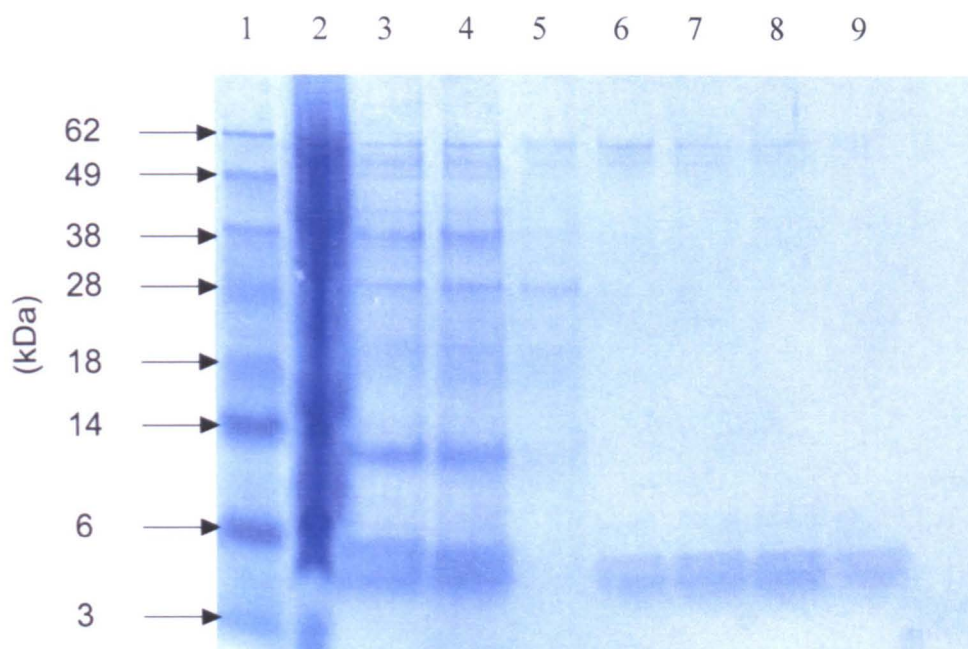


**Figure 6.1 Purification of WT-LH2**

A 12% SDS-PAGE of samples taken at each stage of a WT-LH2 purification.

- Lane 1 – Invitrogen SeeBlue™ MW markers
- Lane 2 – *Rba. sphaeroides* 2.4.1. cell lysate
- Lane 3 – ICM pre-solubilisation
- Lane 4 – ICM post-solubilisation with 3 % LDAO
- Lane 5 – Flow through of first DEAE Sepharose column
- Lane 6 – Sample post first DEAE Sepharose column
- Lane 7 – Sample post second DEAE Sepharose column
- Lane 8 – Sample post Resource-Q™ column
- Lane 9 – Sample post Superdex-200™ gel filtration column

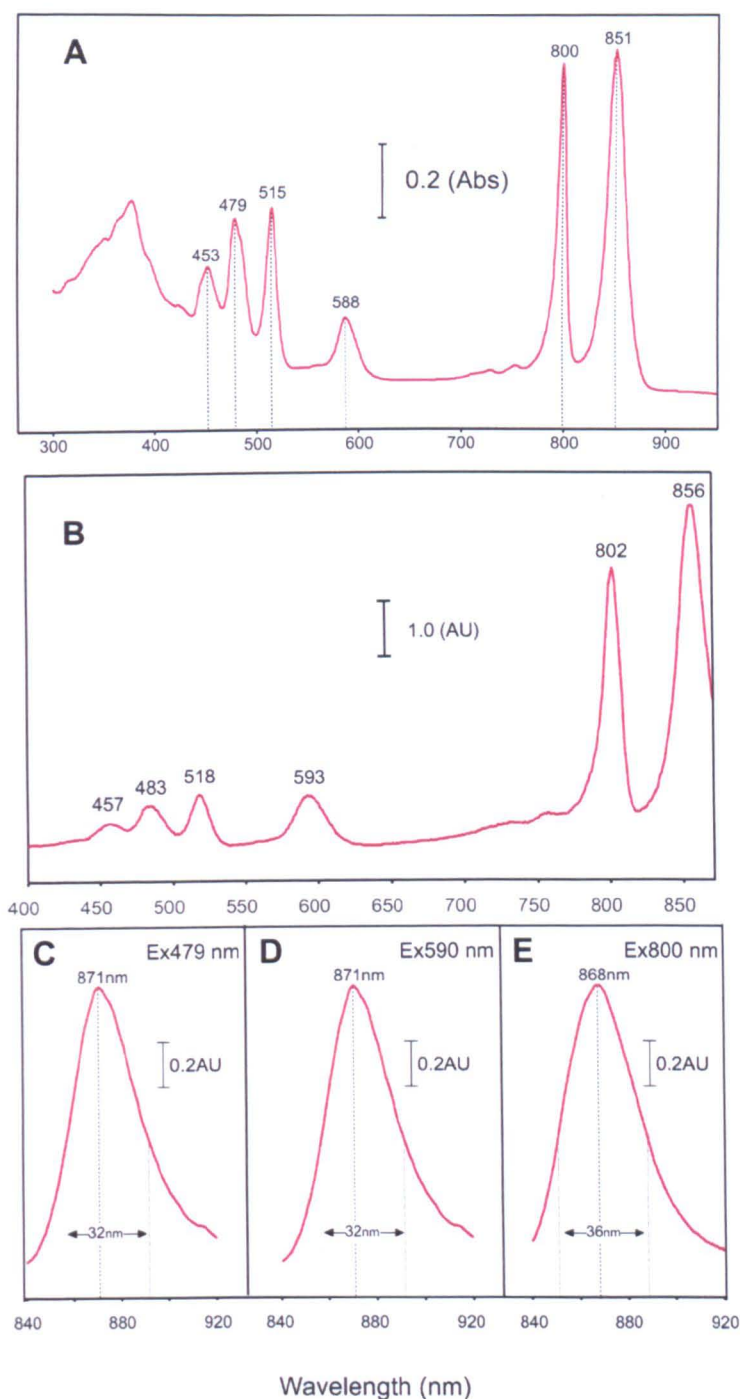


**Figure 6.2 Spectroscopic analysis of WT-LH2 at 77 K**

- F. Absorbance spectrum. Data have been normalised to an absorbance of 1.0 at 850nm
- G. Fluorescence excitation spectrum. Data have been normalised to 1.0 AU at  $Q_x$  maxima. Excitation slit widths of 1.25 mm and emission slit widths of 5 mm were used.
- H. Fluorescence emission spectrum with an excitation wavelength of 479nm.
- I. Fluorescence emission spectrum with an excitation wavelength of 590nm.
- J. Fluorescence emission spectrum with an excitation wavelength of 800nm

All fluorescence emission spectra have their peak maxima and full width half maxima labelled. The spectra have been normalised to 1 AU at peak maxima. Excitation slit widths of 2.5 mm and emission slit widths of 2.5 mm were used.

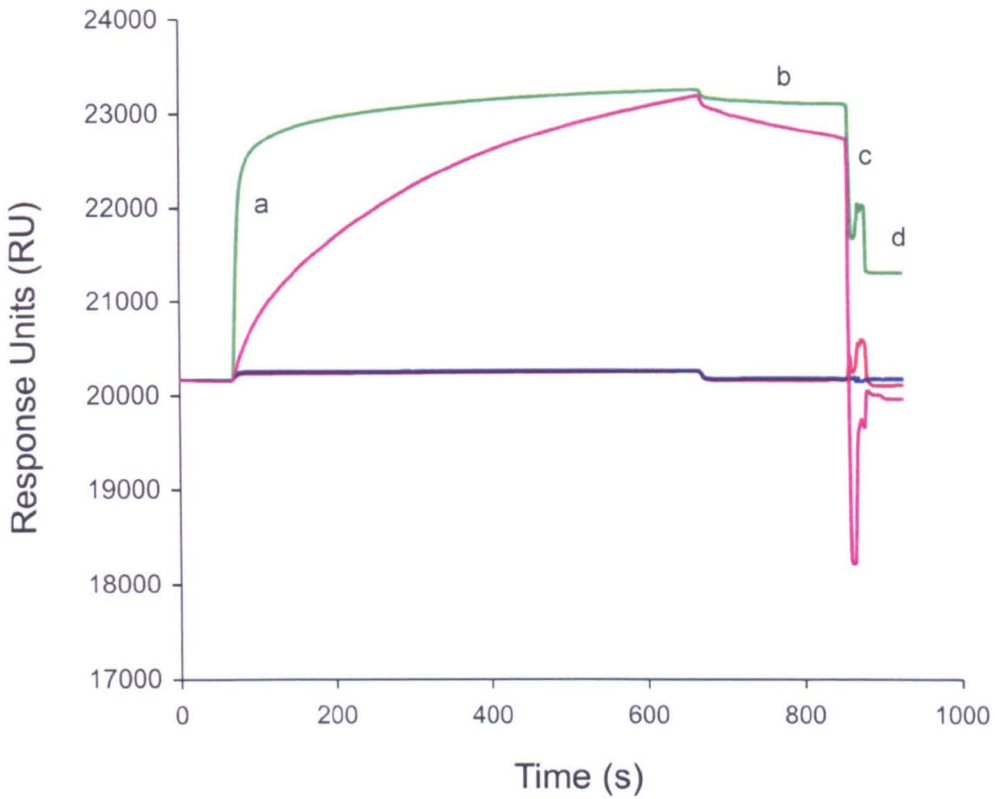
crosslinking to a carboxylic acid terminated SAM (MUA). This crosslinking is depicted in the first reaction shown in Figure 1.17B.

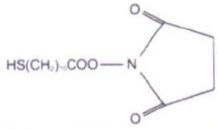
### 6.3.3 SPR

Surface plasmon resonance (SPR) studies were carried out to assess the degree of attractive or repulsive forces which the fabricated SAMs showed towards purified LH2 complexes. The experiments were performed on a Biacore 3000 instrument as described in section 2.17. Figure 6.3 shows the traces obtained for all four SAMs. The data shown are each an average of four individual traces for each sample. Each trace has four distinct phases. Firstly the purified LH2 complex (12.5 AU) was passed over the sensor chip at a rate of  $10 \mu\text{l min}^{-1}$  for 10 min (a). The SAM surface was then washed with Buffer A (20 mM Tris, 0.1 % LDAO, pH 8.0) at  $10 \mu\text{l min}^{-1}$  for 3 min (b). Aggressive washing of the surface using 1 % SDS detergent at  $30 \mu\text{l min}^{-1}$  for 30 sec followed (c). The chip was then exposed to Buffer A at  $10 \mu\text{l min}^{-1}$  for 1 min (d). All four traces have been normalised to a starting value of 20170.0 RU for comparison.

When analysing this data, there are two useful comparisons to make. Firstly, how much LH2 complex is bound to the SAM surface after exposure to the protein, while undergoing washing with Buffer A (phase b) when compared to the period before the SAM was exposed to the protein solution. This gives an indication of the attractiveness or repulsiveness of the surface to the protein at the conditions which further experiments will be performed. Secondly, how much protein remains bound to the surface after washing with SDS detergent (phase d) when compared to after washing with Buffer A (phase b). This comparison gives an indication of the nature of the interaction between the LH2 complex and the SAM. If a significant amount of protein remains bound after SDS washing, it is a strong indication that it is covalently bound to the surface.

These comparisons are made for each SAM and displayed in the table in Figure 6.3. It is evident that PfoT and OEG resist any protein binding to the surface. Both exhibit none or almost no protein binding after washing with Buffer A.



SAM		Bound protein at 0 (S) (RU)	Bound protein at 800(S) (RU)	Bound protein at 930(S) (RU)	% Bound protein after SDS wash	% Bound protein compared to NHS terminated SAM
	Pftot HS(CH <sub>2</sub> ) <sub>2</sub> (CF <sub>2</sub> ) <sub>6</sub>	0	-1.0	-55.0	0	0.0
	OEG HS(CH <sub>2</sub> ) <sub>11</sub> (OCH <sub>2</sub> CH <sub>2</sub> ) <sub>3</sub> OH	0	9.0	4.0	44	0.004
	MUA HS(CH <sub>2</sub> ) <sub>11</sub> COOH	0	2665.0	-200.0	0	0.0
	NHS 	0	2934.0	1120.0	38	100.0

**Figure 6.3 SPR analysis of SAMs after exposure to purified WT-LH2 complex**

The SPR traces shown are the average of four separate exposures at identical conditions. Purified LH2 complex (12.5 AU) was passed over the sensor chip at a rate of 10  $\mu\text{l min}^{-1}$  for 600 sec (a). The SAM surface was then washed with Buffer A (20 mM Tris, 0.1 % LDAO, pH 8.0) at 10  $\mu\text{l min}^{-1}$  for 3 min (b). Aggressive washing of the surface using 1 % SDS detergent at 30  $\mu\text{l min}^{-1}$  for 30 sec followed (c). The chip was then exposed to Buffer A at 10  $\mu\text{l min}^{-1}$  for 1 min (d). All traces have been normalised to a starting value of 20170.0 RU for comparison.

MUA binds a significant amount of protein, 2665.0 RU, after initial exposure to the LH2 complex. However, this is completely removed by washing with SDS. In fact, the trace shows that there is less bound to the surface than before the protein was applied. This may be due the removal of small amounts of contamination from the chip which was present before it was exposed to the LH2 complex.

The NHS terminated SAM initially binds a similar amount of LH2 complex to MUA (2934.0 RU), however, 38 % of this complex remains bound after aggressive washing with SDS.

#### **6.3.4 Micron patterning**

The SPR experiments successfully identified conditions for either binding or repelling LH2. It is important to realise that both of these binding characteristics are needed for successful patterning. Analysis of the SPR data obtained meant that the two SAMs chosen to create the micro-patterns were Ptot (resistant) and an NHS terminated alkane thiol (attractive). The creation of the photopatterned Ptot / MUA SAM is detailed in section 2.15.3. A friction force microscopy image of this SAM is displayed in Figure 6.4A. The light squares seen are areas of MUA, the dark grid seen between the squares is a SAM of protein resistant Ptot.

Before exposure to purified LH2 complex, the patterned SAM was derivatised via N-(3-Dimethylaminopropyl)-N'-ethylcarbodiimide hydrochloride (EDC)/NHS crosslinking to the carboxylic acid tail group of MUA. This created squares comprising an alkane thiol possessing a tail group (NHS) which is capable of covalently binding purified protein. The SAM was then immersed in Buffer A containing purified LH2 complex ( $A_{850} = 0.1$ ) for 15 min.

A Tapping mode™ AFM height image recorded under liquid shows the SAM after immersion in a LH2 protein solution (Figure 6.4B). A clear height difference is seen between the protein resistant grid areas (Ptot) and the squares comprised of NHS tail groups.

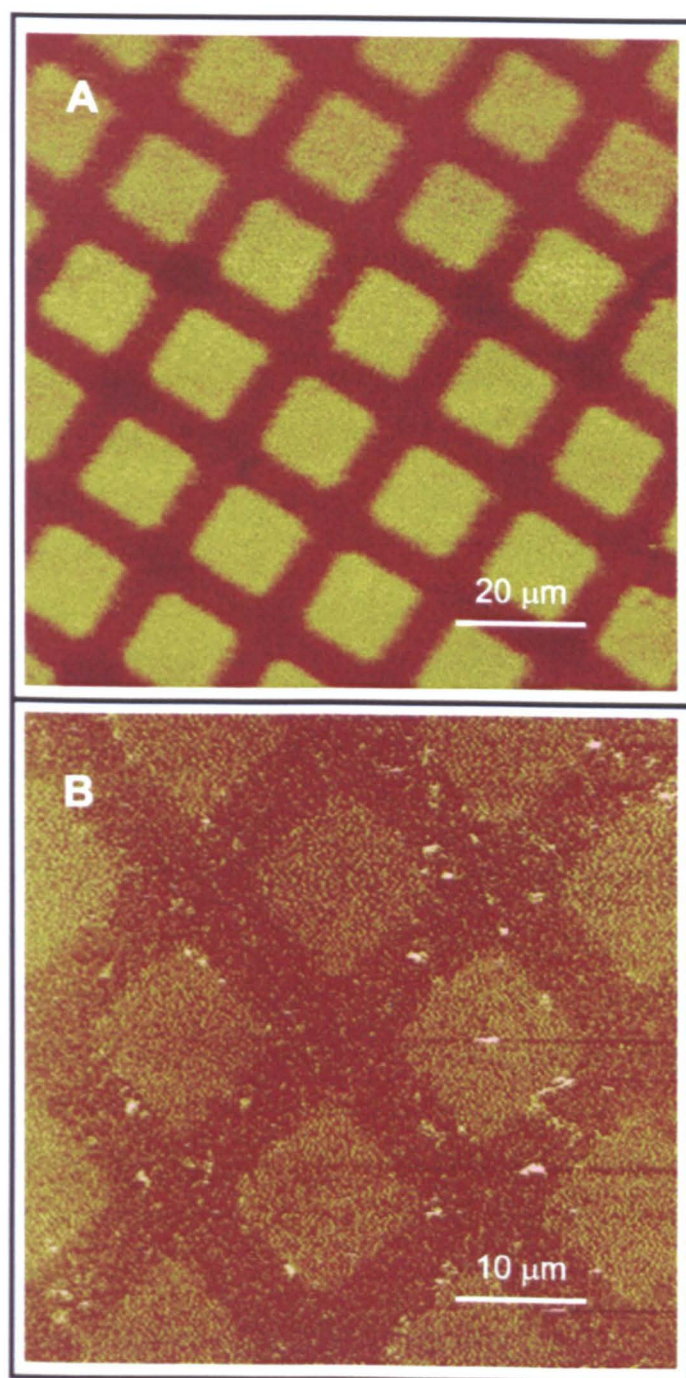


**Figure 6.4** Micron patterning of WT-LH2 imaged by AFM

- A. A friction force image of 1H, 1H, 2H, 2H- pefluorooctanethiol/  $\text{HS}(\text{CH}_2)_{11}\text{COOH}$  (interstitial areas/squares) chemical pattern.
- B. A Tapping Mode™ AFM height image of the pattern displayed in panel A is shown. The functionalisation of the  $\text{HS}(\text{CH}_2)_{11}\text{COOH}$  alkane thiol with (EDC)/NHS has occurred, meaning the square regions now possess an NHS tail group. Purified LH2 complexes have been bound covalently to the functionalised NHS squares, which is shown by the increase in height in these areas.

### 6.3.4 Fluorescence imaging of LH2 bound to photopatterned SAMs

The patterned LH2 complexes shown in Figure 6.4B were then probed using a confocal microscope attached to an AFFM as described in section 2.16.2. The fluorescence images recorded are displayed in Figures 6.5A and 6.5B.

Figure 6.5A shows the fluorescence image recorded using a single photon counting avalanche photo diode (APD), which records light at all wavelengths. The image shown in Figure 6.5B was recorded using a Charge Coupled Device (CCD) camera (Spec-10:100B, Princeton Instruments). Fluorescence recorded using this camera was measured at a wavelength of 890 nm. Both images show an increased fluorescence in the square regions of the pattern where the LH2 is bound.

A more detailed analysis of the CCD fluorescence image obtained is shown in Figure 6.6. The emission spectrum recorded by the CCD of the LH2 complex in solution is shown in Figure 6.6A as a reference. A comparison of the fluorescence in the resistant (Pfort) and attractive (NHS) regions of the SAM is shown in Figure 6.6B. The spectrum collected from the NHS region is an average of 25 pixels along the white line labelled (a). The spectrum collected from the Pfort region is an average of 25 pixels along the white line labelled (b). There is an almost 10 fold increase in fluorescence at 890 nm seen in the NHS regions compared to the Pfort regions. A peak occurring at 820 nm is present in both areas of the SAM, which can be attributed to fluorescence of the underlying gold surface.

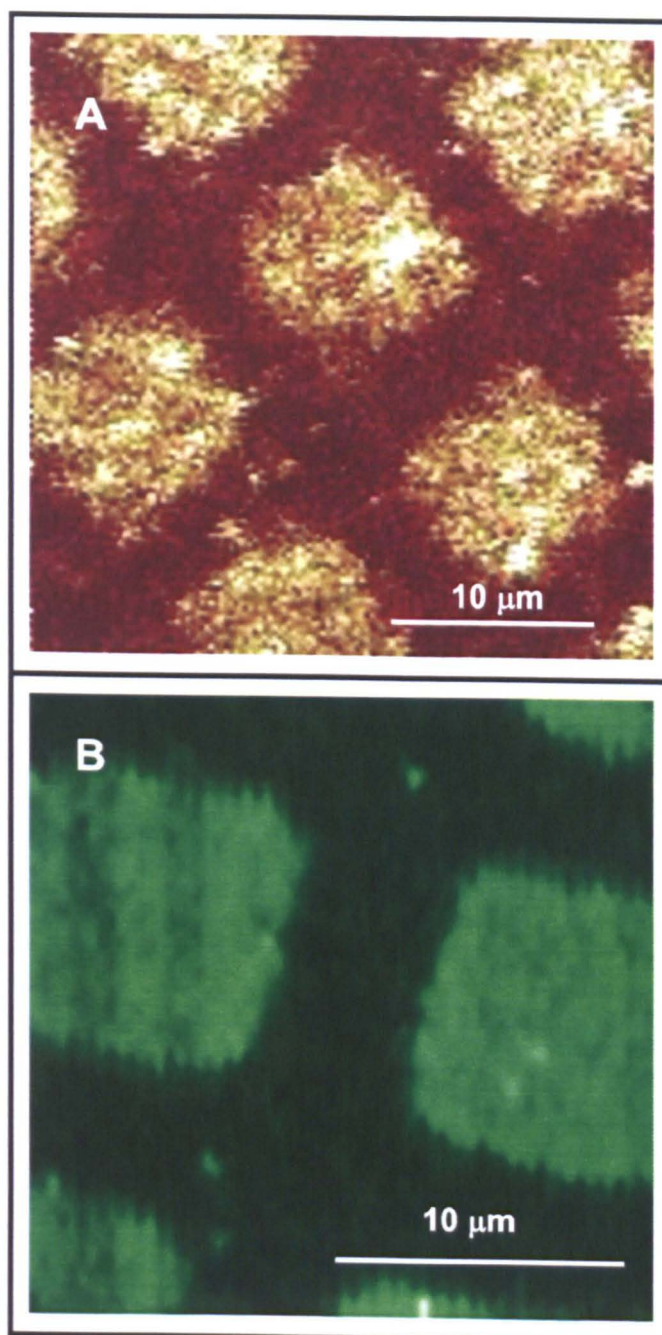


**Figure 6.5** Fluorescence images of patterned purified WT-LH2 complex

- A. Fluorescent images of WT-LH2 immobilized onto PfoT / NHS ester micron pattern captured with a single photon counting APD
- B. Fluorescent images of WT-LH2 immobilized onto PfoT / NHS ester micron pattern captured by a prism based spectrograph equipped with a liquid nitrogen cooled back illuminated CCD camera. The image taken is fluorescence emission recorded at 890 nm.

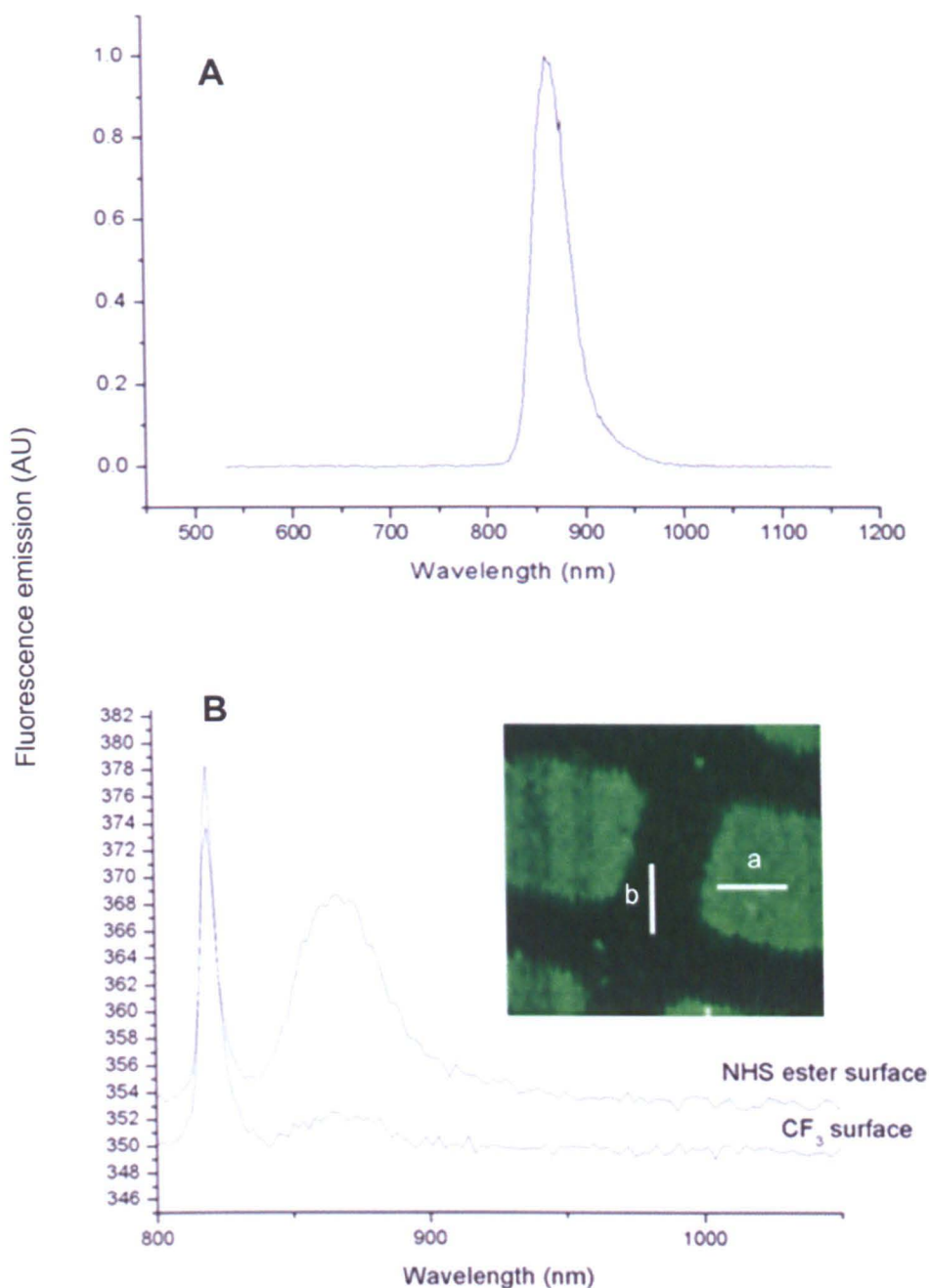


**Figure 6.6 The fluorescence emission spectra of covalently bound purified WT-LH2 complexes**

- A. Fluorescence emission spectra of purified LH2 complexes in solution (20 mM Tris, 0.1 % LDAO, pH 8.0) recorded at room temperature. Spectrum has been normalised to a value of 1.0 AU for clarity.
- B. Fluorescence emission spectra of purified LH2 complexes immobilised onto NHS ester surface (a) and from the protein resistant PfoT surface (b). Spectra collected are an average of 25 pixels along a line chosen from the image inset.

All spectra measured using a prism based spectrograph equipped with a liquid nitrogen cooled, back illuminated CCD camera.

## **6.4 Discussion**

### **6.4.1 Context**

The patterning of proteins at the micron and sub micron scale is becoming increasingly important as the fields of proteomics and bionanotechnology grow. The directed immobilisation of specific proteins in a precise spatial arrangement could herald a new diagnostic technology similar in usefulness to that of DNA and mRNA micro-arrays. The key problem when developing this technology is maintaining the specificity of protein deposition on a surface, whilst reducing the scale at which the proteins are patterned. The work presented in this chapter demonstrates not only highly specific deposition of a purified membrane protein on the micron scale, but it also shows the protein remains functional when bound to the surface.

### **6.4.2 SPR analysis of SAM properties**

The SPR studies presented in Figure 6.3 have provided qualitative evidence which has allowed the identification of suitable protein resistant (Pftot) and attractive (NHS terminated alkane thiol) surfaces from which it is possible to reproducibly fabricate patterned SAMs. The results observed for OEG indicate a level of efficiency similar to that of Pftot in terms of preventing protein binding. However the integrity of the SAMs of this compound upon patterning was degraded (data not shown), meaning the specificity of LH2 patterning would be reduced.

The SPR traces obtained for NHS-terminated SAMs show that the specific covalent attachment of purified LH2 complexes is achieved (for a mechanism of attachment see Figure 1.17B), since a significant amount remains bound even after aggressive washing with the denaturant SDS. The inability of MUA SAMs to bind purified LH2 complexes, when electrostatic interactions are compromised by SDS washing, means that it is not suitable for use in the long term development of this technology.

### 6.4.3 Micron patterning of purified LH2 complexes

The AFM height image presented in Figure 6.4, along with the fluorescence images detailed in Figures 6.5 and 6.6 prove the binding of purified LH2 complexes in specific spatial arrangements has been achieved. The fluorescence images (Figures 6.5A and B) in conjunction with the spectroscopic data (Figure 6.6A and B) prove the LH2 complex remains functional after being covalently attached to the surface. The B850 fluorescence emission which is seen in the squares of liganded complexes is ~10 fold higher than that seen in the protein resistant (Pfort) areas of the pattern (Figure 6.5B), showing that the deposition of the purified complex was specific and controlled.

The micron patterning of proteins per se is not novel; this has been achieved before for soluble proteins such as biotin (Harnett *et al.*, 2001). The work in this chapter is novel, since it has shown for the first time that it is possible to pattern membrane proteins at the micron scale whilst maintaining their intrinsic functionality. This is of importance in not only the wider context of developing protein arrays for use in proteomics, but also the more specific field of creating hybrid photovoltaic technologies. The fact that these techniques have been applied to the LH2 complex means that it is now possible to imagine similar work being carried out using other important membrane proteins. It is possible various cell receptor proteins could be studied, perhaps screening them as possible drug targets in pharmaceutical research.

It should be noted that if the practical application of protein arrays as a diagnostic tool is to become a reality then further work needs to be carried out. This should focus upon reducing the level of protein patterning to the nano-scale, as well as developing methods by which multiple proteins can be specifically patterned in close proximity. Possibilities for achieving this could focus upon the patterning of SAMs using Near Field Scanning Optical Microscopy (NSOM). This technique allows for the circumvention of the diffraction limit (usually  $\lambda/2$  nm) to in some cases  $\lambda/20$  nm (Xia *et al.*, 1998; Piner *et al.*, 1999).

## Appendix I

### *E. coli* strains used in this thesis

Strain	Relevant properties	Source/reference
DH5 $\alpha$	supE44 $\Delta$ lacU169 ( $\Phi$ 80lacZ $\Delta$ M15) hsdR17 recA1 endA1 gyrA96 thi-1 relA1	Hanahan (1985)
S17-1	RP4-2 (Tc::Mu, Nm::Tn7) integrated into the chromosome: thi pro hsdR hsdM <sup>+</sup> recA Tp <sup>R</sup> (Sm <sup>R</sup> )	Simon <i>et al.</i> (1983)

### *Rba. sphaeroides* strains used in this thesis

Strain	Relevant properties	Source/reference
2.4.1.	Wild-type	Samuel Kaplan (University of Texas)
$\Delta$ 1BA- $\Delta$ 2BA	In-frame genomic deletion of <i>puc1BA</i> and <i>puc2BA</i>	Zeng <i>et al.</i> , (2003)
$\Delta$ 2BA	In-frame genomic deletion of <i>puc2BA</i>	Zeng <i>et al.</i> , (2003)
$\Delta$ 1BAC- $\Delta$ 2BA	In-frame genomic deletion of <i>puc1BAC</i> and <i>puc2BA</i>	Zeng <i>et al.</i> , (2003)
$\Delta$ 3	In-frame genomic deletion of <i>puc1BA</i> and <i>puc2BA</i> . Tn5 insertion within <i>puf</i> operon, deleting <i>pufBALM</i> (Km <sup>r</sup> )	Chapter 5 of this thesis
$\Delta$ 4	In-frame genomic deletion of <i>puc1BAC</i> and <i>puc2BA</i> . Tn5 insertion within <i>puf</i> operon, deleting <i>pufBALM</i> (Km <sup>r</sup> )	Chapter 5 of this thesis
DD13	Genomic deletion of <i>puc1BA</i> by insertion of Sm <sup>r</sup> gene. Genomic deletion of <i>pufBALMX</i> + 1.6Kb downstream of the <i>puf</i> operon by insertion of Km <sup>r</sup> gene.	Jones <i>et al.</i> , (1992)

### PCR Primers

Primer Name	Primer sequence 5'→3'	Relevant section of thesis
P1-2B	AGTGACTGACGATCCGAAGAAAGTCTGGCCGAGC	3.2.1.1
P2-2B	GCTCGGCCAGACTTTCTTGCATCGTCAGTCACT	3.2.1.1
P3-2B	CGAGCGGCCTGACCATTGCCGAAGCCGAAGAAG	3.2.1.1
P4-2B	CTTCTTCGGCTTCGGCAATGGTCAGGCCGCTCG	3.2.1.1

**b-series ions generated upon MS/MS of LH2  $\beta$ -polypeptides (section 3.3.3.2)**

#### Puc1B

Residue	Mass	b - ion
M	131.04	132.04
T	101.04	233.10
D	115.02	348.12
D	115.02	463.15
L	113.08	576.23
N	114.04	690.28
K	128.09	818.37
V	99.07	917.44
W	186.08	1103.52

#### Puc2B

Residue	Mass	b - ion
M	131.04	132.04
T	101.04	233.10
D	115.02	348.12
D	115.02	463.15
P	97.05	560.20
K	128.09	688.30
K	128.09	816.40
V	99.07	915.46
W	186.08	1101.54

## Appendix II

Crystallisation screens performed on LH2-1B1A at the University of Sheffield (Chapter 4)

### Screen one

		Concentration
<b>Protein type:</b>	LH2-1B1A	100 A <sub>850</sub> units ml <sup>-1</sup>
<b>Drop conditions:</b>	Phosphate buffer	0.8 M
	Benzamideine Hydrochloride	3.5 %
	Sodium Chloride	300 Mm
<b>Reservoir conditions:</b>	Ammonium sulphate	present at 0.1 M intervals in the range 2.4 M – 3.2 M

### Screen two

		Concentration
<b>Protein type:</b>	LH2-1B1A	100 A <sub>850</sub> units ml <sup>-1</sup>
<b>Drop conditions:</b>	Phosphate buffer	0.9 M
	Benzamideine Hydrochloride	3.5 %
	Sodium Chloride	300 Mm
<b>Reservoir conditions:</b>	Ammonium sulphate	present at 0.1 M intervals in the range 2.4 M – 3.2 M

### Screen three

		Concentration
<b>Protein type:</b>	LH2-1B1A	100 A <sub>850</sub> units ml <sup>-1</sup>
<b>Drop conditions:</b>	Phosphate buffer	0.8 M
	Benzamideine Hydrochloride	3.5 %
	Sodium Chloride	150 Mm
<b>Reservoir conditions:</b>	Ammonium sulphate	present at 0.1 M intervals in the range 2.4 M – 3.2 M

## Screen four

		<b>Concentration</b>
<b>Protein type:</b>	LH2-1B1A	100 A <sub>850</sub> units ml <sup>-1</sup>
<b>Drop conditions:</b>	Phosphate buffer	0.9 M
	Benzamideine Hydrochloride	3.5 %
	Sodium Chloride	150 Mm
<b>Reservoir conditions:</b>	Ammonium sulphate	present at 0.1 M intervals in the range 2.4 M – 3.2 M

## Screen five

		<b>Concentration</b>
<b>Protein type:</b>	LH2-1B1A	100 A <sub>850</sub> units ml <sup>-1</sup>
<b>Drop conditions:</b>	Phosphate buffer	0.8 M
	Benzamideine Hydrochloride	3.5 %
	Magnesium Chloride	300 Mm
<b>Reservoir conditions:</b>	Ammonium sulphate	present at 0.1 M intervals in the range 2.4 M – 3.2 M

## Screen six

		<b>Concentration</b>
<b>Protein type:</b>	LH2-1B1A	100 A <sub>850</sub> units ml <sup>-1</sup>
<b>Drop conditions:</b>	Phosphate buffer	0.9 M
	Benzamideine Hydrochloride	3.5 %
	Magnesium Chloride	300 Mm
<b>Reservoir conditions:</b>	Ammonium sulphate	present at 0.1 M intervals in the range 2.4 M – 3.2 M

## References

- Aagaard, J. and Siström, W.R.**, (1972) Control of synthesis of reaction centre bacteriochlorophyll in photosynthetic bacteria. *Photochemistry And Photobiology* **15**, 209-225.
- Abrahams, J., Leslie, A., Lutter, B. and Walker, B.**, (1994) Structure at 2.8 angstrom resolution of F1-ATPase from bovine heart mitochondria. *Nature* **370**, 621-628.
- Addlesee, H.A. and Hunter, C.N.**, (1999) Physical mapping and functional assignment of the geranylgeranyl-bacteriochlorophyll reductase gene, *bchP*, of *Rhodobacter sphaeroides*. *J. Bacteriol.* **181**, 7248-7255.
- Adams, C.W., Forrest, M.E., Cohen, S.N. and Beatty, J.T.**, (1989) Structural and functional analysis of transcriptional control of the *Rhodobacter capsulatus puf* operon. *J. Bacteriol.* **171**, 473-482.
- Allen, J.P., Feher, G., Yeates, T.O., Komiya, H. and Rees, D.C.**, (1987) Structure of the reaction center from *Rhodobacter sphaeroides* R26: The protein subunits. *Proc. Natl. Acad. Sci. USA* **84**, 6162-6166.
- Allen, J.P., Feher, G., Yeates, T.O., Komiya, H. and Rees, D.C.**, (1987) Structure of the reaction center from *Rhodobacter sphaeroides* R26: The cofactors. *Proc. Natl. Acad. Sci. USA* **84**, 5730-5734.
- Armstrong, G.A., Hundle, B.S. and Hearst, J.E.**, (1993) Evolutionary conservation and structural similarities of carotenoid biosynthesis gene-products from photosynthetic and non photosynthetic organisms. *Met. Enzymol.* **214**, 297-311.
- Armstrong, G.A., Cook, D.N., Ma, D., Alberti, M., Burke, D.H. and Hearst, J.E.**, (1993) Regulation of carotenoid and bacteriochlorophyll biosynthesis genes and identification of an evolutionarily conserved gene required for bacteriochlorophyll accumulation. *J. Gen. Microbiol.* **139**, 897-906.
- Armstrong, G.A.**, (1994) Eubacteria show their true colors - genetics of carotenoid pigment biosynthesis from microbes to plants. *J. Bacteriol.* **176**, 4795-4802.
- Ashby, M.K., Coomber, S.A. and Hunter, C.N.**, (1987) Cloning, nucleotide sequence and transfer of genes for the B800-850 light-harvesting complex of *Rhodobacter sphaeroides*. *FEBS Lett.* **213**, 245-248.
- Bahatyrova, S., Siebert, C.A.; Olsen, J.D. van der Werf, K.O. van Grondelle, R. Niederman, R.A. Bullough, P.A. Otto, C. Hunter, C.N.** (2004). The native architecture of a photosynthetic membrane. *Nature* **430**, 1058-1062.
- Bahatyrova, S.** (2005) Atomic force microscopy of bacterial photosynthetic systems: A new model for native membrane organisation. *Thesis*. University of Twente, Netherlands

- Bain, C.D. Troughton, E.B. Yu-Tai, T. Evall, J. Whitesides, G.M. and Nuzzo, R.G.** (1988) Formation of monolayers films by the spontaneous assembly of organic thiols from solution onto gold. *J. Am. Chem. Soc.* **111**, 321-335
- Bauer, C.E. and Marrs, B.L.**, (1988) *Rhodobacter capsulatus puf* operon encodes a regulatory protein (PufQ) for bacteriochlorophyll biosynthesis. *Proc. Natl. Acad. Sci. USA* **85**, 7074-7078.
- Bauer, C.E., Buggy, J.J., Yang, Z.M. and Marrs, B.L.**, (1991) The superoperonal organization of genes for pigment biosynthesis and reaction center proteins is a conserved feature in *Rhodobacter capsulatus*: analysis of overlapping *bchB* and *pufA* transcripts. *Mol. Gen. Genet.* **228**, 433-444.
- Belasco, J.G., Beatty, J.T., Adams, C.W., Vongabain, A. and Cohen, S.N.**, (1985) Differential expression of photosynthesis genes in *Rhodospseudomonas capsulata* results from segmental differences in stability within the polycistronic *rxcA* transcript. *Cell* **40**, 171-181.
- Beekman, L.M., van Mourik, F., Jones, M.R., Visser, H.M., Hunter, C.N. and van Grondelle, R.**, (1994) Trapping kinetics in mutants of the photosynthetic purple bacterium *Rhodobacter sphaeroides*: influence of the charge separation rate and consequences for the rate-limiting step in the light-harvesting process. *Biochemistry* **33**, 3143-3147.
- Berry, E.A., Guergova-Kuras, M., Huang, L. and Crofts, A.R.**, (2000) Structure and function of cytochrome bc complexes [In process citation]. *Annu. Rev. Biochem.* **69**, 1005-1075.
- Berry, E.A. Huang, Ls Saechao, L.K. Pon, N.G. Valkova-Valchanova, M. Daldal, F.** (2004). X-ray structure of *Rhodobacter capsulatus* cytochrome *bc<sub>L</sub>*: Comparison with its mitochondrial and chloroplast counterparts. *Photosyn. Res.* **81**, 251-275.
- Biebuyck, H.A. Bain, C.D. and Whitesides, G.M.** (1994) Comparison of organic monolayers on polycrystalline gold spontaneously assembled from solutions containing dialkyl disulfides or alkanethiols. *Langmuir*. **10**. 1825-1831
- Biel, A.J. and Marrs, B.L.**, (1983) Transcriptional regulation of several genes for bacteriochlorophyll biosynthesis in *Rhodospseudomonas capsulata* in response to oxygen. *J. Bacteriol.* **156**, 686-694.
- Billsten, H.H., Herek, J.L., GarciaAsua, G., Hashoj, L., Polivka, T., Hunter, C.N. and Sundstrom, V.**, (2002) Dynamics of energy transfer from lycopene to bacteriochlorophyll in genetically-modified LH2 complexes of *Rhodobacter sphaeroides*. *Biochemistry* **41**, 4127-4136.
- Binnig, G., Quate, C. F. and Gerber, C.** (1986) Atomic force microscope. *Phys. Rev. Lett.*, **56**(9), 930-933.
- Bixon, M. and Jortner, J.**, (1999) Electron Transfer - from isolated molecules to biomolecules. *Adv. chem. Phys.* **106**, 35-202.
- Blawas A.S., and Reichert W.M.**, (1998) Protein patterning. *Biomaterials*, **19** 595-609.

- Bollivar,D.W., Wang,S.J., Allen,J.P.and Bauer,C.E.,** (1994) Molecular genetic analysis of terminal steps in bacteriochlorophyll *a* biosynthesis: characterization of a *Rhodobacter capsulatus* strain that synthesizes geranylgeraniol-esterified bacteriochlorophyll *a*. *Biochemistry* **33**, 12763-12768.
- Bollivar,D.W., Jiang,Z.Y., Bauer,C.E.and Beale,S.I.,** (1994) Heterologous expression of the *bchM* gene product from *Rhodobacter capsulatus* and demonstration that it encodes S-adenosyl-L-methionine: Mg-protoporphyrin IX methyltransferase. *J. Bacteriol.* **176**, 5290-5296.
- Boonstra,A.F., Germeroth,L.and Boekema,E.J.,** (1994) Structure of the light-harvesting antenna from *Rhodospirillum molischianum* studied by electron microscopy. *Biochim. et Biophys. Acta - Bioenergetics* **1184**, 227-234.
- Brunisholz, R.A. and Zuber, H.,** (1992) Structure, function and organization of antenna polypeptides and antenna complexes from the three families of *Rhodospirillaneae*. *J. Photochem. Photobiol. B-Biol.* **15**, 113-140.
- Burgess, J.G., Ashby, M.K. and Hunter, C.N.,** (1989) Characterization and complementation of a mutant of *Rhodobacter sphaeroides* with a chromosomal deletion in the light-harvesting (LH2) genes. *J. Gen. Microbiol.* **135**, 1809-1816.
- Chang,C.H., Tiede,D., Tang,J., Smith,U., Norris,J.and Schiffer,M.,** (1986) Structure of *Rhodopseudomonas sphaeroides* R-26 reaction center. *FEBS Lett.* **205**, 82-86.
- Chang,C.H., El-Kabbani,O., Tiede,D., Norris,J.and Schiffer,M.,** (1991) Structure of the membrane-bound protein photosynthetic reaction center from *Rhodobacter sphaeroides*. *Biochemistry* **30**, 5352-5360.
- Chory,J., Donohue,T.J., Varga,A.R., Staehelin,L.A.and Kaplan,S.,** (1984) Induction of the photosynthetic membranes of *Rhodopseudomonas sphaeroides*: biochemical and morphological studies. *J. Bacteriol.* **159**, 540-554.
- Clayton,R.K.and Clayton,B.J.,** (1972) Relations between pigments and proteins in the photosynthetic membranes of *Rhodopseudomonas sphaeroides*. *Biochim. et Biophys. Acta* **283**, 492-504.
- Clayton,R.K.and Haselkorn,R.,** (1972) Protein components of bacterial photosynthetic membranes. *J. Mol. Biol.* **68**, 97-105.
- Cogdell,R.J., Zuber,H., Thornber,J.P., Drews,G., Gingras,G., Niederman,R.A., Parson,W.W.and Feher,G.,** (1985) Recommendations for the naming of photochemical-reaction centers and light-harvesting pigment-protein complexes from purple photosynthetic bacteria. *Biochim. et Biophys. Acta* **806**, 185-186.

**Cogdell,R.J.and Frank,H.A.,** (1987) How carotenoids function in photosynthetic bacteria. *Biochim. et Biophys. Acta* **895**, 63-79.

**Cogdell, R.J., Fyfe, P.K., Barrett, S.J., Prince, S.M., Freer, A.A., Isaacs, N.W., McGlynn, P. and Hunter, C.N.,** (1996) The purple bacterial photosynthetic unit. *Photosyn. Res.* **48**, 55-63.

**Cogdell,R.J., Howard,T.D., Bittl,R., Schlodder,E., Geisenheimer,I.and Lubitz,W.,** (2000) How carotenoids protect bacterial photosynthesis. *Philosophical Transactions of the Royal Society of London Series B-Biological Sciences* **355**, 1345-1349.

**Cohen-Bazire, G., Siström, W.R. and Stanier, R.,** (1957) Kinetic studies of pigment synthesis by non-sulphur purple bacteria. *J. Comp. Cell. Physiol.* **49**, 25-68.

**Conroy,M.J., Westerhuis,W.H., Parkes-Loach,P.S., Loach,P.A., Hunter,C.N.and Williamson,M.P.,** (2000) The solution structure of Rhodobacter sphaeroides LH1beta reveals two helical domains separated by a more flexible region: structural consequences for the LH1 complex. *J. Mol. Biol.* **298**, 83-94.

**Coomber, S.A. and Hunter, C.N.,** (1989) Construction of a physical map of the 45 kb photosynthetic gene cluster of *Rhodobacter sphaeroides*. *Archives of Microbiology* **151**, 454-458.

**Coomber,S.A., Chaudhri,M., Connor,A., Britton,G.and Hunter,C.N.,** (1990) Localized transposon Tn5 mutagenesis of the photosynthetic gene cluster of *Rhodobacter sphaeroides*. *Mol. Microbiol.* **4** , 977-989.

**Crielaard,W., Cotton, N.P.J., Jackson,J.B., Hellingwerf,K.J. and Konings,W.N.** (1988). The transmembrane electrical potential in intact bacteria: simultaneous measurements of carotenoid absorbance changes and lipophilic cation distribution in intact cells of *Rhodobacter sphaeroides*. *Biochim. et Biophys. Acta* **932**, 17-25.

**Crielaard,W. Visschers,R.W.; Fowler,G.J.S.; Vangrondelle,R.; Hellingwerf,K.J.; Hunter,C.N.** (1994) Probing the B800 bacteriochlorophyll binding-site of the accessory light-harvesting complex from *Rhodobacter sphaeroides* using site-directed mutants .1. Mutagenesis, effects on binding, function and electrochromic behavior of its carotenoids. *Biochim. et Biophys. Acta - Bioenergetics* **1183**, 473-482.

**Crofts,A.R.and Berry,E.A.,** (1998) Structure and function of the cytochrome bc(1) complex of mitochondria and photosynthetic bacteria. *Current Opinion In Structural Biology* **8**, 501-509.

**Czajkowsky, D. M. and Shao, Z.** (1998).Submolecular resolution of single macromolecules with atomic force microscopy. *FEBS Lett.* **430**(1-2), 51-54.

- Deckert, A.A., Kelley, A. A., Mullaugh, M.K., and Delaney, C.** (2004) Comprehensive Study of the Formation and Reaction of a Tethered N-Hydroxysulfosuccinimidyl Ester Used to Covalently Tether Proteins to Surfaces. *J. Phys. Chem. B*, **108** (40), 15808 -15814
- Deisenhofer,J., Epp,O., Miki,K., Huber,R.and Michel,H.,** (1985) Structure of the protein subunits in the photosynthetic reaction centre of *Rhodospseudomonas viridis* at 3Å resolution. *Nature* **318**, 618-624.
- Deisenhofer,J. and Michel,H.** (1989) The photosynthetic reaction centre from the purple bacterium *Rhodospseudomonas viridis*. *EMBO J* **8**, 2149-2170.
- Deisenhofer, J. and Norris, J.R.,** (1993) The photosynthetic reaction center, volumes I and II. San Diego Academic Press
- Deisenhofer,J., Epp,O., Sinning,I.and Michel,H.,** (1995) Crystallographic refinement at 2.3 Å resolution and refined model of the photosynthetic reaction centre from *Rhodospseudomonas viridis*. *J. Mol. Biol.* **246**, 429-457.
- Donohue, T.J., Hoger, J.H. and Kaplan, S.,** (1986) Cloning and expression of the *Rhodobacter sphaeroides* reaction center H gene. *J. Bacteriol.* **168**, 953-961.
- Drews, G. and Imhoff, J. F.** (1991) Phototrophic purple bacteria. In *Variations in autotrophic life* (Shively, J. M. and Barton, L. L., eds.) pp51-98, Academic Press, London.
- Ermiler,U., Fritsch,G., Buchanan,S.K.and Michel,H.,** (1994) Structure of the photosynthetic reaction centre from *Rhodobacter sphaeroides* at 2.65 Å resolution: cofactors and protein-cofactor interactions. *Structure* **2**, 925-936.
- Engel,A., Gaub,H.and Muller,D.J.,** (1999) Atomic force microscope: A forceful way with single molecules. *Curr Biol* **9**, R133-R136.
- Engel,A.and Muller,D.J.,** (2000) Observing single biomolecules at work with the atomic force microscope. *Nat Struct. Biol* **7**, 715-718.
- Engelhardt,H., Engel,A.and Baumeister,W.,** (1986) Stoichiometric model of the photosynthetic unit of *Ectothiorhodospira halochloris*. *Proc. Natl. Acad. Sci. USA* **83**, 8972-8976.
- Escoubas, J-M., Lomas, M., LaRoche, J., Falkowski, P.G.,** (1995) Light intensity regulation of *cab* gene transcription is signaled by the redox state of the plastiquinone pool. *Proc. Natl. Acad. Sci. USA* **92**, 10237-10241.
- Farchaus, J.W., Gruenberg, H. and Oesterhelt, D.,** (1990) Complementation of a reaction center-deficient *Rhodobacter sphaeroides* *pufLMX* deletion strain in *trans* with *pufBALM* does not restore the photosynthesis-positive phenotype. *J. Bacteriol.* **172**, 977-985.

- Farchaus, J.W., Barz, W.P., Grunberg, H. and Oesterhelt, D.,** (1992) Studies on the expression of the *pufX* polypeptide and its requirement for photoheterotrophic growth in *Rhodobacter sphaeroides*. *EMBO J.* **11**, 2779-2788.
- Fidai, S., Kalmar, G.B., Richards, W.R. and Borgford, T.J.,** (1993) Recombinant expression of the *pufQ* gene of *Rhodobacter capsulatus*. *J. Bacteriol.* **175**, 4834-4842.
- Fidai, S., Hinchigeri, S.B., Borgford, T.J. and Richards, W.R.,** (1994) Identification of the PufQ protein in membranes of *Rhodobacter capsulatus*. *J. Bacteriol.* **176**, 7244-7251.
- Flemming, G. and van Grondelle, R.,** (1994) The primary steps of photosynthesis. *Physics Today* **47**, 48-55.
- Fotiadis, D., Hasler, L., Müller, D. J., Stahlberg, H., Kistler, J. and Engel, A.** (2000). Surface tongue-and-groove contours on lens MIP facilitate cell-to-cell adherence. *J. Mol. Biol.* **300**(4), 779-789.
- Fotiadis, D., Liang, Y., Filipek, S., Saperstein, D.A., Engel, A. and Palczewski, K.,** (2003) Atomic-force microscopy: Rhodopsin dimers in native disc membranes, *Nature*, **421**, 127-128
- Fotiadis, D., Qian, P., Pilippsen, A., Bullough, P.A., Engel, A. and Hunter, C.N.,** (2004) Structural analysis of the RC-LH1 photosynthetic core complex of *Rhodospirillum rubrum* using atomic force microscopy. *J Biol. Chem.* **279**, 2063-2068.
- Fowler, G.J.S., Visschers, R.W., Grief, G.G., van Grondelle, R. and Hunter, C.N.** (1992) Genetically modified photosynthetic antenna complexes with blueshifted absorbance bands. *Nature* **355**, 848-850.
- Fowler, G.J.S., Sockalingum, G.D., Robert, B. and Hunter, C.N.,** (1994) Blue shifts in bacteriochlorophyll absorbance correlate with changed hydrogen bonding patterns in light-harvesting 2 mutants of *Rhodobacter sphaeroides* with alterations at a-Tyr-44 and a-Tyr-45. *Biochem J* **299**, 695-700
- Fowler, G.J.S., Hess, S., Pullerits, T., Sundström, V. and Hunter, C.N.** The role of  $\beta$ Arg-10 in the B800 bacteriochlorophyll and carotenoid pigment environment within the light-harvesting LH2 complex of *Rhodobacter sphaeroides*. *Biochemistry* **36**, 11282-11291 (1997).
- Francia, F., Wang, J., Venturoli, G., Melandri, B.A., Barz, W.P. and Oesterhelt, D.,** (1999) The reaction center-LH1 antenna complex of *Rhodobacter sphaeroides* contains one PufX molecule which is involved in dimerization of this complex. *Biochemistry* **38**, 6834-6845.
- Francia, F., Wang, J., Zischka, H., Venturoli, G. and Oesterhelt, D.,** (2002) Role of the N- and C-terminal regions of the PufX protein in the structural organization of the photosynthetic core complex of *Rhodobacter sphaeroides*. *Eur J Biochem* **269**, 1877-1885.
- Frank, H.A. and Cogdell, R.J.,** (1996) Carotenoids in photosynthesis. *Photochemistry And Photobiology* **63**, 257-264.

- Freer,A.A., Prince,S., Sauer,K., Papiz,M., Hawthornthwaite-Lawless,A.M., McDermott,G., Cogdell,R.J.and Isaacs,N., (1996) Pigment-pigment interactions and energy transfer in the antenna complex of the photosynthetic bacterium *Rhodospseudomonas acidophila*. *Structure* **4**, 449-462.
- Gall,A., Fowler,G.J.S., Hunter,C.N. and Robert,B. (1997) Influence of the protein binding site on the absorption properties of the monomeric bacteriochlorophyll in *Rhodobacter sphaeroides* LH2 complex. *Biochemistry* **36**, 16282-16287.
- Gall,A., Cogdell,R.J. and Robert,B. (2003) Influence of carotenoid molecules on the structure of the bacteriochlorophyll binding site in peripheral light-harvesting proteins from *Rhodobacter sphaeroides*. *Biochemistry* **42**, 7252-7258 (2003).
- Garcia-Asua, G., Cogdell, R.J. and Hunter, C.N., (2002) Functional assembly of the foreign carotenoid lycopene into the photosynthetic apparatus of *Rhodobacter sphaeroides*, achieved by replacement of the native 3-step phytoene desaturase with its 4-step counterpart from *Erwinia herbicola*. *Mol. Microbiol.* **44**, 233-244.
- Germeroth,L., Lottspeich,F., Robert,B.and Michel,H., (1993) Unexpected similarities of the B800-B850 light-harvesting complex of *Rhodospirillum molischianum* to the B870 light-harvesting complexes from other purple photosynthetic bacteria. *Biochemistry* **32**, 5615-5621.
- Gibson, L.C.D., McGlynn, P., Chaudhri, M. and Hunter, C.N., (1992) A putative anaerobic coproporphyrinogen III oxidase in *Rhodobacter sphaeroides*. II. Analysis of a region of the genome encoding *hemF* and the *puc* operon. *Mol. Microbiol.* **6**, 3171-3186.
- Gibson,L.C.D.and Hunter,C.N., (1994) The bacteriochlorophyll biosynthesis gene, *bchM*, of *Rhodobacter sphaeroides* encodes *S*-adenosyl-L-methionine: Mg protoporphyrin methyltransferase. *FEBS Lett.* **352**, 127-130.
- Gibson,L.C.D., Willows,R.D., Kannangara,C.G., von Wettstein,D.and Hunter,C.N., (1995) Magnesium-protoporphyrin chelatase of *Rhodobacter sphaeroides*: reconstitution of activity by combining the products of the *bchH*, *-I* and *-D* genes expressed in *Escherichia coli*. *Proc. Natl. Acad. Sci. USA* **92**, 1941-1944.
- Gibson,L.C.D., Jensen,P.E.and Hunter,C.N., (1999) Magnesium chelatase from *Rhodobacter sphaeroides*: initial characterization of the enzyme using purified subunits and evidence for a BchI-BchD complex. *Biochem J* **337** ( Pt 2), 243-251.
- Giuliano, G., Pollock, D., Stapp, H. and Scolnik, P.A., (1988) A genetic-physical map of the *Rhodobacter capsulatus* carotenoid biosynthesis gene cluster. *Mol. Gen. Genet.* **213**, 78-83.
- Gong, L.M., Lee, J.K. and Kaplan, S., (1994) The *Q* gene of *Rhodobacter sphaeroides*: its role in *puf* operon expression and spectral complex assembly. *J. Bacteriol.* **176** , 2946-2961.

- Gong, L.M. and Kaplan, S.**, (1996) Translational control of *puf* operon expression in *Rhodobacter sphaeroides* 2.4.1. *Microbiology-Uk* **142**, 2057-2069.
- Goncalves,R.P., Bernadac,A., Sturgis,J.N. and Scheuring,S.** (2005) Architecture of the native photosynthetic apparatus of *Phaeospirillum molischianum*. *J Struct. Biol.* **152**, 221-228.
- Haddon, R.C., Lamola, A.A.**, (1985) The molecular electronic device and the biochip computer: Present status. *Proc. Natl. Acad. Sci. USA* **82** 1874-1878
- Hamblin,P.A., Bourne,N.A.and Armitage,J.P.**, (1997) Characterization of the chemotaxis protein CheW from *Rhodobacter sphaeroides* and its effect on the behaviour of *Escherichia coli*. *Mol. Microbiol.* **24**, 41-51.
- Hanahan, D.**, (1985) Techniques for transformation of *E. coli*. In: Glover, D.M. (ed.), *DNA Cloning*. IRL Press, Oxford, Vol. 1, pp. 109-135.
- Harnett, C. K., Satyalakshmi, K. M., and Craighead, H. G.**, (2001) Bioactive Templates Fabricated by Low-Energy Electron Beam Lithography of Self-Assembled Monolayers. *Langmuir*, **17** (1), 178 -182
- Hess, S., Chachisvilis, M., Timpmann, K., Jones, M.R., Fowler, G.J.S., Hunter ,C.N. and Sundström, V.**, (1995) Temporally and spectrally resolved subpicosecond energy transfer within the peripheral antenna complex (LH2) and from LH2 to the core antenna complex in photosynthetic purple bacteria. *Proc. Natl. Acad. Sci. USA* **92**, 12333-12337.
- Holmes,N.G., Hunter,C.N., Niederman,R.A. and Crofts,A.R.** (1980). Identification of the pigment pool responsible for the flash-induced carotenoid band shift in *Rhodospseudomonas sphaeroides* chromatophores. *FEBS Lett.* **115**, 43-47.
- Hoff,A.J.and Deisenhofer,J.**, (1997) Photophysics of photosynthesis. Structure and spectroscopy of reaction centers of purple bacteria. *Physics Reports-Review Section Of Physics Letters* **287**, 2-247.
- Hu,X.C., Damjanovic,A., Ritz,T.and Schulten,K.**, (1998) Architecture and mechanism of the light-harvesting apparatus of purple bacteria. *Proc. Natl. Acad. Sci. USA* **95**, 5935-5941.
- Hu, X.C., Ritz, T., Damjanovic, A., Autenrieth, F. and Schulten, K.**, (2002) Photosynthetic apparatus of purple bacteria. *Quarterly reviews of Biophysics* **35**, 1-62.
- Huang, J. and Hemminger, J.C.**, (1993) Photooxidation of thiols in self assembled monolayers on gold. *J. Am. Chem. Soc.* **115**, 3342-3343
- Hunter,C.N., Kramer,H.J.M. and van Grondelle,R.** (1985). Linear dichroism and fluorescence emission of antenna complexes during photosynthetic unit assembly in *Rhodospseudomonas sphaeroides*. *Biochim. et Biophys. Acta* **807**, 44-51.

- Hunter, C.N. and Coomber, S.A.,** (1988) Cloning and oxygen-regulated expression of the bacteriochlorophyll biosynthesis genes *bchE*, *bchB*, *bchA* and *bchC* of *Rhodobacter sphaeroides*. *J. Gen. Microbiol.* **134**, 1491-1497.
- Hunter, C.N. and Turner, G.** (1988) Transfer of genes coding for apoproteins of reaction center and light-harvesting LH1 complexes to *Rhodobacter sphaeroides*. *Journal of General Microbiology*, **134**, 1471-1480.
- Hunter, C.N., van Grondelle, R. and van Dorssen, R.J.,** (1989) The construction and properties of a mutant of *Rhodobacter sphaeroides* with the LH1 antenna as the sole pigment protein. *Biochim. et Biophys. Acta* **973**, 383-389.
- Hunter, C.N., McGlynn, P., Ashby, M.K., Burgess, J.G. and Olsen, J.D.,** (1991) DNA sequencing and complementation/deletion analysis of the *bchA-puf* operon region of *Rhodobacter sphaeroides*: *in vivo* mapping of the oxygen-regulated *puf* promoter. *Mol. Microbiol.* **5**, 2649-2661.
- Hunter, C.N., Hundle, B.S., Hearst, J.E., Lang, H.P., Gardiner, A.T., Takaichi, S. and Cogdell, R.J.,** (1994) Introduction of new carotenoids into the bacterial photosynthetic apparatus by combining the carotenoid biosynthetic pathways of *Erwinia herbicola* and *Rhodobacter sphaeroides*. *J. Bacteriol.* **176**, 3692-3697.
- Jamieson, S.J., Wang, P., Qian, P., Kirkland, J.Y., Conroy, M.J., Hunter, C.N. and Bullough, P.A.,** (2002) Projection structure of the photosynthetic reaction centre-antenna complex of *Rhodospirillum rubrum* at 8.5 Å resolution. *EMBO J* **21**, 3927-3935.
- Jensen, P.E., Gibson, L.C.D. and Hunter, C.N.,** (1998) Determinants of catalytic activity with the use of purified I, D and H subunits of the magnesium protoporphyrin IX chelatase from *Synechocystis* sp. PCC6803. *Biochem J* **334** ( Pt 2), 335-344.
- Jones, M.R., Fowler, G.J.S., Gibson, L.C.D., Grief, G.G., Olsen, J.D., Crielaard, W. and Hunter, C.N.,** (1992) Mutants of *Rhodobacter sphaeroides* lacking one or more pigment-protein complexes and complementation with reaction-centre, LH1, and LH2 genes. *Mol. Microbiol.* **6**, 1173-1184.
- Jones, M.R., Visschers, R.W., van Grondelle, R. and Hunter, C.N.,** (1992) Construction and characterization of a mutant of *Rhodobacter sphaeroides* with the reaction center as the sole pigment-protein complex. *Biochemistry* **31**, 4458-4465.
- Jones, M.R., Heer-Dawson, M., Mattioli, T.A., Hunter, C.N. and Robert, B.,** (1994) Site-specific mutagenesis of the reaction centre from *Rhodobacter sphaeroides* studied by Fourier transform Raman spectroscopy: mutations at tyrosine M210 do not affect the electronic structure of the primary donor. *FEBS Lett.* **339**, 18-24.
- Jungas, C., Ranck, J.L., Rigaud, J.L., Joliot, P. and Vermeiglio, A.,** (1999) Supramolecular organization of the photosynthetic apparatus of *Rhodobacter sphaeroides*. *EMBO J.* **18**, 534-542.

- Karrasch,S., Bullough,P.A.and Ghosh,R.,** (1995) The 8.5 Å projection map of the light-harvesting complex I from *Rhodospirillum rubrum* reveals a ring composed of 16 subunits. *EMBO J* **14**, 631-639.
- Kannangara,C.G., Gough,S.P., Bruyant,P., Hooper,J.K., Kahn,A.and von Wettstein,D.,** (1988) tRNA<sup>Glu</sup> as a cofactor in  $\delta$ -aminolevulinic acid biosynthesis: steps that regulate chlorophyll synthesis. *Trends Biochem Sci* **13**, 139-143.
- Kassies, R.** (2005) Atomic Force Fluorescence Microscopy : Combining the best of both worlds. *Thesis*, University of Twente, Netherlands.
- Katona,G., Andreasson,U., Landau,E.M., Andreasson,L.E.and Neutze,R.,** (2003) Lipidic cubic phase crystal structure of the photosynthetic reaction centre from *Rhodobacter sphaeroides* at 2.35 Å resolution. *J. Mol. Biol.* **331**, 681-692.
- Klug, G., Adams, C.W., Belasco, J.G., Doerge, B. and Cohen, S.N.,** (1987) Biological consequences of segmental alterations in mRNA stability: effects of deletion of the intercistronic hairpin loop region of the *Rhodobacter capsulatus puf* operon. *EMBO J.* **6**, 3515-3520.
- Klug, G. and Cohen, S.N.,** (1988) Pleiotropic effects of localized *Rhodobacter capsulatus puf* operon deletions on production of light-absorbing pigment-protein complexes. *J. Bacteriol.* **170**, 5814-5821.
- Klug, G. and Cohen, S.N.,** (1991) Effects of translation on degradation of mRNA segments transcribed from the polycistronic *puf* operon of *Rhodobacter capsulatus*. *J. Bacteriol.* **173**, 1478-1484.
- Kobayashi,M.,** (1995) Waste remediation and treatment using anoxygenic phototrophic bacteria. In: Blankenship,R.E., Madigan,M.T.and Bauer,C.E. (eds.), *Anoxygenic Photosynthetic Bacteria*. Kluwer Academic Publishers, The Netherlands, pp. 1269-1282.
- Koepke, J., Hu, X.C., Muenke, C., Schulten, K. and Michel, H.,** (1996) The crystal structure of the light-harvesting complex II (B800-B850) from *Rhodospirillum rubrum*. *Structure* **4**, 581-597.
- Kiley, P.J. and Kaplan, S.,** (1987) Cloning, DNA sequence, and expression of the *Rhodobacter sphaeroides* light-harvesting B800-850a and B800-850b genes. *J. Bacteriol.* **169**, 3268-3275.
- Kiley, P.J., Donohue, T.J., Havelka, W.A. and Kaplan, S.,** (1987) Dna sequence and *in vitro* expression of the B875 light-harvesting polypeptides of *Rhodobacter sphaeroides*. *J. Bacteriol.* **169**, 742-750.
- Laibinis, P.E. Whitesides, G.M. Allara, D.L. Yu-Tai, T. Parikh, A.N. Nuzzo, R.G.** (1991) Comparison of the structures and wetting properties of self-assembled monolayers of *n*-alkanethiols on the coinage metal surfaces Cu, Ag, Au. *J. Am. Chem. Soc.* **113**, 7152-7167
- Lang,H.P. and Hunter,C.N.** (1994).The relationship between carotenoid biosynthesis and the assembly of the light-harvesting LH2 complex in *Rhodobacter sphaeroides*. *Biochem J* **298**, 197-205.

- Lang, H.P., Cogdell, R.J., Takaichi, S. and Hunter, C.N.,** (1995) Complete DNA sequence, specific Tn5 insertion map, and gene assignment of the carotenoid biosynthesis pathway of *Rhodobacter sphaeroides*. *J. Bacteriol.* **177**, 2064-2073.
- Lebedev, N., Trammel, S.A. Spano, A. Lukashov, E. Griva, I., Schnur., J.** (2006) Conductive wiring of immobilized photosynthetic reaction centre to electrode by cytochrome C. *J. Am. Chem. Soc. Comm.* **128** 12044-12045
- Lee, J.K., DeHoff, B.S., Donohue, T.J., Gumpert, R.I. and Kaplan, S.,** (1989a) Transcriptional analysis of *puf* operon expression in *Rhodobacter sphaeroides* 2.4.1. and an intercistronic transcription terminator mutant. *J. Biol. Chem.* **264**, 19354-19365.
- Lee, J.K., Kiley, P.J. and Kaplan, S.,** (1989b) Posttranscriptional control of *puc* operon expression of B800-850 light-harvesting complex formation in *Rhodobacter sphaeroides*. *J. Bacteriol.* **171**, 3391-3405.
- Lee, J.K. and Kaplan, S.,** (1992) Isolation and characterization of *trans*-acting mutations involved in oxygen regulation of *puc* operon transcription in *Rhodobacter sphaeroides*. *J. Bacteriol.* **174**, 1158-1171.
- Lee, J.K. and Kaplan, S.,** (1992) *cis*-acting regulatory elements involved in oxygen and light control of *puc* operon transcription in *Rhodobacter sphaeroides*. *J. Bacteriol.* **174**, 1146-1157.
- Li, Z. Chang, S. and Williams, R.S.** (2003) Self-assembly of alkanethiol molecules onto platinum and platinum oxide surfaces. *Langmuir.* **19**. 6744-6749
- Lilburn, T.G., Haith, C.E., Prince, R.C. and Beatty, J.T.,** (1992) Pleiotropic effects of *pufX* gene deletion on the structure and function of the photosynthetic apparatus of *Rhodobacter capsulatus*. *Biochim. et Biophys. Acta* **1100**, 160-170.
- Love, C. Wolfe, D.B. Haasch, R. Chabinyk, M.L. Paul, K.E. Whitesides, G.E. and Nuzzo, R.G.** (2003) Formation and structure of self-assembled monolayers of alkanethiolates on palladium. *J. Am. Chem. Soc.*, **125** (9), 2597 -2609
- Madigan, M.T.,** (1988) Microbiology, physiology and ecology of phototrophic bacteria. In: Zehnder, A. (ed.), *Biology of anaerobic micro-organisms*. Wiley, New York, pp. 39-112
- Madigan, M. and Gest, H.,** (1979) Growth of the photosynthetic bacterium *Rhodospseudomonas capsulatus* chemoautotrophically in darkness with H<sub>2</sub> as the energy source. *J. Bacteriol.* **137**, 524-530
- Marrs, B.,** (1981) Mobilization of the genes for photosynthesis from *Rhodospseudomonas capsulata* by a promiscuous plasmid. *J. Bacteriol.* **146**, 1003-1012.

- Mattioli, T.A., Williams, J.C., Allen, J.P. and Robert, B.**, (1994) Changes in primary donor hydrogen-bonding interactions in mutant reaction centres from *Rhodobacter sphaeroides* - identification of the vibrational frequencies of all the conjugated carbonyl groups. *Biochemistry* **33**, 1636-1643.
- Monger, T. and Parson, W.W.**, (1977) Singlet-triplet fusion in *Rhodospseudomonas sphaeroides*. *Biochim. et Biophys. Acta* **460**, 393-407
- McAuley, K.E., Fyfe, P.K., Cogdell, R.J., Isaacs, N. and Jones, M.R.**, (1999) Structural details of an interaction between cardiolipin and an integral membrane protein. *Proc Natl Acad Sci U S A* **96**, 14706-14711.
- McAuley, K.E., Fyfe, P.K., Cogdell, R.J., Isaacs, N.W. and Jones, M.R.**, (2000) X-ray crystal structure of the YM210W mutant reaction centre from *Rhodobacter sphaeroides*. *FEBS Lett.* **467**, 285-290.
- McCarty, R.E., Evron, Y., Johnson, E.A.** (2000) The chloroplast ATP-synthase: A rotary enzyme? *Annu Rev Plant Physiol Plant Mol Biol* **51**: 83-109
- McLuskey, K., Prince, S.M., Cogdell, R.J. and Isaacs, N.W.** (2001). The crystallographic structure of the B800-820 LH3 light-harvesting complex from the purple bacteria *Rhodospseudomonas acidophila* strain 7050. *Biochemistry* **40**, 8783-8789.
- McDermott, G., Prince, S.M., Freer, A.A., Hawthornthwaite-Lawless, A.M., Papiz, M.Z., Cogdell, R.J. and Isaacs, N.W.**, (1995) Crystal structure of an integral membrane light-harvesting complex from photosynthetic bacteria. *Nature* **374**, 517-521.
- McGlynn, P., Hunter, C.N. and Jones, M.R.**, (1994) The *Rhodobacter sphaeroides* PufX protein is not required for photosynthetic competence in the absence of a light harvesting system. *FEBS Lett.* **349**, 349-353.
- Michel, H., Deisenhofer, J.**, (1986) X-ray diffraction studies on a crystalline bacterial photosynthetic reaction centre: A progress report and conclusions on the structure of Photosystem II reaction centres. In: Staehelin, L.A. and Arntzen, C.J. (eds.), *Encyclopedia of Plant Physiology*. Springer, Berlin, Vol. 19, pp. 371-381.
- Mitchell, P.** (1968) Chemiosmotic Coupling in Oxidative and Photosynthetic phosphorylation. Glynn Research Ltd, Bodmin U.K.
- Müller, D. J., Büldt, G. and Engel, A.** (1995). Force-induced conformational change of bacteriorhodopsin. *J. Mol. Biol.* **249**(2), 239-243.
- Naylor, G.W., Adlesee, H.A., Gibson, L.C.D. and Hunter, C.N.**, (1999) The photosynthesis gene cluster of *Rhodobacter sphaeroides*. *Photosyn. Res.* **62**, 121-139

- Niederman, R.A., Mallon, D.E. and Langan, J.J.,** (1976) Membranes of *Rhodospseudomonas sphaeroides*. IV. Assembly of chromatophores in low-aeration cell suspensions. *Biochim. et Biophys. Acta* **440**, 429-447.
- Norrod, K.L. Rowlen, K.L.** (1998) Ozone-Induced Oxidation of Self-Assembled Decanethiol: Contributing Mechanism for "Photooxidation"? *J. Am. Chem. Soc.* **120**. 2656
- O'Gara JP, Gomelsky M, Kaplan S.** (1997) Identification and molecular genetic analysis of multiple loci contributing to high-level tellurite resistance in *Rhodobacter sphaeroides* 2.4.1. *Appl Environ Microbiol.* Dec; **63**(12):4713-20.
- Ogawa, M., Kanda., R., Dewa. T., Iida, K., Nango, M.,** (2002) Molecular Assembly of Light-harvesting Antenna Complex on ITO Electrode. *Chem Lett* **31** 2004 446-450
- Oh-Hama,T., Seto,H.and Miyachi,S.,** (1985) <sup>13</sup>C nuclear magnetic resonance studies on bacteriochlorophyll *a* biosynthesis in *Rhodospseudomonas sphaeroides* S. *Arch. Biochem. Biophys.* **237**, 72-79.
- Okamura,M.Y., Steiner,L.A.and Feher,G.,** (1974) Characterisation of reaction centres from photosynthetic bacteria: Subunit structure of the protein mediating the primary photochemistry in *Rhodospseudomonas sphaeroides*. *Biochemistry* **13**, 1394-1403.
- Olsen,J.D.and Hunter,C.N.,** (1994) Protein structure modelling of the bacterial light-harvesting complex. *Photochem Photobiol* **60**, 521-535.
- Olsen, J.D., Sturgis, J.N., Westerhuis, W.H., Fowler, G.J.S., Hunter, C.N. and Robert, B.,** (1997) Site-directed modification of the ligands to the bacteriochlorophylls of the light-harvesting LH1 and LH2 complexes of *Rhodobacter sphaeroides*. *Biochemistry* **36**, 12625-12632.
- Oster,U., Bauer,C.E.and Rüdiger,W.,** (1997) Characterization of chlorophyll *a* and bacteriochlorophyll *a* synthases by heterologous expression in *Escherichia coli*. *J. Biol. Chem.* **272**, 9671-9676.
- Ostuni, E. Grzybowski,B.A., Mrksich, M. Roberts, C.S., and Whitesides, G.M.,**(2003) Adsorption of Proteins to Hydrophobic Sites on Mixed Self-Assembled Monolayers. *Langmuir* **19**, 1861-1872
- Pan, W. Durning, C. J. and Turro, N. J.** (1996) Kinetics of alkanethiol adsorption on gold. *Langmuir*, **12**, 4469-4473
- Papiz,M., Prince,S.M., Howard,T., Cogdell,R.J.and Isaacs,N.W.,** (2003) The structure and thermal motion of the B800-850 LH2 complex from *Rps. acidophila* at 2.0 Å resolution and 100K: New structural features and functionally relevant motions. *J Mol Biol* **326**, 1523-1538.

- Parkes-Loach, P.S., Law, C.J., Recchia, P.A., Kehoe, J., Nehrlich, S., Chen, J. and Loach, P.A.,** (2001) Role of the core region of the PufX protein in inhibition of reconstitution of the core light-harvesting complexes of *Rhodobacter sphaeroides* and *Rhodobacter capsulatus*. *Biochemistry* **40**, 5593-5601.
- Pemberton, J.M. and Bowen, A.R. St.G.,** (1981) High-frequency chromosome transfer in *Rhodospseudomonas sphaeroides* promoted by broad-host-range plasmid RP-1 carrying mercury transposon Tn501. *J. Bacteriol.* **147**, 110-117.
- Pemberton, J.M. and Harding, C.M.,** (1986) Cloning of carotenoid biosynthesis genes from *Rhodospseudomonas sphaeroides*. *Current Microbiology* **14**, 25-29.
- Pfennig, N.,** (1978) General physiology and ecology of photosynthetic bacteria. In *The photosynthetic bacteria* (Clayton, R.K. and Sistrom, W.R., eds.) 3-78, Plenum Press, New York.
- Piner, R. D. Zhu, J. Xu, F. Mirkin, C. A.** (1999) Dip-pen Nanolithography. *Science*, **283**, 661-663
- Prince, S.M., Papiz, M.Z., Freer, A.A., McDermott, G., Hawthornthwaite-Lawless, A.M., Cogdell, R.J. and Isaacs, N.W.,** (1997) Apoprotein structure in the LH2 complex from *Rhodospseudomonas acidophila* strain 10050: modular assembly and protein pigment interactions. *J. Mol. Biol.* **268**, 412-423.
- Pugh, R.J., McGlynn, P., Jones, M.R. and Hunter, C.N.,** (1998) The LH1-RC core complex of *Rhodobacter sphaeroides*: interaction between components, time-dependent assembly, and topology of the PufX protein. *Biochim. Biophys. Acta* **1366**, 301-316.
- Pullerits, T., Chachisvilis, M. and Sundström, V.,** (1996) Exciton delocalization length in the B850 antenna of *Rhodobacter sphaeroides*. *Journal of Physical Chemistry* **100**, 10787-10792.
- Puskas, A., Greenberg, E.P., Kaplan, S. and Schaeffer, A.L.,** (1997) A quorum-sensing system in the free-living photosynthetic bacterium *Rhodobacter sphaeroides*. *J. Bacteriol.* **179**, 7530-7537.
- Qian, P., Hunter, C.N. and Bullough, P.A.** (2005). The 8.5 Å projection structure of the core RC-LH1-PufX dimer of *Rhodobacter sphaeroides*. *J. Mol. Biol.* **349**, 948-960.
- Recchia, P.A., Davis, C.M., Lilburn, T.G., Beatty, J.T., Parkes-Loach, P.S., Hunter, C.N. and Loach, P.A.,** (1998) Isolation of the PufX protein from *Rhodobacter capsulatus* and *Rhodobacter sphaeroides*: Evidence for its interaction with the  $\alpha$ -polypeptide of the core light-harvesting complex. *Biochemistry* **37**, 11055-11063.
- Robert, B. and Lutz, M.,** (1985) Structures of antenna complexes of several *Rhodospirillaceae* from resonance Raman spectra. *Biochim. et Biophys. Acta* **807**, 10-23.

- Roszak, A.W., Howard, T.D., Southall, J., Gardiner, A.T., Law, C.J., Isaacs, N.W. and Cogdell, R.J.,** (2003) Crystal structure of the RC-LH1 core complex from *Rhodospseudomonas palustris*. *Science* **302**, 1969-1972.
- Rüdiger, W., Schoch, S.,** (1988) Chlorophylls. In: Goodwin, T.W. (ed.), *Chlorophylls*. Academic Press, London, pp. 1-59
- Sambrook, J., Fritsch, E.F. and Maniatis, T.,** (1989) *Molecular Cloning. A Laboratory Manual*, 2nd edition. Cold Spring Harbour Laboratory Press, New York.
- Savage, H., Cyrklaff, M., Montoya, G., Kühlbrandt, W. and Sinning, I.,** (1996) Two-dimensional structure of light harvesting complex II (LHII) from the purple bacterium *Rhodovulum sulfidophilum* and comparison with LHII from *Rhodospseudomonas acidophila*. *Structure* **4**, 243-252.
- Schabert, F. A., Henn, C. and Engel, A.** (1995). Native *Escherichia coli* OmpF porin surfaces probed by atomic force microscopy. *Science* **268**, 92-94.
- Scheer, H.,** (1991) Structure and occurrence of chlorophylls. In: Scheer, H. (ed.), *Chlorophylls*. CRC Press Inc, Cleveland, pp. 3-30.
- Schmidt, K.** (1978) Biosynthesis of carotenoids. In: Clayton, R.K. and Siström, W.R. (eds.), *Photosynthetic bacteria*. Plenum Press, New York, pp. 729-750.
- Shemin, D.,** (1956) The biosynthesis of porphyrins. In: Graf, S. (ed.), *Essays In Biochemistry*. Wiley and Sons, New York, pp. 241-258
- Scheuring, S., Ringler, P., Borgnia, M., Stahlberg, H., Müller, D. J., Agre, P. and Engel, A.** (1999). High resolution topographs of the *Escherichia coli* waterchannel aquaporin Z. *EMBO J.* **18**, 4981-4987.
- Scheuring, S., Reiss-Husson, F., Engel, A., Rigaud, J.L. and Ranck, J.L.,** (2001) High-resolution AFM topographs of *Rubrivivax gelatinosus* light- harvesting complex LH2. *EMBO J* **20**, 3029-3035.
- Scheuring, S., Seguin, J., Marco, S.; Levy, D; Robert, B.; Rigaud, J.L.** (2003) Nanodissection and high-resolution imaging of the *Rhodospseudomonas viridis* photosynthetic core complex in native membranes by AFM. *Proc Natl Acad Sci U S A* **100**, 1690-1693
- Scheuring, S., Rigaud, J.L. and Sturgis, J.** (2004). Variable LH2 stoichiometry and core clustering in native membranes of *Rhodospirillum photometricum*. *EMBO J* **23**, 4127-4133
- Scheuring, S., Francia, F., Busselez, J., Melandri, B.A., Rigaud, J.L. and Levy, D.,** (2004) Structural role of PufX in the dimerization of the photosynthetic core-complex of *Rhodobacter sphaeroides*. *J Biol. Chem.* **279**, 3620-3626.

- Scheuring,S. and Sturgis,J.N.** (2005) Chromatic adaption of photosynthetic membranes. *Science* **309**, 484-487
- Scheuring,S., Busselez,J. and Levy,D.** (2005) Structure of the dimeric PufX-containing core complex of *Rhodobacter blasticus* by *in situ* atomic force microscopy. *J Biol. Chem.* **280**, 1426-1431.
- Scheuring,S., Goncalves,R.P., Prima,V. and Sturgis,J.N.** (2006).The Photosynthetic Apparatus of *Rhodospseudomonas palustris*: Structures and Organization. *J. Mol. Biol.* **358**, 83-96.
- Shreve, A.P., Trautman, J., Frank, H.A., Owens, T.G. and Albrecht, A.,** (1991) Femtosecond energy-transfer processes in the B800-850 light-harvesting complex of *Rhodobacter sphaeroides* 2.4.1. *Biochim. et Biophys. Acta* **1058**, 280-288.
- Schumacher, A. and Drews, G.,** (1978) The formation of bacteriochlorophyll-protein complexes of the photosynthetic apparatus of *Rhodospseudomonas capsulata* during the early stages of development. *Biochim. et Biophys. Acta* **501**, 183-194.
- Senaratne, W., Andruzzi, L., and Ober, C. K.,** (2005) Self-Assembled Monolayers and Polymer Brushes in Biotechnology: Current Applications and Future Perspectives. *Biomacromolecules*, **6**, (5), 2427 -2448
- Siebert, C.A., Qian, P., Fotiadis, D., Engel, A., Hunter, C.N. and Bullough, P.A.,** (2004) Molecular architecture of photosynthetic membranes in *Rhodobacter sphaeroides*: the role of PufX. *EMBO J.* **23**, 690-700
- SiefermannHarms,D.,** (1987) The light-harvesting and protective functions of carotenoids in photosynthetic membranes. *Physiol. Plantarum* **69**, 473-568.
- Smith,C.A., Suzuki,J.Y.and Bauer,C.E.,** (1996) Cloning and characterization of the chlorophyll biosynthesis gene *chlM* from *Synechocystis* PCC 6803 by complementation of a bacteriochlorophyll biosynthesis mutant of *Rhodobacter capsulatus*. *Plant Mol. Biol.* **30**, 1307-1314.
- Stamouli,A., Kafi,S., Klein,D.C.G., Oosterkamp,T.H., Frenken,J.W.M., Cogdell,R.J.and Aartsma,T.J.,** (2003) The ring structure and organization of light harvesting 2 complexes in a reconstituted lipid bilayer, resolved by atomic force microscopy. *Biophys J* **84**, 2483-2491.
- Stark,W., Kühlbrandt,W., Wildhaber,I., Wehrli,E.and Muhlethaler,K.,** (1984) The structure of the photoreceptor unit of *Rhodospseudomonas viridis*. *EMBO J.* **3**, 777-783.
- Sturgis,J.N., Hagemann,G., Tadros,M.H.and Robert,B.,** (1995) Biochemical and spectroscopic characterization of the B800-850 light-harvesting complex from *Rhodobacter sulphidophilus* and its B800-830 spectral form. *Biochemistry* **34**, 10519-10524.

**Sturgis, J.N., Jirsakova, V., Reiss-Husson, F., Cogdell, R.J. and Robert, B.,** (1995) Structure and properties of the bacteriochlorophyll binding site in peripheral light-harvesting complexes of purple bacteria. *Biochemistry* **34**, 517-523.

**Sturgis, J.N., Olsen, J.D., Robert, B. and Hunter, C.N.,** (1997) Functions of conserved tryptophan residues of the core light-harvesting complex of *Rhodobacter sphaeroides*. *Biochemistry* **36**, 2772-2778.

**Suzuki, J.Y. and Bauer, C.E.,** (1995) Altered monovinyl and divinyl protochlorophyllide pools in *bchJ* mutants of *Rhodobacter capsulatus* - possible monovinyl substrate discrimination of light-independent protochlorophyllide reductase. *J. Biol. Chem.* **270**, 3732-3740.

**Tadros, M.H. and Waterkamp, K.** Multiple copies of the coding regions for the light-harvesting B800-850 alpha- and beta-polypeptides are present in the *Rhodospseudomonas palustris* genome. *EMBO J.* **8**, 1303-1308 (1989).

**Tadros, M.H., Katsiou, E., Hoon, M.A., Yurkova, N. and Ramji, D.P.** (1993). Cloning of a new antenna gene cluster and expression analysis of the antenna gene family of *Rhodospseudomonas palustris*. *Eur. J. Biochem.* **217**, 867-875.

**Tai, T.-N., Moore, M.D. and Kaplan, S.,** (1988) Cloning and characterization of the 5-aminolevulinate synthase gene(s) from *Rhodobacter sphaeroides*. *Gene* **70**, 139-151.

**Taylor, D.P., Cohen, S.N., Clark, W.G. and Marrs, B.L.,** (1983) Alignment of genetic and restriction maps of the photosynthesis region of the *Rhodospseudomonas capsulata* chromosome by a conjugation-mediated marker rescue technique. *J. Bacteriol.* **154**, 580-590.

**Tichy, H.V., Oberlé, B., Stiehle, H., Schiltz, E. and Drews, G.,** (1989) Genes downstream from *pucB* and *pucA* are essential for formation of the B800-850 complex of *Rhodobacter capsulatus*. *J. Bacteriol.* **171**, 4914-4922.

**Tichy, H.V., Albien, K.U., Gad'on, N. and Drews, G.,** (1991) Analysis of the *Rhodobacter capsulatus* *puc* operon: the *pucC* gene plays a central role in the regulation of LHII (B800-850 complex) expression. *EMBO J.* **10**, 2949-2955.

**Topoglidis, E. Campbell, C.J. Cass, A.E.G. and Durrant, J.R.** (2001) Factors that affect protein adsorption on nanostructured titania films. A novel spectroelectrochemical application to sensing. *Langmuir*, **17** (25), 7899 -7906.

**Trammel, S.A., Wang, L., Zullo, J.M., Shashidhar, R., Lebedev, N.,** (2004) Orientated binding of photosynthetic reaction centres on gold using Ni-NTA self-assembled monolayers. *Biosens Bioelectronics* **19** 1649-1655

- Tunncliffe, R.B Ratcliffe, E.C. Hunter, C.N. Williamson, M.P.** (2006) The solution structure of the PufX polypeptide from *Rhodobacter sphaeroides*. *FEBS Lett.* **508**, 6967-6971
- Vanderah, D.J. Valincius, G. and Meuse, C.W.** (2002) Self-assembled monolayers of methyl 1-thiahexa(ethylene oxide) for the inhibition of protein adsorption. *Langmuir*, **18** (12), 4674 -4680, 2002.
- Van Niel, C.B.** (1962) The present status of the comparative study of photosynthesis. *Ann. Rev. Plant Physiol.* **13**, 1-26.
- Verméglio, A. and Joliot, P.** (2002) Supramolecular organisation of the photosynthetic chain in anoxygenic bacteria. *Biochimica Et Biophysica Acta-Bioenergetics*, **1555**, 60-64.
- Visscher, K.J., Bergström, H., Sundström, V., Hunter, C.N. and van Grondelle, R.,** (1989) Temperature-dependence of energy-transfer from the long wavelength antenna bacteriochlorophyll<sub>896</sub> to the reaction centre in *Rhodospirillum rubrum*, *Rhodobacter sphaeroides* (WT and M2 mutant) from 77 to 177K, studied by picosecond absorption spectroscopy. *Photosyn. Res.* **22**, 211-217.
- Vos, M.H., van Dorssen, R.J., Amesz, J., van Grondelle, R. and Hunter, C.N.,** (1988) The organisation of the photosynthetic apparatus of *Rhodobacter sphaeroides*: studies of antenna mutants using singlet-singlet quenching. *Biochim. et Biophys. Acta* **933**, 132-140.
- Walz, T., Jamieson, S.J., Bowers, C.M., Bullough, P.A. and Hunter, C.N.,** (1998) Projection structures of three photosynthetic complexes from *Rhodobacter sphaeroides*: LH2 at 6 Å, LH1 and RC-LH1 at 25 Å. *J. Mol. Biol.* **282**, 833-845.
- Wellington, C.L. and Beatty, J.T.,** (1991) Overlapping mRNA transcripts of photosynthesis gene operons in *Rhodobacter capsulatus*. *J. Bacteriol.* **173**, 1432-1443.
- Westerhuis, W.H.J., Farchaus, J.W. and Niederman, R.A.,** (1993) Altered spectral properties of the B875 light-harvesting pigment-protein complex in a *Rhodobacter sphaeroides* mutant lacking *pufX*. *Photochemistry And Photobiology* **58**, 460-463.
- Williams, J.C., Steiner, L.A., Ogden, R.C., Simon, M.I. and Feher, G.,** (1983) Primary structure of the M subunit of the reaction center from *Rhodopseudomonas sphaeroides*. *Proc. Natl. Acad. Sci. USA - Bio. Sci.* **80**.
- Williams, J.C., Feher, G. and Simon, M.I.,** (1983) Sequencing of the gene encoding the M subunit of the reaction center of *Rhodopseudomonas sphaeroides*. *Biophysical Journal* **41**.
- Williams, J.C., Steiner, L.A., Feher, G. and Simon, M.I.,** (1984) Primary structure of the L subunit of the reaction center from *Rhodopseudomonas sphaeroides*. *Proc. Natl. Acad. Sci. USA - Bio. Sci.* **81**.

- Williams, J.C., Steiner, L.A. and Feher, G.,** (1986) Primary structure of the reaction center from *Rhodospseudomonas sphaeroides*. *PROTEINS: Structure, Function and Genetics* **1**, 312-325.
- Willows, R.D.,** (2003) Biosynthesis of chlorophylls from protoporphyrin IX. *Natural Product Reports* **20**, 327-341.
- Woodbury, N.W., Allen, J.P.,** (1995) The pathway, kinetics and thermodynamics of electron transfer in wild type and mutant reaction centers of purple nonsulfur bacteria. In: Blankenship, R.E., Madigan, M.T. and Bauer, C.E. (eds.), *The Anoxygenic Photosynthetic Bacteria*. Kluwer Academic Publishers, The Netherlands, pp. 527-557.
- Xia, Y.; Whitesides, G. M.** 1998. Soft Lithography. *Angew. Chem., Int. Ed.* **37**, 550-575.
- Youvan, D.C., Bylina, E.J., Alberti, M., Begusch, H. and Hearst, J.E.,** (1984a) Nucleotide and deduced polypeptide sequences of the photosynthetic reaction center, B870 antenna and flanking polypeptides from *Rhodospseudomonas capsulata*. *Cell* **37**, 949-957.
- Youvan, D.C., Alberti, M., Begusch, H., Bylina, E.J. and Hearst, J.E.,** (1984b) Reaction center and light-harvesting I genes from *Rhodospseudomonas capsulata*. *Proc. Natl. Acad. Sci. USA - Bio. Sci.* **81**, 189-192.
- Zeng, X., Choudhary, M. and Kaplan, S.,** (2003) A second and unusual pucBA operon of *Rhodobacter sphaeroides* 2.4.1: genetic and function of the encoded polypeptides. *J. Bacteriol.* **185**, 6171-6184.
- Zhang, Y. Terril, R.H. Bohm, P.W.** (1999) Ultraviolet photochemistry and ex situ ozonolysis of alkanethiol self-assembled monolayers on gold. *Chem. Mater.* **11**. 2191-
- Zinth, W., Kaiser, W. and Michel, M.,** (1983) Efficient photochemical activity and strong dichroism of single crystals of reaction centres from *Rhodospseudomonas viridis*. *Biochim Biophys Acta* **723**, 128-131.
- Zhu, Y.S., Kiley, P.J., Donohue, T.J. and Kaplan, S.,** (1986) Origin of the mRNA stoichiometry of the *puf* operon in *Rhodobacter sphaeroides*. *J. Biol. Chem.* **261**, 10366-10374.
- Zhu, Y.S. and Hearst, J.E.,** (1986) Regulation of expression of genes for light-harvesting antenna proteins LH-I and LH-II; reaction center polypeptides RC-L, RC-M and RC-H; and enzymes of bacteriochlorophyll and carotenoid biosynthesis in *Rhodobacter capsulatus* by light and oxygen. *Proc. Natl. Acad. Sci. USA* **83**, 7613-7617.
- Zsebo, K.M. and Hearst, J.E.,** (1984) Genetic-physical mapping of a photosynthetic gene cluster from *Rhodospseudomonas capsulata*. *Cell* **37**, 937-947.
- Zuber, H.,** (1985) Structure and function of light-harvesting complexes and their polypeptides. *Photochemistry And Photobiology* **42**, 821-844.